

**DESIGN, SYNTHESIS AND STUDIES OF GUANIDINIUM-BASED INHIBITORS  
FOR ISOPRENOID BIOSYNTHETIC PATHWAY ENZYMES**

by

Walid Abdelmagid

MChem., The University of Liverpool, 2011

A THESIS SUBMITTED IN PARTIAL FULFILLMENT OF  
THE REQUIREMENTS FOR THE DEGREE OF

Doctor of Philosophy

in

THE FACULTY OF GRADUATE AND POSTDOCTORAL STUDIES  
(Chemistry)

THE UNIVERSITY OF BRITISH COLUMBIA

(Vancouver)

October 2019

© Walid Abdelmagid, 2019

The following individuals certify that they have read, and recommend to the Faculty of Graduate and Postdoctoral Studies for acceptance, the dissertation entitled:

**DESIGN, SYNTHESIS AND STUDIES OF GUANIDINIUM-BASED INHIBITORS  
FOR ISOPRENOID BIOSYNTHETIC PATHWAY ENZYMES**

---

submitted by Walid Abdelmagid in partial fulfillment of the requirements for

the degree of Doctor of Philosophy

in Chemistry

**Examining Committee:**

Martin Tanner

Supervisor

Stephen Withers

Supervisory Committee Member

Glenn Sammis

Supervisory Committee Member

Kathryn Ryan

University Examiner

David Chen

University Examiner

**Additional Supervisory Committee Members:**

Supervisory Committee Member

Supervisory Committee Member

## Abstract

In this thesis an inhibition strategy was developed to target enzymes that utilize allylic diphosphates. Positively-charged inhibitors that mimic the transition states/intermediates formed with these enzymes were synthesized. In chapter two, inhibitor **2** containing a guanidinium moiety appended to a phosphonylphosphinate was designed to mimic the transition state for the dissociation of dimethylallyl diphosphate into an allylic carbocation-pyrophosphate ion-pair. To test for the effectiveness of incorporating a guanidinium functionality into inhibitors of human farnesyl diphosphate synthase, inhibitors **3** and **4** were also prepared. Inhibitor **3** has a positive charge localized onto one atom, and inhibitor **4** is isosteric to inhibitor **2**, but lacks positive charge. The inhibitors displayed  $IC_{50}$  values that were significantly higher than the substrate  $K_m$  value, indicating that the positive charge did not result in tight binding to the enzyme.

We decided to apply our inhibition strategy on other allylic diphosphate utilizing-enzymes. In chapter three, inhibitors bearing a guanidinium/amidinium moiety appended to a phosphonylphosphinate and flanked by a hydrocarbon tail (inhibitors **26** and **36**) were synthesized. A neutral inhibitor **34** was also prepared as control. These inhibitors were tested against human squalene synthase (HSQS) and bacterial dehydrosqualene synthase (DSQS) from *Staphylococcus aureus*. It was anticipated that the lipid chain might increase the enzyme's affinity towards the inhibitors. The positively-charged inhibitors acted as competitive inhibitors (low micromolar  $K_I$  values) against DSQS. Similar trends were observed for the first half reaction of HSQS. Surprisingly, the neutral inhibitor was the most

potent for both enzymes. These results indicated that the active site of both enzymes does not directly stabilize the allylic carbocation. We reasoned that these positively-charged inhibitors might be effective with enzymes that generate carbocation intermediates that are not stabilized by resonance or ion-pair interactions. Such a strategy was applied in chapter four, where inhibitors **2** – **4** were tested against isopentenyl diphosphate isomerase (IDI), and acted as competitive inhibitors of IDI. Notably, inhibitor **2** bound 400 times more tightly than its neutral isostere, inhibitor **4**. We reasoned that inhibitor **2** allows for proper positioning of the positive charge in the active site, leading to favorable electrostatic interactions.

## Lay Summary

In this thesis, I synthesized inhibitors that target enzymes involved in vital biological processes and have been considered potential drug targets for many diseases. Inhibitors of these enzymes could be used as cholesterol-lowering drugs, or in the treatment of cancer, progeria, *plasmodium falciparum* resistant malaria and cardiovascular diseases. Our inhibition strategy was found to be ineffective with enzymes that involve the ionization of an allylic diphosphate into an allylic carbocation-pyrophosphate ion pairs, but was very effective with enzymes that involve the formation of carbocations that are less stabilized.

## Preface

A version of Chapter three has been published and some figures are reproduced with permission from: Abdelmagid, Walid M., Adak, Taiya, Freeman, Jon O., Tanner, Martin E., *Biochemistry*, 2018, 57 (38), pp 5591–5601. The plasmid carrying the doubly truncated human squalene synthase (residues 31–370) was provided to us by Dr. Jon Freeman at the Pacific Lutheran University. All the studies reported in this publication and the rest of Chapter three, except for the synthesis of inhibitor **36** made by Taiya Adak, were performed by the author of this thesis under the supervision of Professor Martin Tanner.

The second and the fourth chapters of this thesis are original unpublished work. All the synthetic experiments and kinetic studies were completed by the author of this thesis under the supervision of Professor Martin Tanner.

## Table of Contents

<b>Abstract.....</b>	<b>iii</b>
<b>Lay Summary .....</b>	<b>v</b>
<b>Preface.....</b>	<b>vi</b>
<b>Table of Contents .....</b>	<b>vii</b>
<b>List of Tables .....</b>	<b>xi</b>
<b>List of Figures.....</b>	<b>xii</b>
<b>List of Abbreviations and Symbols .....</b>	<b>xxii</b>
<b>Acknowledgements .....</b>	<b>xxv</b>
<b>Dedication .....</b>	<b>xxvi</b>
<b>Chapter 1: Introduction .....</b>	<b>1</b>
1.1 Terpenes and Terpenoids .....	1
1.1.1 A Brief History and Classification.....	1
1.1.2 Terpene Cyclases .....	3
1.2 Mevalonate Pathway .....	6
1.3 Protein Prenylation.....	8
1.4 The Prenyltransferase Family of Enzymes .....	10
1.4.1 Isoprenyl Diphosphate Synthases (Metal Ion-Dependent Prenyltransferases) :Farnesyl Diphosphate Synthase (FPPS) .....	11
1.4.2 Protein Prenyltransferases: Protein Farnesyltransferase (Ftase).....	23
1.4.3 Aromatic Prenyltransferases (Metal Ion-Independent Prenyltransferases): 4- Dimethylallyl Tryptophan Synthase (4-DMATS) .....	29

1.5	Other Enzymes Involved in Isoprenoid Biosynthesis that generate Carbocationic Intermediates.....	32
1.5.1	Human Squalene Synthase.....	32
1.5.2	Bacterial Dehydrosqualene Synthase of <i>Staphylococcus aureus</i> .....	49
1.5.3	Isopentenyl Diphosphate Isomerase (IDI) (Type 1) .....	59
1.6	Mechanism-Based Inhibition of carbocation-forming enzymes.....	68
1.6.1	Inhibition Studies of Glycosidases.....	68
1.6.2	Inhibition Studies of Isomerases: Isopentenyl Diphosphate Isomerase.....	74
1.6.3	Inhibition Studies of Prenyltransferases: Geranylgeranyl Diphosphate Synthase	75
1.6.4	Bisphosphonates .....	77
1.7	Thesis Goals.....	80

## **Chapter 2: Design, Synthesis and Evaluation of Guanidinium based inhibitors of Human**

	<b>Farnesyl Diphosphate Synthases (HFPPS).....</b>	<b>84</b>
2.1	Introduction.....	84
2.2	Design of Inhibitors .....	85
2.3	Synthesis of Inhibitors <b>2 – 4</b> .....	88
2.3.1	Attempts towards the Synthesis of Inhibitor 2: Pathway A.....	88
2.3.2	Synthesis of Inhibitor 2: Pathway B .....	92
2.3.3	Synthesis of Inhibitors <b>3</b> and <b>4</b> .....	96
2.4	Overproduction and Purification of Human Farnesyl Diphosphate Synthase .....	98
2.5	Measurements of Kinetic Parameters .....	99
2.5.1	Measurements of Kinetic Parameters for the human farnesyl diphosphate synthase reaction.....	99

2.5.2	Inhibition Assays .....	102
2.6	Conclusion and Summary .....	104
2.7	Future Directions .....	110
2.8	Experimental Procedures .....	111
2.8.1	Materials and Methods.....	111
2.8.2	Synthesis of Inhibitors .....	112
2.8.3	General Enzyme Methods.....	116
<b>Chapter 3: Studies with Guanidinium-Based Inhibitors Suggest Minimal Stabilization of Allylic Carbocation Intermediates by Dehydrosqualene and Squalene Synthase.....</b>		<b>120</b>
3.1	Introduction.....	120
3.2	Design of Inhibitors .....	124
3.3	Synthesis of Inhibitors .....	128
3.3.1	Synthesis of Inhibitor <b>26</b> .....	128
3.3.2	Synthesis of Inhibitor <b>34</b> .....	134
3.3.3	Synthesis of Inhibitor <b>36</b> .....	138
3.4	Characterization of Inhibitors .....	138
3.5	Overproduction and Purification of HSQS and DSQS .....	139
3.6	Measurement of Enzyme Kinetics .....	140
3.6.1	Continuous Coupled Assay.....	140
3.6.2	Inhibition Results and Discussion.....	143
3.7	Conclusion and Summary .....	151
3.8	Experimental Procedures .....	162
3.8.1	Materials and Methods.....	162

3.8.2	Synthesis of Inhibitors .....	163
3.8.3	General Enzyme Methods.....	167
<b>Chapter 4:</b>	<b>The Inhibition of Type 1 Isopentenyl Diphosphate Isomerase by Guanidinium-</b>	
<b>Based Inhibitors .....</b>	<b>.....</b>	<b>171</b>
4.1	Introduction.....	171
4.2	Design of Inhibitors .....	172
4.3	Enzyme Kinetics .....	174
4.3.1	Overproduction and Purification of IDI and 4-DMATS.....	176
4.3.2	Measurements of Kinetic Parameters for the 4-DMATS reaction.....	176
4.3.3	Measurement of Kinetics Parameters for the IDI reaction and Inhibition Kinetics	
	177	
4.4	Summary of Chapter Four and Overall Thesis Conclusion .....	184
4.5	Overall Thesis Future Directions .....	190
4.6	Experimental Procedures .....	192
4.6.1	Synthesis of Inhibitors .....	192
4.6.2	General Enzyme Methods.....	192
<b>Bibliography .....</b>	<b>.....</b>	<b>196</b>
<b>Appendix.....</b>	<b>.....</b>	<b>219</b>

## List of Tables

<b>Table 1: Summary of kinetic constants measured with DSQS and SQS,<sup>a</sup>measured with [FPP] = 50 <math>\mu</math>M. <sup>b</sup>measured for first half reaction in absence of NADPH .....</b>	<b>152</b>
--	------------

## List of Figures

Figure 1.1: Examples of mono-, sesqui- and di-terpenoids found in nature, and the structure of isoprene .....	3
Figure 1.2 Structures of the substrates of terpene cyclases. (P denotes a phosphate group) .....	4
Figure 1.3: Examples of the conversion of geranyl diphosphate to myrcene, limonene, and $\beta$ -phellandrene by terpene cyclases.....	5
Figure 1.4: The Mevalonate Pathway .....	7
Figure 1.5: Scheme showing protein farnesylation and the localization of prenylated proteins within a cellular membrane.....	8
Figure 1.6: Prenylation catalyzed by prenyltransferase .....	10
Figure 1.7: The overall reaction catalyzed by farnesyl diphosphate synthase (FPPS) .....	11
Figure 1.8: Stereochemical investigation of the trans-farnesyl diphosphate synthase, using tritiated substrates. ....	14
Figure 1.9: $S_N2$ mechanism for FPPS proposed by Cornforth and Popjak.....	15
Figure 1.10: Proposed $S_N1$ mechanism for FPPS .....	16
Figure 1.11: The structures of trifluoromethyl dimethylallyl diphosphate and dimethylallyl methanesulfonate analogues. ....	17
Figure 1.12: The structures of fluorinated geranyl diphosphate analogue and the corresponding fluorinated methanesulfonate analogue. ....	18
Figure 1.13: The structures of fluorinated geranyl diphosphate analogues and fluorinated methanesulfonate analogues. ....	20

Figure 1.14: (A) Crystal structure of avian FPPS is shown using a ribbon diagram, orange arrows refer to the active sites. B) Graphical representation of the enzyme active site on the right is showing the two DDxxD motifs, and the black circle represents Phe112.....	22
Figure 1.15: Scheme showing the formation of FPP by FPPS and the covalent attachment of a farnesyl unit to the C-terminus of a protein substrate via farnesylation by Ftase.....	24
Figure 1.16: Potential mechanisms employed by Ftase.....	26
Figure 1.17: Structures of FPP analogues used in mechanistic studies of Ftase. ....	27
Figure 1.18 Structure of tipifarnib. ....	28
Figure 1.19: The C-4 prenylation of L-Trp catalyzed by 4-DMATS .....	29
Figure 1.20: The structure of the unreactive analogue of DMAPP, DMSPP. ....	30
Figure 1.21: The crystal structure of DMATS in complex with the thiol analog of DMAPP (DMSPP) and L-Trp. ....	31
Figure 1.22: Structures of regular and irregular connected isoprene units in different isoprenoids. ....	33
Figure 1.23: The structures of squalene and phytoene. ....	34
Figure 1.24: The reaction catalyzed by SQS to form squalene, a precursor in the biosynthesis of cholesterol. ....	36
Figure 1.25: Accepted mechanism of the biosynthesis of squalene catalyzed by squalene synthase (SQS).....	38
Figure 1.26: Products formed from reaction of squalene synthase and FPP in either the absence of NADPH or in the presence of the unreactive NADPH analogue, NADPH <sub>3</sub> .....	40
Figure 1.27: Proposed mechanisms for the conversion of PSPP to squalene.....	42
Figure 1.28: The reaction catalyzed by PSY. ....	44

Figure 1.29: Ribbon diagram showing the "isoprenoid fold" of the HSQS enzyme. The first, second, and third conserved regions (shown in red, green and gold, respectively) are common to both SQS and PYS and cluster around the putative active site. Shown in blue is the aspartate/glutamate-rich regions. .... 45

Figure 1.30: The reactions catalyzed by SQS and DSQS. .... 46

Figure 1.31: Crystal structure of human squalene synthase. FLAP (ball and stick representation) is an inhibitor bound to SQS. .... 47

Figure 1.32: Human squalene synthase's core architecture is structurally homologous to that of three other class I isoprenoid biosynthetic enzymes, FPPS, PLS and EAS. .... 48

Figure 1.33: The structure of staphyloxanthin. .... 49

Figure 1.34: The biosynthetic pathway of staphyloxanthin from FPP. .... 52

Figure 1.35: Mechanism of the biosynthesis of dehydrosqualene catalyzed by dehydrosqualene synthase (DSQS). .... 54

Figure 1.36: Crystal structure of DSQS from *Staphylococcus aureus* complexed with a bisphosphonate inhibitor. .... 55

Figure 1.37: (A and B) Two possible mechanistic scenarios of the two FPP condensation, S1 = donor or S1 = acceptor. Only that scenario shown in A, where S1 = donor, was consistent with the crystallographic data. .... 56

Figure 1.38: Crystallographic data for DSQS-FSPP complex and the intermediate PSPP. (A) DSQS-FSPP complex (B) DSQS/PSPP complex (C) Superposition of A and B (D) Close-up view of A and B superposition. The arrows indicate the movements of the C1', C2, and C3 atoms. .... 58

Figure 1.39: Isomerization of DMAPP and IPP catalyzed by IDI. .... 59

Figure 1.40: IDI type I enzyme utilizes a protonation/deprotonation mechanism. ....	60
Figure 1.41: IDI type I overall structure shown by ribbon representation of the secondary structure. (A) Shows metal-free IDI type I structure. (B) Shows metal-bound IDI type I structure, and two additional $\beta$ -strands at the N-terminus. The metal ion is shown as (M). ....	61
Figure 1.42: A stereoview of distorted octahedral metal coordination site, that contains H25, H32, H69, E114 and E116. ....	62
Figure 1.43: Proposed mechanism of IDI type I. ....	63
Figure 1.44: Labelling experiment on the reaction catalyzed by IDI. ....	64
Figure 1.45: Mechanism of the isomerization reaction employed by IDI (the inset shows the structure of inhibitor <b>48</b> ). ....	65
Figure 1.46: Structure of inhibitor 48 bound to the active site of <i>E. coli</i> IDI. The lower diagram outlines the role of the metal ions in catalysis. ....	67
Figure 1.47: Reactions catalyzed by retaining and inverting glycosidases. ....	69
Figure 1.48: Catalytic mechanism employed by retaining glycosidases. (The inset shows the structure of an oxocarbenium ion). ....	70
Figure 1.49: Catalytic mechanism employed by inverting glycosidases. ....	71
Figure 1.50: Structures of amino-sugars (in their neutral form) used as glycosidase inhibitors. .	72
Figure 1.51: Structures of the imidazole, triazole, and tetrazole analogues of amino-sugar inhibitors. (The inset illustrates the protonation of the imidazole by a catalytic carboxylic acid residue). <sup>100</sup> The structure of the oxocarbenium ion is given to compare with the protonated imidazole. ....	74
Figure 1.52: Top box show the structure of the carbocation intermediate formed by IPP and the bottom box shows the structure of inhibitor <b>48</b> . ....	75

Figure 1.53: Catalytic mechanism of geranylgeranyl diphosphate synthase (GGPPS).The top inset shows the tertiary carbocation formed in the reaction catalyzed by GGPPS. The bottom inset shows the protonated form of inhibitor <b>49</b> .....	76
Figure 1.54: Structures of pyrophosphate, bisphosphonate and the hydroxylated bisphosphonate. ....	77
Figure 1.55: Structures of common nitrogen-containing bisphosphonates (N-BPs).....	78
Figure 1.56: Structures of bisphosphonates and their novel lipophilic analogues.....	79
Figure 1.57: Scheme showing ionization of a prenyl substrate. The inset shows the structure of inhibitor <b>1</b> , and comparison between inhibitor <b>1</b> and the putative transition state. ....	80
Figure 1.58: The structures of inhibitors <b>2</b> , <b>3</b> and <b>4</b> .....	81
Figure 1.59: The structures of farnesyl diphosphate, inhibitors <b>26</b> and <b>36</b> .....	82
Figure 1.60: Structure of Inhibitor <b>34</b> , negative control. ....	83
Figure 2.1: Scheme showing how FPP is involved in the biosynthesis of many vital biological molecules. ....	85
Figure 2.2: Scheme showing the phosphorolysis and hydrolysis of the P-O-P linkage in inhibitor <b>1</b> .....	86
Figure 2.3: The structure of the transition state formed in the reaction catalyzed by FPPS on the left, and the structure of inhibitor <b>2</b> is shown on the right.....	87
Figure 2.4: The structures of inhibitors <b>3</b> and <b>4</b> .....	87
Figure 2.5: Structure of inhibitor <b>2</b> . ....	88
Figure 2.6: Literature-known synthetic route of amine <b>12</b> . <sup>118</sup> ....	88
Figure 2.7: First route towards inhibitor <b>2</b> . ....	90
Figure 2.8: Guanidinylation reagent (1, 3-bis (tert-butoxycarbonyl)-2-methyl-2-thiourea).....	91

Figure 2.9: New synthetic route for inhibitor <b>2</b> .	93
Figure 2.10: <sup>1</sup> H NMR spectrum of inhibitor <b>2</b> (D <sub>2</sub> O – Dioxane 1mM, 400 MHz).	94
Figure 2.11: <sup>31</sup> P NMR spectrum of inhibitor <b>2</b> (D <sub>2</sub> O, 162 MHz).	95
Figure 2.12: Structures of inhibitors <b>3</b> and <b>4</b> .	96
Figure 2.13: Deprotection of amine <b>12</b> to yield inhibitor <b>3</b> .	96
Figure 2.14: Synthetic route of inhibitor <b>4</b> .	97
Figure 2.15: A modified version of the continuous coupled assay for phosphate release for the reaction catalyzed by HFPPS.	100
Figure 2.16: A plot of initial velocity vs. GPP concentration for the reaction catalyzed by HFPPS. The kinetic parameters were determined by fitting the data to the Michaelis-Menten equation and are as follows: $k_{cat} = 0.57 \pm 0.01 \text{ s}^{-1}$ and $K_m = 4.9 \pm 0.5 \text{ }\mu\text{M}$ .	101
Figure 2.17: A, B and C are the IC <sub>50</sub> Curves of inhibitors <b>2</b> , <b>3</b> and <b>4</b> , respectively, against HFPPS.	103
Figure 2.18: IC <sub>50</sub> values for inhibitors <b>2</b> – <b>4</b> .	105
Figure 2.19: Structures of selected bisphosphonates and their IC <sub>50</sub> values studied by Oldfield and coworkers.	108
Figure 2.20: The structure of DMAPP is on the left. On the right is the structure of inhibitor <b>2</b> , showing the replaced two oxygens with two CH <sub>2</sub> groups in green.	109
Figure 2.21: A fluorinated version of inhibitor <b>2</b> .	110
Figure 3.1: Structures of squalene and dehydrosqualene.	120
Figure 3.2: The reactions catalyzed by squalene synthase (SQS) and bacterial dehydrosqualene synthase (DSQS), and the structures of staphyloxanthin and cholesterol.	122
Figure 3.3: Structure of Lapaquistat, a potent squalene synthase inhibitor	123

Figure 3.4: The reactions catalyzed by HSQS and DSQS to produce squalene and dehydrosqualene, respectively. (P denotes a phosphate group).....	125
Figure 3.5: Structure of the desired inhibitor mimicking the transition state of FPP dissociation. ....	126
Figure 3.6: Structure of inhibitors <b>26</b> , <b>36</b> and <b>34</b> .....	127
Figure 3.7: Synthesis of the thiourea compound <b>23</b> via coupling of amine <b>12</b> and N,N' diBoc-thiourea. ....	128
Figure 3.8: Guanidinylation reaction and failed final inhibitor deprotection. ....	129
Figure 3.9: Scheme showing side reactions encountered when using 30 equivalents of TMSBr in the deprotection of compound <b>25</b> . ....	130
Figure 3.10: Scheme showing side reactions encountered when using 50 equivalents of TMSBr and collidine in the deprotection of compound <b>25</b> .....	131
Figure 3.11: Structures of the unsaturated and saturated inhibitor <b>26</b> . ....	132
Figure 3.12: Hydrogenation of unsaturated amine <b>24</b> to form the saturated racemic amine <b>31</b> . ....	132
Figure 3.13: Successful synthetic route for inhibitor ( $\pm$ ) <b>26</b> . ....	133
Figure 3.14: Pathway A, an unsuccessful route towards inhibitor <b>34</b> . ....	135
Figure 3.15: Pathway B, unsuccessful route towards inhibitor <b>34</b> . ....	136
Figure 3.16: Protection of the amine functional group by reacting it with diBoc. ....	137
Figure 3.17: Pathway C, the synthesis of inhibitor <b>34</b> .....	137
Figure 3.18: Synthesis of inhibitor <b>36</b> . (this compound was synthesized by Taiya Adak).....	138
Figure 3.19: Continuous coupled assay for phosphate release in the reaction catalyzed by DSQS. The inset shows the chromophore.....	140

Figure 3.20: The reaction catalyzed by SQS. The inset outlines the first half of the enzymatic reaction.....	141
Figure 3.21: The reaction catalyzed by DSQS.....	142
Figure 3.22: A plot of initial velocity vs [FPP] for the reaction catalyzed by DSQS. Kinetic parameters were obtained by fitting the data to the Michaelis Menten equation and were found to be as follows: $k_{cat} = 0.39 \pm 0.01 \text{ s}^{-1}$ , $K_m = 25 \pm 5 \text{ }\mu\text{M}$ , and $k_{cat}/K_m = 16 \times 10^3 \text{ M}^{-1}\text{s}^{-1}$ .....	143
Figure 3.23: A scheme showing how inhibitors <b>26</b> and <b>36</b> mimic the proposed transition state. The bottom structure shows the neutral urea-containing inhibitor <b>34</b> as a negative control. ....	144
Figure 3.24: IC <sub>50</sub> determinations for the inhibition of the reaction catalyzed by HSQS ([FPP] = 50 $\mu\text{M}$ ). Graphs A, B and C show data for inhibitors <b>26</b> , <b>36</b> and <b>34</b> , respectively.....	145
Figure 3.25: IC <sub>50</sub> determinations for the inhibition of the reaction catalyzed by DSQS ([FPP] = 50 $\mu\text{M}$ ). Graphs A, B and C show data for inhibitors <b>26</b> , <b>36</b> and <b>34</b> , respectively.....	146
Figure 3.26: Plot of rate versus FPP concentration for the inhibition of the DSQS reaction with fitting to the Michaelis-Menten equation for competitive inhibition. A) Data for inhibitor <b>26</b> . B) Data for inhibitor <b>36</b> . C) Data for inhibitor <b>34</b> .....	148
Figure 3.27: Lineweaver-Burk plots for the inhibition of DSQS by inhibitors <b>26</b> , <b>36</b> , and <b>34</b> . The color codes for the above Lineweaver-Burk plots are as follows: A) Inhibition by inhibitor <b>26</b> at the following concentrations: light blue = 8.25 $\mu\text{M}$ , yellow = 3.3 $\mu\text{M}$ , grey = 1.6 $\mu\text{M}$ , orange = 0.8 $\mu\text{M}$ , dark blue = 0 $\mu\text{M}$ . B) Inhibition by inhibitor <b>36</b> at the following concentrations: green = 36 $\mu\text{M}$ , light blue = 18 $\mu\text{M}$ , yellow = 12 $\mu\text{M}$ , grey = 9 $\mu\text{M}$ , orange = 4.5 $\mu\text{M}$ , dark blue = 0 $\mu\text{M}$ . C) Inhibition by inhibitor <b>34</b> at the following concentrations: light blue = 8.25 $\mu\text{M}$ , yellow = 3.3 $\mu\text{M}$ , grey = 1.6 $\mu\text{M}$ , orange = 0.8 $\mu\text{M}$ , dark blue = 0 $\mu\text{M}$ . ....	149

Figure 3.28: Structures of inhibitors <b>37 – 40</b> , with their IC <sub>50</sub> values.....	155
Figure 3.29: The top box shows the structure and IC <sub>50</sub> value of inhibitor <b>40</b> . The bottom box shows the structures and IC <sub>50</sub> values for both inhibitors <b>26</b> and <b>36</b> from our current study. ....	156
Figure 3.30: Structures of inhibitors <b>41</b> and <b>42</b> , with their IC <sub>50</sub> values.....	157
Figure 3.31: The transition state for PSPP dissociation and structure of inhibitor <b>43</b> , with its IC <sub>50</sub> value.....	158
Figure 3.32: Structures of inhibitors <b>44 – 47</b> , with their IC <sub>50</sub> values.....	159
Figure 3.33: Structure of the tertiary cation intermediate formed in the reaction of isopentenyl diphosphate isomerase and inhibitor <b>48</b> .....	160
Figure 3.34: Structure of inhibitor <b>49</b> . ....	161
Figure 4.1: The reaction catalyzed by IDI. ....	171
Figure 4.2: The structures of inhibitor <b>48</b> and the carbocation intermediate formed in the IDI reaction.....	172
Figure 4.3: The three red boxes show the structures of inhibitors <b>2</b> , <b>3</b> and <b>4</b> , respectively. The blue box shows the structure of the carbocation intermediate formed in the IPP-catalyzed reaction.....	173
Figure 4.4: The continuous coupled assay for the reaction catalyzed by isopentenyl diphosphate isomerase (IDI). The blue inset shows the continuous coupled assay for the reaction catalyzed by 4-DMATS. ....	175
Figure 4.5: A plot of initial velocity vs. DMAPP concentration for the reaction catalyzed by 4-DMATS. The kinetic parameters were determined by fitting the data to the Michaelis-Menten equation and are as follows: $k_{cat} = 0.51 \pm 0.05 \text{ s}^{-1}$ and $K_m = 10.5 \pm 0.5 \text{ }\mu\text{M}$ .....	177

Figure 4.6: A plot of initial velocity vs. IPP concentration for the reaction catalyzed by IDI-1. The kinetic parameters were determined by fitting the data to the Michaelis-Menten equation and are as follows:  $k_{\text{cat}} = 0.88 \pm 0.08 \text{ s}^{-1}$  and  $K_m = 8.5 \pm 0.5 \text{ }\mu\text{M}$ . ..... 178

Figure 4.7: IC<sub>50</sub> curves for inhibitors **2** – **4** against IDI-1. A, B and C are data for inhibitors **2**, **3** and **4**, respectively. .... 180

Figure 4.8: Plot of rate versus IPP concentration for the inhibition of the IDI reaction with fitting to the Michaelis-Menten equation for competitive inhibition. A) Data for inhibitor **2**. B) Data for inhibitor **3**. C) Data for inhibitor **4**. .... 182

Figure: Figure 4.9: Lineweaver-Burk plots for the inhibition of IDI by inhibitors **2**, **3**, and **4**. The color codes for the above Lineweaver-Burk plots are as follows: A) Inhibition by inhibitor **2** at the following concentrations: dark blue = 1  $\mu\text{M}$ , yellow = 0.7  $\mu\text{M}$ , grey = 0.3  $\mu\text{M}$ , orange = 0.1  $\mu\text{M}$ , light blue = 0  $\mu\text{M}$ . B) Inhibition by inhibitor **3** at the following concentrations: dark blue = 16.5  $\mu\text{M}$ , yellow = 8.2  $\mu\text{M}$ , grey = 3.3  $\mu\text{M}$ , orange = 1.6  $\mu\text{M}$ , light blue = 0  $\mu\text{M}$ . C) Inhibition by inhibitor **4** at the following concentrations: green = 400  $\mu\text{M}$ , dark blue = 200  $\mu\text{M}$ , yellow = 100  $\mu\text{M}$ , grey = 60  $\mu\text{M}$ , orange = 30  $\mu\text{M}$ , light blue = 0  $\mu\text{M}$ . .... 183

Figure 4.10: Structures of inhibitors **2**, **3** and **4**. .... 184

Figure 4.11: Structures of inhibitor **49** and the tertiary carbocation intermediate formed in the reaction catalyzed by GGPPS. .... 187

Figure 4.12: Structures of the IPP carbocationic intermediate, inhibitor **2** and the proposed inhibitors **50** and **51**. .... 191

## List of Abbreviations and Symbols

$\epsilon$	molar absorptivity
$\epsilon_{360}$	extinction coefficient at 360 nm
$\lambda_{\max}$	absorption maximum
Ac	acetyl
AcOH	acetic acid
Ado	adenosine
ADP	adenosine diphosphate
ATP	adenosine triphosphate
Boc	tert-butyloxycarbonyl
Bn	benzyl
BSA	bovine serum albumin
D	deuterium ( $^2\text{H}$ )
Da	Dalton
DMAPP	dimethylallyl diphosphate
DMAT	dimethylallyltryptophan
DMATS	dimethylallyltryptophan synthase
DNA	deoxyribonucleic acid
DSQS	bacterial dehydrosqualene synthase from <i>Staphylococcus aureus</i>
<i>E. coli</i>	<i>Escherichia coli</i>
ESI-MS	electrospray ionization mass spectrometry
$\text{Et}_3\text{N}$	triethylamine
$\text{EtNH}_2$	ethylamine
$\text{Et}_2\text{O}$	diethyl ether
$\text{EtOAc}$	ethyl acetate
<i>fgaPT</i> <sub>2</sub>	gene of dimethylallyltryptophan synthase from <i>Aspergillus fumigatus</i>
FPP	farnesyl diphosphate
FPPS	farnesyl diphosphate synthase
Ftase	farnesyltransferase
GPP	geranyl diphosphate
GPPS	geranyl diphosphate synthase
GGtase	geranylgeranyl transferase
HPLC	high performance liquid chromatography
HSQS	human squalene synthase
iPrOH	isopropyl alcohol
IPP	isopentenyl diphosphate
IPTG	isopropyl 1-thio- $\beta$ -D-galactopyranoside
IDI	isopentenyl diphosphate
<i>J</i>	coupling constant (NMR); subscripts indicate coupling partners
$k_{\text{cat}}$	catalytic constant
$k_{\text{cat}}/K_{\text{m}}$	specificity constant; second-order rate constant
$K_{\text{I}}$	inhibition constant

kDa	kilodalton
KIE	kinetic isotope effect
$K_m$	Michaelis constant
LB	Luria-Bertani medium
$m/z$	mass to charge ratio (mass spectrometry)
M	molar
Me	methyl
MeOH	methanol
MESG	2-amino-6-mercapto-7-methylpurine ribonucleoside
MgSO <sub>4</sub>	magnesium sulfate
MHz	megahertz
MW	molecular weight
NaH	sodium hydride
NaHCO <sub>3</sub>	sodium bicarbonate
NaCl	sodium chloride
Na <sub>2</sub> CO <sub>3</sub>	sodium carbonate
NaOH	sodium hydroxide
NEt <sub>3</sub>	triethylamine
NiSO <sub>4</sub>	nickel sulfate
NMR	nuclear magnetic resonance
OD <sub>600</sub>	optical dispersion at 600 nm
Pi	inorganic phosphate
PNP	purine nucleoside phosphorylase
PPi	pyrophosphate
ppm	parts per million
PSY	phytoene synthase
PT	prenyltransferase
RT	room temperature
SDS-PAGE	sodium dodecyl sulfate polyacrylamide gel electrophoresis
TB	Terrific Broth
T	Tritium ( <sup>3</sup> H)
TEAB	triethylammonium bicarbonate
TFA	trifluoroacetic acid
THF	tetrahydrofuran
TLC	thin layer chromatography
TMSBr	trimethylsilyl bromide
Tris	tris(hydroxymethyl)aminomethane
UV	ultraviolet
UV-Vis	ultraviolet-visible
$v$	initial reaction velocity (rate)
WT	wild type

## Common Amino Acid Abbreviations

A	Ala	alanine
C	Cys	cysteine
D	Asp	aspartate
E	Glu	glutamate
F	Phe	phenylalanine
G	Gly	glycine
H	His	histidine
I	Ile	isoleucine
K	Lys	lysine
L	Leu	leucine
M	Met	methionine
N	Asn	asparagine
P	Pro	proline
Q	Gln	glutamine
R	Arg	arginine
S	Ser	serine
T	Thr	threonine
V	Val	valine
W	Trp	tryptophan
Y	Tyr	tyrosine

## **Acknowledgements**

I would like to extend my sincere gratitude to my supervisor, Professor Martin Tanner for his wonderful and great support throughout my entire PhD from day one. It would have been definitely different and harder without his guidance. So, "Thank you" so much.

I would also like to thank my supervisory committee; Professor Stephen Withers for his great support and for being a wonderful listener, and Professor Glenn Sammis for his guidance and advices. Special Thank you to Professor Marco Ciufolini for being very supportive and a wonderful professor friend, and to Professor Mike Wolf for being such a great graduate advisor for me.

I would like to thank the members of the Tanner lab; I will really miss them. I also offer my enduring gratitude to the faculty, staff and my fellow students at UBC, who have inspired me to continue my work in this field.

## **Dedication**

To whom I can't live without, I take my energy from, who taught me how to be strong, how to fight hard, how not to give up and never to lose a battle without trying to win, not to fear fail since every fail is a new start for a new battle. To my whole world, My queen, My beloved Mother (Solly). You have always supported me, throughout my whole life, you never let me down. To my beloved siblings, Dr. Nourhan, Esraa, Ahmed and Menna. To my beautiful nephew Joey (Jojo). To my cousin, Sam Cheir, who helped me to start.

# Chapter 1: Introduction

## 1.1 Terpenes and Terpenoids

### 1.1.1 A Brief History and Classification

Terpenes encompass an expansive and assorted class of unsaturated hydrocarbons produced biosynthetically by all organisms from the five carbon "isoprene sub-unit".<sup>1</sup> In Nature, terpenes play a vital role in various biological activities. The pleasant taste in many of our food items is owed to the presence of biosynthetic terpenes.<sup>1-4</sup> Owing to their strong odor, terpenes are employed by plants to deter herbivores directly or, more subtly, attract predators or parasites that may prey upon herbivores.<sup>1</sup> Furthermore, numerous insects accumulate and/or modify the terpenes that they receive in their diet and use them to produce hormones and pheromones.<sup>5-7</sup> Pheromones are used by insects and several other organisms as signaling molecules to help them communicate with other individuals of their own kind and to mark their territory and/or resources. A wide array of structurally varied natural products is generated from acyclic terpenes that undergo oxidations, cyclizations, and rearrangements.<sup>1</sup> The broad diversity of these "terpenoids" (oxygen containing derivatives of terpenes) is reflected in the wide range of biological properties: ranging from anti-cancer and anti-malarial activities to tumor promotion and ion-channel binding.<sup>1-4</sup>

While active molecules in their own right, terpenoids serve other biological roles as precursors to sterols and steroids or as a source of isoprene moieties for the isoprenylation of proteins, an important post-translational modification (PTM) that enables protein localization to cellular membranes.<sup>1,8</sup> There is tremendous diversity in the synthesis and derivatization of terpenoids, yielding a myriad array of molecules with varied biologically relevant roles.<sup>1</sup>

Terpenoids are biosynthesized from branched five-carbon isoprene substrates and they can be distinguished by the number of isoprene units presented in the molecule: hemi- (C5), mono- (C10), sesqui- (C15), di- (C20), sester- (C25), and tri-terpenoids (C30) (Figure 1.1).<sup>2-4,9</sup> Essential oils and floral scents are mainly made from monoterpenes. Citronellol, an interesting acyclic monoterpene found in citronella oils, has inhibitory properties against *Mycobacterium tuberculosis* and it has long been recognized as an insect repellent.<sup>10</sup> Perillyl alcohol, another notable monoterpene, is used as a chemopreventive agent that helps to slow down or prevent the progress of liver cancer in rats.<sup>11</sup>

The sesquiterpene lactone artemisinin (Figure 1.1) has antimalarial properties and is commonly used around the world to treat both drug-resistant and cerebral malaria.<sup>12</sup> Bisabolol oxide A, another sesquiterpene, is a common herbal remedy used to treat skin inflammation – it is also an antibacterial and an antifungal agent.<sup>13</sup> Paclitaxel (Taxol®) is an example of a cyclic diterpene which is used to treat lung, ovarian, and breast cancer.<sup>3</sup>

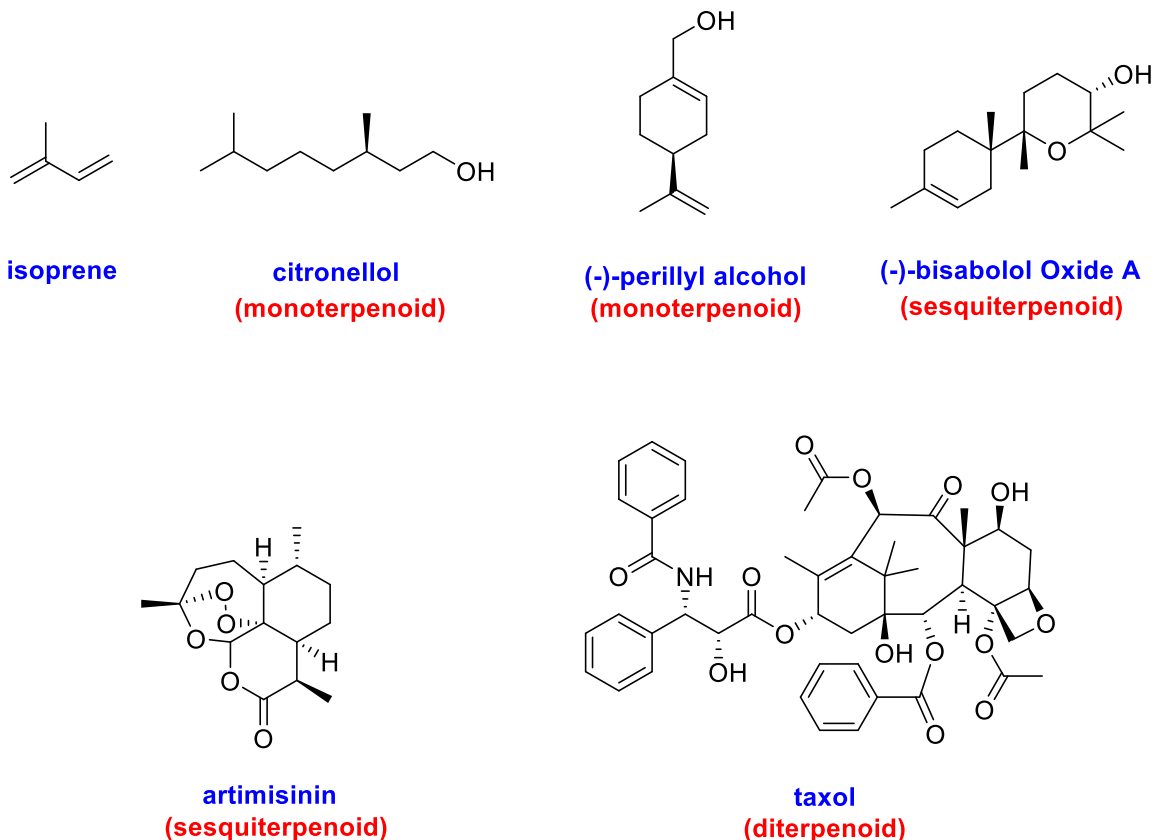


**Figure 1.1: Examples of mono-, sesqui- and di-terpenoids found in nature, and the structure of isoprene**

### 1.1.2 Terpene Cyclases

The strategy that Nature employs to produce terpenes/terpenoids involves the chemistry of allylic diphosphates. <sup>3</sup> Five-carbon allylic diphosphates are sequentially elongated to form longer chain allylic diphosphates, each of which retains a terminal pyrophosphate moiety (Figure 1.2). Dimethylallyl diphosphate (DMAPP) and isopentenyl diphosphate (IPP) are the building blocks from which all isoprenoid substrates are synthesized. <sup>14,15</sup> A group of enzymes, known as

prenyltransferases (PTs), use DMAPP and IPP to catalyze the synthesis of the linear prenyl diphosphates that eventually serve as the substrates in the subsequent synthesis of numerous terpenoids.<sup>3</sup>

IPP is first added to DMAPP in a head-to-tail manner to generate geranyl diphosphate (GPP, 10 carbons). Subsequent additions of IPP give farnesyl diphosphate (FPP, 15 carbons), and geranylgeranyl diphosphate (GGPP, 20 carbons) (Figure 1.2).<sup>16</sup>

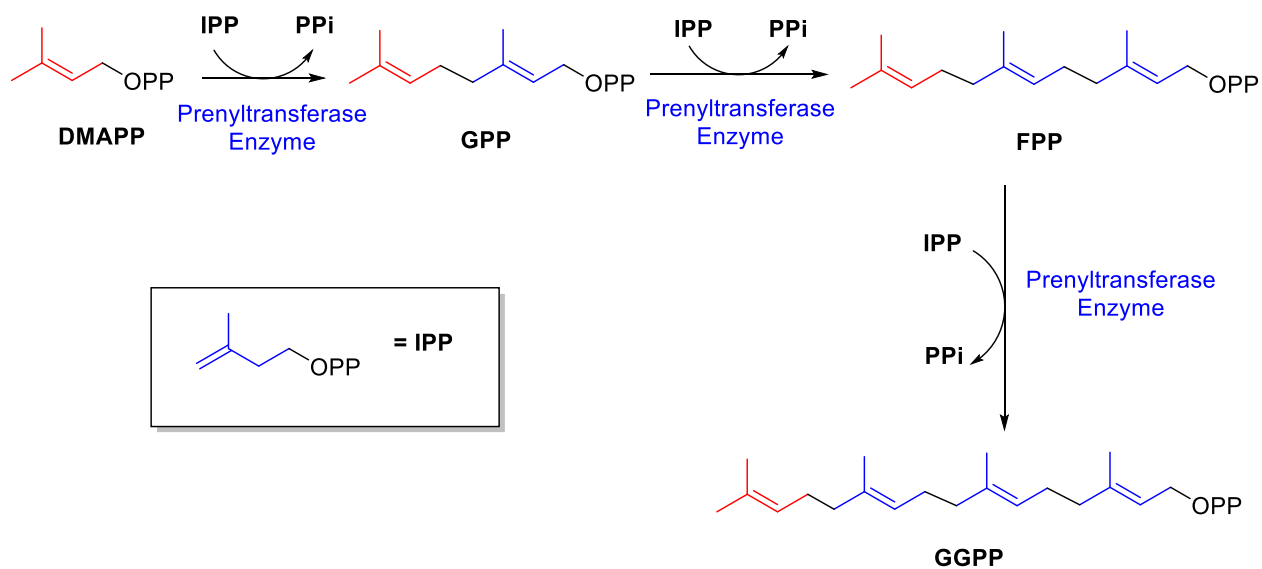


**Figure 1.2 Structures of the substrates of terpene cyclases. (P denotes a phosphate group)**

Terpene cyclases, also referred to as terpene synthases, are enzymes that catalyze unique multistep cyclization reactions to produce chiral carbocyclic structures (Figure 1.3).<sup>1,3,17,18</sup> The cyclase first binds the allylic diphosphate substrate and promotes the dissociation of the pyrophosphate moiety. This heterolytic dissociation results in the formation of an allylic carbocation which may undergo extensive structural rearrangements before it is quenched. Interestingly, terpene cyclases control the precise structural rearrangements and cyclizations, as shown in (Figure 1.3), in order to produce a specific terpene.<sup>3</sup> For instance, geranyl diphosphate, which is a linear prenyl diphosphate, can be converted by monoterpene synthases to myrcene, 4*S*-limonene, and 4*S*-β-phellandrene (Figure 1.3).<sup>3,13,19</sup>

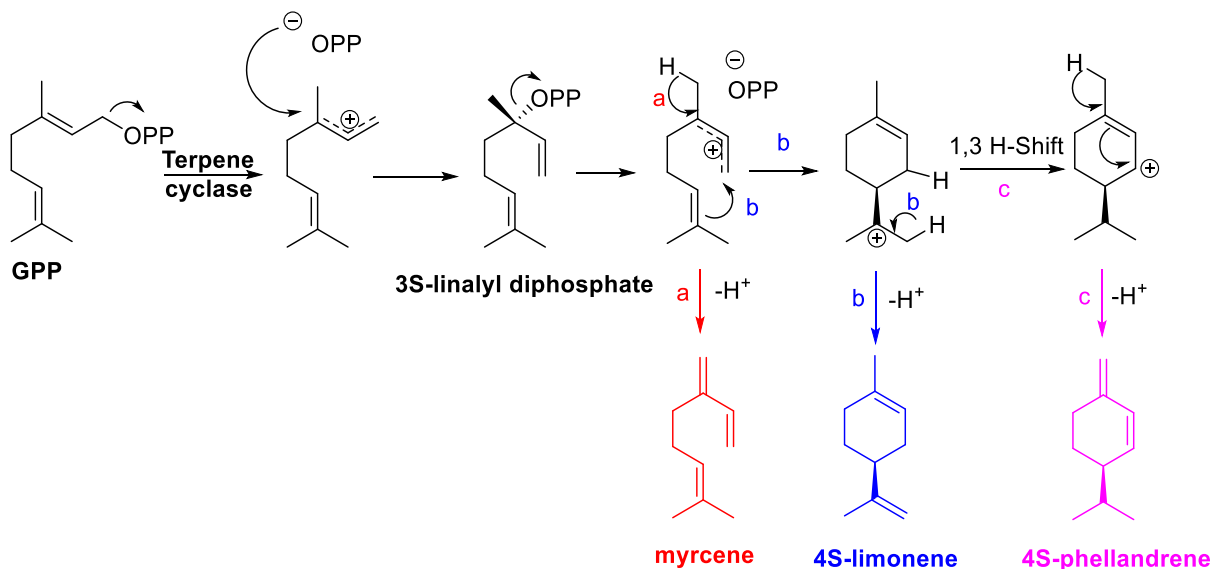


**Figure 1.3: Examples of the conversion of geranyl diphosphate to myrcene, limonene, and β-phellandrene by terpene cyclases.**

## 1.2 Mevalonate Pathway

As seen in section 1.1.2, isoprenoids are biosynthesized from the two common C5 precursors, isopentenyl diphosphate (IPP) and its corresponding isomer dimethylallyl diphosphate (DMAPP). These C5 precursors are generated via two independent pathways: (i) the classical mevalonate (MVA) pathway (Figure 1.4) or (ii) the 1- deoxy-D-xylulose 5-phosphate/2-C-methyl-D-erythritol 4-phosphate (DOXP/MEP) pathway. Archaeobacteria, fungi and animals (including humans) are restricted to the classical MVA pathway; while most bacteria can only employ the MEP pathway.<sup>20</sup> In contrast, plants and algae may utilize either pathway, depending on the species. The mevalonate (MVA) pathway, also known as the isoprenoid pathway or the HMG-CoA reductase pathway, is a pivotal pathway in humans that plays a vital role in many essential cellular processes.<sup>20</sup> It is involved in the synthesis of sterol and non-sterol isoprenoids, such as cholesterol and isopentenyl tRNA, respectively. Owing to its involvement in the biosynthesis of cholesterol and its implications in cardiovascular diseases, the mevalonate pathway has been extensively studied in recent years.<sup>21</sup> In addition, numerous studies have suggested that the inhibition of the production of the non-sterol isoprenoids might have a great impact on human pathology.<sup>20-25</sup> The MVA pathway utilizes acetyl CoA as it is a carbon source and can be subdivided into two parts: the “upper” mevalonate pathway and the “lower” mevalonate pathway (Figure 1.4). The upper mevalonate pathway is the same throughout all the eukaryotes, archaea, and select strains of bacteria and is comprised of three steps to give mevalonate. In contrast, the lower mevalonate pathway is different amongst eukaryotes, archaea, and bacteria and is comprised of four to five steps.<sup>20</sup>



### 1.3 Protein Prenylation

Proteins play vital roles in the structure and function of cells - and post-translational modification performed on them leads to an increase in their functional diversity.<sup>26</sup> Post-translational modification (PTM) is a biochemical process in which amino-acid residues in a protein are covalently modified after the protein has been biosynthesized.<sup>27-29</sup> Another significant role of the isoprene diphosphates is their involvement in protein prenylation, which is a post-translational modification involving either farnesylation or geranylgeranylation (Figure 1.5).<sup>26</sup> This modification is considered crucial for the function of a range of proteins, since it controls the localization and activity of the prenylated protein within the appropriate cellular membrane. In addition, prenylation permits certain proteins to function properly and to interact with other proteins at a sub-cellular level.<sup>27-30</sup>

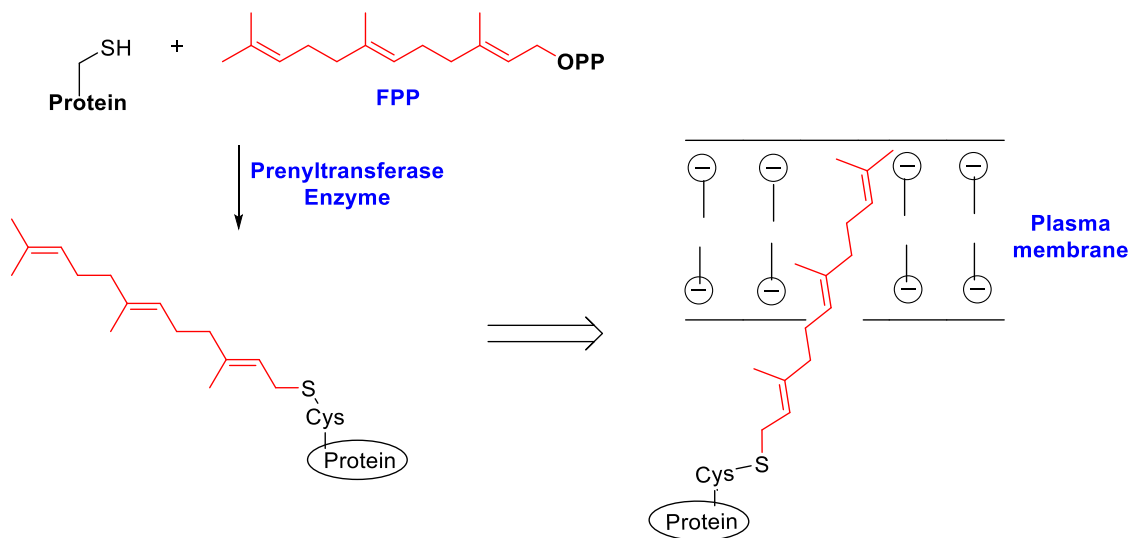


**Figure 1.5: Scheme showing protein farnesylation and the localization of prenylated proteins within a cellular membrane**

Protein prenylation is an important post-translation modification process in a vast array of proteins. For instance, it is crucial to the function of members of the Ras family that play a vital role in cell signaling.<sup>31,32</sup> The Ras family is expressed in all animal cell lineages and organs. Moreover, all members of the Ras family are classified as small GTPases and are involved in cellular signal transduction. When Ras proteins are activated by incoming signals, they subsequently signal other proteins; which induce genes responsible for cell growth, differentiation, and survival. It is well known that, mutations in Ras genes can lead to an uncontrollable growth of cells; which in turn leads to the transformation of these normal cells into malignant ones, a process named oncogenesis.<sup>26,33</sup>

The post-translational farnesylation of Ras proteins was found to be critical for healthy cellular function. The presence of overexpressed farnesylated Ras proteins in more than 30% of human cancer has led to extensive research on mammalian protein prenylation; especially protein farnesylation.<sup>34</sup> Interestingly, it was found that unfarnesylated mutant Ras proteins do not attach to cell membranes, thus cannot stimulate the aforementioned oncogenic transformation.<sup>23,26-28</sup> Consequently, farnesyltransferases (Ftases) were considered as promising targets for cancer therapy. It is anticipated that by “targeting” the farnesylation of Ras proteins (through perhaps the inhibition of farnesyltransferases), the function of oncogenic Ras proteins may be disrupted.

<sup>26,33</sup>

## 1.4 The Prenyltransferase Family of Enzymes

Prenyltransferases (PTs) are enzymes that catalyze the prenylation process, which is the transfer of an isoprenyl moiety to an acceptor molecule and results in the formation of C-C, C-S, C-O or C-N bonds (Figure 1.6). In a prenyltransferase reaction, an electron-rich nucleophile serves as a "prenyl acceptor", and gets alkylated by an isoprenyl diphosphate forming a prenylated compound and pyrophosphate (PPi) as products. <sup>26</sup>

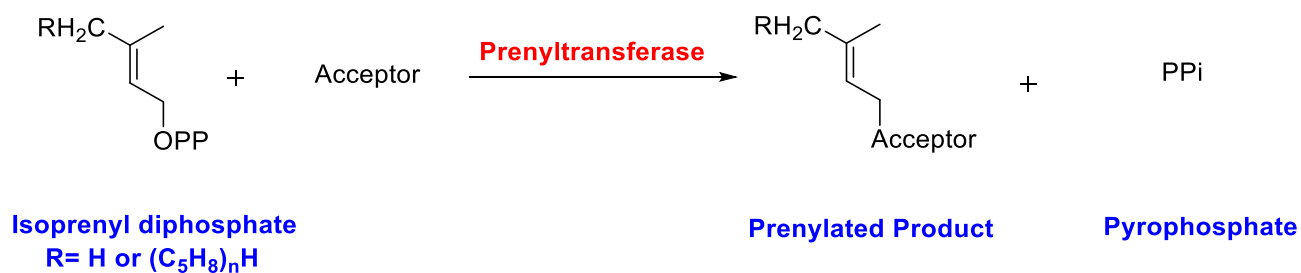


**Figure 1.6: Prenylation catalyzed by prenyltransferase**

Most prenyltransferases (PTs) can be categorized into three main groups based on the type of reaction they catalyze <sup>26</sup>:

- Isoprenyl diphosphate synthases: synthesis of an isoprenyl diphosphate
- Protein prenyltransferases: prenylation of a protein
- Aromatic prenyltransferases: prenylation of an aromatic substrate

## 1.4.1 Isoprenyl Diphosphate Synthases (Metal Ion-Dependent Prenyltransferases): Farnesyl Diphosphate Synthase (FPPS)

### 1.4.1.1 Introduction

Isoprenyl diphosphate synthases (IPPSs) constitute the first family of prenyltransferases (PTs). These enzymes catalyze the chain elongation reactions of allylic diphosphates by employing a vast array of isoprenyl diphosphates as electrophiles, thus producing a variety of linear allylic diphosphates with well-defined chain lengths (Figure 1.7).<sup>36-38</sup>

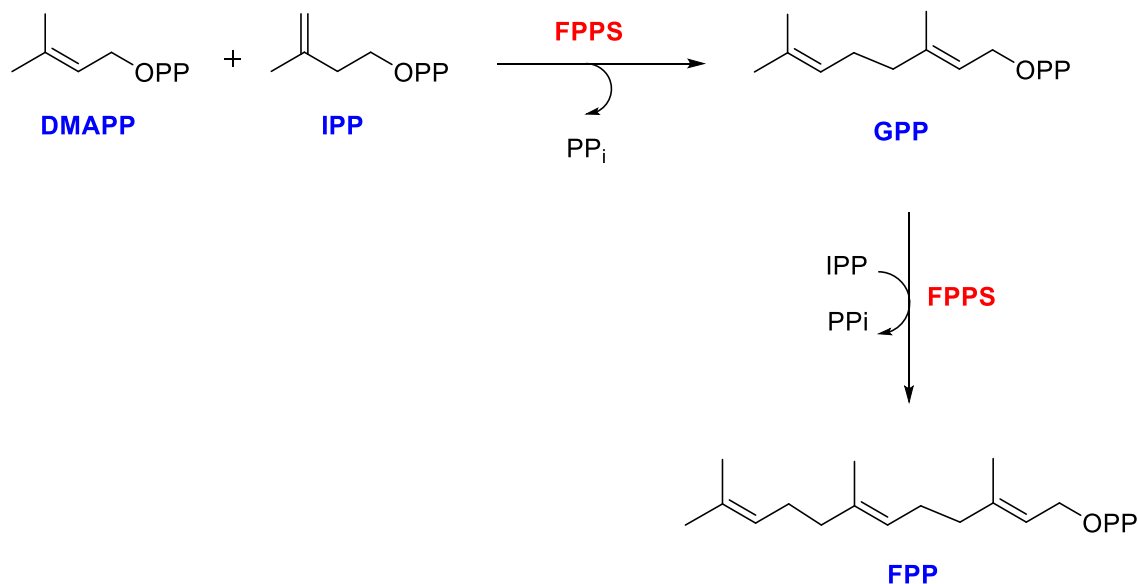


**Figure 1.7: The overall reaction catalyzed by farnesyl diphosphate synthase (FPPS)**

The IPPS family can be further subdivided into *trans*- and *cis*-isoprenyl diphosphate synthases, based on the stereochemistry of the newly formed double bonds in their end products. Notably, all members of this family are believed to have evolved from a common ancestor, since they all show amino acid sequence homology, in addition to containing two aspartate-rich DDxxD motifs.<sup>39</sup> The *trans* class of isoprenyl diphosphate synthases have been extensively studied over the past few decades, their basic catalytic and chain length determination mechanisms have been identified by site directed mutagenesis in conjunction with X-ray crystallography data. Contrarily, there is much less known about the *cis* class. Since the focus of this thesis is on the *trans* family, all further discussion will be focused on this class. *Trans*-farnesyl diphosphate synthase (FPPS), found in mammals, plants and bacteria, is involved in the biosynthesis of a great array of important terpenes such as sterols (the major structural components of eukaryotic membranes), polyprenyl pyrophosphates (pivotal membrane-soluble carriers of sugars), and carotenes (photoreceptors in the visual and photosynthetic systems).

26,39,40

#### 1.4.1.2 Mechanistic Studies

The Porter and Popjak research groups were the first groups to study and purify farnesyl diphosphate synthase enzyme in the 1960's.<sup>4,39</sup> It was proposed that FPPS catalyzes the successive transfer of IPP onto allylic diphosphates with the necessary assistance of a divalent metal ion - either Mg<sup>2+</sup> or Mn<sup>2+</sup>.<sup>39</sup> The metal ions are bound to the enzyme active site by several chelating aspartate residues in the DDxxD motifs. These metal ions act as Lewis acids and facilitate the binding and dissociation of the diphosphate substrates during catalytic turnover.<sup>4,39</sup>

Cornforth and Popjak have investigated the stereochemistry of the *trans*-farnesyl diphosphate synthase. They prepared the following compounds and used them as substrates for the enzyme: (S)-[1-<sup>3</sup>H<sub>1</sub>]-DMAPP, *trans*-[4-<sup>3</sup>H<sub>1</sub>]-IPP and (R)-[2-<sup>3</sup>H<sub>1</sub>]-IPP (Figure 1.8). They demonstrated that a stereochemical inversion occurred at the C-1 position of the starting material when using the tritiated (S)-[1-<sup>3</sup>H<sub>1</sub>]-DMAPP. When they used *trans*-[4-<sup>3</sup>H<sub>1</sub>]-IPP, they found that the newly formed bond was generated by addition to the *Si* face of the IPP alkene, since the enzymatic reaction only produces products with an (S)-configuration. Finally, when using tritiated (R)-[2-<sup>3</sup>H<sub>1</sub>]-IPP, they showed that the tritium was always lost to the solvent during generation of the new *trans* double bond (Figure 1.8).<sup>25,41</sup>

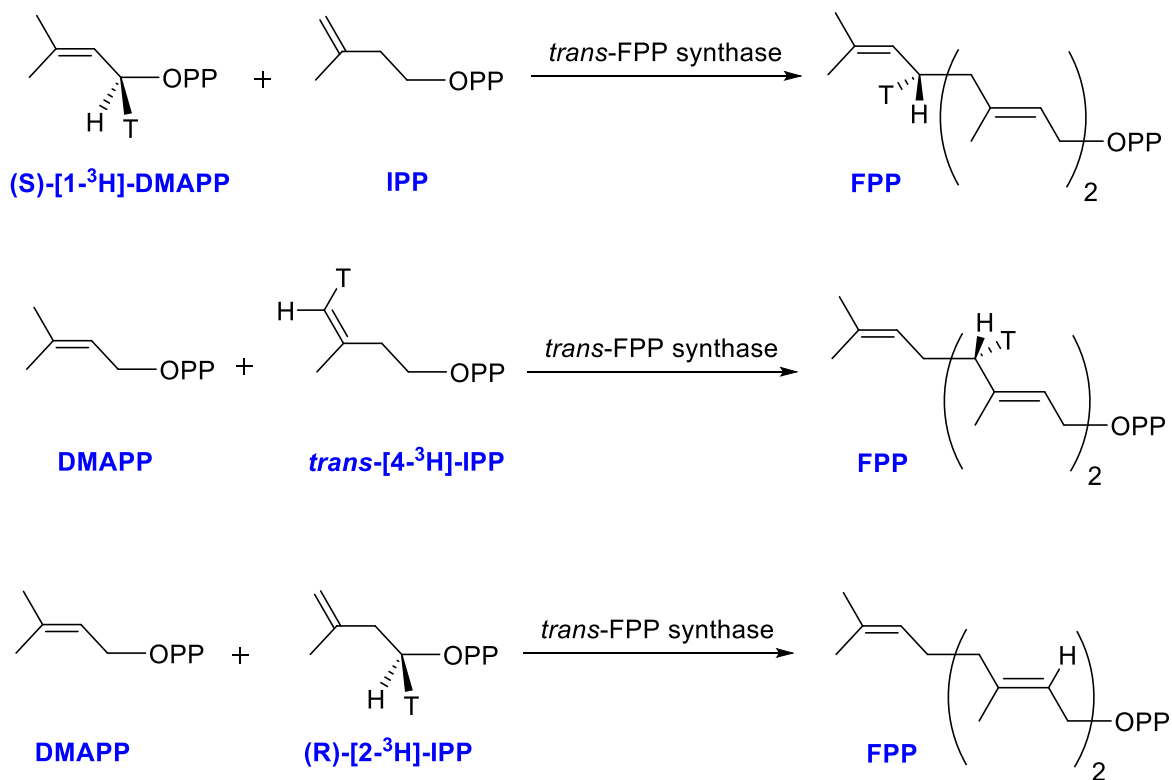


**Figure 1.8: Stereochemical investigation of the *trans*-farnesyl diphosphate synthase, using tritiated substrates.**

These observations led Cornforth and Popjak to propose a  $S_N2$  mechanism for the *trans*-farnesyl diphosphate synthase reaction (Figure 1.9). In this mechanism, IPP is attacked by an unknown nucleophile (X group) at the C-3 position, which in turn promotes a subsequent nucleophilic attack of the C-4 of IPP onto the C-1 of DMAPP (or GPP), thus displacing the pyrophosphate group, and generating an enzyme-linked intermediate. This is followed by a *trans* elimination of the X group and the pro (*R*) proton at the C-2 position in the intermediate, generating the product.<sup>25,39,41</sup>

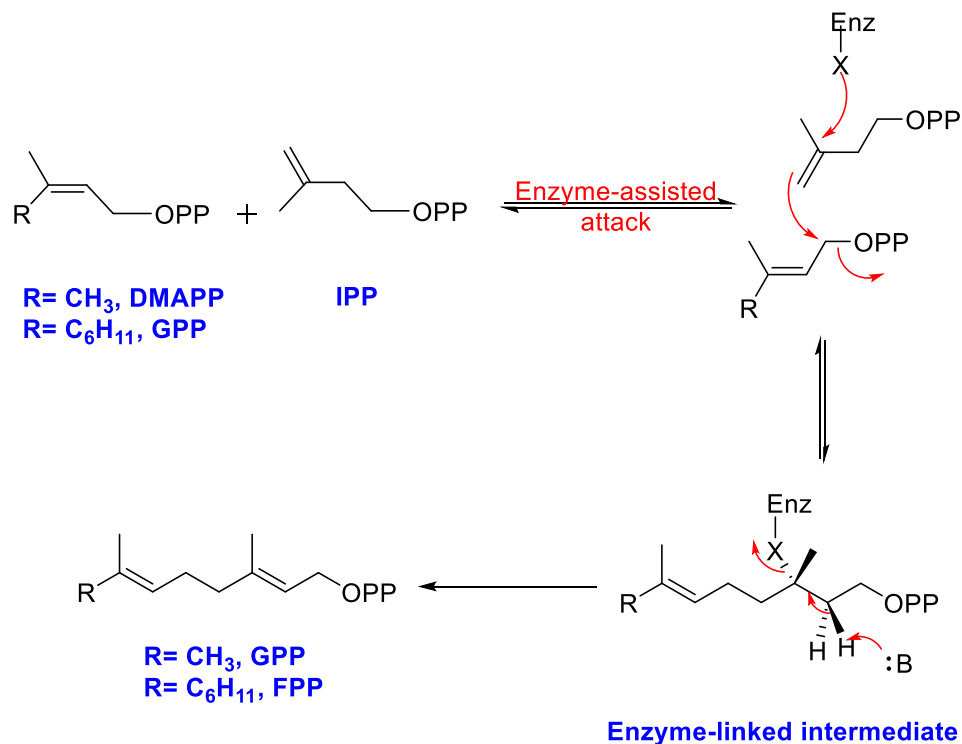


**Figure 1.9:  $\text{S}_{\text{N}}2$  mechanism for FPPS proposed by Cornforth and Popjak.**

Poulter disagreed with the aforementioned proposal and argued that these stereochemical studies were not sufficient to support the  $\text{S}_{\text{N}}2$  mechanism. Since enzymatic reactions are stereoselective regardless of the mechanism, and both  $\text{S}_{\text{N}}1$  and  $\text{S}_{\text{N}}2$  mechanisms have the potential to cause a stereochemical inversion at the C-1 position of DMAPP based on how the substrates are held at specific positions in the active site of the enzyme.<sup>4,42</sup>

Poulter then suggested an  $S_N1$  mechanism (also denoted as an "ionization-condensation-elimination" mechanism) for the reactions catalyzed by farnesyl diphosphate synthase (FPPS). The first step of catalysis involves a dissociation of the pyrophosphate moiety from DMAPP/GPP to produce an allylic carbocation. Thereafter, there is a nucleophilic attack onto the allylic carbocation by the IPP alkene, which produces a tertiary carbocation. Finally, after a deprotonation step, GPP/FPP is formed (Figure 1.10).<sup>4</sup>

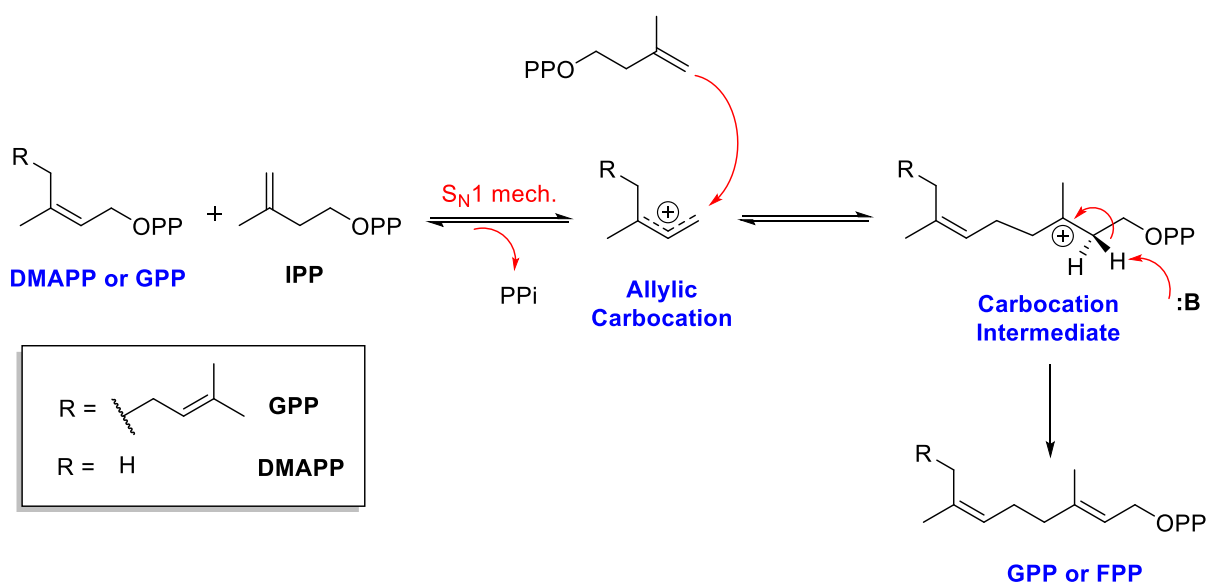


**Figure 1.10: Proposed  $S_N1$  mechanism for FPPS**

Poulter and his coworkers conducted further studies to verify their suggested  $S_N1$  mechanism for *trans*-farnesyl diphosphate synthase.<sup>4,43,44</sup> They prepared a series of fluorinated compounds: (E) and (Z) trifluoromethyl analogues of DMAPP ((E)-CF<sub>3</sub>-DMAPP and (Z)-CF<sub>3</sub>-DMAPP) and (E) and (Z) trifluoromethyl-2-butenyl mesylates ((E)-CF<sub>3</sub>-DMA-Ms and (Z)-CF<sub>3</sub>-

DMA-Ms) (Figure 1.11). The latter two compounds were used in non-enzymatic solvolysis studies. It should be noted that the allylic cations formed from these DMAPP analogues are expected to be higher in energy than the dimethylallyl cations, since all the analogues contain the strongly electron-withdrawing group CF<sub>3</sub> (substituent constant of  $\sigma^+ = 0.612$ ). This should destabilize any forming carbocation and dramatically reduce its rate of formation. On the other hand, the CF<sub>3</sub> group was known for enhancing the rate of S<sub>N</sub>2 nucleophilic substitution of chloride by iodide in the (E)-2-butenyl systems.<sup>4,43</sup>

Poulter and his coworkers predicted that the rate of the enzymatic reaction would be enhanced if the S<sub>N</sub>2 mechanism was employed, and reduced in the S<sub>N</sub>1 mechanism. The fact that fluorination could also slow down the rate in an ‘exploded’- S<sub>N</sub>2 mechanism, made Poulter’s prediction somewhat controversial.<sup>4,43</sup>

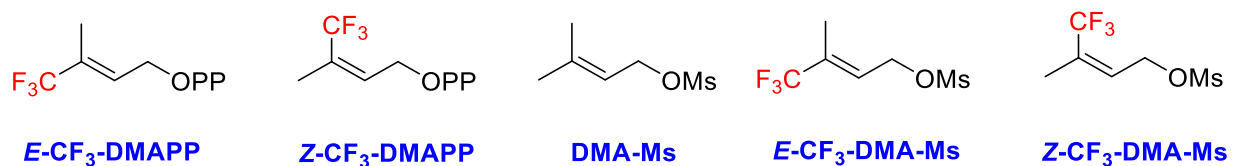


**Figure 1.11: The structures of trifluoromethyl dimethylallyl diphosphate and dimethylallyl methanesulfonate analogues.**

The authors measured the rate of the non-enzymatic solvolysis reactions of the fluorinated mesylates (presumably pure  $S_N1$  reactions), as well as the enzymatic reactions of the fluorinated DMAPP analogues. In both cases, the reaction rates were markedly lower than those with the corresponding non-fluorinated compounds as expected for reactions that proceed via carbocationic intermediates/transition states. The relative reaction rates ( $k^{rel}$ ) between fluorinated and non-fluorinated compounds were used to assess the magnitude of the effects of fluorination.

The relative reaction rates ( $k^{rel}$ ) for the solvolysis of the (*E*)- $CF_3$ -DMA-Ms and (*Z*)- $CF_3$ -DMA-Ms compounds were found to be similar to that for the enzymatic reaction of the (*E*)- $CF_3$ -DMAPP and (*Z*)- $CF_3$ -DMAPP substrates. The similarity between the  $k^{rel}$  values for the enzymatic and non-enzymatic solvolysis reactions provides a strong support to the  $S_N1$  pathway, in which an allylic carbocation is generated during catalysis.<sup>4,43</sup> Poulter and his coworkers prepared also a series of fluorinated GPP analogues and tested them: 2-fluorogeranyl diphosphate (2-F-GPP) and 2-fluorogeranyl methanesulfonate (Figure 1.12).<sup>4</sup>

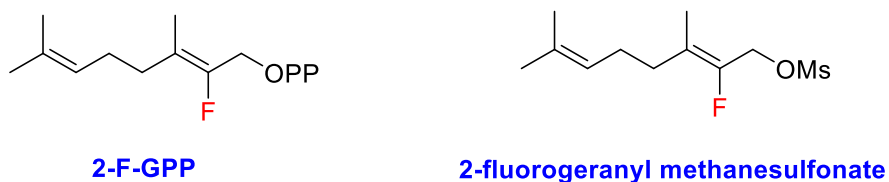


**Figure 1.12: The structures of fluorinated geranyl diphosphate analogue and the corresponding fluorinated methanesulfonate analogue.**

A rate depression by a factor of  $8.4 \times 10^{-4}$  was observed in the enzymatic reaction utilizing the fluorinated analogue, 2-F-GPP, when compared to GPP itself. This was similar to the depression factor ( $4.4 \times 10^{-3}$ ) value observed in the non-enzymatic  $S_N1$  solvolysis reaction of 2-fluoromethyl methanesulfonate when compared to the corresponding non-fluorinated compounds. Moreover, the  $K_m$  values for 2-F-GPP analogue and GPP substrate were found to be very similar,  $K_m = 1.1 \mu\text{M}$  and  $0.8 \mu\text{M}$ , respectively. These results provide further evidence for the involvement of a  $S_N1$  mechanism.<sup>4,43</sup>

Poulter and his coworkers conducted more experiments to further investigate the mechanism by preparing another series of C-3 fluorinated GPP analogues, 3- $\text{CH}_2\text{F}$ -GPP, 3- $\text{CHF}_2$ -GPP and 3- $\text{CF}_3$ -GPP, and a series of C-3 fluorinated geranyl methanesulfonates analogues, 3- $\text{CH}_2\text{F}$ -G-Ms, 3 $\text{CHF}_2$ -G-Ms and 3- $\text{CF}_3$ -G-Ms (Figure 1.13). Interestingly, they found similarities between the  $k^{\text{rel}}$  values of the first order solvolysis reactions of the methanesulfonates and the  $k^{\text{rel}}$  values of the enzymatic reactions of the fluorinated GPP analogues.<sup>4,43</sup> Consequently, they concluded that *trans*-farnesyl diphosphate synthase employs a  $S_N1$  dissociation mechanism, which involves the formation of an allylic carbocation during catalysis.

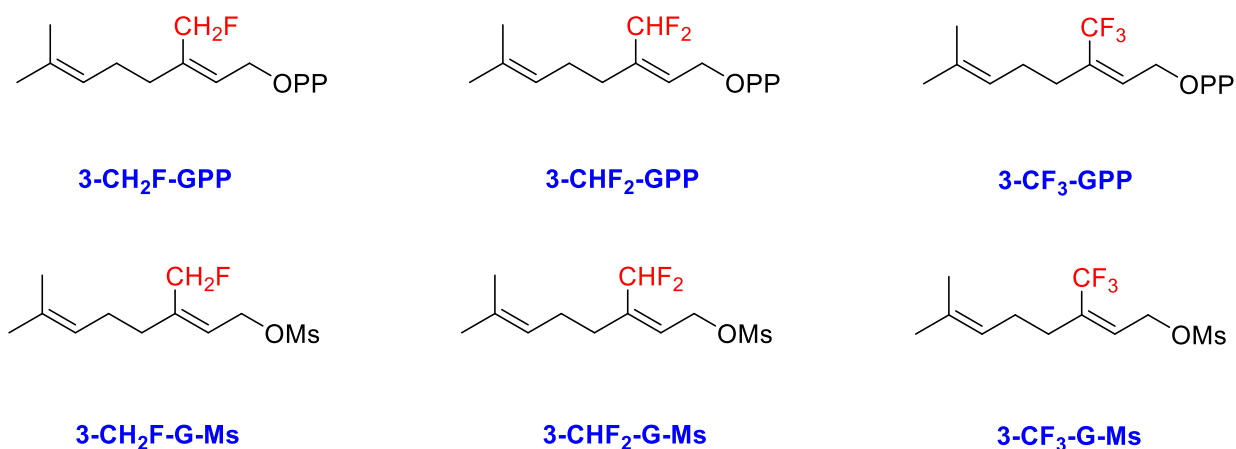


**Figure 1.13: The structures of fluorinated geranyl diphosphate analogues and fluorinated methanesulfonate analogues.**

### 1.4.1.3 Structural Studies

The Poulter group were the first to reveal the crystal structure of the avian *trans*-farnesyl diphosphate synthase with a resolution of 2.6 Å. Avian FPP synthase was the first prenyltransferase enzyme to be analysed by X-ray crystallography (Figure 1.14A). The X-ray structure revealed that it is dimeric and has 13  $\alpha$ -helices; 10 of which form a central “cavity” to surround the active site of the enzyme. In addition, the two oppositely located aspartate-rich motifs (DDxxD) on walls of this cavity define the substrate binding pockets for IPP and DMAPP/GPP, and chelate to the Mg<sup>2+</sup> cations that bind to the diphosphate moieties of the substrates to aid in the ionization step during catalysis (Figure 1.14B).<sup>44</sup> Site directed mutagenesis has revealed the essential role of aspartate residues in the DDxxD motifs for enzyme activity, since mutations of Asp to Ala have resulted in rate depression by 5 – 7 orders of magnitude.<sup>16,45</sup>

It is clearly revealed from the structure of the FPPS enzyme complexed with GPP and IPP that GPP binds to the DDxxD motif closer to the N-terminus, while IPP binds to the second such motif closer to the C-terminus. The hydrocarbon tail of the final product resides in a large hydrophobic pocket.<sup>44</sup> It should be noted that the X-ray structure of FPPS revealed the vital role that the aromatic residue Phe-112 (which is located 12 Å from the GPP binding DDxxD motif) plays in determining the definitive length of the hydrocarbon chain in the final product (Figure 1.14B). Further chain extensions would cause severe steric interactions with this residue, and therefore the reaction ends at FPP formation. Moreover, site directed mutagenesis was used to show that the size of this hydrophobic pocket can be altered to accommodate different sizes of isoprene units. Replacing Phe-112 with smaller amino acids such as alanine and serine allowed for the formation of C20 (geranylgeranyl diphosphate, GPP) and C25 (geranyl farnesyl diphosphate, GFP), respectively.<sup>16</sup>

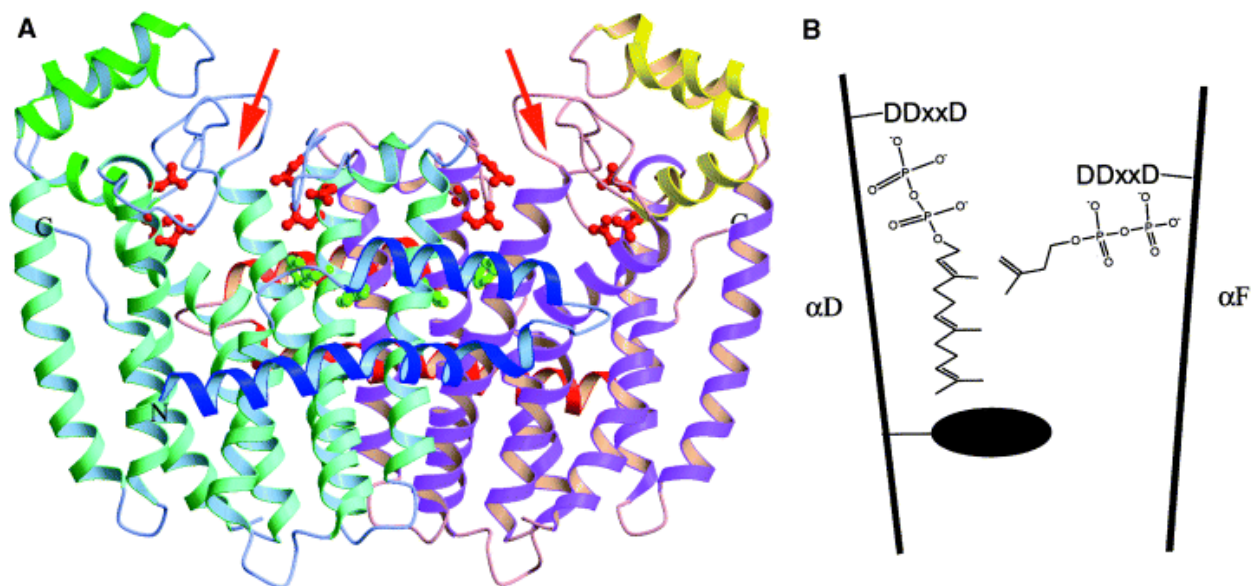


**Figure 1.14: (A) Crystal structure of avian *trans*-FPPS is shown using a ribbon diagram, orange arrows refer to the active sites. B) Graphical representation shows the enzyme active site with FPP and IPP bound, the two DDxxD motifs, and the black circle represents Phe112. This figure is obtained from the crystallographic report on the enzyme.<sup>26</sup>**

Farnesyl diphosphate (FPP) is an essential metabolite for several important biological processes and it plays a vital role as a precursor in the biosynthesis of several classes of crucial metabolites, including sterols and dolichols.<sup>14,46,47</sup> Furthermore, FPP is used by farnesyltransferase (FTase) as a substrate to prenylate proteins that are involved in many crucial biological processes. Due to the importance of farnesyl diphosphate to all organisms, it has become a vital target for drug design. This will be discussed further at the end of this chapter and in chapter two.<sup>26</sup>

## 1.4.2 Protein Prenyltransferases: Protein Farnesyltransferase (Ftase)

### 1.4.2.1 Introduction

As mentioned previously, prenyltransferases (PTs) can be categorized into three main groups based on the reaction they catalyze; protein prenyltransferase enzymes constitute the second family of PTs. This family of enzymes consists of three different protein prenyltransferases in humans.<sup>32</sup> The first two are farnesyltransferase (Ftase) and geranylgeranyltransferase 1 (GGTase 1), both of which recognize the same motif (the CaaX motif) around the cysteine in their substrate and are known as CaaX prenyltransferases. The CaaX motif consists of two aliphatic residues (denoted by the two a's) and an 'X' residue: either methionine, serine, or glutamine depending on the nature of the prenyltransferase enzyme.<sup>34</sup> It is anticipated that almost 2% of mammalian proteins are farnesylated or geranylgeranylated by the covalent attachment of an isoprenoid moiety of either a farnesyl (C15) or a geranylgeranyl (C20) groups, respectively.<sup>31</sup> The third protein prenyltransferase is geranylgeranyltransferase 2 (GGTase 2, also known as Rab geranylgeranyltransferase), which recognizes a different motif, and is called a non-CaaX prenyltransferase. It is noteworthy that the most widely studied enzyme in this family is protein farnesyltransferase (Ftase).<sup>48</sup> Farnesyltransferase catalyzes the covalent attachment of a farnesyl unit (which is produced by FPPS) to a cysteine residue, which is part of a CaaX motif, of a protein substrate (Figure 1.15). The newly attached isoprenoid units help to localize proteins at the cell membrane, to maintain proper protein function, and to permit specific protein-protein interactions at a sub-cellular level (e.g. prenylated proteins of the Ras and G protein families that are crucial to cell signaling systems).<sup>30,49,50</sup>

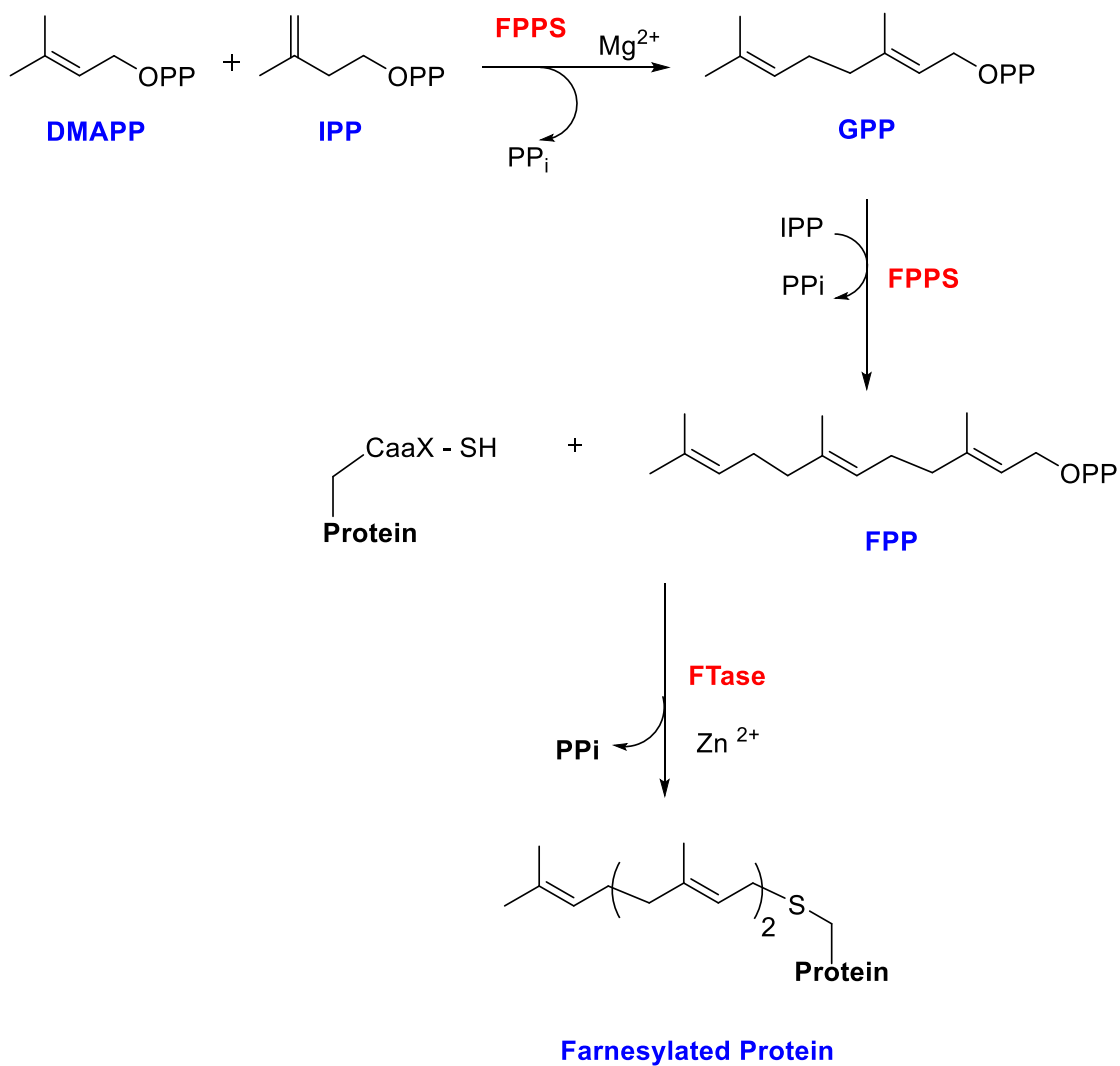


**Figure 1.15: Scheme showing the formation of FPP by FPPS and the covalent attachment of a farnesyl unit to the C-terminus of a protein substrate via farnesylation by Ftase.**

Protein farnesyltransferases (Ftase) are metal ion-dependent enzymes: the presence of a  $Zn^{2+}$  ion cofactor is crucial for them to retain their activities. The metal plays a vital role in coordinating with the cysteine thiolate of the protein substrate. It is worth noting that the active sites of the Ftase enzymes lack the Asp-rich DDxxD motif responsible for the binding of  $Mg^{2+}$ /diphosphate in other prenyltransferases (such as the previously mentioned farnesyl diphosphate synthase (FPPS)). The isoprenyl diphosphate synthase and the farnesyltransferase employ different mechanisms for catalysis, consistent with the absence of any sequence homology between the genes encoding for them. Due to the key role that the enzymes FPPS and Ftase play in cell division and cancer progression, they have been accepted as valid anti-cancer drug targets.

34,48,51,52

#### 1.4.2.2 Mechanistic Studies

Two different mechanisms were proposed for farnesyltransferase (Ftase) catalysis,  $S_N1$  (dissociative) and  $S_N2$  (associative) (Figure 1.16). In both mechanisms a deprotonated cysteine residue first coordinates to the  $Zn^{2+}$  cofactor in the active site. From this point the mechanisms differ. In the  $S_N1$  pathway, the pyrophosphate dissociates from FPP forming an allylic carbocation intermediate, which is then attacked by the thiolate anion to furnish the farnesylated protein. In the  $S_N2$  mechanism, the thiolate anion attacks FPP and displaces the pyrophosphate in a single transition state.

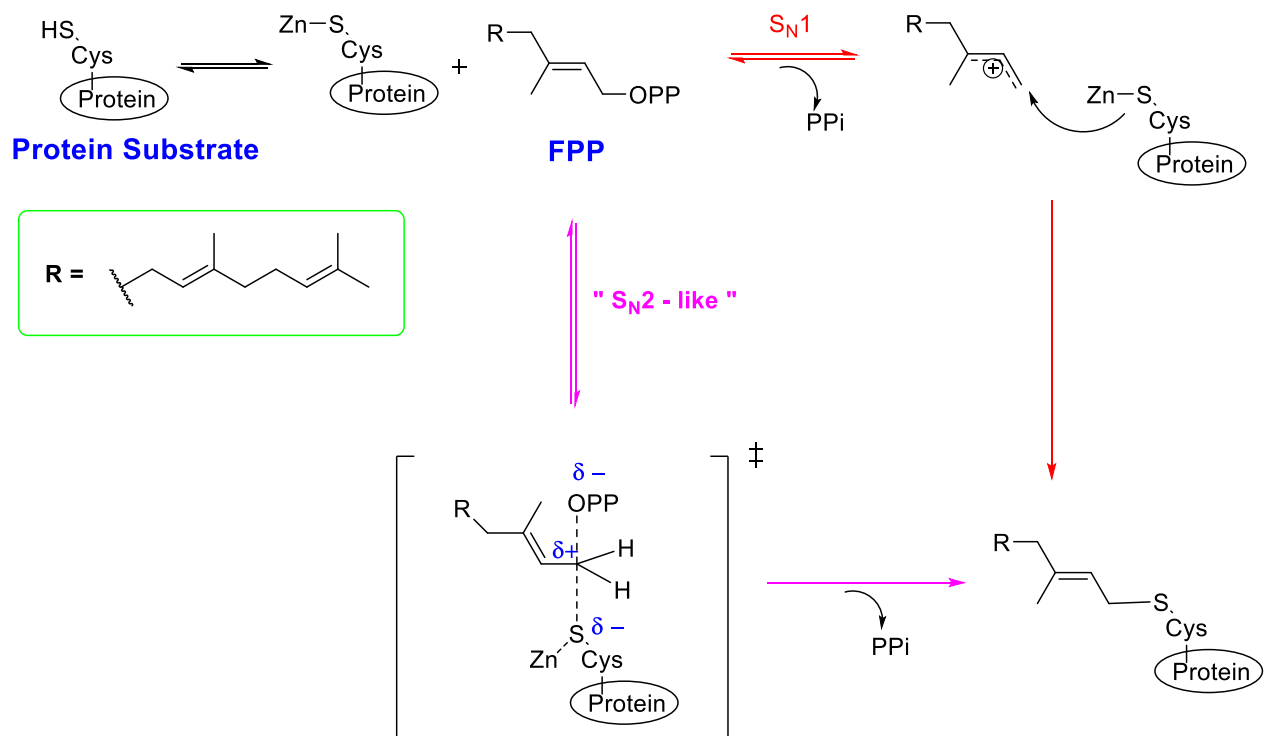


**Figure 1.16: Potential mechanisms employed by Ftase**

Mechanistic investigations were conducted on Ftase by the research groups of Poulter and Fierke.<sup>34</sup> They used fluorinated FPP analogues, since fluorine substitution is believed to destabilize the forming allylic carbocation thus slowing down the reaction rates (Figure 1.17). The relative rate values obtained with the fluorinated FPP substrates reflected the presence of a significant carbocationic character that is generated during catalysis. However, the rate depressions were less severe than that of other known S<sub>N</sub>1 enzymatic reactions.

It was generally accepted that this reaction proceeds via an  $S_N2$ -like transition state with a considerable carbocationic character generated in the allylic moiety of FPP during catalysis.<sup>53</sup> This finding has been further analyzed with KIE experiments by the research group of Distefano. They used a deuterium-labeled FPP substrate (Figure 1.17) in the measurement of the kinetic isotope effect (KIE).<sup>53</sup> Since the pyrophosphate dissociation step in an  $S_N1$  reaction would be the rate determining step (RDS), they predicted a large secondary isotope effect of about (1.1 – 1.4), because there is a change of the hybridization from  $sp^3$  to  $sp^2$  at the C-1 position of FPP. Surprisingly, the KIE measured close to unity indicating that the deuterium substitution did not have a significant effect on the barrier to reaction. They concluded that Ftase enzymatic reaction proceeds via an  $S_N2$  mechanism, which agrees with the aforementioned experiments.<sup>48,53</sup>

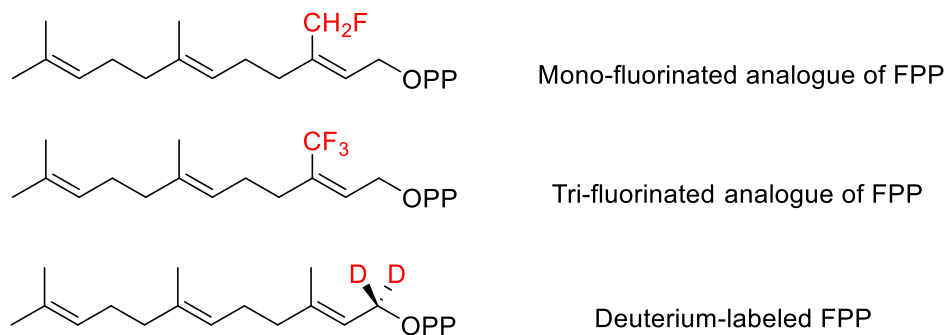


**Figure 1.17: Structures of FPP analogues used in mechanistic studies of Ftase.**

### 1.4.2.3 Ftase Inhibitors

Surprisingly, farnesyltransferase (Ftase) inhibitors were found to be ineffective drugs, partially because there is an alternative pathway for Ras prenylation via the related enzyme geranylgeranyl transferase (GGTase I). It is noteworthy that the protein prenyltransferase enzymes, Ftase and GGTase I and II do not have a strict substrate specificity - often leading to cross prenylation - and that this promiscuity is the major reason behind the failure of Ftase inhibitors such as tipifarnib (Figure 1.18).<sup>21,30,54</sup> The inhibition of farnesyl diphosphate synthase (FPPS) and/or geranylgeranyl diphosphate synthase (GGPPS) provides an attractive alternative to Ftase. The inhibition of these enzymes leads to decreased levels of farnesyl diphosphate and/or geranylgeranyl diphosphate and corresponding decreased levels of protein prenylation.<sup>34</sup>

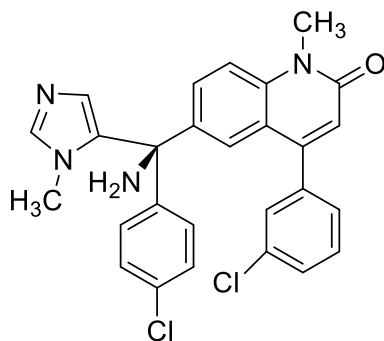


**Figure 1.18 Structure of Tipifarnib.**

### 1.4.3 Aromatic Prenyltransferases (Metal Ion-Independent Prenyltransferases): 4-Dimethylallyl Tryptophan Synthase (4-DMATS)

Indole prenyltransferases have been identified in several fungal species. These enzymes catalyze the attachment of a prenyl group onto a large diversity of aromatic substrates that possess an indole ring-system. The enzyme 4-dimethylallyl-tryptophan synthase (4-DMATS) utilizes dimethylallyl diphosphate (DMAPP) in the C-4 prenylation of L-Trp to give 4-dimethylallyl-tryptophan (4-DMAT) and an inorganic pyrophosphate (PP<sub>i</sub>) as products (Figure 1.19).<sup>55</sup>

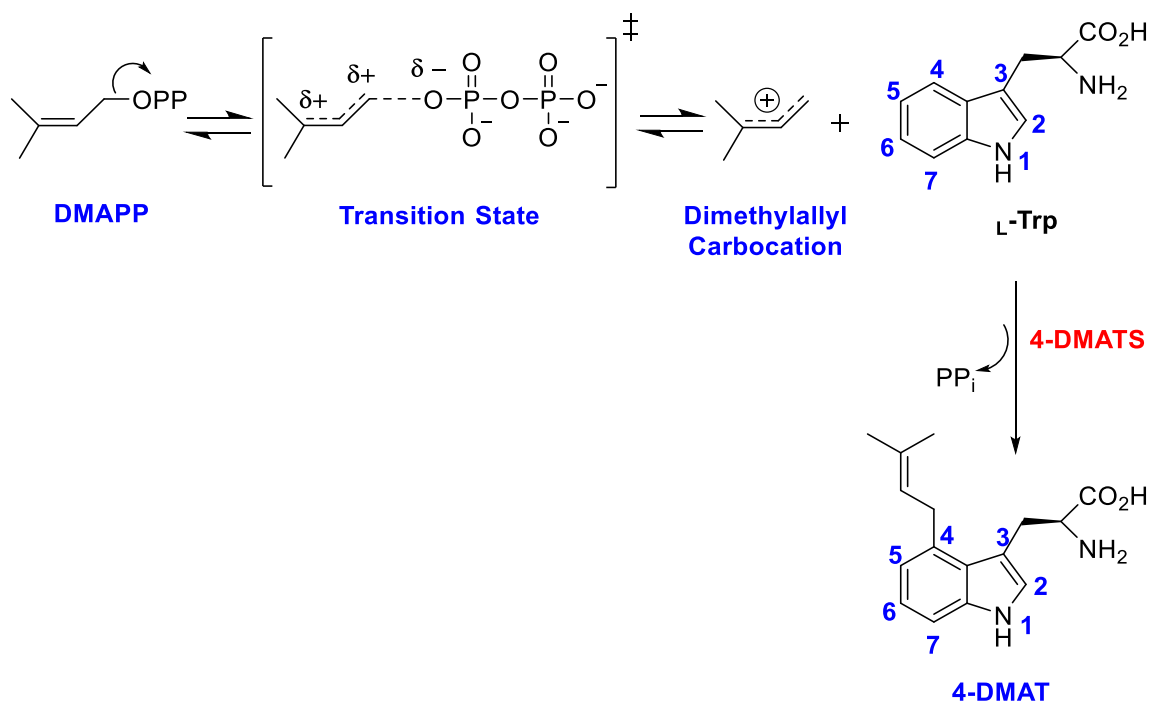
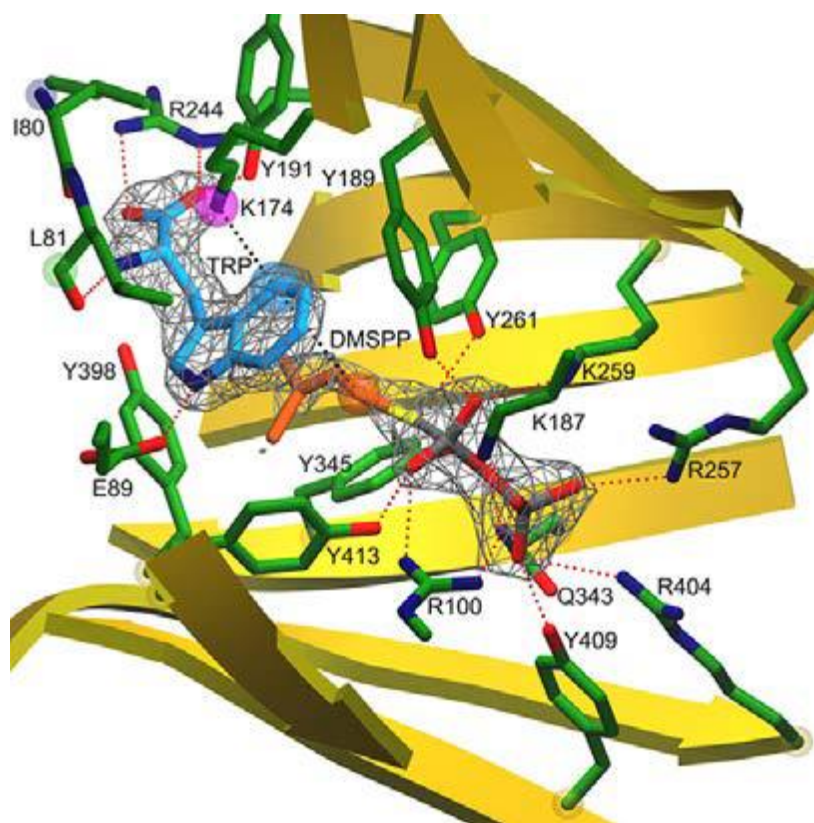


Figure 1.19: The C-4 prenylation of L-Trp catalyzed by 4-DMATS

A 2009 report of the crystal structure of 4-DMATS has shown that it adopts the rare ABBA fold (or PTs barrel fold).<sup>56</sup> This crystal structure of 4-DMATS was obtained in a complex with DMSPP, the unreactive thiol analogue of DMAPP, and L-tryptophan (Figure 1.20). Five residues were found to coordinate to the diphosphate moiety of the DMAPP; three positive arginine residues and two lysine residues. Furthermore, a series of tyrosine residues form a network of hydrogen bonds with the diphosphate group of DMAPP - this network of H-bonds is believed to be vital for the binding of the substrate. The prenyl group of DMAPP (or its unreactive analog, DMSPP) is sandwiched between a Tyr side chain (Tyr 345) and the indole ring of L-tryptophan (Figure 1.21), which is believed to promote ionization and help stabilize the resultant allylic carbocation via cation- $\pi$  interactions.<sup>56</sup> In this thesis 4-DMATS has been used only as a coupling enzyme in chapter 4, since it releases pyrophosphate (PPi) as a byproduct.



**Figure 1.20: The structure of the unreactive analogue of DMAPP, DMSPP.**



**Figure 1.21: The crystal structure of DMATS in complex with the thiol analog of DMAPP (DMSPP) and L-Trp.** This figure is obtained from the crystallographic report on the enzyme. <sup>56</sup>

## **1.5 Other Enzymes Involved in Isoprenoid Biosynthesis that generate Carbocationic Intermediates.**

In this thesis we will describe our efforts to design inhibitors that mimic the carbocation intermediate formed by isoprenoid biosynthetic enzymes. In the following three sections we will introduce enzymes that are thought to generate carbocation intermediates and were the subject of studies in this work.

### **1.5.1 Human Squalene Synthase**

#### **1.5.1.1 Introduction**

In humans, the isoprenoid biosynthetic pathway is involved in the production of critical end-products with a diversity of vital physiological functions such as cholesterol, dolichol, steroids, hormones, and prenylated proteins.<sup>20,57-62</sup> As discussed previously, the consecutive addition of isopentenyl diphosphate (IPP) to the growing isoprene chain in a head-to-tail manner - thus forming a series of linear isoprenoid diphosphates (C10 to C25) - is catalyzed by the prenyltransferase family of enzymes. The enzymes discussed thus far produce, or rely upon, linear isoprenoids formed by head-to-tail addition of isopentenyl diphosphates (IPP).<sup>63</sup>

In Nature, there are more than 33 000 different isoprenoid compounds. In the majority of these isoprenoids their carbon frameworks consist of isoprene units connected in a regular 1'-4, head-to-tail manner, while many others have them connected in an irregular 1'-1, head-to-head pattern. Essential oils of plants in the *Asteraceae* family are known for containing a vast array of different irregular monoterpenes with 1'-1, 1'-2, 1'-3, 2-1'-3, c1'-2-3 and c1'-1-2 structures (Figure 1.22).<sup>64</sup>

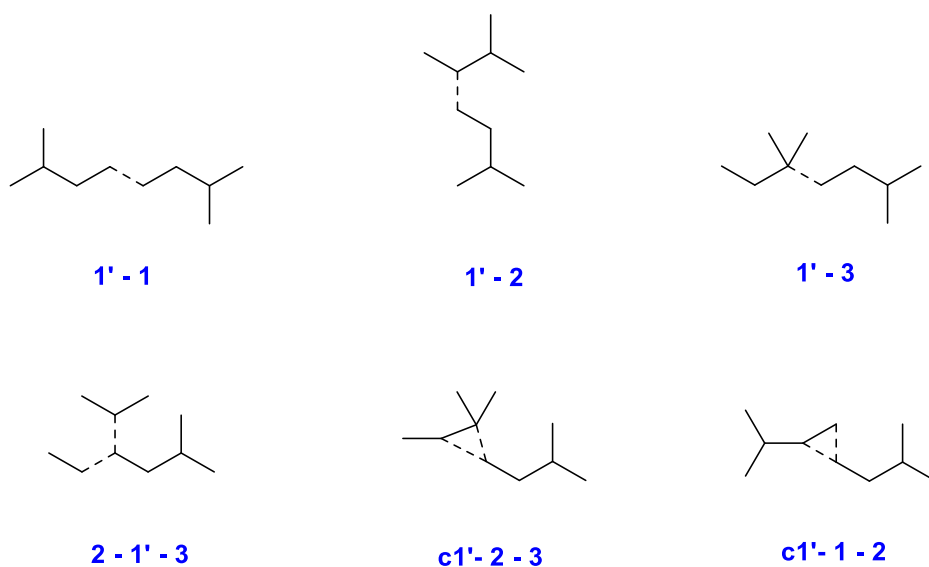


**Figure 1.22: Structures of regular and irregular connected isoprene units in different isoprenoids.**

The most well-known head-to-head terpenes are squalene (SQ) and phytoene (PT) (Figure 1.23), with a 1'–1 linkage between two farnesyl diphosphate moieties and 1'–1 linkage between two geranylgeranyl diphosphate residues, respectively.<sup>64</sup> It is noteworthy that squalene and phytoene are essential precursors involved in the biosynthesis of sterol and carotenoid, respectively.<sup>63,64</sup>

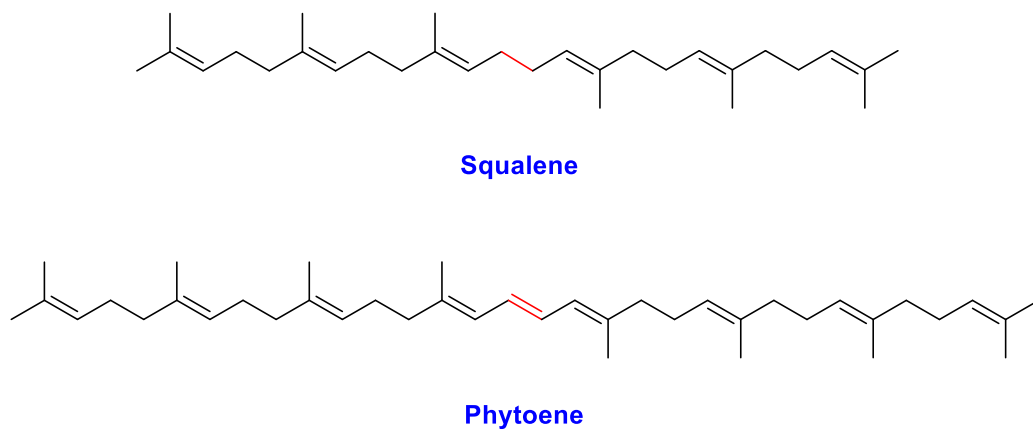


**Figure 1.23: The structures of Squalene and Phytoene.**

Squalene is formed in a head-to-head manner by condensation of two FPP molecules via the prenyltransferase-like enzyme squalene synthase (SQS). Subsequently, a class II terpene cyclase catalyzes the conversion of the linear terpene, squalene, into its corresponding cyclic derivative, and this product is carried forward towards cholesterol (Figure 1.24).<sup>64</sup> In 1966 Rilling discovered that the squalene synthase reaction proceeds via a triterpene intermediate with a c1'–2–3 structure (Figure 1.22), presqualene diphosphate (PSPP) (Figure 1.24).<sup>64</sup> This discovery sparked considerable attention to the biogenesis of isoprenoids with 1'–1 linkages in

their carbon skeleton. Interestingly, Altman and his coworkers reported shortly thereafter that the reaction catalyzed by phytoene synthase, which involves the biosynthesis of phytoene from geranylgeranyl diphosphate, proceeds via an analogous cyclopropane-containing intermediate, prephytoene diphosphate (PPPP).<sup>65</sup>



### 1.5.1.2 Mechanistic Studies

Washburn and Ortiz de Montellano have proposed that the catalytic machinery of squalene synthase (SQS), a 47-kDa membrane associated enzyme, is comprised of two distinct catalytic reaction centers (Figure 1.25).<sup>66</sup> In the first catalytic reaction center, there are two different FPP binding sites. In the first binding site, the first FPP molecule is bound in an orientation facilitating its dissociation to yield an allylic carbocation and an inorganic pyrophosphate. In the second binding site, a second molecule of FPP is bound in a conformation that allows a nucleophilic attack of its allylic double bond onto the aforementioned allylic tertiary carbocation.<sup>64,67</sup> Subsequently, a deprotonation step induces a ring closure to form a stable intermediate (PSPP), which is a remarkable cyclopropylcarbinyl diphosphate with a  $1^{\circ}-2-3$  structure (Figure 1.22).<sup>64</sup> In the second catalytic reaction center, dissociation of a pyrophosphate from PSPP gives a cyclopropylmethyl cation which undergoes a carbocation rearrangement and a final reduction by NADPH to form squalene (Figure 1.25).

Poulter and Popjak have postulated a sequential binding of the two molecules of FPP, whereby the donor FPP binds first and the cyclopropylcarbinyl diphosphate intermediate (PSPP) translocates from the first to the second reaction center within the enzyme, without its release.

<sup>64,68,69</sup>

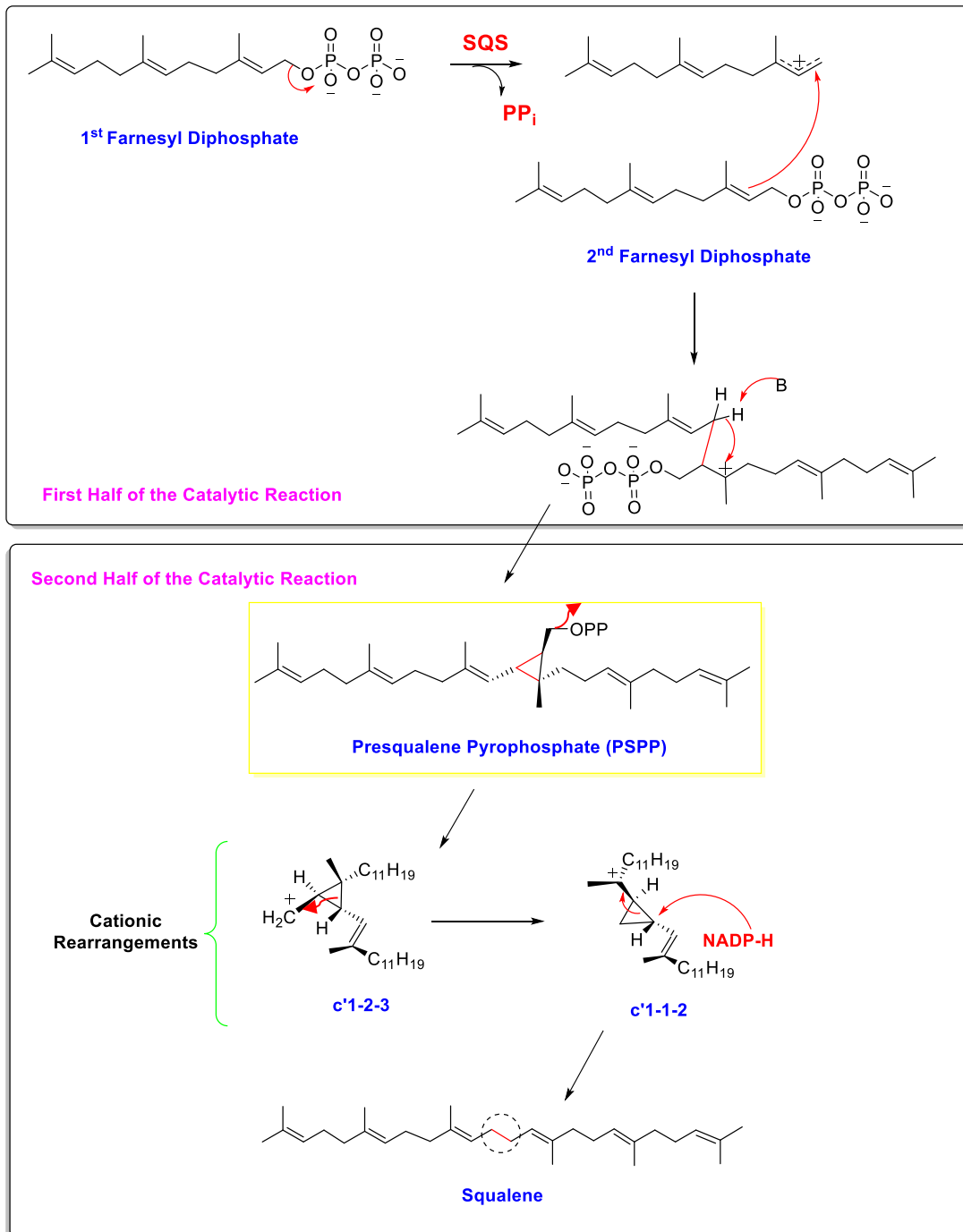


**Figure 1.25: Accepted mechanism of the biosynthesis of squalene catalyzed by squalene synthase (SQS).**

After the discovery of PSPP, several research groups proposed mechanisms for the second half of the squalene synthase reaction, based on known cationic rearrangements of cyclopropylcarbinyl cations.<sup>64,65,68-70</sup> One proposal which took into consideration all of the known regio- and the stereochemical factors, involved the rearrangements of a c'1-2-3 cation to a c'1-1-2 cation, followed by reduction with the cofactor NADPH at C-1' (Figure 1.25). Zhang and Poulter conducted some mechanistic studies, from which they obtained strong evidence for the involvement of carbocationic intermediates formed during the cationic rearrangements of PSPP to produce SQ.<sup>64</sup> They noticed a rapid conversion of FPP to PSPP upon incubating the recombinant form of squalene synthase enzyme with FPP in the absence of NADPH.<sup>64</sup> This conversion was followed by a slow enzyme-catalyzed solvolysis of the cyclopropylcarbinyl intermediate (PSPP), to yield a mixture of products (Figure 1.26). The mixture was found to contain: 24% (*Z*)-dehydrosqualene (DSQ), 14% hydrobotryococcene (HBO) and 58% hydrosqualene (HSQ). After interpretation, it was suggested that DSQ was generated upon eliminating a proton from carbocation c'1-1-2, while both alcohols HBO and HSQ were generated upon nucleophilic attack by water on cations c'1-2-3 and c'1-1-2, respectively.<sup>70</sup>

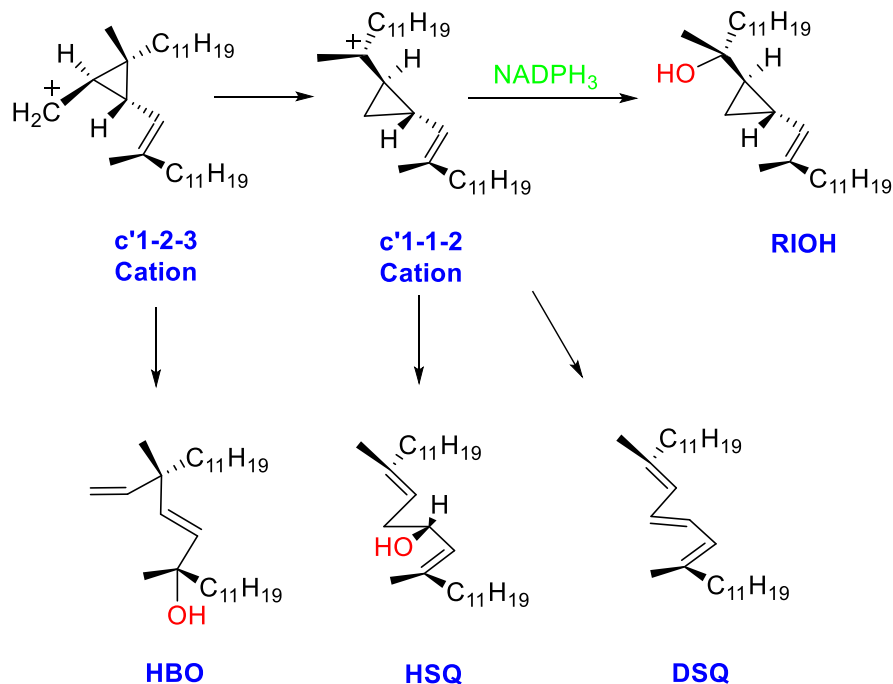


**Figure 1.26: Products formed from reaction of squalene synthase and FPP in either the absence of NADPH or in the presence of the unreactive NADPH analogue,  $\text{NADPH}_3$ .** <sup>70</sup>

In an attempt to test for the effect of occupying the cofactor binding site on the distribution of the aforementioned mixture of products, they repeated the above experiment but in the presence of an unreactive analogue of the cofactor,  $\text{NADPH}_3$  (an unreactive analogue lacking the 5,6-double bond in the nicotinamide ring). <sup>70</sup> The results they obtained were interesting, since both  $\text{DSQ}$  and  $\text{HSQ}$  still formed (23% and 58%, respectively) but the  $\text{HBO}$  was not detected. Instead, there was a new compound comprising 17% of the products. Mass spectrometry and  $^1\text{H}$  NMR analysis revealed its identity, it was a cyclopropylcarbinyl alcohol with isomeric structure to  $\text{DSQ}$  and  $\text{HSQ}$ , namely presqualene alcohol ( $\text{RIOH}$ ). <sup>64,68-70</sup>

Poulter and his coworkers positively identified the structure and the relative stereochemistry of RIOH by synthesizing it from farnesol. Also, they found that the distribution of this mixture of products was not affected upon switching the metal ion from  $Mg^{2+}$  to  $Mn^{2+}$ , however it was sensitive to its presence.<sup>69,70</sup> Poulter suggested that the isolation of RIOH, which was formed upon incubation with FPP in the presence of  $NADPH_3$ , to be very strong evidence for the cationic rearrangement of a c'1-2-3 cation to a c'1-1-2 cation.<sup>64,70</sup> Also, he suggested that these rearrangements are known to be highly stereoselective and can be dealt with as a net outcome of two consecutive superficial [1,2] rearrangements, where the primary c'1-2-3 cation rearranges forming a c'1-1-3 cyclobutyl cation, which then rearranges again to form the tertiary c'1-1-2 cation (Figure 1.27). He first proposed that a c'1-1-3 cation is a discrete intermediate in these cationic rearrangements, but since it couldn't be trapped, he later suggested that this c'1-1-3 cation might be a transition state linking the c'1-2-3 cation to the c'1-1-2 cation.<sup>68</sup>

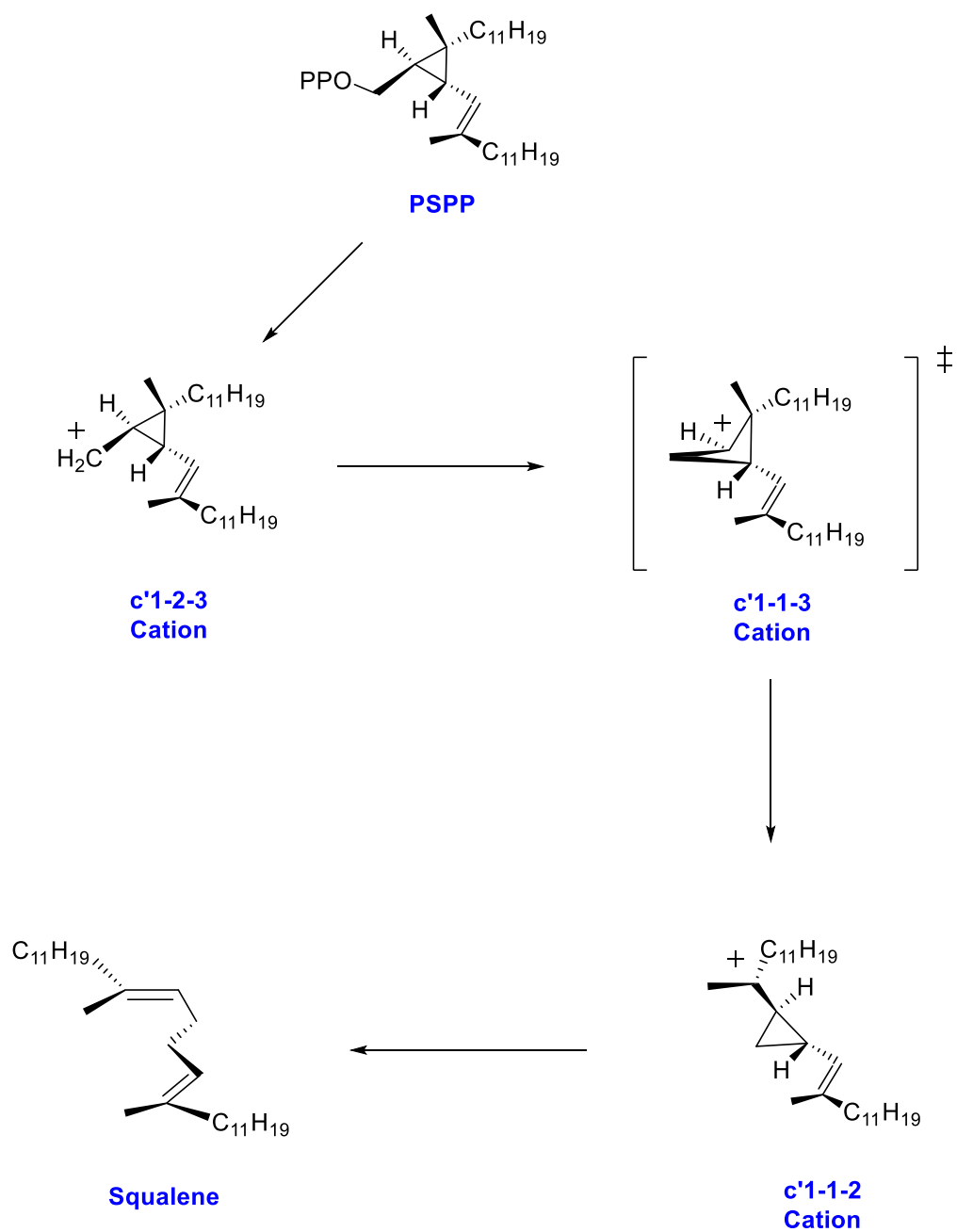


**Figure 1.27: Proposed mechanisms for the conversion of PSPP to squalene.** <sup>68</sup>

Poulter and his coworkers also found that incubation of a recombinant form of squalene synthase enzyme with NADPH and (*R*)-[1-H<sup>2</sup>] FPP produced a squalene with a molecular ion at *m/z* 412, and when incubated with NADPH and (*S*)-[1-H<sup>2</sup>] FPP produced a squalene with a molecular ion at *m/z* 411. These results agree with those obtained by Cornforth and Popjak and show that the *si*-hydrogen on C-1 of FPP is deprotonated by a basic residue in the first half of the catalytic reaction. <sup>64,68</sup>

With these results Poulter and his coworkers concluded that the catalytic machinery of squalene synthase (SQS) is designed to enhance the rearrangements of cations c'1-2-3 to c'1-1-2, (Figure 1.27). <sup>68</sup> In addition, Poulter proposed that the pyrophosphate group (PPi) released from the PSPP intermediate has a vital role in the second half reaction. It is anticipated that the electrostatic interactions in the c'1-2-3 cation : PPi and c'1-1-2 cation : PPi ion pairs may control the regioselectivity in the cationic rearrangements. Finally, he concluded that, in the absence of the cofactor, the formation of PSPP was much slower than in its presence. <sup>64,68,69</sup>

### 1.5.1.3 Structural Studies

Both enzymes, squalene synthase (SQS) and phytoene synthase (PYS) (Figure 1.28) are believed to have evolved from a common ancestor despite the fact that SQS catalyzes a reductive dimerization and PYS catalyzes redox neutral dimerization. Both SQS and PYS catalyze a head-to-head dimerization involving a stable cyclopropylcarbinyl intermediate, and do so with the same absolute stereochemistry. <sup>63,68</sup> DSQ, a C<sub>30</sub> analogue of phytoene, is produced when incubating SQS with FPP in the absence of NADPH (Figure 1.26). Evidence that both enzymes

are genetically related comes from the alignments of multiple amino acid sequences from different organisms. Three regions of conserved amino acids were identified in both enzymes, that cluster around the putative active site of SQS (Figure 1.29).<sup>68</sup>

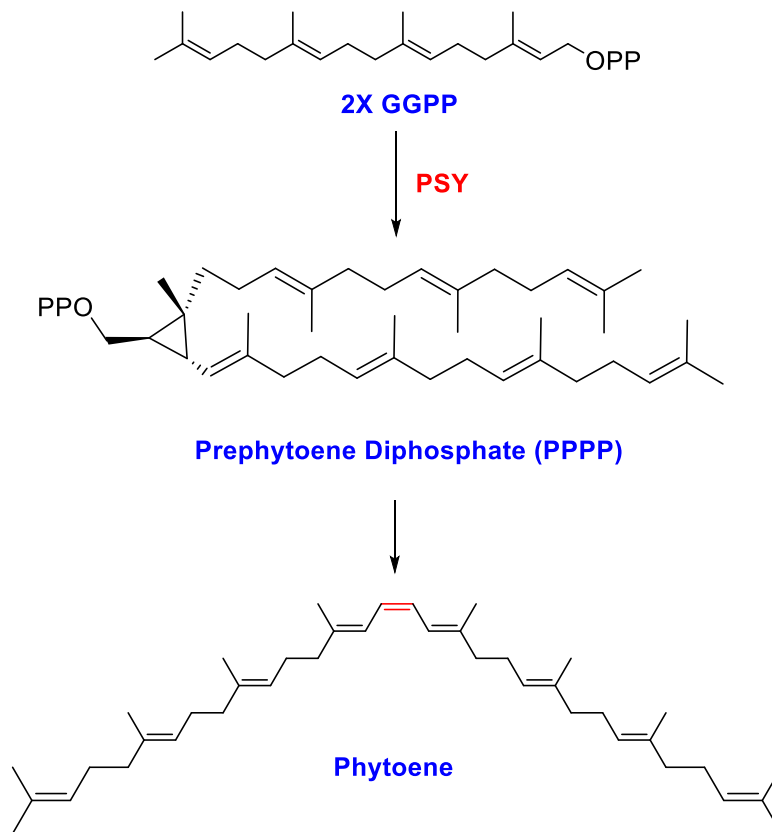


**Figure 1.28: The reaction catalyzed by PSY.**

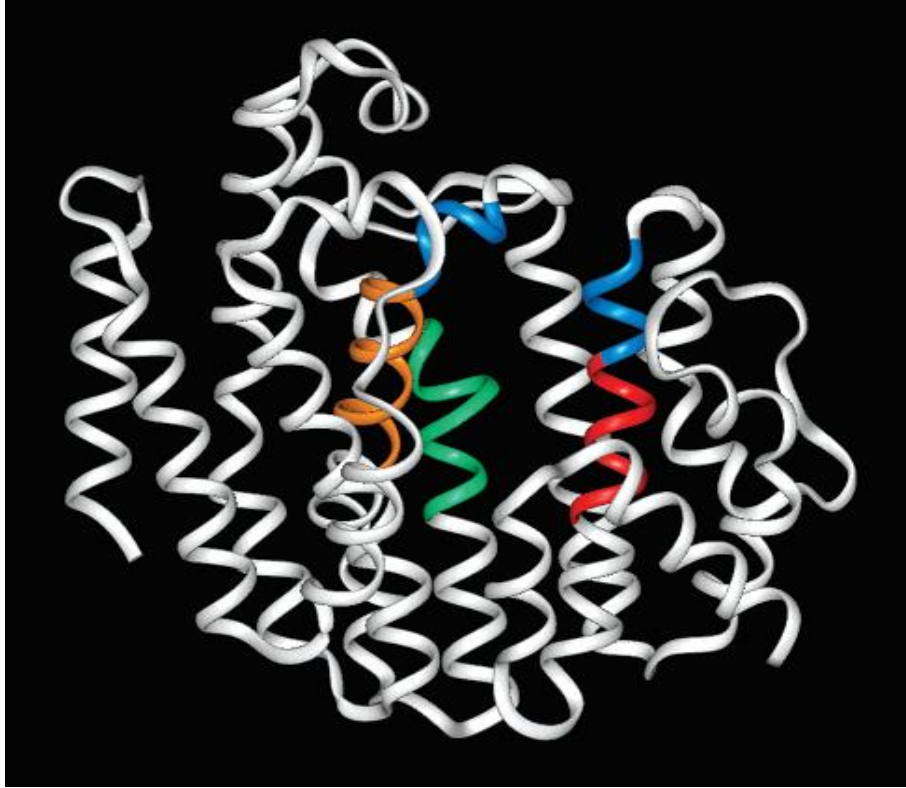


**Figure 1.29: Ribbon diagram showing the "isoprenoid fold" of the HSQS enzyme. The first, second, and third conserved regions (shown in red, green and gold, respectively) are common to both SQS and PYS and cluster around the putative active site. Shown in blue are the aspartate/glutamate-rich regions. This figure is obtained from the crystallographic report on the enzyme.<sup>68</sup>**

Another enzyme that is known to be evolutionarily and structurally similar to squalene synthase (SQS) is dehydrosqualene synthase (DSQS), despite the fact that SQS catalyzes a reductive dimerization and DSQS catalyzes redox neutral dimerization. Both enzymes catalyze the head-to-head dimerization of two FPP molecules and generate the common presqualene diphosphate intermediate (PSPP), then reactions diverge from this point (Figure 1.30). SQS has

an additional NADPH-binding cleft that allows for reduction to take place, while DSQS does not utilize NADPH.<sup>2,71-73</sup>

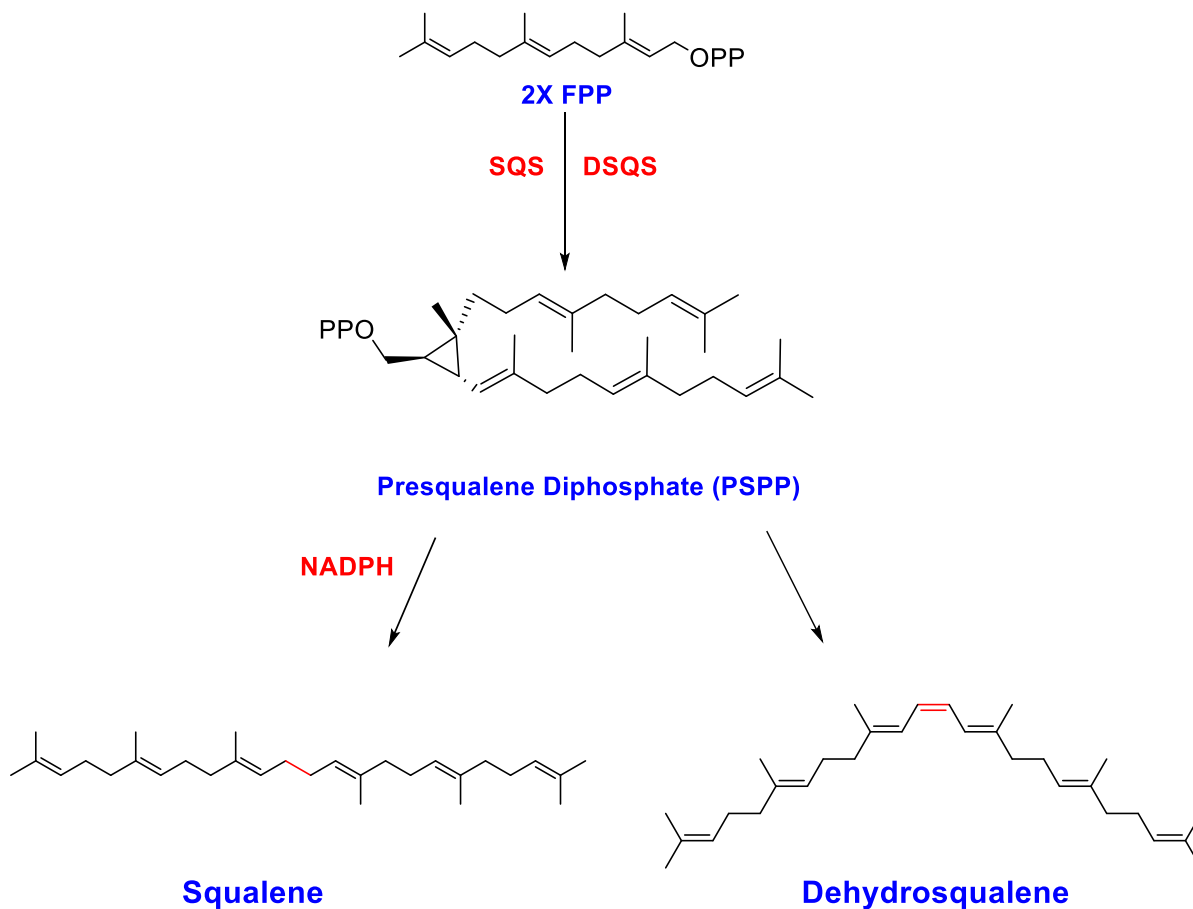


**Figure 1.30: The reactions catalyzed by SQS and DSQS.**

In 2000, Harwood and his coworkers were the first to identify the crystal structure of the recombinant form of human squalene synthase complexed with different inhibitors.<sup>63</sup> The X-ray structure revealed that the enzyme is entirely  $\alpha$ -helical with axes of all the helices arranged in three main layers, the first layer contains helices A, B and K, second one is formed by helices E,

C, J and L, are the last layer contains helices D, F, G, H, I and M. The enzyme is folded as a single domain with a large central channel surrounded by the five  $\alpha$ -helices C, F, G, H and J (Figure 1.31).<sup>63</sup> The two FPP binding sites in the first half reaction of squalene synthase are located in the central channel lined with conserved aspartate and arginine residues, and have been implicated in FPP binding by site directed mutagenesis studies. One end of this channel is predominantly hydrophobic while the other end is exposed to the solvent and contains a signature aspartate-rich sequence.<sup>63</sup> It should be noted that there are no crystal structures with NADPH bound, and there is no Rossmann fold in the structure. It has been postulated that the J-K loop and part of helix K comprise the nucleotide binding site.

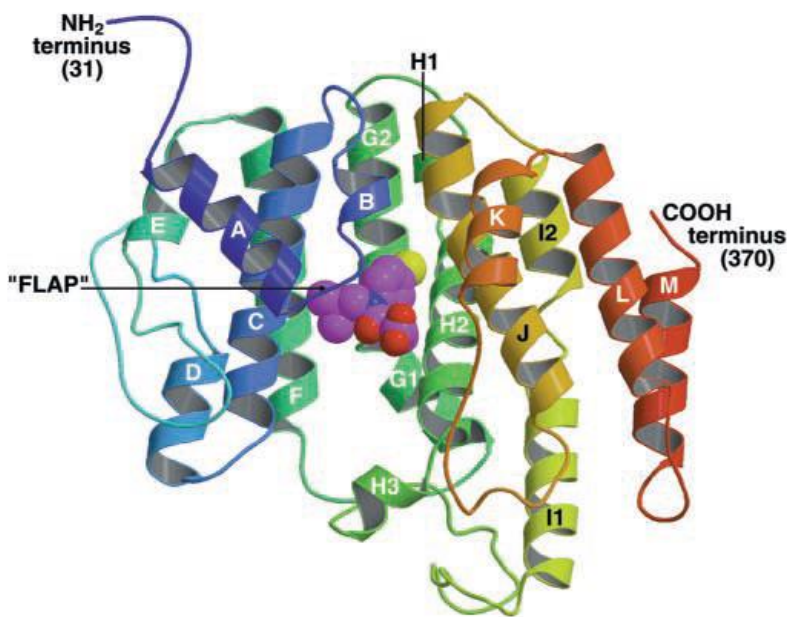


**Figure 1.31: Crystal structure of human squalene synthase. FLAP (ball and stick representation) is an inhibitor bound to SQS.** This figure is obtained from the crystallographic report on the enzyme.<sup>63</sup>

Interestingly, the five  $\alpha$ -helices that surround the active site in the core of human squalene synthase are structurally similar to the cores of three other class I isoprenoid biosynthetic enzymes with known crystal structures; avian farnesyl diphosphate synthase (FPPS), pentalenene synthase (PLS) and 5-epi-aristolochene synthase (EAS) (Figure 1.32).<sup>63</sup> This finding agrees with the early suggestion made by Schulz that all class I isoprenoid biosynthetic enzymes have evolved from a common ancestor.<sup>1,74</sup>

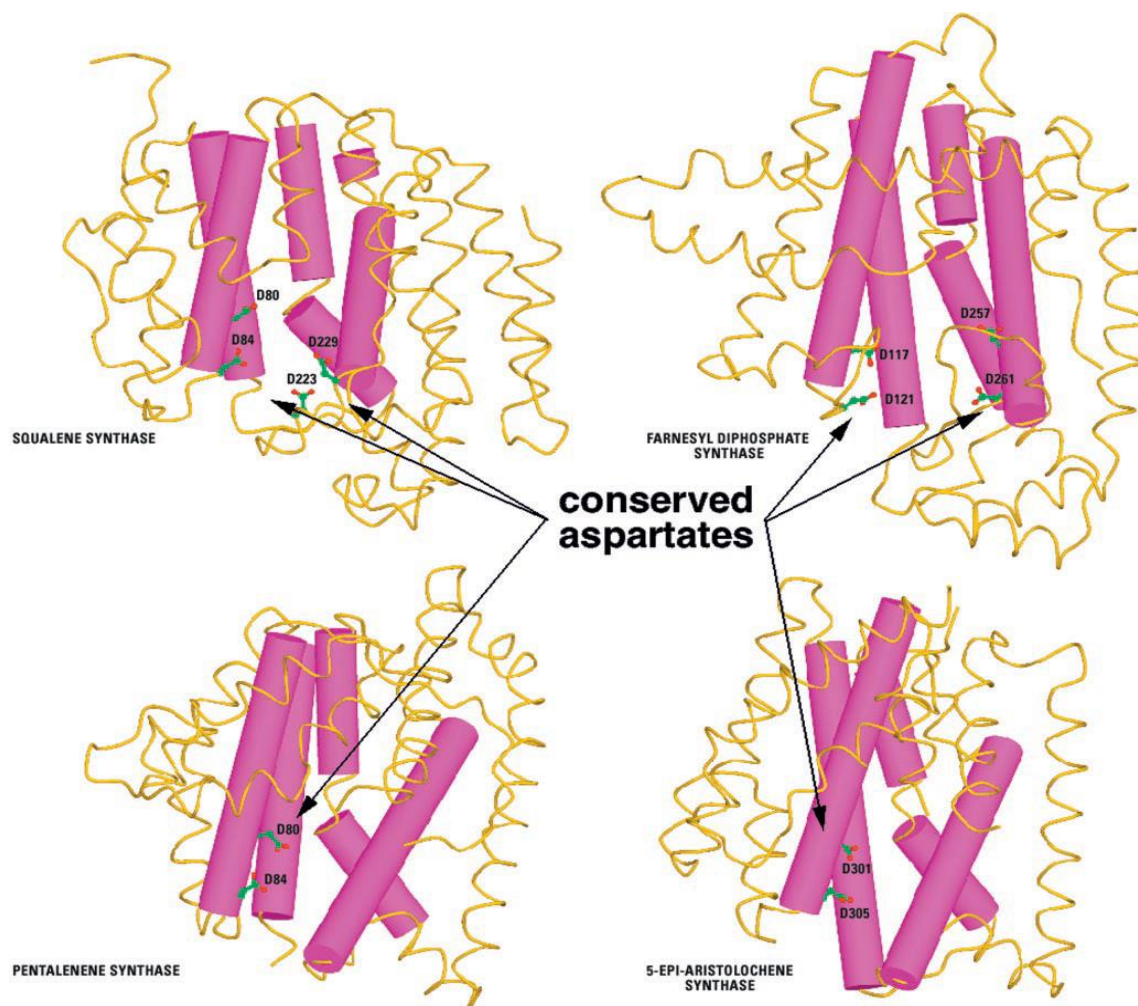


**Figure 1.32: Human squalene synthase's core architecture is structurally homologous to that of three other class I isoprenoid biosynthetic enzymes, FPPS, PLS and EAS. This figure is obtained from the crystallographic report on the enzyme.<sup>63</sup>**

## 1.5.2 Bacterial Dehydrosqualene Synthase of *Staphylococcus aureus*

### 1.5.2.1 Introduction

As discussed previously, allylic diphosphate synthases catalyze the condensation of isoprene units in either a head-to-head or head-to-tail manner to produce linear terpenes that are involved in the biosynthesis of sterols and carotenoid pigments.<sup>1,75</sup> In humans, plants, fungi, protozoa as well as many pathogenic yeasts squalene synthase (SQS) catalyzes the reductive head-to-head condensation of two FPP molecules to give squalene (Figure 1.30).<sup>75</sup> In plants, phytoene synthase (PSY), a related isoprenoid enzyme, catalyzes the non-reductive head-to-head condensation of two molecules of geranylgeranyl diphosphate (GGPP) resulting in the formation of the linear C<sub>40</sub> isoprenoid, phytoene (Figure 1.28), which is an intermediate in the biosynthesis of carotenoid pigments.<sup>75</sup> Finally, in the bacterium *Staphylococcus aureus*, dehydrosqualene synthase (DSQS) catalyzes the head-to-head condensation of two molecules of FPP, to furnish the linear C<sub>30</sub> isoprenoid, dehydrosqualene (Figure 1.30), which is an essential intermediate in the biosynthesis of the carotenoid pigment, staphyloxanthin (STX) (Figure 1.33).<sup>75</sup>

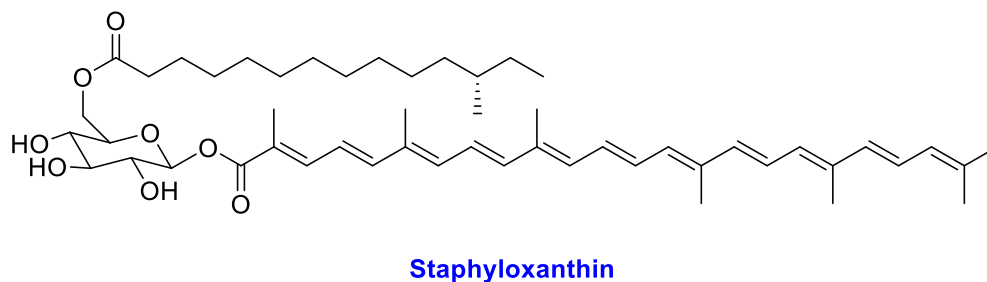


**Figure 1.33: The structure of staphyloxanthin.**

Interestingly, all the enzymatic reactions catalyzed by these three head-to-head terpene synthases; SQS, DSQS and PSY, occur over two distinctive steps. The first step involves the formation of the cyclopropylcarbinyl intermediates PPPP or PSPP.<sup>75,76</sup> The second step involves the conversion of the cyclopropylcarbinyl diphosphate intermediates into linear hydrocarbon chains, either in a reductive sense, as in the case of SQS, or in a redox neutral sense, as in the case of DSQS and PSY. Our focus in this thesis is on squalene synthase and bacterial dehydrosqualene synthase from *Staphylococcus aureus*.<sup>75,76</sup>

Nowadays, there is a growing concern regarding the decreased rate of introduction of new anti-infective agents, and the world-wide development of antibiotic drug resistance, especially with the widespread infections caused by *Staphylococcus aureus*. This has led to the employment of alternative approaches which involve targeting bacterial virulence factors. Virulence factors such are molecules responsible for the infectivity of bacteria and/or their intrusiveness *in vivo*.<sup>76,77</sup> The screening for inhibitors that target the biosynthesis of virulence factors was considered to be challenging, since they are not required for survival *in vitro*. In the case of *Staphylococcus aureus*, the major virulence factor is staphyloxanthin (STX), which is a colored carotenoid pigment. Marshall and Rodwell were the first to report STX. In 1972 it was isolated from *S. aureus* and chemically analyzed by Marshall and Wilmoth, who identified it as  $\beta$ -D-glucopyranosyl 1-O-(4,4'-diaponeurosporen-4-oate)-6-O-(12-methyltetradecanoate) (Figure 1.33).<sup>76</sup>

The biosynthetic genes for staphyloxanthin are organized in an operon, *CrtOPQMN*. The biosynthesis of STX starts with the head-to-head condensation of two molecules of farnesyl diphosphates (FPP) to yield dehydrosqualene as catalyzed by dehydrosqualene synthase (CrtM). This is converted to the yellow main intermediate 4,4'-diaponeurosporene by dehydrosqualene desaturase (CrtN) (Figure 1.35). Then diaponeurosporene oxidase (CrtP) oxidizes 4,4'-diaponeurosporene to 4,4'-diaopeurosporenic acid. A glycosyl transferase (CrtQ) adds glucose to the carboxylate of 4,4'-diaopeurosporenic acid to yield glycosyl 4,4'- diaopeurosporenoate. Finally, CrtO, an acyl transferase, esterifies glucose at the C-6'' position to yield staphyloxanthin (Figure 1.34).<sup>76</sup>

Interestingly, the inhibition of any of the steps mentioned above results in colorless bacteria. Studies by Liu *et al.* have revealed that the loss of the STX pigment makes *S. aureus* susceptible to killing by reactive oxygen species generated by the host neutrophils. Accordingly, it is anticipated that the inhibition of the biosynthetic pathway of staphyloxanthin is a promising drug target against pigmented *Staphylococcus aureus* strains.<sup>15,76,78</sup>

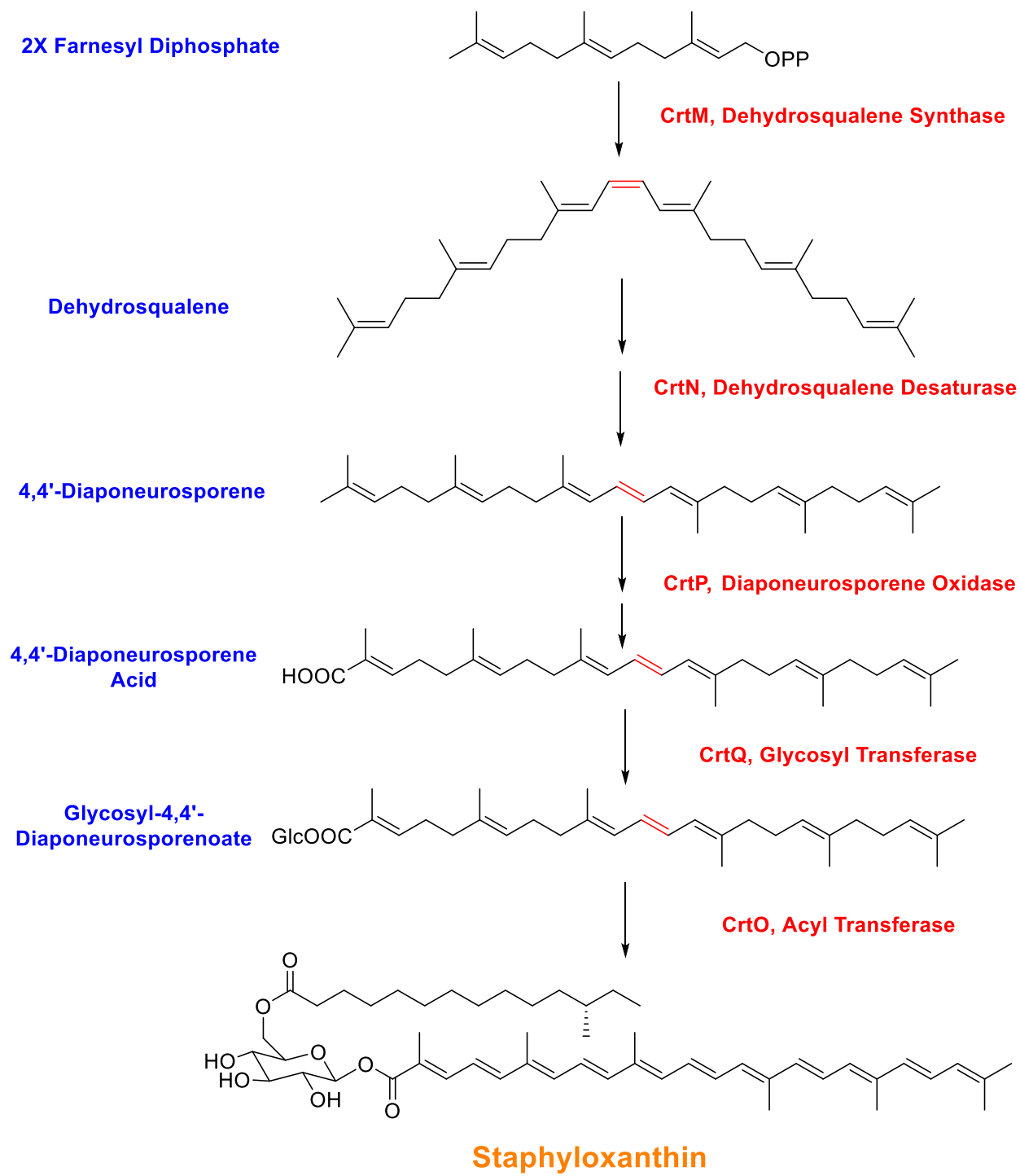


**Figure 1.34: The biosynthetic pathway of staphyloxanthin from FPP.** <sup>76</sup>

### 1.5.2.2 Mechanistic and Structural Studies of DSQS

Bacterial dehydrosqualene synthase (DSQS) catalyzes the redox neutral head-to-head condensation of two molecules of farnesyl diphosphate (FPP) to form dehydrosqualene. As was seen in the case of squalene synthase (SQS), the reaction proceeds via an initial ionization of farnesyl diphosphate (FPP) to generate an allylic carbocation-pyrophosphate ion pair (Figure 1.35).<sup>77</sup> A deprotonation and cyclization then forms presqualene diphosphate intermediate (PSPP) completing the first half of the catalytic reaction. In the second half reaction, PSPP ionizes to form a cyclopropylmethyl cation. With analogy to the SQS reaction, it is thought that this cation rearranges to give a cyclopropyl tertiary cation (Figure 1.35). Then instead of reducing with NADPH, DSQS promotes a deprotonation and ring opening to produce dehydrosqualene. Due to similarity in the reactions catalyzed, it is anticipated that HSQS and DSQS might be evolutionarily related. This is supported by an amino acid sequence alignment that shows a sequence identity of 30% identity and a sequence similarity of 36%.<sup>77</sup>

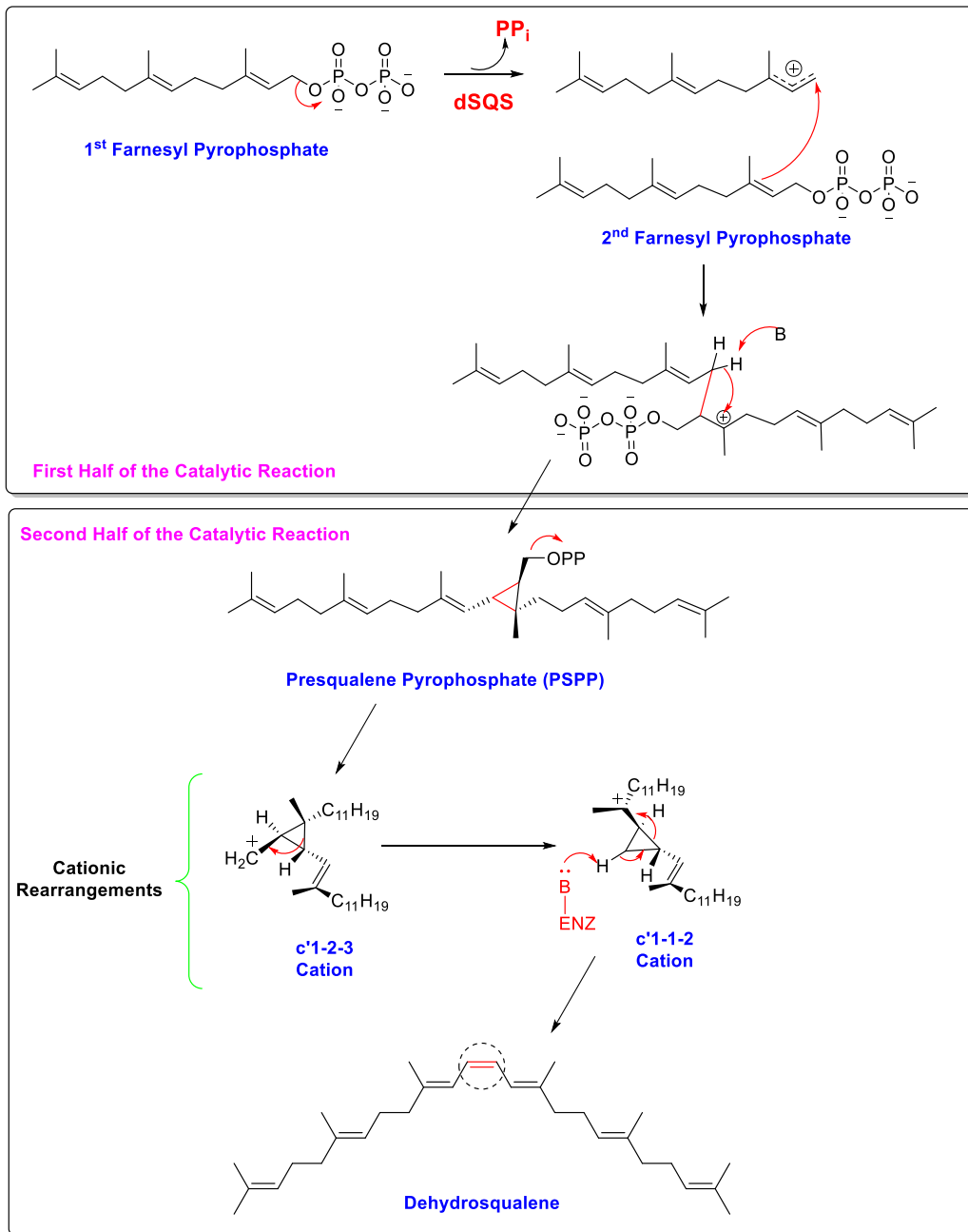


**Figure 1.35: Mechanism of the biosynthesis of dehydrosqualene catalyzed by dehydrosqualene synthase (DSQS).**

Oldfield and coworkers reported the X-ray crystal structure of bacterial dehydrosqualene synthase from *Staphylococcus aureus* complexed with a bisphosphonate inhibitor with a resolution of 1.58 Å (Figure 1.36).<sup>75</sup> The crystal structure of DSQS shows that the protein is all helical and contains a large channel running through the center that can fit the linear C<sub>30</sub> isoprenoid product, dehydrosqualene, as well as two FPP binding sites. As expected, the general fold of the enzyme is similar to that of the human squalene synthase (HSQS), but it lacks the putative NADPH binding region.

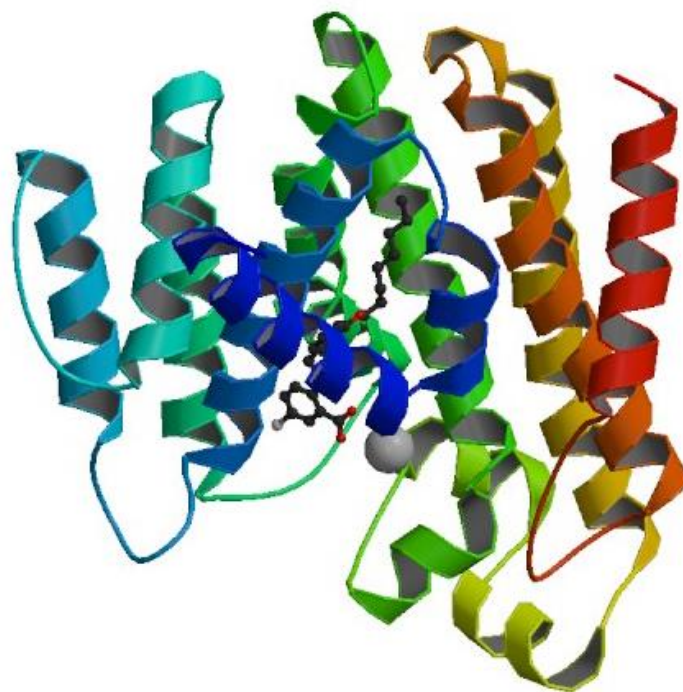


**Figure 1.36: Crystal structure of DSQS from *Staphylococcus aureus* complexed with a bisphosphonate inhibitor.** This figure is obtained from the crystallographic report on the enzyme.<sup>75</sup>

They conducted extensive structural studies on the enzyme, in an attempt to define which of the two enzymatic sites (S1 and S2) hosts the initial ionization (donor FPP) and which site hosts the alkene (FPP receptor), and how PSPP binds to the enzyme active site.<sup>75</sup> Oldfield proposed two different mechanistic scenarios for the prenyl diphosphate binding sites; either S1 = donor or S1 = acceptor (Figure 1.37).<sup>75</sup>

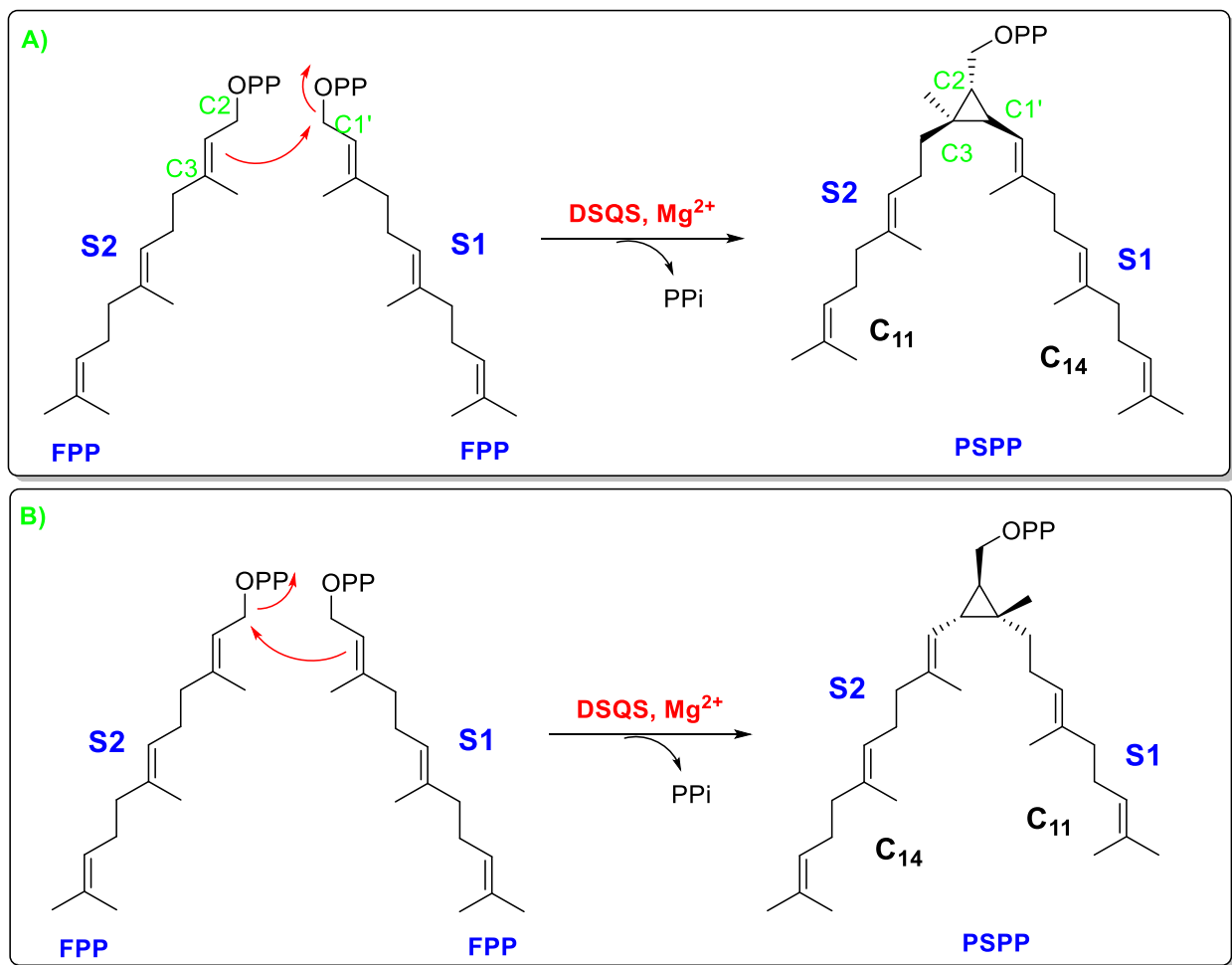


**Figure 1.37: (A and B) Two possible mechanistic scenarios of the two FPP condensation, S1 = donor or S1 = acceptor. Only that scenario shown in A, where S1 = donor, was consistent with the crystallographic data.**

In order to define the two FPP binding sites S1 and S2, Oldfield and coworkers prepared an unreactive analogue of farnesyl diphosphate, *S-thiolo*-farnesyl diphosphate (FSPP). They crystallized the enzyme-FSPP complex and obtained the structure shown in Figure 1.38. The crystal structure they obtained showed that the distances between C-1' and C-2,3 for both proposed mechanistic models were almost the same (5 – 5.4 Å), which is insufficient for any donor-acceptor site assignments.<sup>75</sup> Consequently, they decided to use an inactive mutant version of the enzyme Y129A which was based on an alignment of amino acid sequence with rat SQS. With the inactive mutant, they were able not only to obtain a structure with FSPP (Figure 1.38A), but also with the intermediate PSPP bound (Figure 1.38B). Superimposing the two crystal structures (Figures 1.38C and 1.38D), allowed them to make the following observations.<sup>75</sup> Firstly, site S1 contains the donor FPP, which forms the C1' carbocation after ionization, since the pyrophosphate group (PPi) which was seen in the S1 site of the DSQS-FSPP structure is no longer present in the S1 site of the DSQS/PSPP structure.<sup>75</sup> Furthermore, the longer side chain of PSPP was found to occupy the S1 site, indicating that the S1 FPP initially ionizes.<sup>75</sup>

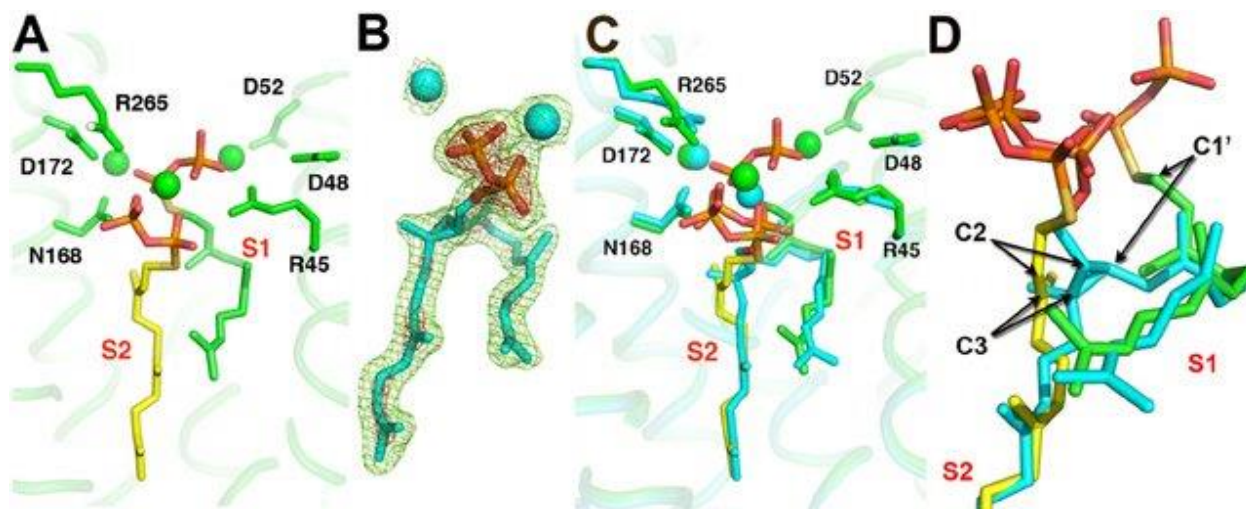


**Figure 1.38: Crystallographic data for DSQS-FSPP complex and the intermediate PSPP. (A) DSQS-FSPP complex (B) DSQS/PSPP complex (C) Superposition of A and B (D) Close-up view of A and B superposition. The arrows indicate the movements of the C1', C2, and C3 atoms. This figure is obtained from the crystallographic report on the enzyme.<sup>75</sup>**

These results are consistent with the following mechanistic scenario; S1 FPP ionizes and then reacts with the allylic double bond of the S2 FPP to form the stable intermediate cyclopropylcarbiny diphosphate PSPP. Presumably the diphosphate of PSPP flips back towards the S1 site to interact with the  $Mg^{2+}$  cluster that promotes the second ionization forming the cyclopropylmethyl carbocation, which undergoes further cationic rearrangements.<sup>75</sup>

### 1.5.3 Isopentenyl Diphosphate Isomerase (IDI) (Type 1)

#### 1.5.3.1 Introduction

Isopentenyl Diphosphate Isomerase (IDI) catalyzes the isomerization reaction that interconverts isopentenyl diphosphate (IPP) and dimethylallyl diphosphate (DMAPP) (Figure 1.39). The loss of IDI activity is fatal for organisms utilizing the MVA pathway; given that IDI is critically involved in the biosynthesis of DMAPP from IPP. But in organisms that utilize the MEP pathway, IPP and DMAPP are biosynthesized as a mixture from 4-hydroxy-DMAPP and it is believed that the IDI activity is maintained just to balance the pools of IPP and DMAPP.<sup>79</sup>



**Figure 1.39: Isomerization of DMAPP and IPP catalyzed by IDI.**

The IDI enzyme has two convergently evolved forms; type I and type II. Both forms of the enzyme are known to catalyze the same isomerization reaction; although they are architecturally different in terms of their active site arrangement and the mechanism employed in the isomerization process. The type I enzyme utilizes a protonation/deprotonation mechanism that is facilitated by the presence of two divalent metals: typically,  $\text{Zn}^{2+}$  and  $\text{Mg}^{2+}$  or  $\text{Mn}^{2+}$  (Figure 1.40).<sup>79-81</sup> In contrast, only a single divalent metal is present in the type II enzyme (IDI-2), typically  $\text{Mg}^{2+}$ , and a fully reduced flavin mononucleotide (FMN) is bound in its active site.

Based on the presence of a fully reduced FMN, it is believed that IDI-2 enzyme catalyzes the net addition or abstraction of hydrogen atoms.<sup>81</sup> As the focus of this thesis is on carbocation-generating enzymes, all further discussion will center on the type I enzyme.

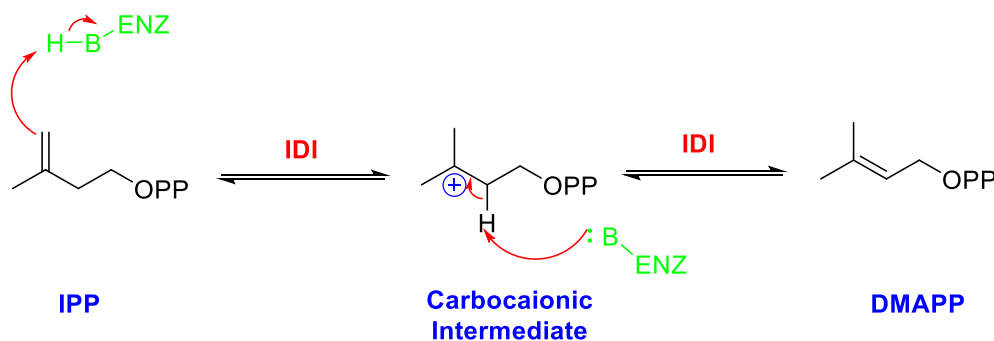


**Figure 1.40: IDI type I enzyme utilizes a protonation/deprotonation mechanism.**

### 1.5.3.2 Structural and Mechanistic Studies

Durbecq and coworkers have reported the crystal structure of IDI type I, which is composed of 182 amino acids.<sup>80</sup> The structure showed that the enzyme folds in a compact globular form that belongs to the  $\alpha,\beta$  family of proteins. In the absence of metal ions the protein's secondary structure shows three  $\beta$ -sheets going through the center surrounded by four  $\alpha$ -helices (Figure 1.41A).<sup>80</sup> The central  $\beta$ -sheet has four strands (S3, S6, S7 and S10), which possess mixed polarities, it also contains the catalytic cysteine in the S6 strand facing the H1 helix, and it is anticipated that this cysteine is involved in the protonation/deprotonation mechanism.<sup>80</sup> The other two  $\beta$ -sheets surround the central  $\beta$ -sheet and they are composed of three and two antiparallel strands (S4, S5, S11, and S8, S9, respectively). It should be noted that,

in the metal-free IDI crystal structure the first 31 N-terminal residues and many other amino acids in the 103 – 116 regions are not clearly identified in the electron-density map, and some of their side chains were disordered. But upon metal binding, the first 31 N-terminal residues become well defined and they fold into another  $\beta$ -sheet, which is small and composed of two antiparallel strands (Figure 1.41B). Moreover, the residues in the regions of 103 – 116 become well defined (Figure 1.41B).<sup>80</sup> The authors concluded that, first 31 N-terminal amino acids are probably flexible and not folded properly in the absence of metal ions.<sup>80</sup>

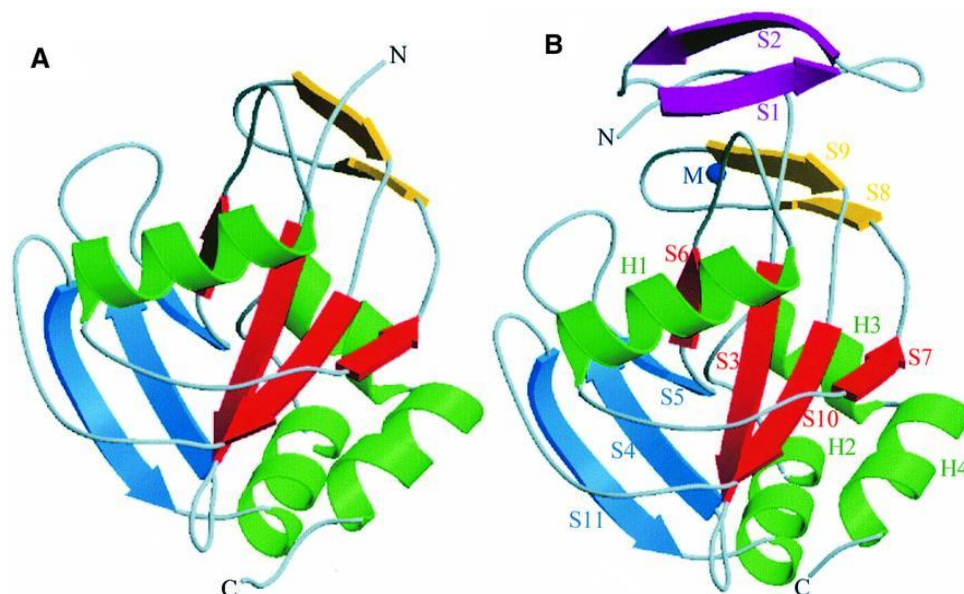


**Figure 1.41: IDI type I overall structure shown by ribbon representation of the secondary structure. (A) Shows metal-free IDI type I structure. (B) Shows metal-bound IDI type I structure, and two additional  $\beta$ -strands at the N-terminus. The metal ion is shown as (M).**

This figure is obtained from the crystallographic report on the enzyme.<sup>80</sup>

The metal binding promotes conformational changes that create a distorted octahedral metal coordination site containing the residues H25, H32, H69, E114 (which has both of its carboxylate oxygens participating in the metal coordination site) and E116 (Figure 1.42).<sup>80</sup> Moreover, a deeply buried cavity was formed in the active site as a result of these conformational changes. It is believed that such a cavity is designed by the enzyme to protect the highly reactive tertiary carbocation, and to shield it from water.<sup>80</sup>

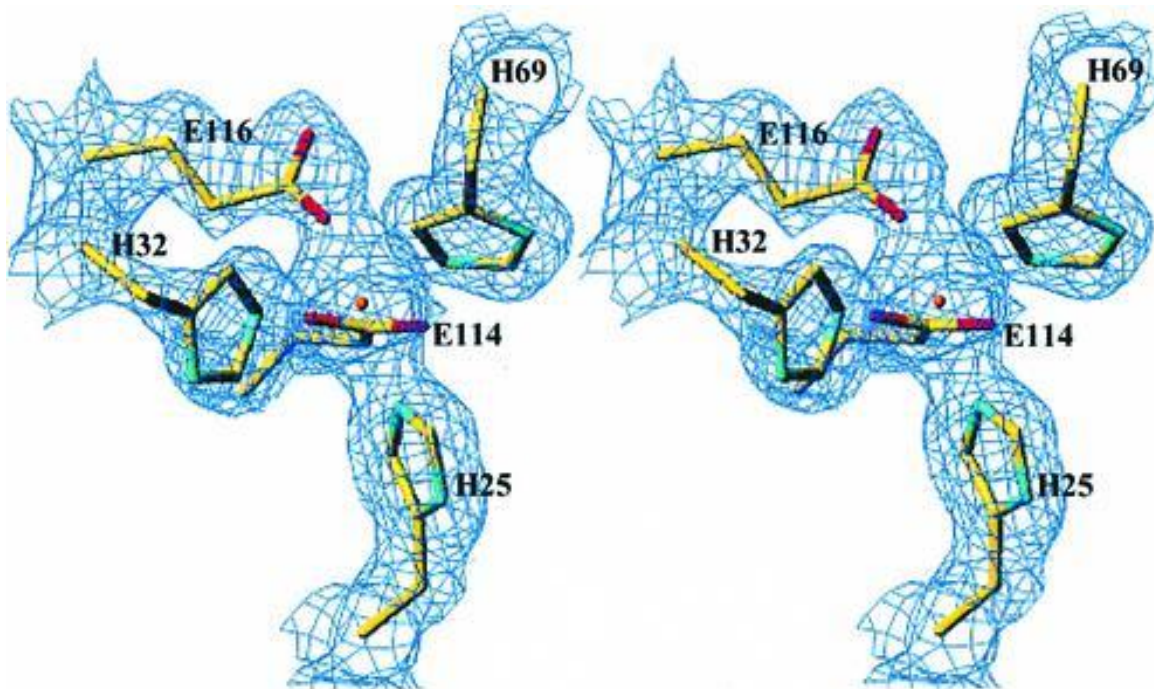


**Figure 1.42: A stereoview of a distorted octahedral metal coordination sphere in the active site, formed by H25, H32, H69, E114 and E116. This figure is obtained from the crystallographic report on the enzyme.<sup>80</sup>**

An inspection of the active site shows that C67 and E116 are the only available residues that could participate in the protonation/deprotonation step.<sup>80-83</sup> The C67 residue can initiate the reaction via protonation of the double bond (C-4) of the IPP substrate, generating the highly reactive tertiary carbocation intermediate (Figure 1.43). This cation could be electrostatically stabilized by the E116 carboxylate, which could then participate in the final deprotonation of the carbocation intermediate forming the final product, DMAPP (Figure 1.43).<sup>80</sup> Site-directed mutagenesis studies on E116 supported its proposed role in catalysis.<sup>80</sup>

The indole ring of tryptophan 161 is also thought to help stabilize the tertiary carbocation via quadrupole-charge interactions (Figure 1.43).<sup>79,80,84</sup> Site-directed mutagenesis studies showed that replacing the tryptophan 161 residue with phenylalanine 161F produced an inactive mutant.<sup>80</sup> These results agree with the suggestion that the tryptophan residue is not only there to define the active site borders but also has a role in stabilizing the carbocation during catalysis.<sup>81</sup>

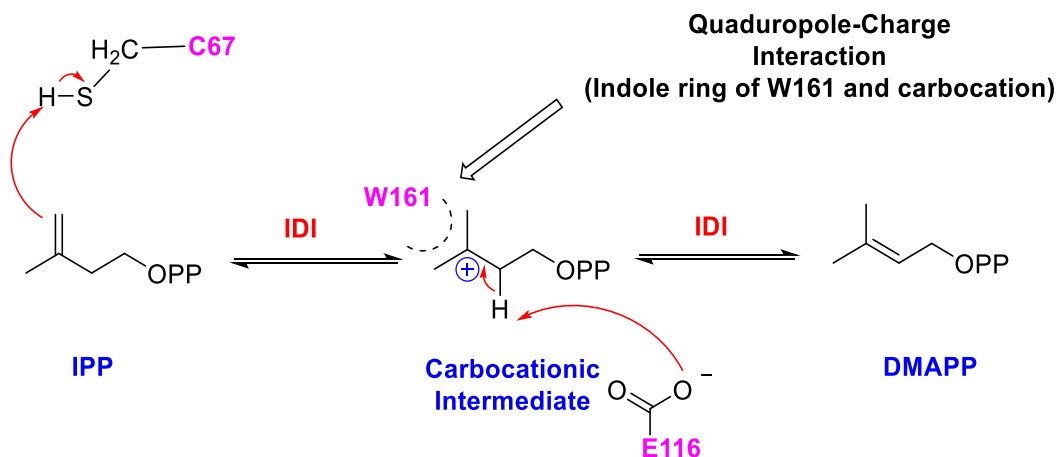


**Figure 1.43: Proposed mechanism of IDI type I.**

Extensive studies by Poulter and coworkers concluded that the isomerization reaction catalyzed by IDI proceeds by a stepwise protonation-deprotonation reaction mechanism involving a tertiary carbocation intermediate (Figure 1.40). They found that upon running multiple turnovers of the isomerization reaction in D<sub>2</sub>O buffer, there was a rapid exchange of one of the hydrogens at C-2, and both of the hydrogens at C-4, in IPP, as well as all three of the *E*-methyl hydrogens in DMAPP (Figure 1.44). These results are consistent with the proposed protonation/deprotonation mechanism and show that the enzyme selectively deprotonates the *pro-R* position of the carbocation intermediate.

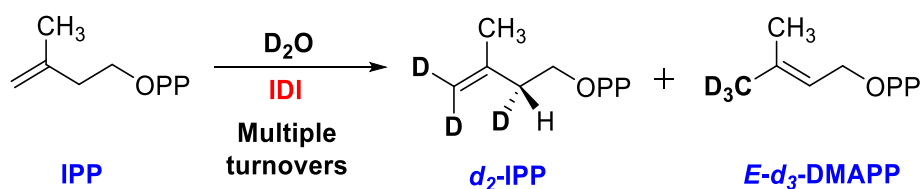


**Figure 1.44: Labelling experiment on the reaction catalyzed by IDI.**

In 1986, Reardon and Abeles reported the inactivation of IDI with the thiol-selective reagent iodoacetamide, and they found that the rate of inactivation of the enzyme was dependent on an ionizable group that has a pK<sub>a</sub> of 9.3.<sup>85</sup> Their finding suggested the presence of a protonated cysteine that may act as a catalytic acid. In addition, Street *et al.* reported in 1994 a reduced activity of the IDI enzyme upon replacing C67 with a serine residue, presumably because of the higher pK<sub>a</sub> of the serine hydroxyl.<sup>82,83</sup> In 2004, Poulter and coworkers also reported site-directed mutagenesis studies that showed replacing cysteine with alanine or valine abolished enzymatic activity.<sup>86</sup>

Abeles and Poulter independently tested the inhibitory effect of inhibitor **48** (nitrogen isopentenyl diphosphate analogue).<sup>85,87</sup> The ammonium-containing inhibitor, **48**, provides a close mimic to the carbocationic intermediate, as it places a positively charged nitrogen atom in an analogous position to the putative carbocation intermediate (Figure 1.45). They found that inhibitor **48** effectively behaved as an irreversible inhibitor of isopentenyl diphosphate isomerase.<sup>87</sup> Later studies by Poulter and coworkers confirmed that this compound was actually a non-covalent reversible inhibitor of the enzyme with a very tight binding constant ( $K_{dis} = 120$  pM) ( $K_{dis}$  was calculated from  $K_{dis} = \frac{k_{off}}{k_{on}}$ ).<sup>88</sup>

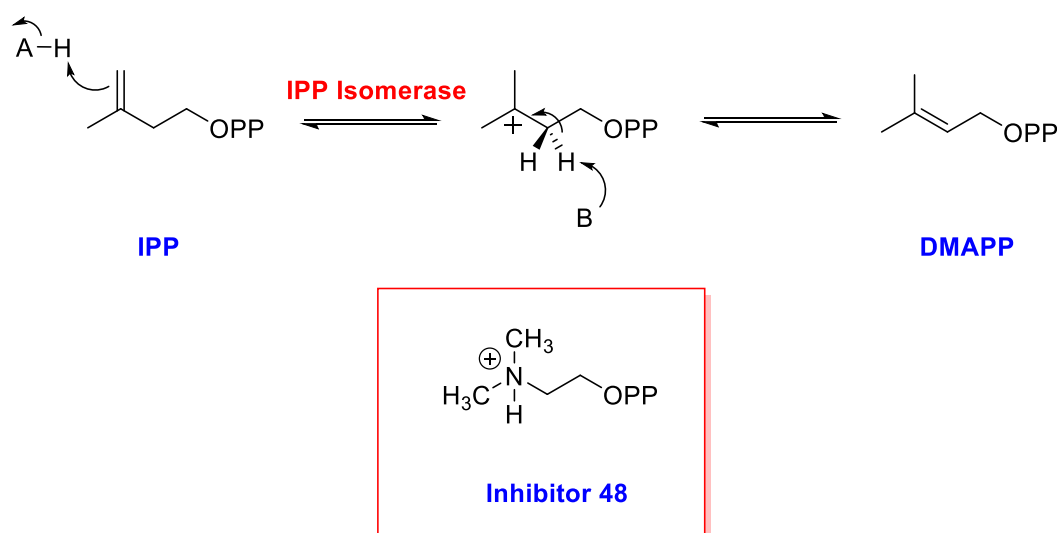


**Figure 1.45: Mechanism of the isomerization reaction employed by IDI (the inset shows the structure of inhibitor 48).**

The inhibition of isopentenyl diphosphate isomerase (IDI) by inhibitor **48** provides strong evidence for the presence of a carbocation intermediate. The notable potency of inhibitor **48** suggests that electrostatic interactions are of great importance with this enzyme. It is likely that during catalysis, a negatively charged residue (such as E116) in the active site of the enzyme stabilizes the carbonium ion.<sup>81,83,87,89</sup> Poulter and coworkers analyzed the metal ions in the complex of IDI with inhibitor **48**.<sup>81</sup> The X-ray crystal structure showed the presence of two metal ions. Moreover, the crystal structure reveals the critical roles that the metal ions play during catalysis. It is found that a magnesium metal ion coordinates to the diphosphate of the substrate to promote its binding to the enzyme active site, while zinc (or manganese) organizes the structure of the protein as well as coordinates to the E116 residue, thereby lowering the pKa of its carboxyl group (Figure 1.46).<sup>81</sup>

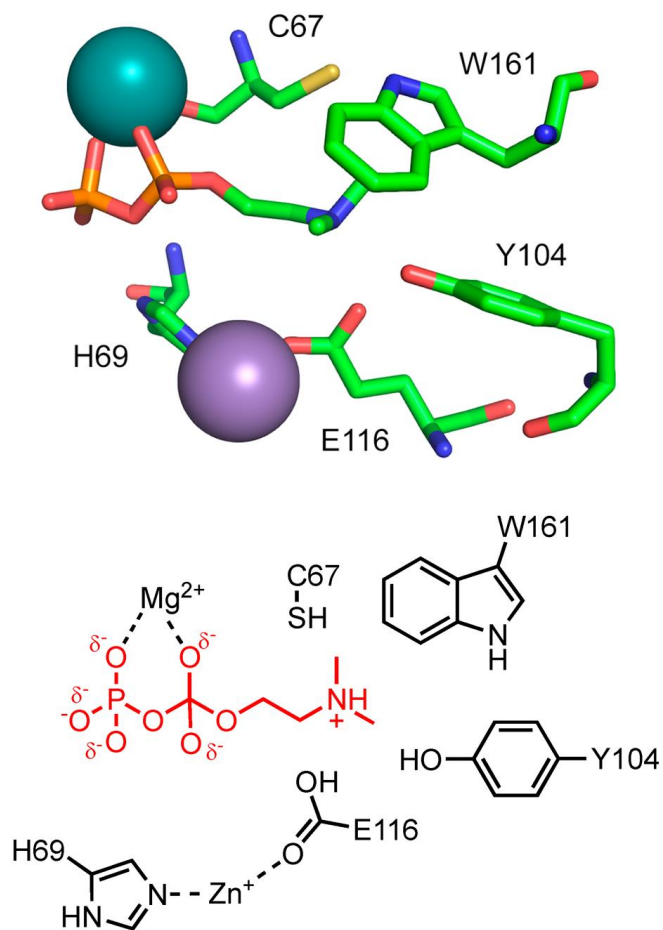


**Figure 1.46: Structure of inhibitor 48 bound to the active site of *E. coli* IDI. The lower diagram outlines the role of the metal ions in catalysis.** This figure is obtained from the crystallographic report on the enzyme.<sup>89</sup>

## **1.6 Inhibition of Carbocation-Forming Enzymes using Transition State-Analogues**

The focus of this thesis is on the design and synthesis of positively-charged inhibitors that mimic the transition state/intermediate formed with allylic diphosphate utilizing-enzymes. Therefore, in this section we will provide a brief overview on transition state-analogues used as inhibitors of carbocation-forming enzymes. These inhibitors tend to have a great affinity for their respective enzyme since they are electronically and structurally similar to the transition states/intermediates, yet are stable in solution. Since enzymes have evolved to tightly bind to the transition states during the enzymatic reactions, these compounds are expected to be potent inhibitors of the enzyme. Such strategies have been employed to inhibit a variety of enzymes that include glycosidases, isomerases, cyclases and prenyltransferases.<sup>90</sup>

### **1.6.1 Inhibition Studies of Glycosidases**

Glycosidases encompass a huge family of mechanistically related enzymes that catalyze the hydrolysis of glycosidic bonds in complex sugars, whereupon, a sugar hemiacetal is formed with either a retention of the anomeric configuration (in the case of so-called retaining glycosidases) or less commonly an inversion of the anomeric configuration (in the case of inverting glycosidases) (Figure 1.47).<sup>90,91</sup>

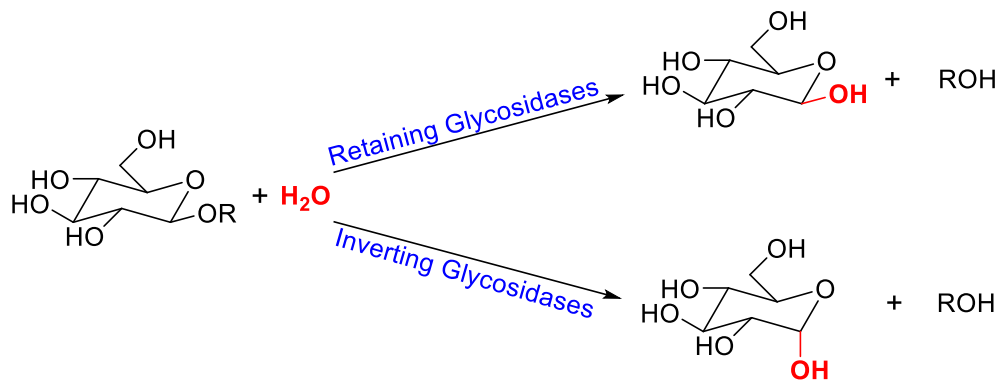


**Figure 1.47: Reactions catalyzed by retaining and inverting glycosidases.**

Extensive research has been directed towards the study and development of new glycosidase inhibitors, as enzyme-catalyzed hydrolysis of polysaccharides is a widespread biological process.<sup>90,91,91-93</sup> Glycosidase inhibitors have many potential applications as agrochemicals and pharmaceuticals. In addition, they can play a vital role in probing the mechanisms and structures of glycosidases.<sup>91</sup>

Koshland has proposed that, in retaining glycosidases, the hydrolysis of substrates takes place through a double-displacement mechanism involving the formation of a covalent bond with an enzyme residue (Figure 1.48). Alternatively, a single-displacement mechanism is employed by inverting glycosidases, in which a water molecule displaces the aglycon portion through a nucleophilic attack (Figure 1.49). It is anticipated that each step in the mechanism proceeds via an oxocarbenium ion-like transition state.<sup>91,94</sup>

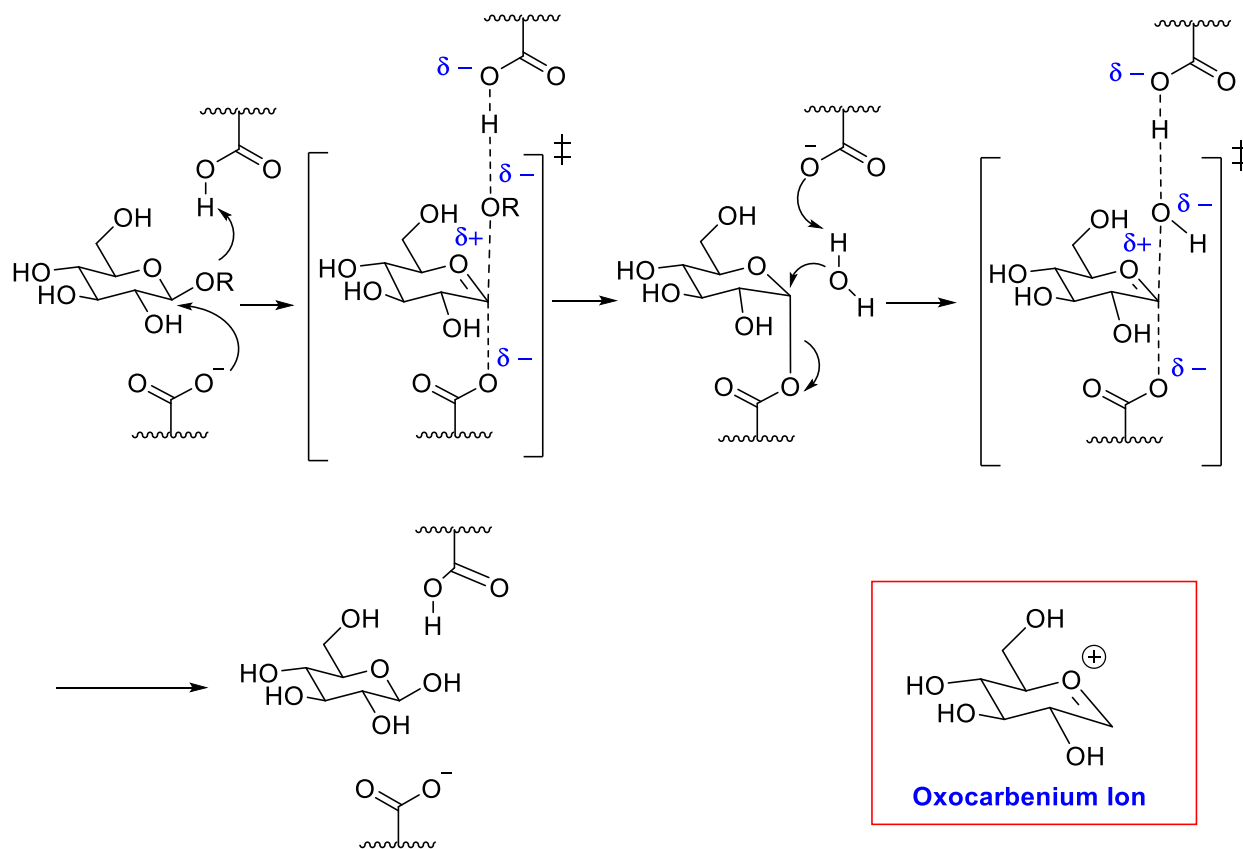


**Figure 1.48: Catalytic mechanism employed by retaining glycosidases. (The inset shows the structure of an oxocarbenium ion).**

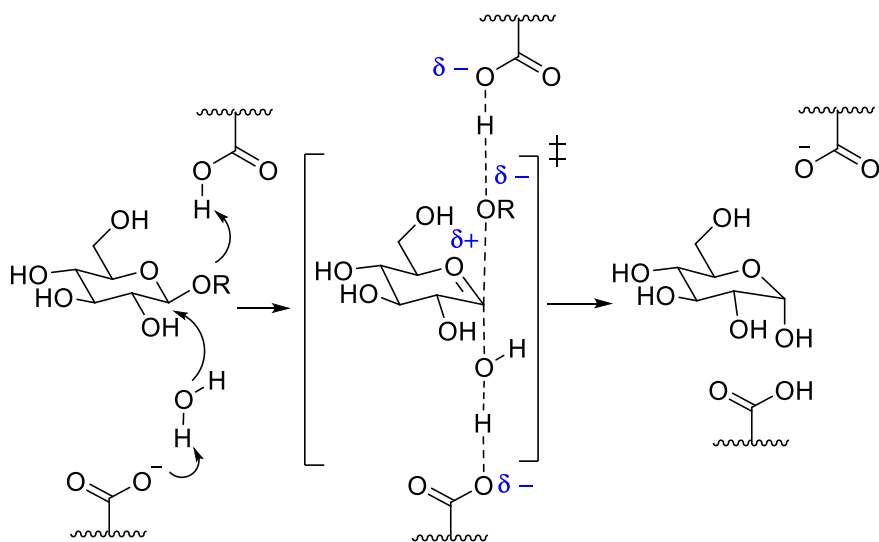


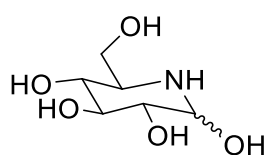
**Figure 1.49: Catalytic mechanism employed by inverting glycosidases.**

As mentioned previously in section 1.6, transition state analogues are expected to have high affinity for the enzyme and thus be potent inhibitors. This notion has led to the synthesis of several inhibitors bearing a positive charge that mimics the oxocarbenium ion. In some cases, a flattened chair structure is also incorporated into the design.

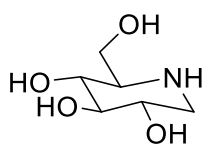
### 1.6.1.1 Amino-Sugars as Transition State-Analogues of Glycosidases

To better mimic the oxocarbenium ion, several potent glycosidase inhibitors have been designed with a basic nitrogen atom in their chemical structures (Figure 1.50). A pivotal example is nojirimycin, a natural product isolated from *Streptomyces* and the first N-glucose analogue.<sup>90,91,94</sup> It acts as a potent inhibitor of both the  $\alpha$ -, and  $\beta$ -glucosidases of numerous organisms.<sup>95</sup> A more stable deoxy-analogue of nojirimycin, which was isolated from the roots of the mulberry

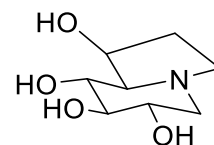
tree and lacks the anomeric OH, is 1-deoxynojirimycin, which acts as an inhibitor of  $\alpha$ -glucosidases.<sup>96</sup> Castanospermine, which was extracted from the seeds of the Australian plant *Castanospermum australe*, is yet another potent inhibitor of  $\alpha$ -glucosidases (Figure 1.50).<sup>97</sup> Extensive research has been directed towards the preparation of new derivatives of the above natural amino-sugars with increased potency. For example, *N*-Butyl-1-deoxynojirimycin (Zavesca) and *N*-hydroxyethyl-1-deoxynojirimycin (Miglitol) are *N*-alkylated derivatives of deoxynojirimycin that have been demonstrated to be exceedingly biologically active: both are clinically used drugs against type I Gaucher disease and type II diabetes, respectively (Figure 1.50).<sup>92,98</sup>



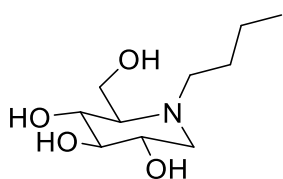
**Nojirimycin**



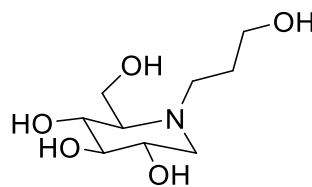
**Deoxynojirimycin**



**Castanospermine**



**Zavesca**

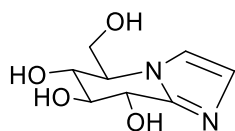


**Miglitol**

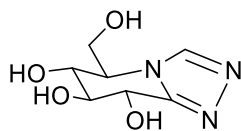
**Figure 1.50: Structures of amino-sugars (in their neutral form) used as glycosidase inhibitors.**

Owing to their  $sp^3$ -hybridized anomeric carbon atom, polyhydroxylated piperidines possess minimal conformational similarity to the  $sp^2$ -hybridized oxocarbenium ion; nevertheless, it is anticipated that binding is facilitated by favorable electrostatic interactions with negatively charged, catalytically relevant, carboxylate residues in the enzyme active site. Polyhydroxylated piperidines exist as their conjugate acids at physiological pH, and the ammonium ions serve as a close mimic to the developing charge of an oxocarbenium ion-like transition state.<sup>92</sup>

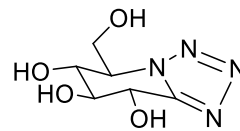
The preparation of even more potent piperidine derivatives was achieved by further modifications of the amino sugar inhibitors mentioned above. Glucose-derived fused imidazoles, triazoles, and tetrazoles (Figure 1.51) are derivatives of polyhydroxylated piperidines fused with aromatic rings: imidazole, triazole, and tetrazole rings, respectively. These inhibitors were found to be potent inhibitors of  $\beta$ -glucosidase from almonds with  $K_I$  values of 0.1, 19, and 150  $\mu\text{M}$ , respectively.<sup>92,98-100</sup> These glucose-derivatives are likely transiently protonated to bear a positive charge and mimic the oxocarbenium-like transition state. The  $sp^2$ -hybridized nitrogen in these compounds serves to mimic the flattened conformation of an oxocarbenium ion.<sup>92</sup>



Imidazole analogue



Triazole analogue



Tetrazole analogue

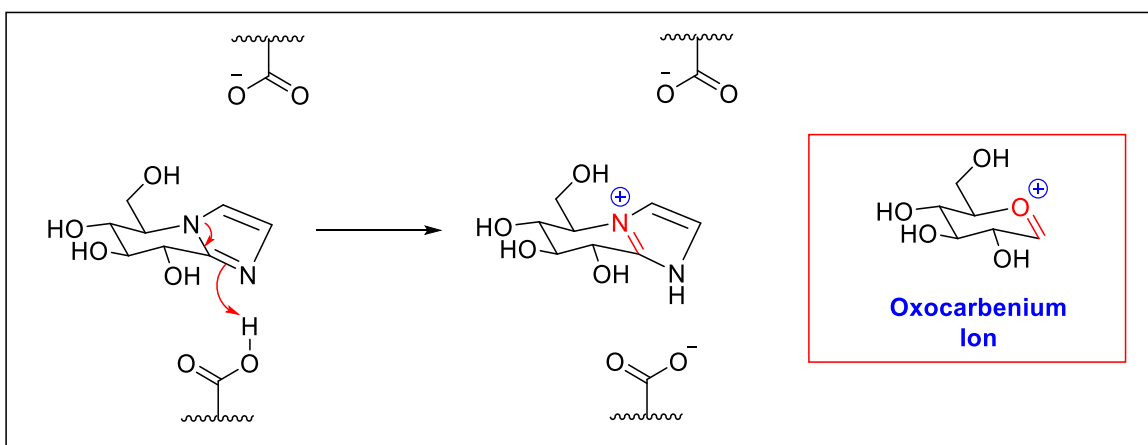


**Figure 1.51: Structures of the imidazole, triazole, and tetrazole analogues of amino-sugar inhibitors. (The inset illustrates the protonation of the imidazole by a catalytic carboxylic acid residue).<sup>100</sup> The structure of the oxocarbenium ion is given to compare with the protonated imidazole.**

### 1.6.2 Inhibition Studies of Isomerases: Isopentenyl Diphosphate Isomerase

Several non-carbohydrate handling enzymes that generate discrete carbocationic intermediates were found to be inhibited with ammonium-containing inhibitors.<sup>90</sup> One of these enzymes, isopentenyl diphosphate isomerase (IDI), which was discussed in section 1.5.3. The isomerase enzyme (IDI) was found to be inhibited by inhibitor **48** (with a  $K_{dis}$  value of 120 pM).

<sup>85,87</sup> The appropriately positioned positively charged nitrogen atom makes inhibitor **48** a good mimic to the intermediate carbocation (Figure 1.52).<sup>85</sup>

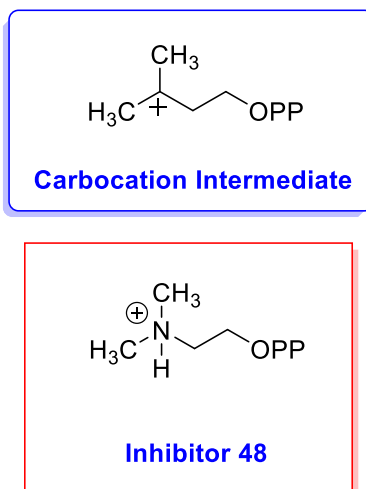


**Figure 1.52: Top box show the structure of the carbocation intermediate formed by IPP and the bottom box shows the structure of inhibitor 48.**

### 1.6.3 Inhibition Studies of Prenyltransferases: Geranylgeranyl Diphosphate Synthase

Geranylgeranyl diphosphate synthase (GGPPS) from rat liver is an interesting example that highlights the application of nitrogen-containing inhibitors. GGPP synthase catalyzes the biosynthesis of geranylgeranyl diphosphate (GGPP), which involves the condensation of farnesyl diphosphate (FPP) with isopentenyl diphosphate (IPP) (Figure 1.53). Steiger and coworkers have designed inhibitor **49** to mimic the GGPP synthase reaction intermediate (Figure 1.53).<sup>101</sup> As shown below, inhibitor **49** mimics the positive charge on the tertiary carbocation intermediate, as

it almost certainly binds in its conjugate acid form. When tested against GGPP synthase, this competitive inhibitor showed more than 90% inhibition at a concentration of 0.9  $\mu\text{M}$ .<sup>101</sup>

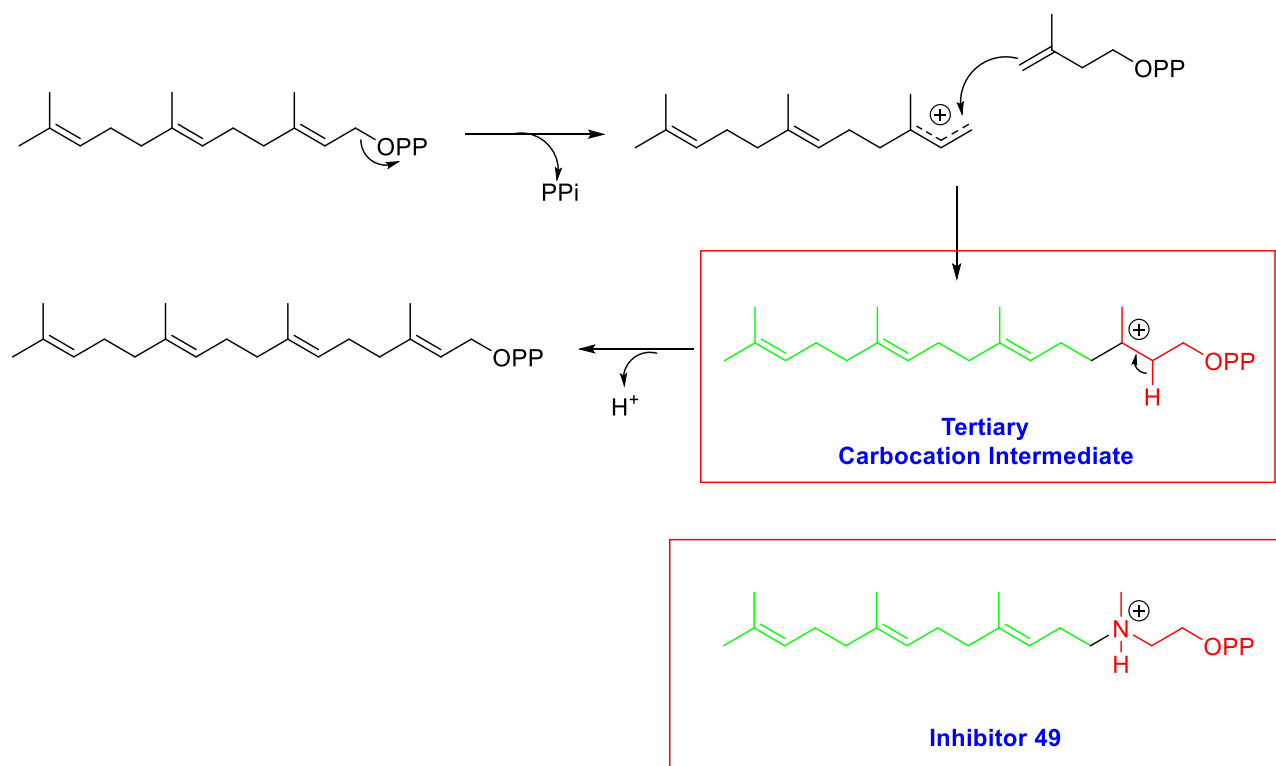


**Figure 1.53: Catalytic mechanism of geranylgeranyl diphosphate synthase (GGPPS). The top inset shows the tertiary carbocation formed in the reaction catalyzed by GGPPS. The bottom inset shows the protonated form of inhibitor 49**

## 1.6.4 Bisphosphonates

Bisphosphonates (BPs) were first developed as complexing agents in the fertilizer and oil industries, they were also commonly used as anticorrosive agents.<sup>102</sup> In the late 1960s, bisphosphonates were explored as therapeutic agents, and it was found that they can be used as a treatment for bone-related diseases. They help prevent the bone-mass loss associated with many diseases, such as Paget's disease of the bone, and osteoporosis. The methylene bisphosphonates, also referred to as bisphosphonates (BP's), are pyrophosphate analogues, wherein the bridging oxygen atom has been replaced with a methylene group (Figure 1.54).<sup>103-107</sup>

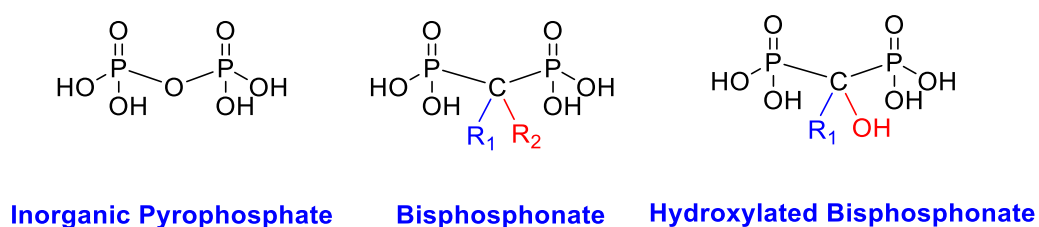


**Figure 1.54: Structures of pyrophosphate, bisphosphonate and the hydroxylated bisphosphonate.**

Interestingly, this replacement allows the possibility of installing two different side chains, R<sub>1</sub> and R<sub>2</sub>, on the bridging carbon. Hydroxylated BPs are known for their great affinity for bones as they bind the bone calcium ions using their hydroxyl and their two phosphate groups, thereby forming what is known as tridentate "Bone Hook".<sup>108</sup> Eventually, the incorporation of a basic amino alkyl group onto the BP's backbone introduced a new member to

the BP family, known as Nitrogen-containing Bisphosphonates (N-BPs). Examples of the N-BPs are alendronate and ibandronate, which are in current clinical use for treatment of osteoporosis (Figure 1.55).<sup>102,108,109</sup>

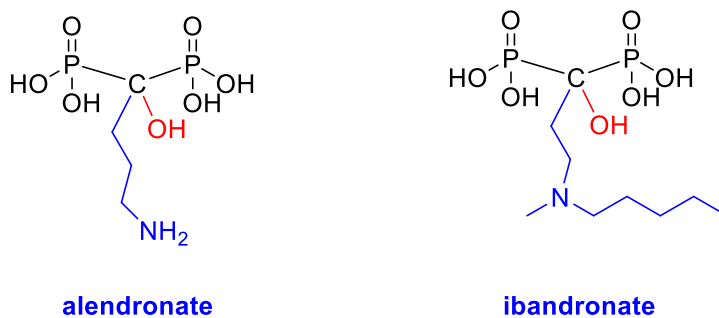


**Figure 1.55: Structures of common nitrogen-containing bisphosphonates (N-BPs).**

Although their mechanism of action was not known until the early 2000s, bisphosphonates were used for over 30 years as a treatment for different bone resorption diseases.<sup>109–113</sup> After their mechanism of action came to light in the early 2000s, it was confirmed that bisphosphonates target osteoclasts at the cellular level, whereas: at the molecular level, they inhibit farnesyl diphosphate synthase (FPPS) and geranylgeranyl diphosphate synthase (GGPPS).<sup>102</sup> The most potent of these are N-BPs and it is thought that the protonated amines mimic carbocation intermediates formed during catalysis and aid in binding.

Inhibition of these enzymes results in decreased prenylation of proteins (such as the previously mentioned oncogenic Ras proteins), a disruption of intercellular signaling, and eventual cell death. Drawback of bisphosphonates is their low bioavailability, which is a consequence of their poor cell-membrane permeability due to their highly charged nature.<sup>108</sup> In addition, BPs have a very short lifetime in the bloodstream resulting from their tight interactions with bone minerals. To deal with these problems, compounds BPH-811 and BPH-703 were synthesized, wherein the hydroxyl groups in risedronate and zoledronate were removed and hydrophobic side chains were appended to the aromatic amine (Figure 1.56). These modifications helped increase the lipophilicity of the new bisphosphonates, resulting in greater cellular uptake and less affinity for bone minerals. This latest finding opens the possibility of using these modified bisphosphonates in cancer chemotherapy.<sup>102,114,115</sup>

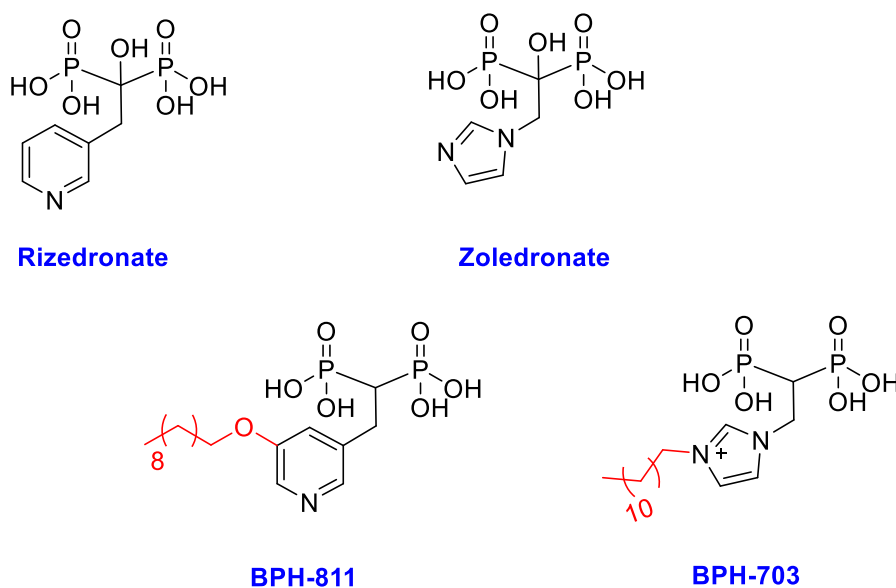


**Figure 1.56: Structures of bisphosphonates and their novel lipophilic analogues.**

## 1.7 Thesis Goals

This thesis will focus on the development of a general inhibition strategy that can be applied to prenyltransferases and other enzymes that generate carbocation intermediates from allylic diphosphates. Our approach will be to use a guanidinium group as a mimic of an allylic carbocation. In prior work in the Tanner lab, attempts were made to synthesize inhibitor **1** (Figure 1.57). This inhibitor contains a guanidinium moiety appended to a pyrophosphate analogue that is designed to mimic the transition state/intermediate formed with allylic diphosphate utilizing-enzymes.

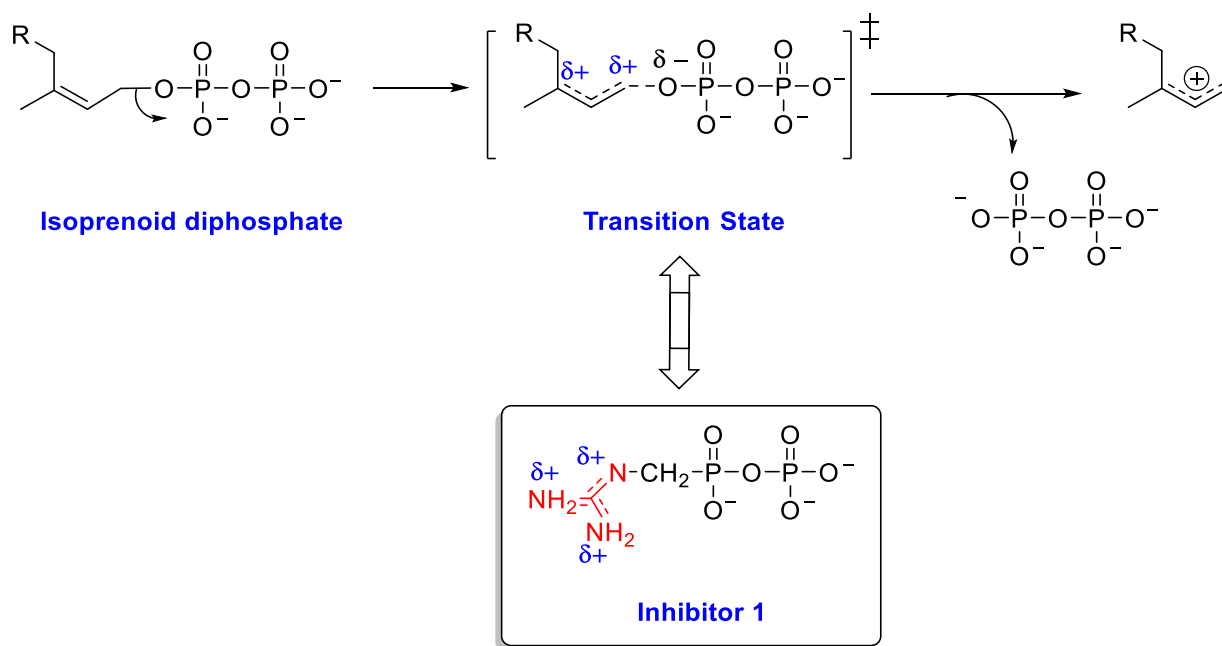


**Figure 1.57:** Scheme showing ionization of a prenyl diphosphate substrate. The inset shows the structure of inhibitor **1**, and comparison between inhibitor **1** and the putative transition state.

Unfortunately, inhibitor **1** suffered from instability and decomposed upon extended handling (explained in detail in chapter two), so work on inhibitor **1** was discontinued. In **Chapter Two**, we describe the synthesis of a DMAPP mimic, inhibitor **2**, in which the phosphorous atoms are bridged by a methylene group instead of an oxygen (Figure 1.58). This imparts total stability towards hydrolysis. We tested this inhibitor as a DMAPP analogue in the enzymatic reaction catalyzed by human farnesyl diphosphate synthase (HFPPS). To test the effectiveness of incorporating a guanidinium moiety into inhibitors of human farnesyl diphosphate synthase, three potential inhibitors were prepared. Inhibitor **2** has a guanidinium moiety appended onto a pyrophosphate analogue, thus introducing a planar, delocalized cation in a position analogous to that of the putative allylic carbocation in the active site of the FPPS. To further test for the importance of the delocalized positive charge, inhibitors **3** and **4** were prepared. Inhibitor **3** has the positive charge, but it is localized on a single atom, while inhibitor **4** is isosteric to inhibitor **1** but it lacks a positive charge.

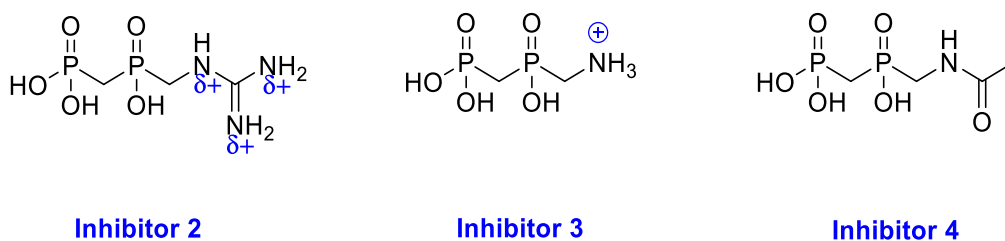


**Figure 1.58: The structures of inhibitors 2, 3 and 4.**

In **Chapter Three**, the design and synthesis of extended guanidinium and amidinium inhibitors with appended alkyl chains are described. They are tested as inhibitors of two enzymes that utilize farnesyl diphosphate (FPP) as a substrate (Figure 1.59), human squalene synthase (HSQS) and bacterial dehydrosqualene synthase (DSQS).

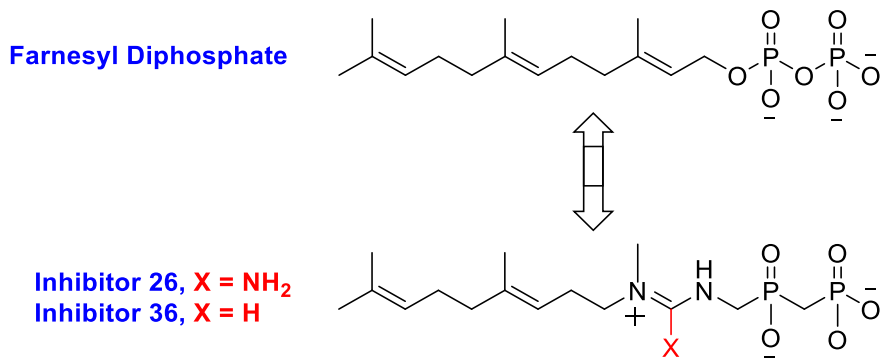


**Figure 1.59: The structures of farnesyl diphosphate, inhibitors 26 and 36.**

Inhibitor **26** contains a guanidinium as an allylic carbocation mimic, whereas amidinium inhibitor **36** (made by another PhD student in the lab) contains a positive charge that is delocalized over two nitrogen atoms, instead of three. It was anticipated that inhibitor **36** would benefit through the removal of the extra amine group, as it mispositions a portion of the positive charge and might cause steric hindrance in the enzymatic active site. Inhibitor **34**, a neutral urea analogue, was synthesized as a control (Figure 1.60)

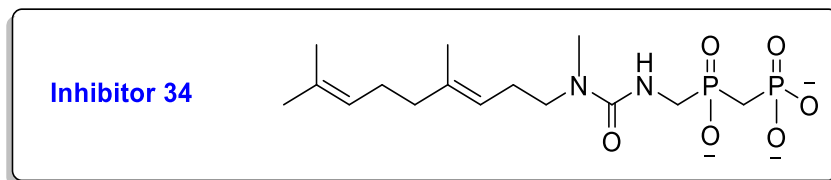


**Figure 1.60: Structure of Inhibitor 34, negative control.**

Finally, ammonium containing compounds have been reported to be effective inhibitors of enzymes that proceed via non-resonance-stabilized carbocationic intermediates. Since our guanidinium-based inhibitors bear a planar cation, they may be more effective at mimicking a carbocation than an  $sp^3$ -hybridized ammonium-based inhibitor. Our inhibitory strategy can therefore be tested on enzymes that also proceed via a non-resonance stabilized tertiary carbocationic intermediates.<sup>85</sup> In **Chapter Four** the efficacies of our positively charged guanidinium-based inhibitor **2** and inhibitors **3** and **4** are tested against isopentenyl diphosphate isomerase (IDI).

## Chapter 2: Design, Synthesis and Evaluation of Guanidinium based inhibitors of Human Farnesyl Diphosphate Synthase (HFPPS)

### 2.1 Introduction

Despite the fact that bisphosphonate inhibitors were originally used to treat bone-related diseases, as discussed in section 1.6.4, recent studies revealed that bisphosphonates might also be used to treat cancer.<sup>102</sup> This is due to their ability to inhibit prenyltransferase enzymes, such as farnesyl diphosphate synthase (FPPS) and geranylgeranyl diphosphate synthase (GGPPS).<sup>24,106,111,116</sup> In theory, the inhibition of the FPPS and GGPPS enzymes might be more effective than the direct inhibition of FTase, since inhibition of these enzymes would deplete the substrate (FPP) used in protein prenylation via protein farnesyltransferase (FTase).<sup>102</sup> Since nitrogen-containing bisphosphonates are known for their metal binding affinity, and they are thought to mimic the putative allylic carbocation substrate formed by the FPPS enzyme, using them as inhibitors for this enzyme has proven to be effective.<sup>102,114</sup> However, there are some drawbacks to the use of bisphosphonates in that they are poorly bioavailable due to their affinity to bone. Therefore, alternative inhibitors against allylic diphosphate synthases are desirable.<sup>14,106,106,107,109</sup>

In this chapter we will prepare an inhibitor that resembles DMAPP in structure, but bears a planar delocalized cation that is designed to mimic an allylic carbocation. This inhibitor will be tested against the reaction catalyzed by farnesyl diphosphate synthase (FPPS), which is an

important enzyme in the mevalonate pathway that plays a vital role in many biological processes (Figure 2.1).

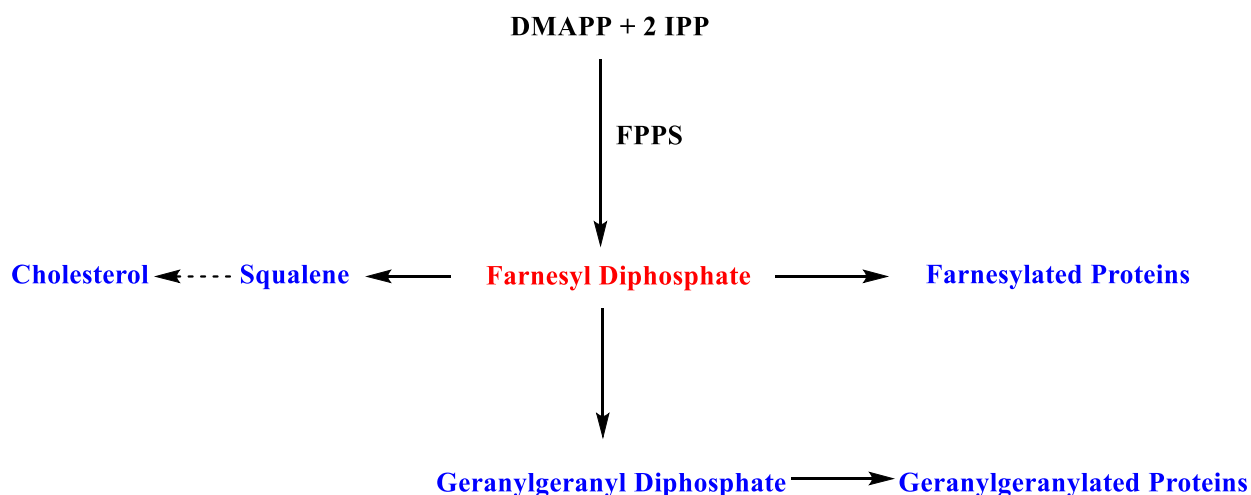


**Figure 2.1: Scheme showing how FPP is involved in the biosynthesis of many vital biological molecules.**

## 2.2 Design of Inhibitors

Previously in the Tanner lab, a former PhD student Niusha Mahmoudi worked on the synthesis of the 1<sup>st</sup> generation of our proposed prenyltransferase inhibitors. Inhibitor **1** contained a guanidinium moiety attached to a phosphoryl phosphonate group.<sup>117</sup> The compound could be prepared but was never isolated in a pure form, as it co-eluted with phosphate during ion-exchange chromatography. In addition, the compound was unstable, since traces of a guanidinium phosphonate impurity and either pyrophosphate or phosphate accumulated upon extended handling of the compound. This is due to the phosphorolysis and hydrolysis of the P-O-

P linkage, respectively (Figure 2.2). It was suggested that the positively charged guanidinium facilitated attack at the terminal phosphate and displacement of the guanidinium phosphate.

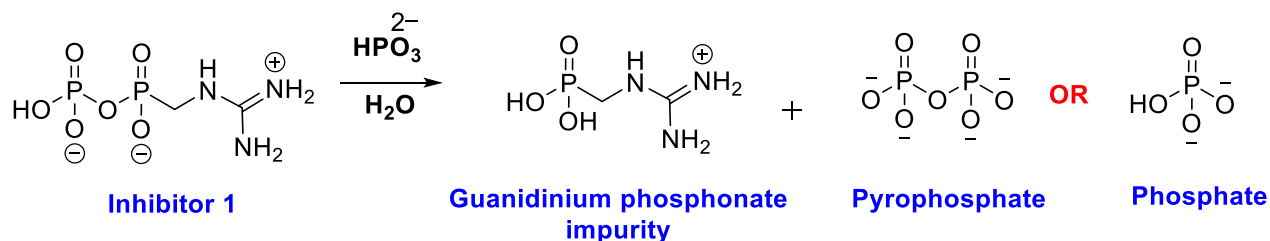


**Figure 2.2: Scheme showing the phosphorolysis and hydrolysis of the P-O-P linkage in inhibitor 1.**

Due to the instability problems with inhibitor 1<sup>117</sup>, we designed another analogue (Inhibitor 2) in which the phosphoryl phosphonate P-O-P linkage is replaced with a non-hydrolyzable phosphinyl phosphonate P-CH<sub>2</sub>-P linkage (Figure 2.3). To test our inhibition strategy against human farnesyl diphosphate synthase (HFPPS), three potential inhibitors were synthesized: inhibitors 2, 3 and 4. Inhibitor 2, containing a guanidinium moiety attached to a diphosphate analogue, was designed to mimic the transition state for the ionization of dimethylallyl diphosphate (DMAPP) into an allylic carbocation and pyrophosphate. This inhibitor bears a positive charge delocalized over three nitrogen atoms in a planar arrangement. To test for the effectiveness of a guanidinium functionality, inhibitor 3 was prepared (Figure 2.4). Inhibitor 3 contains an amine group instead of the guanidinium group: it bears the positive charge but lacks charge-delocalized atoms and the planarity of inhibitor 2. Inhibitor 4, a neutral

control, and an isosteric analogue of inhibitor 2, was prepared to test for the necessity of the positive charge.

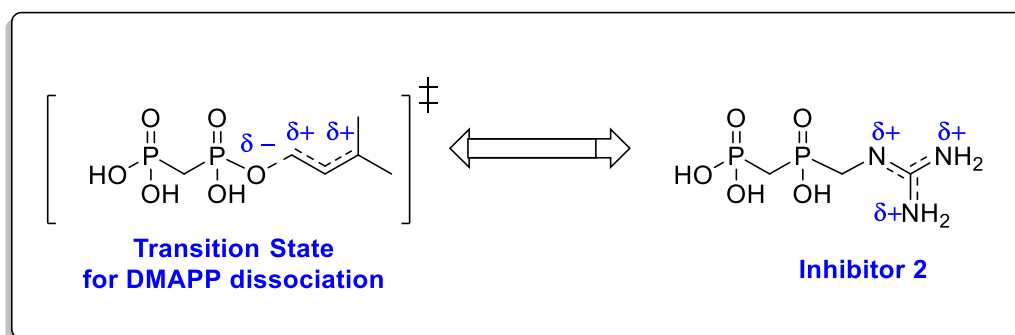


**Figure 2.3:** The structure of the transition state formed in the reaction catalyzed by FPPS on the left, and the structure of inhibitor 2 is shown on the right.

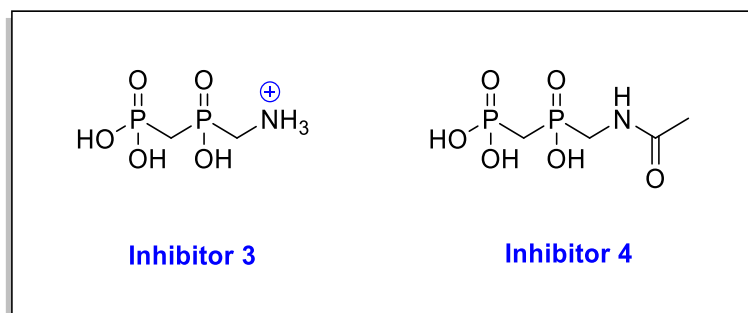


**Figure 2.4:** The structures of inhibitors 3 and 4

## 2.3 Synthesis of Inhibitors 2 – 4

### 2.3.1 Attempts towards the Synthesis of Inhibitor 2: Pathway A



Figure 2.5: Structure of inhibitor 2.

Inhibitor **2** (Figure 2.5) was synthesized from the literature known amine **12**, which was synthesized using the following synthetic route (Figure 2.6).<sup>118</sup>

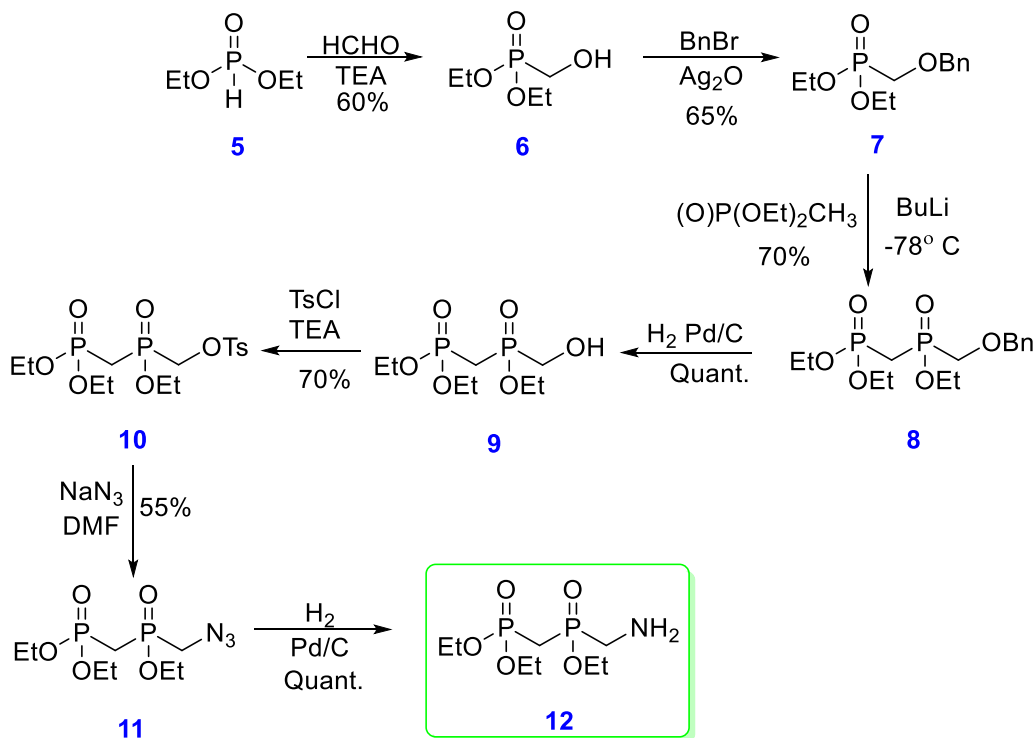
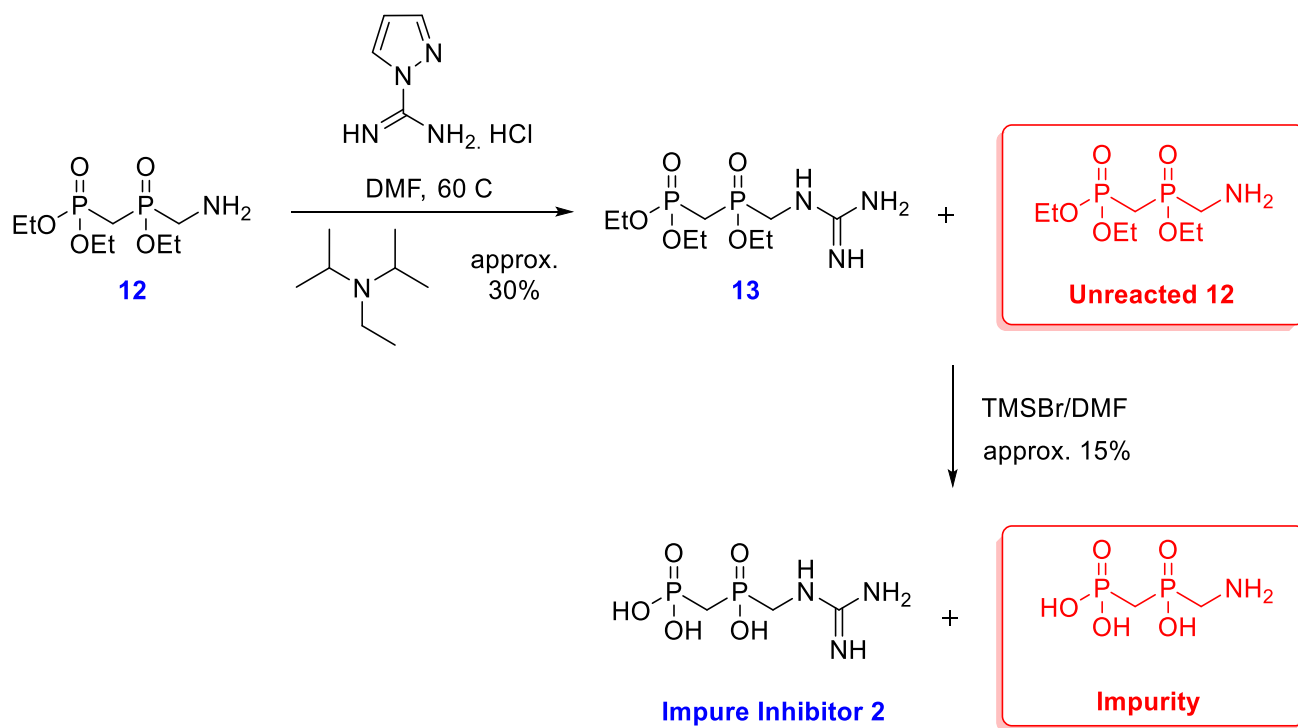


Figure 2.6: Literature-known synthetic route of amine **12**.<sup>118</sup>

Alcohol **9** was synthesized in gram quantities starting from diethyl phosphite **5** in a four-step sequence. Addition of formaldehyde to diethyl phosphite **5** gave alcohol **6**. Protection of the hydroxymethyl group with benzyl bromide/silver (I) oxide yielded **7**. The latter was coupled with lithiated diethyl methylphosphonate to give compound **8**. Deprotection of compound **8** by catalytic hydrogenation gave alcohol **9**. Compound **9** then reacted with tosylchloride in the presence of triethylamine to give tosylated compound **10**. Treatment of compound **10** with sodium azide in DMF at 60 °C gave compound **11** which was then converted to amine **12** by catalytic hydrogenation. <sup>118</sup>

To form the guanidine functionality, amine **12** was treated with the guanidinylation reagent, 1H-pyrazole-1-carboxamide-hydrochloride, to yield guanidine **13** which was found to be accompanied with some unreacted amine **12** as an impurity (Figure 2.7). <sup>119</sup>



**Figure 2.7: First route towards inhibitor 2.**

In spite of several attempts to optimize this route, this reaction never went to completion and was always low yielding. We first let the reaction run for a longer time (up to 48 hours), but these conditions never forced the reaction to completion. Secondly, we raised the reaction temperature to 90 °C, but this alteration led to decomposition of the formed guanidine and the formation of many other impurities according to mass spectrometry and NMR. All attempts to purify the product by column chromatography failed, due to its polarity and the low yield of formation. Therefore, it was decided to carry the reaction forward despite the impurities and then purify it at the next step. Deprotection of compound **13** with trimethylsilyl bromide yields inhibitor **2** along with a deprotected version of compound **12** as confirmed by NMR and mass spectrometry.

Silica gel chromatography was not a valid option for purification due to the high polarity of both the compound and the impurity. In an attempt to purify the inhibitor, we used ion-exchange chromatography, but the deprotected amine impurity co-eluted with inhibitor **2**, since both have a similar number of negative charges. Therefore, an alternate synthetic route (pathway B) to make the guanidine from the literature known amine **12** was designed. The new route utilizes the alternate guanidinyllating reagent (1, 3-bis (tert-butoxycarbonyl)-2-methyl-2-thiourea) (Figure 2.8).

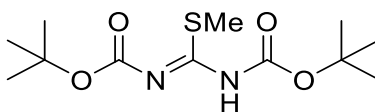


**Figure 2.8: Guanidinyllating reagent (1, 3-bis (tert-butoxycarbonyl)-2-methyl-2-thiourea).**

### 2.3.2 Synthesis of Inhibitor 2: Pathway B

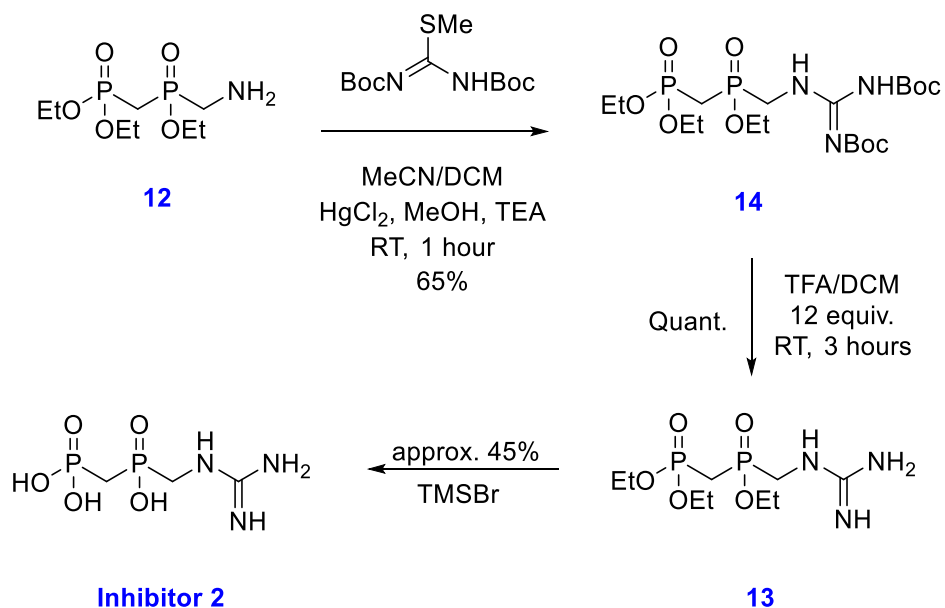


**Figure 2.9: New synthetic route for inhibitor 2.**

Treatment of compound **12** with 1, 3-bis (tert-butoxycarbonyl)-2-methyl-2-thiourea in combination with HgCl<sub>2</sub> yields the protected guanidine **14** in 65% yield (much higher than previous route) (Figure 2.9).<sup>120</sup> We were able to purify compound **14**, because the two Boc groups that are installed on the guanidine functionality helped to decrease the polarity of the compound, which in turn facilitated its purification with silica gel chromatography.<sup>120</sup> Thus, the problem that was encountered in pathway A had been overcome.

In order to remove the Boc groups, compound **14** was treated with trifluoroacetic acid to yield compound **13**. The final deprotection of compound **13** was difficult to optimize, we tried different numbers of equivalencies (10 – 100 equiv.) and for different durations (18 – 48 hours) in order to find the best conditions for the deprotection. Compound **13** was ultimately deprotected with 100 equiv. of trimethylsilyl bromide for 48 h yielding inhibitor **2**, which was purified using ion-exchange chromatography. The crude reaction mixture was loaded onto a column of DE 52 resin and was eluted with various concentrations of freshly prepared triethylammonium bicarbonate buffer (TEAB). All collected fractions were lyophilized and analyzed by  $^1\text{H}$  and  $^{31}\text{P}$  NMR spectroscopy. The final compound was fully characterized by  $^1\text{H}$  and  $^{31}\text{P}$  NMR spectroscopy and mass spectrometry. The  $^1\text{H}$  NMR spectrum showed a signal for the 8 H of dioxane (the internal standard) at 3.68 ppm which appears as a singlet (Figure 2.10). The signal at 3.42 ppm is from the methylene group attached to the guanidine and it appears as a doublet due to coupling to the adjacent P atom. Finally, there is a signal at 1.94 ppm for the bridging methylene group which appears as a doublet of doublets due to the coupling to both adjacent P atoms. It should be noted that the two phosphorus peaks in the  $^{31}\text{P}$  NMR spectrum (Figure 2.11) did not appear to be coupled. This could be due to signal broadening caused by traces of metal ions in the sample since protected precursors (such as compound **13**) showed weak P-P coupling (approximately 3 Hz). The yield of the last step of synthesis was also determined by  $^1\text{H}$  NMR spectroscopy with the addition of an internal standard of 1 mM 1,4-dioxane and integration of the appropriate signals. In this manner a yield of approximately 45% was calculated.

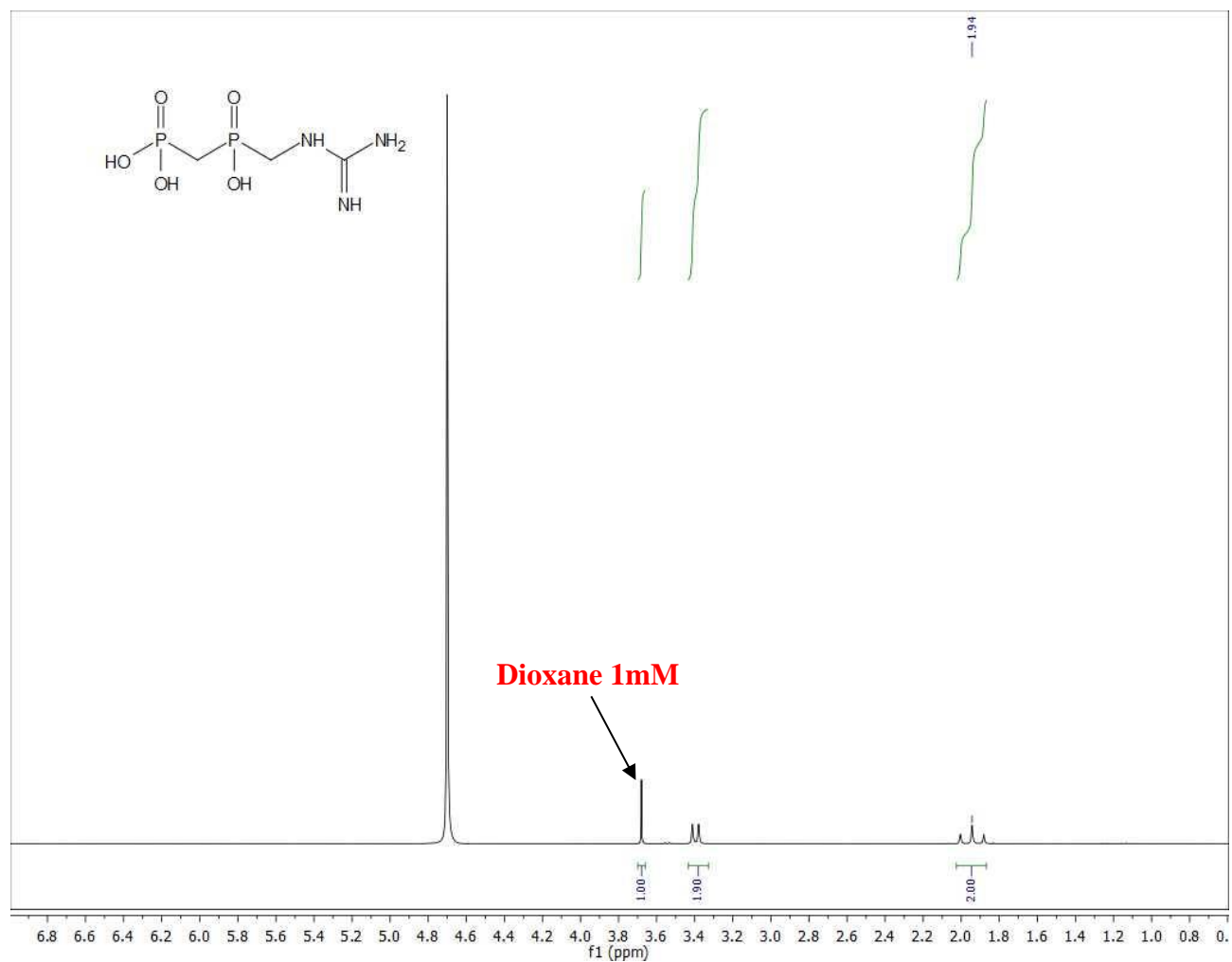


**Figure 2.10:** <sup>1</sup>H NMR spectrum of inhibitor 2 (D<sub>2</sub>O – Dioxane 1mM, 400 MHz).

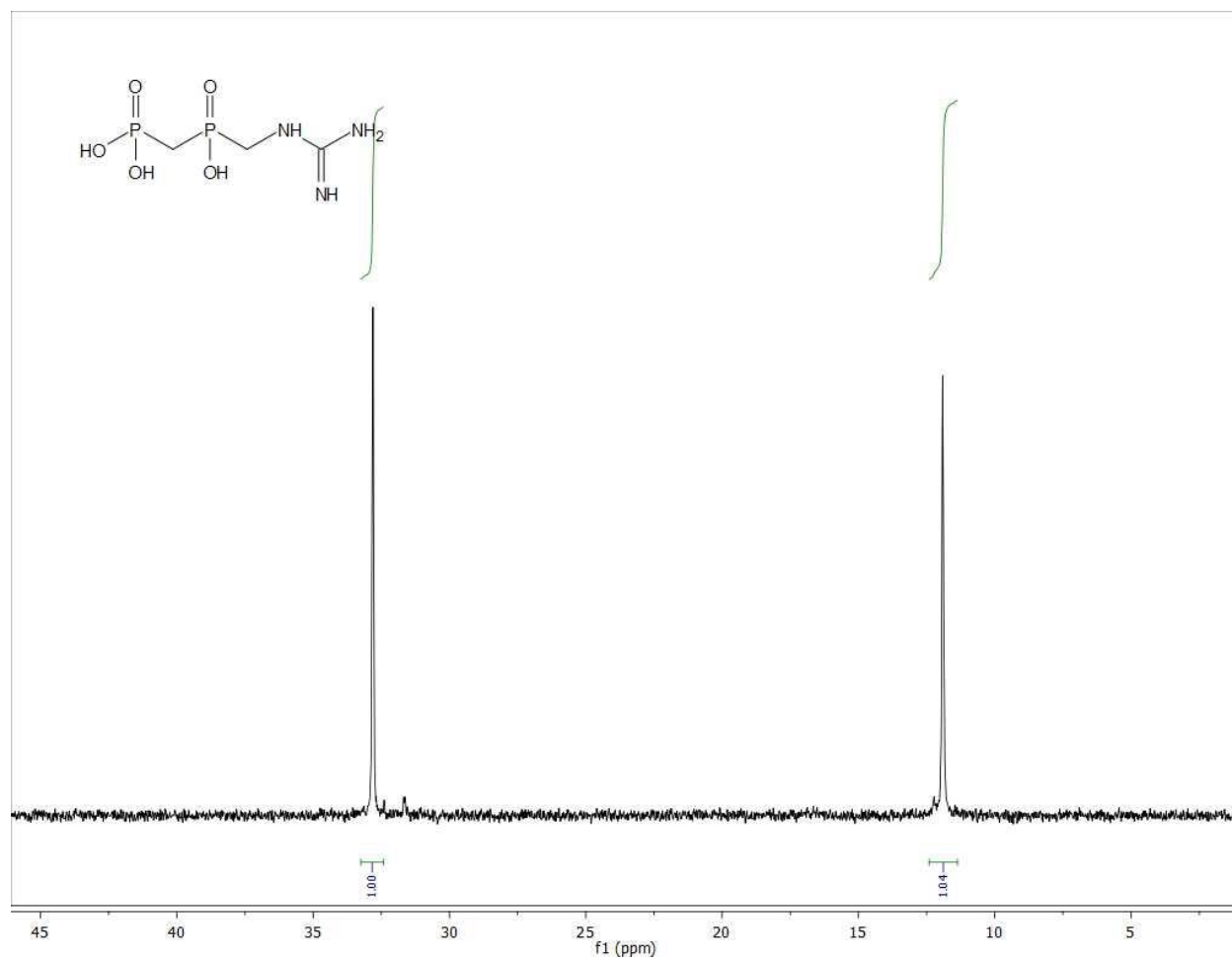


**Figure 2.11:  $^{31}\text{P}$  NMR spectrum of inhibitor 2 ( $\text{D}_2\text{O}$ , 162 MHz).**

### 2.3.3 Synthesis of Inhibitors 3 and 4

The necessity of the guanidinium moiety for tight binding was tested by synthesizing some analogues of inhibitor **2**: inhibitor **3** (amine) and inhibitor **4** (acetylated version) (Figure 2.12). Inhibitor **3** contains a positive charge but lacks  $sp^2$  hybridization/delocalization. Inhibitor **4** is isosteric to inhibitor **2** (still retains the planarity) but lacks any positive charge.

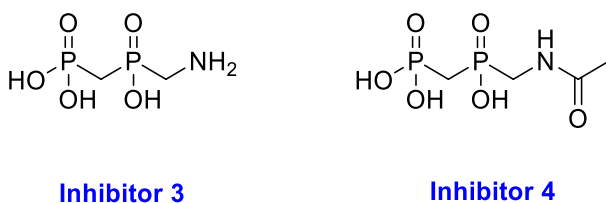


**Figure 2.12: Structures of inhibitors 3 and 4.**

Inhibitor **3** was synthesized from the literature known amine **12** in one step (Figure 2.13). Treatment of compound **12** with trimethylsilyl bromide yields inhibitor **3**, which was purified using DE 52 ion-exchange chromatography, eluting with various concentrations of freshly prepared triethylammonium bicarbonate buffer (TEAB).

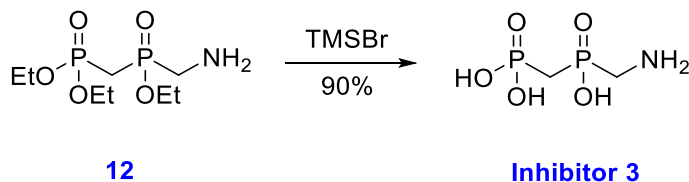


**Figure 2.13: Deprotection of amine 12 to yield inhibitor 3.**

Inhibitor **4** was also synthesized from the literature known amine **12** in a two-step procedure (Figure 2.14). Amine **12** was treated with acetic anhydride in the presence of pyridine to yield the protected version of inhibitor **4**, compound **15**, which was purified by column chromatography. Treatment of compound **15** with trimethylsilyl bromide yields inhibitor **4**, which was purified using ion-exchange chromatography.

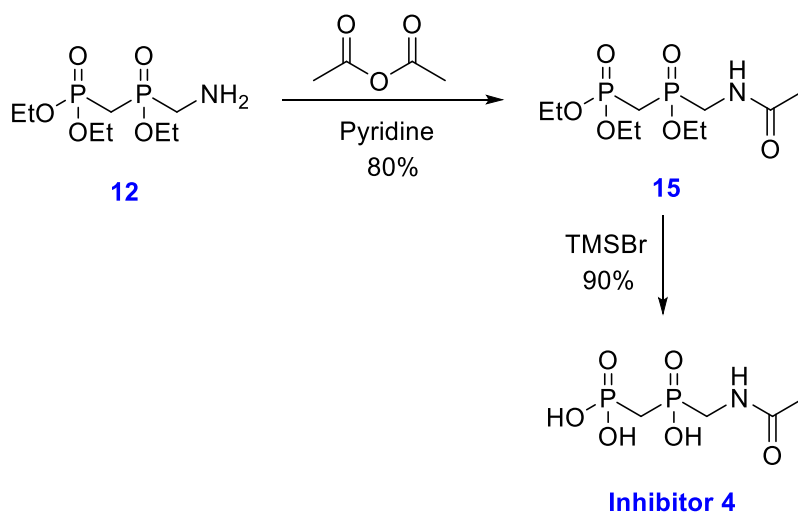


**Figure 2.14: Synthetic route to inhibitor 4.**

Similar to inhibitor **2**, all collected fractions from ion-exchange chromatography for both inhibitors **3** and **4** were lyophilized and analyzed by  $^1\text{H}$  and  $^{31}\text{P}$  NMR spectroscopy. Then the final compounds were fully characterized by  $^1\text{H}$  and  $^{31}\text{P}$  NMR spectroscopy and mass spectrometry. The yield of the last step of synthesis was also determined by  $^1\text{H}$  NMR spectroscopy with the addition of an internal standard of 1 mM 1,4-dioxane and integration of the appropriate signals. In this manner a yield of approximately 90% was calculated for the final deprotection step with both inhibitors.

Following the characterization of all the inhibitors; we proceeded to the next step, which involved the overproduction and purification of human farnesyl diphosphate synthase (HFPPS); and then the testing of inhibitors 2 – 4. The following sections will describe in detail the overproduction and purification of the enzyme, as well as our inhibition studies.

## **2.4 Overproduction and Purification of Human Farnesyl Diphosphate Synthase**

To prepare recombinant human FPPS we used the same strategy as Oldfield and coworkers who found that a truncated version of the enzyme (residues 6 – 353) was soluble and stable upon expression in *E. coli*.<sup>121</sup> Therefore, the gene encoding for truncated (residues 6 – 353) human farnesyl diphosphate synthase (*FPPS* from *Homo sapiens*), was synthesized and cloned into a pET28a(+) vector (Novagen/EMD Millipore) at the *NdeI* and *BamHI* restriction sites, with codon optimization for expression in *E. coli*, by Genscript. This includes a sequence encoding for an N-terminal hexa-histidine tag that allows for protein purification by immobilized metal affinity chromatography, a kanamycin resistance gene that facilitates the selection of transformed bacteria, and a T7 promoter/lac operon system for IPTG induction and protein expression. Approximately, 40 mg of HFPPS was obtained from 1 liter of cell culture and it was found to be more than 90% pure as analyzed by SDS-PAGE (Figure A.1). The enzyme could be stored under – 80 °C without a significant loss of activity for at least 4 months.

## 2.5 Measurements of Kinetic Parameters

### 2.5.1 Measurements of Kinetic Parameters for the human farnesyl diphosphate synthase reaction

Since the reaction catalyzed by HFPPS releases pyrophosphate (PPi) as a byproduct, kinetic constants ( $k_{\text{cat}}$  and  $K_{\text{m}}$ ) could be obtained by a modified continuous coupled assay for phosphate release (Figure 2.15).<sup>122</sup> Pyrophosphatase is added to catalyze the hydrolysis of the released byproduct (PPi) into two equivalents of phosphate (Pi), which is then used as a substrate by another coupling enzyme: purine nucleoside phosphorylase (PNPase). The coupling enzyme (PNPase) acts on 2-amino-6-mercapto-7-methylpurine ribonucleoside (MESG) to generate ribose-1-phosphate and 2-amino-6-merapto-7-methylpurine as products. Since MESG shows a maximum UV absorbance at 330 nm at neutral pH, and 2-amino-6-merapto-7-methylpurine shows a maximum UV absorbance at 360 nm, the reaction kinetics can be followed by an increase in absorption at 360 nm. It should be noted that GPP was used as a substrate (instead of DMAPP), so that we only monitored the second half of the overall reaction. This was done to simplify the reaction kinetics.

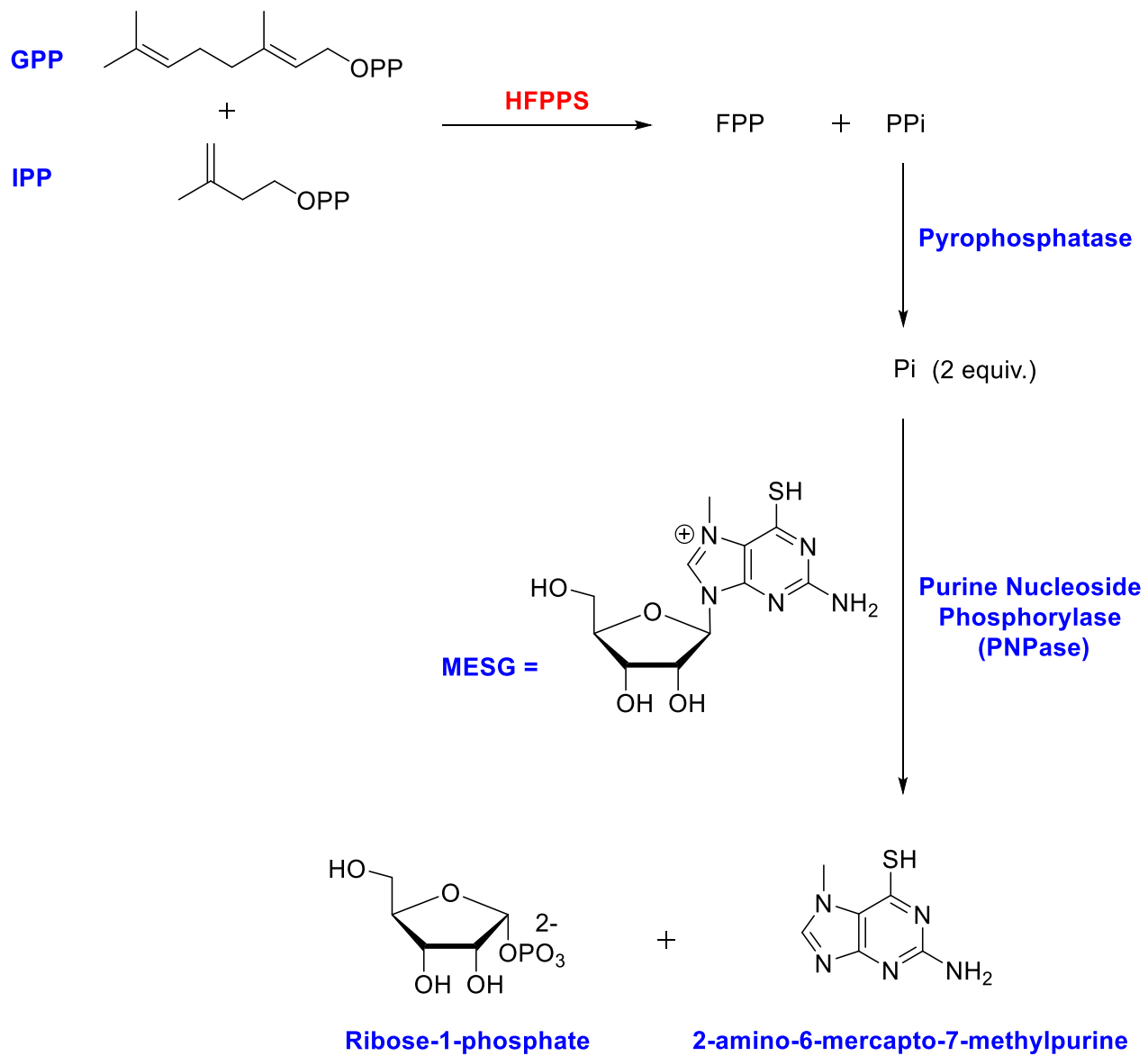


**Figure 2.15: A modified version of the continuous coupled assay for phosphate release for the reaction catalyzed by HFPPS.**

Kinetic parameters were measured from the fit of initial velocities of the reaction to the Michaelis-Menten equation. The initial velocities were measured at a series of different concentrations of geranyl diphosphate (prepared by Dr. James Morrison) (1  $\mu\text{M}$  – 60  $\mu\text{M}$ ) while keeping the concentration of isopentenyl diphosphate constant at a saturating level (30  $\mu\text{M}$ ). A hyperbolic kinetic profile was observed (Figure 2.16) with the following kinetic parameter values:  $k_{\text{cat}} = 0.57 \pm 0.01 \text{ s}^{-1}$  and  $K_{\text{m}} = 4.9 \pm 0.5 \mu\text{M}$ .

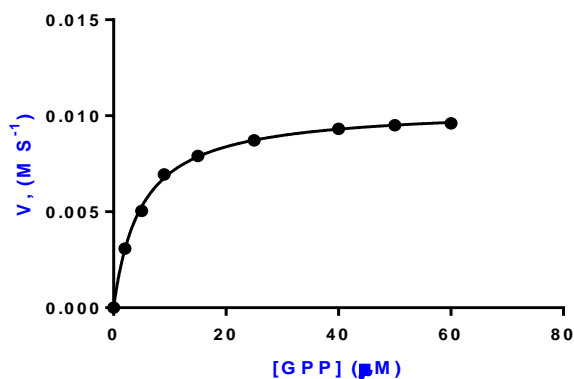


**Figure 2.16: A plot of initial velocity vs. GPP concentration for the reaction catalyzed by HFPPS. The kinetic parameters were determined by fitting the data to the Michaelis-Menten equation and are as follows:  $k_{\text{cat}} = 0.57 \pm 0.01 \text{ s}^{-1}$  and  $K_{\text{m}} = 4.9 \pm 0.5 \mu\text{M}$ .**

## 2.5.2 Inhibition Assays

The inhibitory effects of inhibitors **2** – **4** towards the activity of human farnesyl diphosphate synthase (HFPPS) were studied using the previously described continuous coupled assay for phosphate release (Figure 2.15). Inhibition kinetics were performed as described in section 2.5.1, but with the inclusion of inhibitors **2** – **4** at different concentrations. The  $IC_{50}$  values for all three inhibitors were first obtained by measuring the initial velocities at a series of different concentrations of inhibitors **2** – **4** (varying from 0  $\mu\text{M}$  – 1500  $\mu\text{M}$ , approximately) while keeping the concentrations of IPP (30  $\mu\text{M}$ ) and of GPP (10  $\mu\text{M}$ ) constant. The  $IC_{50}$  values for inhibitors **2**, **3** and **4** were found to be  $233 \pm 15 \mu\text{M}$ ,  $150 \pm 7 \mu\text{M}$  and  $177 \pm 10 \mu\text{M}$  respectively (Figures 2.17). The results show that all three  $IC_{50}$  values were substantially higher than the  $K_m$  values for the substrates (GPP,  $K_m = 5 \mu\text{M}$  and DMAPP,  $K_m = 12 \mu\text{M}$ ). Since potent inhibition was not observed, no attempt was made to obtain the individual kinetic constant  $K_I$  for any of the inhibitors.

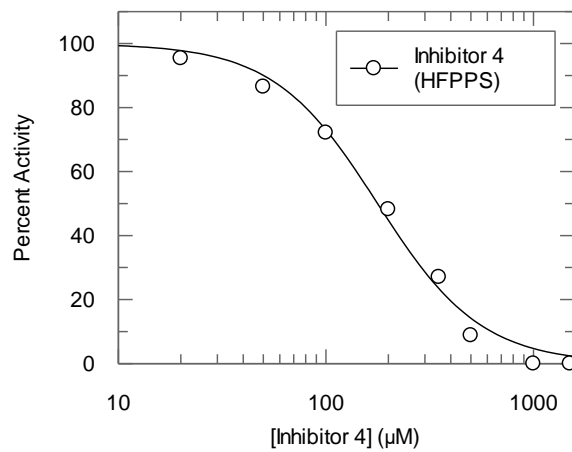
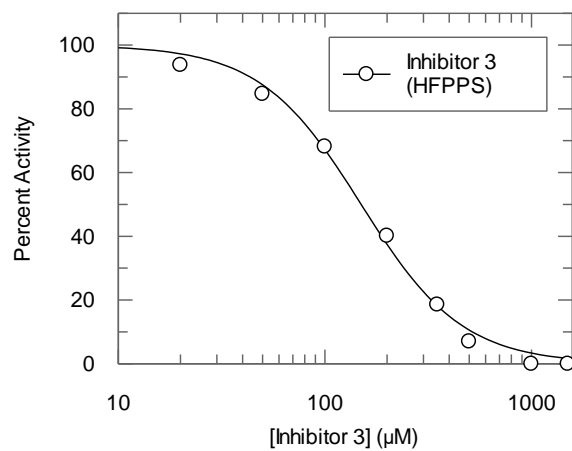
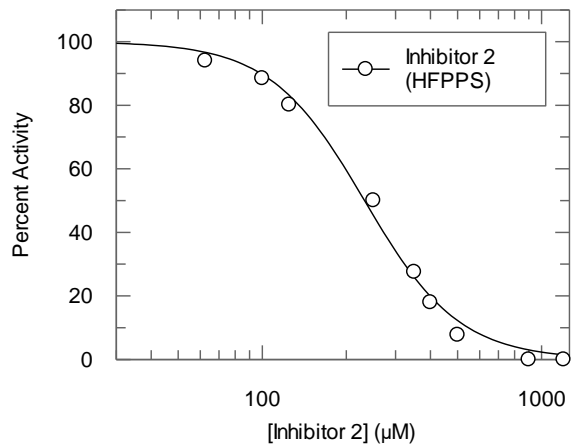
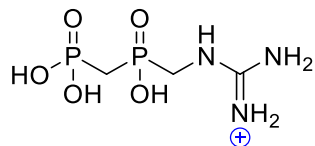


**Figure 2.17: The three  $\text{IC}_{50}$  Curves of inhibitors 2, 3 and 4, respectively, against HFPPS.**

## 2.6 Conclusion and Summary

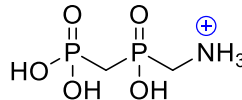
In this study, we prepared three potential inhibitors to probe the effectiveness of incorporating a guanidinium moiety into inhibitors of human farnesyl diphosphate synthase. As discussed previously, inhibitor **2** contains the guanidinium functionality, which provides a planar positive charge that is delocalized over three nitrogen atoms and is designed to mimic a putative allylic carbocation. An appended phosphoryl phosphonate group serves to mimic the pyrophosphate group in the transition state/ion pair. Inhibitor **3** has an ammonium functionality, thus retains the charge, but not the planarity or delocalization. Inhibitor **4** contains a urea functionality, and is therefore uncharged but is isosteric to inhibitor **2**. Inhibitor **4** plays the role as a negative control to test for the significant contribution of a positively charged group.

The three inhibitors were synthesized from the literature-known amine, compound **12**.<sup>118</sup> The final concentrations of all inhibitors were determined by <sup>1</sup>H NMR spectroscopy with the addition of an internal standard, 1,4-dioxane, of a known concentration, and integration of the appropriate signals. HFPPS was overexpressed and purified, and the kinetic parameters ( $K_m$  and  $k_{cat}$ ) were determined using the coupled assay for phosphate release. Inhibition kinetics were measured using the same assay, and the following  $IC_{50}$  values (Figure 2.18) were obtained for inhibitors **2**, **3** and **4**:  $233 \pm 15 \mu\text{M}$ ,  $150 \pm 7 \mu\text{M}$  and  $177 \pm 10 \mu\text{M}$ , respectively.



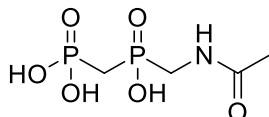
**Inhibitor 2**

**IC<sub>50</sub> = 233 μM**



**Inhibitor 3**

**IC<sub>50</sub> = 150 μM**



**Inhibitor 4**

**IC<sub>50</sub> = 177 μM**

**Figure 2.18: IC<sub>50</sub> values for inhibitors 2 – 4**

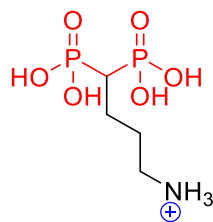
Tight binding of the inhibitors was expected, due to their electronic and structural similarity to the transition state and/or allylic carbocation-pyrophosphate ion pair formed during catalysis. It was anticipated that the inhibitors would benefit from the same favorable active site interactions that lower the activation energy for ionization of DMAPP.<sup>4,90</sup> Instead, the inhibitors displayed IC<sub>50</sub> values that were significantly higher than the substrate *K<sub>m</sub>* value. Furthermore, the uncharged control, inhibitor **4**, bound equally well as the cationic inhibitors. This indicates that the positive charge does not coordinate to the potency of these compounds.

There are many scenarios that could account for the failure of these inhibitors. The first scenario could be that the presence of the positive charge does not necessarily increase potency, since the enzyme may have not evolved an active site that stabilizes a carbocation by electrostatic interactions. While a carbocation is thought to be formed during catalysis, it is a relatively stable one as it is both tertiary and resonance stabilized.<sup>4</sup> Furthermore, it is electrostatically stabilized by the adjacent pyrophosphate anion.<sup>4,43</sup> Therefore, one can imagine that the enzyme may not need to utilize many binding interactions to directly stabilize the cation. This notion goes against literature reports that cationic bisphosphonates are the most potent inhibitors due to the presence of nitrogen atoms in their structures.<sup>102,109,114</sup>

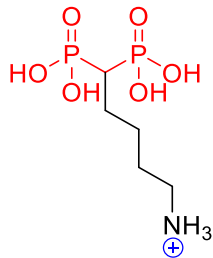
A report by Oldfield and coworkers illustrates the modest effect that the presence of a positive charge has on binding to FPPS.<sup>123</sup> Furthermore, it shows that the positioning of the positive charge is not crucial for potent inhibition. He conducted inhibition studies on 66 bisphosphonate inhibitors that bind in the DMAPP binding site. One can imagine that if these inhibitors were mimicking a carbocation, then the location of the positive charge in these inhibitors will be very crucial to their binding, but this was not found to be the case.<sup>123</sup> For instance, inhibitors **16**, **17** and **20** (Figure 2.19) position the positive charge three, four and five carbons away from the P-C-P of the bisphosphonate backbone, respectively, yet all exhibit IC<sub>50</sub> values in the low micromolar range.

Furthermore, Inhibitors **18** and **19** ( Figure 2.19) have the protonated pyridine ring attached via one or two methylenes to the P-C-P of the bisphosphonate backbone, and show similar  $IC_{50}$  values of 1.3  $\mu$ M and 5.4  $\mu$ M, respectively. We can see that the location of the positive charge in these inhibitors does not have a dramatic effect on potency which argues against a specific electrostatic interaction leading to tight binding.

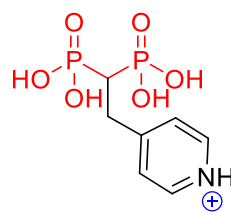
Most notably, inhibitors **20** and **21** (Figure 2.19) have a similar length of side chain, but one has a protonated amine group and the other lacks any positive charge. These two inhibitors have similar  $IC_{50}$  values of 4.6  $\mu$ M and 5.9  $\mu$ M, respectively, which are only 5 fold higher than the most potent inhibitor **16**, and reveals that the presence of a positive charge does not dramatically increase the potency of the inhibitors. Instead, most of the binding energy in these bisphosphonates likely comes from tight interactions with the metal ions in the active site of the enzyme. This is unlike the findings with glycosidase inhibitors, where a positive charge placed at an analogous position to that of the putative oxocarbenium ion, dramatically increases potency. This indicates that glycosidase enzymes had to evolve an active site to stabilize the higher energy oxocarbenium ion that is not formed as an ion pair. <sup>124-128</sup>



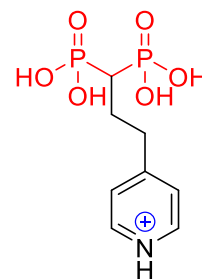
**Inhibitor 16**  
 $IC_{50} = 0.9 \mu\text{M}$



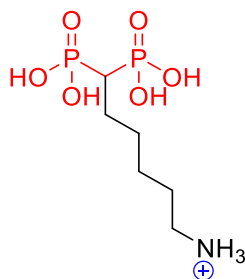
**Inhibitor 17**  
 $IC_{50} = 4.4 \mu\text{M}$



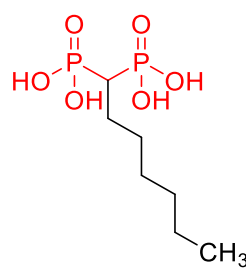
**Inhibitor 18**  
 $IC_{50} = 1.3 \mu\text{M}$



**Inhibitor 19**  
 $IC_{50} = 5.4 \mu\text{M}$



**Inhibitor 20**  
 $IC_{50} = 4.6 \mu\text{M}$



**Inhibitor 21**  
 $IC_{50} = 5.9 \mu\text{M}$

**Figure 2.19: Structures of selected bisphosphonates and their  $IC_{50}$  values studied by Eric Oldfield and his coworkers.** <sup>123</sup>

A second scenario is that the inhibitor cannot access the DMAPP binding site, and only binds to the IPP binding site. This behavior could be due to the replacement of the two oxygen atoms (bridging and terminal) with methylene groups (Figure 2.20), which may affect the compound's binding ability to coordinate to the metal ion clusters. This could be caused by the P-O-P and P-CH<sub>2</sub>-P bond angles, as the latter no longer has a bridging oxygen whose lone pairs would be conjugated with the adjacent P=O groups. In addition, the electronegativity differences between the bridging oxygen versus the methylene group could affect the pK<sub>a</sub> of the terminal phosphonate group.

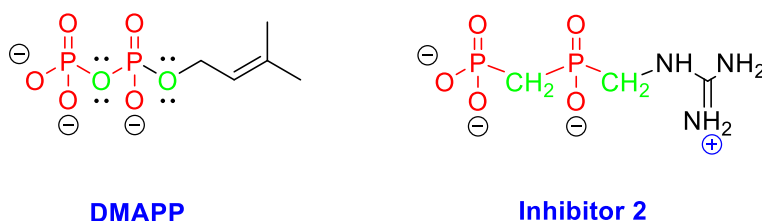
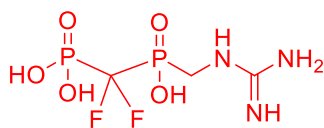


**Figure 2.20: The structure of DMAPP is on the left. On the right is the structure of inhibitor 2, showing the replaced two oxygens with two CH<sub>2</sub> groups in green.**

Overall, we conclude that both the delocalized positive charge of the guanidinium moiety and the localized positive charge of the ammonium group do not contribute significantly to binding affinity in this study, since the neutral control inhibitor binds almost as well as the charged ones. One possible explanation is that the HFPPS enzyme did not have to evolve a high affinity for the allylic carbocation intermediate, as it could be sufficiently stabilized by electrostatic interactions with the pyrophosphate byproduct. Alternatively, the inhibitors may be unable to access the DMAPP binding site of the enzyme.

## 2.7 Future Directions

In the first scenario, FPP synthase does not significantly recognize cationic species. In this event, the strategy outlined in this chapter does not lead to future inhibitor design with FPP synthase. Instead, our inhibitor may be useful with other carbocation-generating enzymes that do not involve an ionization of an allylic diphosphate. Such a strategy will be discussed and tested in chapter four. In the light of the second scenario, the very low affinity for the guanidinium-based inhibitor towards the farnesyl diphosphate synthase (FPPS) enzyme could be due to replacement of the bridging oxygen atom with a methylene group which might result in a higher pKa of the terminal phosphonate and two overall negative charges instead of three, thus less favorable interactions in the active site. To address this problem, we could introduce electron-withdrawing groups (EWGs) on the bridging carbon (such as fluorine, inhibitor **22**) (Figure 2.21). The EWGs would help lower the pKa of the bisphosphonate, perhaps leading to more favorable interactions in the active site.



**Inhibitor 22**

**Figure 2.21: A fluorinated version of inhibitor 2.**

## 2.8 Experimental Procedures

### 2.8.1 Materials and Methods

All reagents were purchased from Sigma-Aldrich, Fluka, Toronto Research Chemicals Inc. (TRC), or Advanced ChemTech (Louisville, KY) and used without further purification unless otherwise stated. Isopropyl  $\beta$ -D-1-galactopyranoside (IPTG) was purchased from Invitrogen. D<sub>2</sub>O (99.9%) was purchased from Cambridge Laboratories. Dowex® 50WX8 (H<sup>+</sup> form) resin was purchased from Sigma-Aldrich. Triethylamine was distilled over CaH<sub>2</sub> under an atmosphere of Ar. Silica gel chromatography was performed using Silica Gel SiliaFlash F60 (230-400 mesh, Silicycle). <sup>1</sup>H NMR spectra were recorded on a Bruker AV400 spectrometer at a field strength of 400 MHz. Proton-decoupled <sup>31</sup>P NMR spectra were recorded on Bruker AV400 spectrometer at a field strength of 162 MHz. Mass spectra were obtained on a Waters Micromass LCT mass spectrometer using electrospray ionization (ESI-MS). Neutral compounds were detected as positive ions, and negatively charged compounds were detected as negative ions.

## 2.8.2 Synthesis of Inhibitors

### 2.8.2.1 Synthesis of compound 14

1, 3-Bis (*tert*-butoxycarbonyl )-2-methyl-2-thiourea (760 mg, 2.64 mmol, 5.5 equiv.) was added to a solution of HgCl<sub>2</sub> (165 mg, 0.59 mmol, 1.25 equiv.) in 20 mL anhydrous MeCN and the mixture was stirred under an argon atmosphere at rt for 20 min. To this solution was added Et<sub>3</sub>N (200 μL, 1.4 mmol, 3equiv.); a white precipitate appeared immediately. After 5 min, stirring was halted and 10 mL of the colourless supernatant was withdrawn by a syringe. The content of the syringe was added dropwise to amine **12** (130 mg, 0.47 mmol) in 20 mL 4:1 MeCN/DCM. The reaction was stirred for 1 h and quenched by the addition of 3 mL of MeOH. Concentration of the reaction mixture under reduced pressure afforded an oily residue. Purification by chromatography on silica gel (70% hexane/30% EtOAc–80% EtOAc/20% MeOH) furnished the guanidine **14**, in a 65% yield. <sup>1</sup>H NMR (CDCl<sub>3</sub>, 400 MHz): δ ppm 8.68 (s, 1H), 4.11 - 4.27 (m, 6H), 3.77 – 3.89 (m, 2H), 2.5 (t, *J* = 24.4 Hz, 2H), 1.42 (s, 9H), 1.40 (s, 9H), 1.25 - 1.33 (m, 9H). <sup>31</sup>P NMR (CDCl<sub>3</sub>, 162 MHz): δ ppm 21.34 (d, *J* = 6.6 Hz), 43.24 (d, *J* = 6.6 Hz). MS (ESI) *m/z* for [M + H]<sup>+</sup> = 516.4

### 2.8.2.2 Synthesis of compound 13

Guanidine **14** (200 mg, 0.38 mmol) was dissolved in 5 mL 1:1 TFA/DCM and stirred at rt for 3 h. The reaction mixture was concentrated under reduced pressure to yield guanidine **13** as a yellowish solid in a quantitative yield.  $^1\text{H}$  NMR (MeOD, 400 MHz):  $\delta$  ppm 4.14-4.29 (m, 6H), 3.87 (d,  $J = 8.1$  Hz, 2H), 2.85 – 2.99 (m, 2H), 1.36 – 1.42 (m, 9H).  $^{31}\text{P}$  NMR (MeOD, 162 MHz):  $\delta$  ppm 20.21 (d,  $J = 3$  Hz), 40.50 (d,  $J = 3$  Hz). MS (ESI)  $m/z$  for  $[\text{M} + \text{H}]^+ = 316.4$ .

### 2.8.2.3 Synthesis of Inhibitor 2

Guanidine **13** (200 mg, 0.8 mmol) was treated with 1 ml TMSBr in 10 ml of DMF and stirred at rt for 18 h. The reaction mixture was concentrated under reduced pressure to yield inhibitor **2** as yellow oil. The oil was dissolved in 3 mL triethylammonium bicarbonate buffer (1 mM, pH = 7.5) and loaded onto a 15 mL column of DEAE cellulose (DE 52, Whatman® Inc.) and eluted with a stepwise gradient of 5 to 100 mM triethylammonium bicarbonate buffer (pH = 7.5). All fractions were lyophilized to dryness and analyzed using  $^1\text{H}$  and  $^{31}\text{P}$  NMR spectroscopy. Selected fractions containing inhibitor were dissolved in water and treated with Dowex® 50WX8 ( $\text{H}^+$  form) resin until the pH reached 1. The acidified solution was neutralized with NaOH (0.1 M) and then lyophilized. To a solution of lyophilized solids in water (200  $\mu\text{L}$ ) was added EtOH (800  $\mu\text{L}$ ) and the cloudy mixture was centrifuged (10 K rpm, 30 min) to yield a pellet. The supernatant was removed, and the pellet was dissolved in 1.0 mM 1, 4-dioxane in  $\text{D}_2\text{O}$ .  $^1\text{H}$  NMR spectroscopy with integration of the appropriate signals was used to quantify the concentration. A yield of approximately 45% was estimated for this reaction.

$^1\text{H}$  NMR ( $\text{D}_2\text{O}$ , 400 MHz):  $\delta$  ppm 3.41 (d,  $J = 9.7$  Hz, 2H), 1.94 (t,  $J = 24.3$  Hz, 2H).  $^{31}\text{P}$  NMR ( $\text{D}_2\text{O}$ , 162 MHz):  $\delta$  ppm 11.95 ((d,  $J = 3$  Hz), 32.81 ((d,  $J = 3$  Hz). HRMS (ESI)  $m/z$  calcd for  $[\text{C}_3\text{H}_{10}\text{N}_3\text{O}_5\text{P}_2]^-$ , 230.0096, found 230.0096.

#### 2.8.2.4 Synthesis of inhibitor 3

Amine **12** (100 mg, 0.5 mmol) was treated with 1 ml TMSBr in 10 ml DMF and stirred at rt for 18 h. The reaction mixture was concentrated under reduced pressure to yield inhibitor **3** as a pale-yellow oil. The oil was dissolved in 3 mL triethylammonium bicarbonate buffer (1 mM, pH = 7.5) and loaded onto a 15 mL column of DEAE cellulose (DE 52, Whatman® Inc.) and eluted with a stepwise gradient of 5 to 100 mM triethylammonium bicarbonate buffer (pH = 7.5). All fractions were lyophilized, for 48 hours, to dryness and analyzed using  $^1\text{H}$  and  $^{31}\text{P}$  NMR spectroscopy. Selected fractions containing inhibitor were dissolved in water and treated with Dowex® 50WX8 ( $\text{H}^+$  form) resin until the pH reached 1. The acidified solution was neutralized with NaOH (0.1 M) and then lyophilized. The final product was dissolved in 1.0 mM 1, 4-dioxane in  $\text{D}_2\text{O}$ .  $^1\text{H}$  NMR spectroscopy with integration of the appropriate signals was used to quantify the concentration. A yield of approximately 90% was estimated for this reaction.  $^1\text{H}$  NMR ( $\text{D}_2\text{O}$ , 400 MHz):  $\delta$  ppm 2.71 (d,  $J = 8.3$  Hz, 2H), 1.85 – 1.94 (t,  $J = 17.7$  Hz, 2H).  $^{31}\text{P}$  NMR ( $\text{D}_2\text{O}$ , 162 MHz):  $\delta$  ppm 13.35 (d,  $J = 4.4$  Hz), 39.44 (d,  $J = 5$  Hz). MS (ESI)  $m/z$  for  $[\text{M} + \text{H}]^+ = 190.10$ .

### 2.8.2.5 Synthesis of compound 15

To a solution of compound **12** (100 mg, 0.3 mmol) in 5 ml of DCM was added 1 ml of acetic anhydride and pyridine (50  $\mu$ l, 0.6 mmol). The reaction mixture was stirred at rt for 14 h. Concentration of the reaction mixture under reduced pressure afforded an oily residue. Purification by silica gel chromatography (70% hexane/30% EtOAc) furnished the pure compound **15** as a yellow oil in a 80% yield.  $^1\text{H}$  NMR (MeOD, 400 MHz):  $\delta$  ppm 4.15-4.22 (m, 6H), 3.75-3.85 (m, 2H), 2.75-2.84 (m, 2H), 2.23 (s, 3H), 1.33-1.39 (m, 9H).  $^{31}\text{P}$  NMR (MeOD, 162 MHz):  $\delta$  ppm 20.52 (d,  $J = 8.6$  Hz), 42.26 (d,  $J = 8.6$  Hz). MS (ESI)  $m/z$  for  $[\text{M} + \text{H}]^+ = 316.3$ .

### 2.8.2.6 Synthesis of inhibitor 4

Compound **15** (50 mg, 0.1 mmol) was treated with 1 ml TMSBr in 10 ml DMF and stirred at rt for 18 h. The reaction mixture was concentrated under reduced pressure to yield inhibitor **4** as yellow oil. The oil was dissolved in 3 mL triethylammonium bicarbonate buffer (1 mM, pH = 7.5) and loaded onto a 15 mL column of DEAE cellulose (DE 52, Whatman® Inc.) and eluted with a stepwise gradient of 5 to 100 mM triethylammonium bicarbonate buffer (pH = 7.5). All fractions were lyophilized to dryness and analyzed using  $^1\text{H}$  and  $^{31}\text{P}$  NMR spectroscopy. Selected fractions containing inhibitor were dissolved in water and treated with Dowex® 50WX8 ( $\text{H}^+$  form) resin until the pH reached 1. The acidified solution was neutralized with NaOH (0.1 M) and then lyophilized. The final product was dissolved in 1.0 mM 1, 4-dioxane in  $\text{D}_2\text{O}$ .  $^1\text{H}$  NMR spectroscopy with integration of the appropriate signals was used to quantify the concentration. A yield of approximately 90% was estimated for this reaction.

<sup>1</sup>H NMR (D<sub>2</sub>O, 400 MHz): δ ppm 3.59 (d, *J* = 9.1 Hz, 2H), 2.31 – 2.47 (m, 2H), 1.95 (s, 3H). <sup>31</sup>P NMR (D<sub>2</sub>O, 162 MHz): δ ppm 17.11 (d, *J* = 8.2 Hz), 38.85 (d, *J* = 8.3 Hz). MS (ESI) *m/z* for [M + H]<sup>+</sup> = 232.10.

### 2.8.3 General Enzyme Methods

Centrifugal filters (4 mL 10 000 MWCO) were purchased from Millipore. Acryl-cuvettes used in enzyme kinetic assays were from Sarstedt. Chelating Sepharose® Fast resin was purchased from Pharmacia Biotech. Protein concentrations were determined by the method of Bradford on a Cary 3E UV-Vis spectrophotometer using bovine serum albumin as standard.<sup>129</sup> All measurements were performed at 37 °C. Protein purity was assessed using SDS-PAGE, stained with Coomassie blue according to Laemmli. 185 Molecular weight standards for SDS-PAGE were BSA (66 kDa) and carbonic anhydrase (29 kDa), both purchased from Sigma. The enzyme kinetic assays were carried out on a Cary 300 UV-Vis spectrometer with a Cary temperature controller attached. Protein concentrations were determined by the Bradford assay using a commercial kit (Bio-Rad). All kinetic parameters were determined from the fit of initial velocities to the Michaelis-Menten equation:  $v_0 = \frac{V_{max} \cdot [S]}{K_M + [S]}$ . IC<sub>50</sub> values were calculated using this equation:  $y = \frac{100\%}{1 + \left(\frac{x}{IC_{50}}\right)^s}$ , where "s" is the slope factor, x is the inhibitor concentration and y is the percent activity.

### 2.8.3.1 Overproduction and Purification of Human Farnesyl Diphosphate Synthase (HFPPS)

The gene encoding for truncated human farnesyl diphosphate synthase FPPS from *Homo sapiens* (residues 6 – 353), was synthesized by GenScript® with codon optimization for expression in *E. coli* and was cloned into a pET28a(+) vector (Novagen/EMD Millipore) via *NdeI* and *BamHI* restriction sites. A stop codon was added after the FPPS open reading frame to prevent expression of pET28a's optional C-terminal His tag. Expression of the resulting plasmid, *FPPS/pET28a* results in a protein expressed with an N-terminal His tag and T7 tag. The plasmid *FPPS/pET28a* was used to transform chemically competent *Escherichia coli* expression strain Rosetta (DE3) pLysS (Novagen) following the Inoue method.<sup>130</sup>

Overproduction of human farnesyl diphosphate synthase (HFPPS) was achieved following a previously described procedure.<sup>44,45</sup> Transformed cells were grown at 37 °C in 1 L of Terrific Broth (TB) medium containing 35 µg/mL chloramphenicol and 30 µg/mL kanamycin until an OD<sub>600</sub> of 0.5 was reached. Cells were induced for overproduction by the addition of 120 mg (1 mM) of isopropyl-β-D-1-thiogalactopyranoside (IPTG). After growing at 22 °C for an additional 24 hours, cells were harvested and lysed with a French press in Tris-HCl buffer (50 mM, pH 8.0) containing dithiothreitol (2 mM), NaCl (500 mM), MgCl<sub>2</sub> (2 mM), imidazole (20 mM), aprotinin (1 µg mL<sup>-1</sup>), and pepstatin A (1 µg mL<sup>-1</sup>).

The lysate was cleared by centrifugation (34 155g, 45 min) and filtration through a 0.22 mm filter. A column containing chelating Sepharose fast flow resin (GE Healthcare, 10 mL) was charged with 100 mM NiSO<sub>4</sub> and washed with Tris-HCl buffer (50 mM, pH 8.0) containing NaCl (500 mM) and imidazole (5 mM). The clarified lysate was loaded onto the column and eluted with same buffer but containing imidazole at 5, 20, 100, and 500 mM. Fractions containing the desired enzyme eluted after the addition of 500 mM imidazole as analyzed by Bradford assay. Glycerol (10%) was added to the resulting eluent before flash freezing with liquid N<sub>2</sub>. Typically, 40 mg of enzyme was purified from 1 L of culture. Enzymes were found to be more than 90% pure as analyzed by SDS-PAGE (Figure A.1).

### 2.8.3.2 Measurements of Inhibition Kinetics

Kinetic constants for the inhibition of farnesyl diphosphate synthase (FPPS) by inhibitors **2 – 4** were measured by a modification of a previously described continuous coupled assay for phosphate release.<sup>122</sup> A cuvette containing 50 mM HEPES buffer (pH 7.5, final volume 1000  $\mu\text{L}$ ),  $\text{MgCl}_2$  (10 mM), geranyl diphosphate (GPP) (10  $\mu\text{M}$ ), isopentenyl diphosphate (IPP) (30  $\mu\text{M}$ ), 2-amino-6-mercapto-7-methylpurine ribonucleoside (MESG) (20  $\mu\text{M}$ ), purine nucleoside phosphorylase (PNPase) (1 unit), and inorganic pyrophosphatase (PPase) (0.5 unit) was thermally equilibrated for 5 min at 37 °C. The enzymatic reaction was initiated by the addition of farnesyl diphosphate synthase (MW = 36000 g/mol, 0.08 nmol/ml) and the rate was calculated from the observed increase of absorption at 360 nm ( $\epsilon = 11000 \text{ M}^{-1} \cdot \text{cm}^{-1}$ ). Kinetic parameters were determined from the fit of initial velocities to the Michaelis-Menten equation. Inhibition kinetics were described as above, but with the inclusion of inhibitors **2 – 4** at various concentrations. The kinetic parameters  $k_{\text{cat}}$  and  $K_{\text{m}}$ , the inhibition constants  $\text{IC}_{50}$ , and their associated errors, were determined by fitting the initial velocity data to the Michaelis-Menten equation using non-linear regression. Every experiment was repeated 3 times and the resulting kinetic constants never differed by more than 20%. Data obtained on different days with different batches of enzyme could result in kinetic constants that differed from those reported above by up to 25%.

## Chapter 3: Studies with Guanidinium-Based Inhibitors Suggest Minimal Stabilization of Allylic Carbocation Intermediates by Dehydrosqualene and Squalene Synthase.

### 3.1 Introduction

In this chapter, I describe studies on two enzymes that utilize the same substrate, farnesyl diphosphate (FPP), and have very similar mechanisms of action. Human squalene synthase (HSQS) and bacterial dehydrosqualene synthase (DSQS) produce important biological molecules and their inhibitors can be used as anti-cancer agents, cholesterol-lowering drugs and antibacterial agents.<sup>63</sup> Despite the fact that both enzymes share a class I terpenoid synthase fold, in addition to the three conserved consensus sequences which comprise the FPP binding site, the sequence similarity between the enzymes is only 10%.<sup>1,15,131</sup> Both enzymes catalyze the head-to-head condensation reactions of two identical molecules of farnesyl diphosphate to form squalene and dehydrosqualene, respectively (Figure 3.1).<sup>75,131</sup>

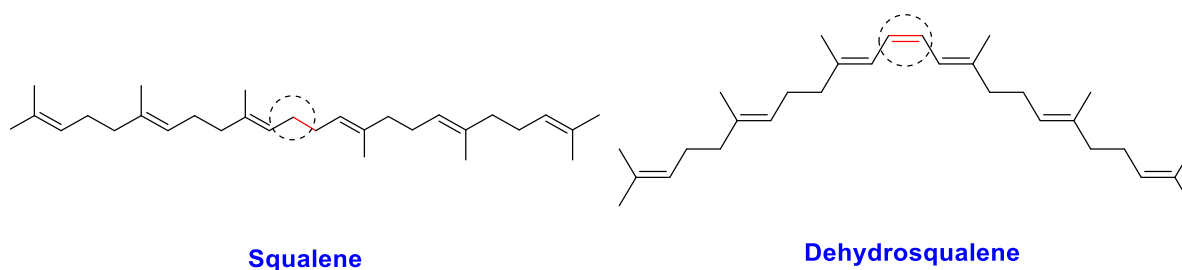


**Figure 3.1: Structures of squalene and dehydrosqualene.**

Squalene, which has a saturated central C-C bond, is biosynthesized via a reductive dimerization reaction utilizing NADPH as a cofactor, in a reaction catalyzed by squalene synthase (SQS).<sup>15,72,131</sup> Conversely dehydrosqualene, which has a distinctive cis central alkene, is made via a redox neutral reaction that is catalyzed by dehydrosqualene synthase (DSQS).<sup>75,131</sup> This first part of the catalytic reaction in both HSQS and DSQS involves the head-to-head condensation of two FPP molecules and the formation of the common stable intermediate, presqualene diphosphate (PSPP). This is followed by the conversion of PSPP into squalene or dehydrosqualene by squalene synthase or dehydrosqualene synthase, respectively (Figure 3.2).<sup>25,75,131</sup>

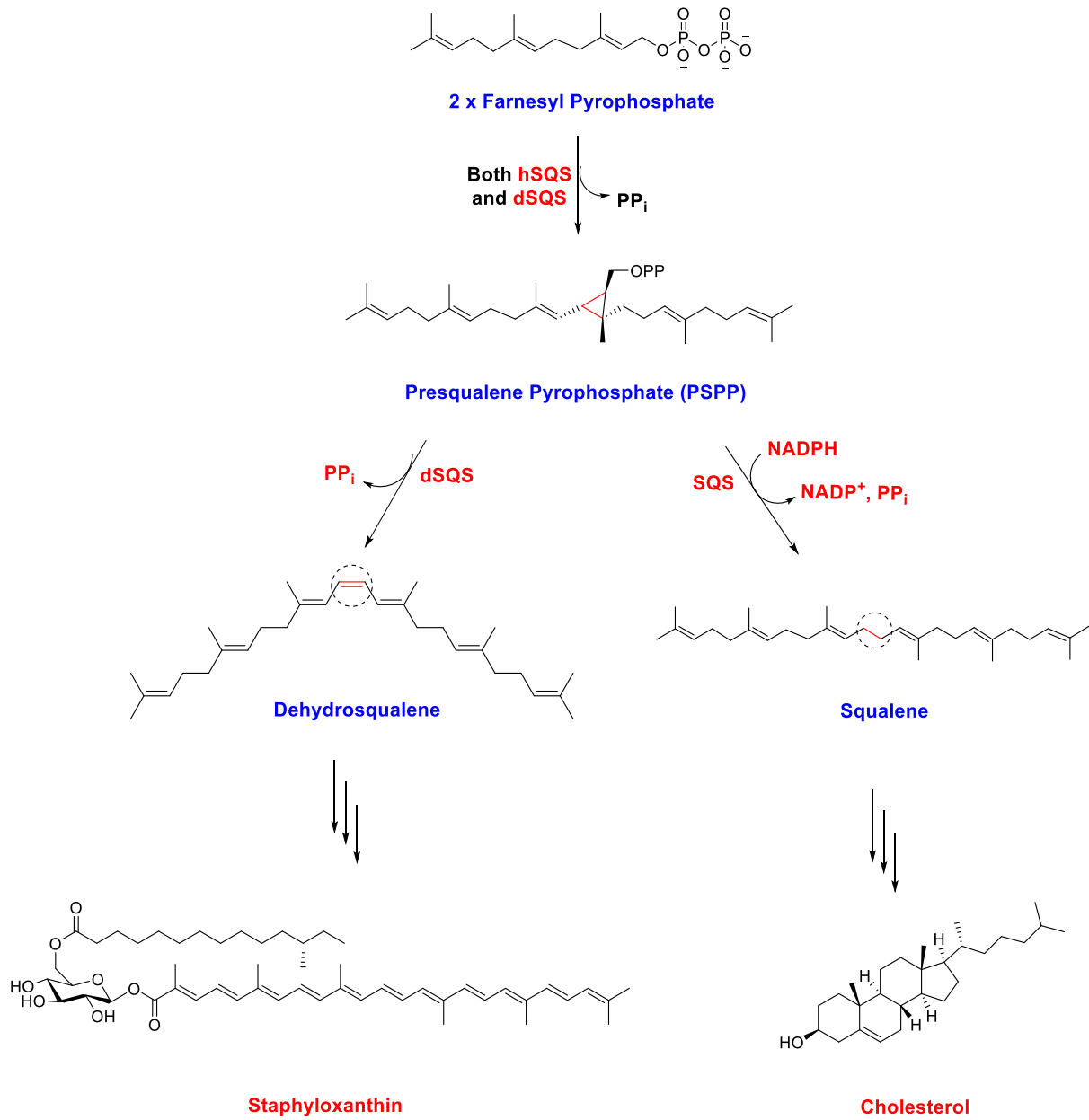


**Figure 3.2: The reactions catalyzed by squalene synthase (SQS) and bacterial dehydrosqualene synthase (DSQS), and the structures of staphyloxanthin and cholesterol.**

Owing to its vital role in the biosynthesis of steroids in general, and cholesterol in particular, human squalene synthase (HSQS) has long been a target for inhibitor design.<sup>15,63,131</sup> Human squalene synthase inhibitors have the ability to disrupt the biosynthetic pathway of cholesterol, thus may can act as cholesterol lowering agents.<sup>15</sup> Interestingly, drugs developed based on this strategy could be used as a replacement to statin drugs, inhibitors that target the second step of the mevalonate pathway<sup>15,29</sup>; thereby halting the production of terpenes entirely. Lapaquistat is an example of a potent squalene synthase inhibitor that was anticipated to be one of the most promising cholesterol lowering drugs after reaching a late stage of development. However, the accompanying liver toxicity resulted in the halting of trials and preventing it from being marketed (Figure 3.3).<sup>132</sup>

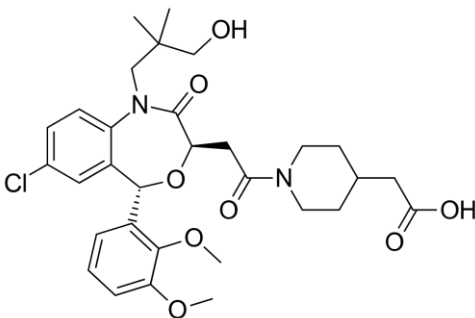


**Figure 3.3: Structure of Lapaquistat, a potent squalene synthase inhibitor**

Interest in designing inhibitors of the bacterial dehydrosqualene synthase (DSQS) of *Staphylococcus aureus* centers on the potential for antibiotic development.<sup>29,76</sup> The bacterial enzyme is involved in the biosynthesis of staphyloxanthin (Figure 3.2); which is a membrane-bound carotenoid that functions as an antioxidant to protect *S. aureus* against reactive oxygen species and helps to enhance its survival during harsh conditions.<sup>29,76,78</sup> The coloured pigment is responsible for the bacteria's distinctive yellow colour. Since inhibition of the biosynthesis of staphyloxanthin increases the bacteria's susceptibility to the immune system, it has become a potential novel target of anti-infective therapy against pigmented *Staphylococcus aureus* strains.<sup>75,78</sup>

In the following sections, we will outline our strategy towards the design of cationic inhibitors targeting human squalene synthase (HSQS) and the bacterial dehydrosqualene synthase (DSQS) as well as a neutral control inhibitor.

### **3.2 Design of Inhibitors**

The first step in catalysis for both the HSQS and DSQS enzymes involves the dissociation of a molecule of farnesyl diphosphate (FPP) resulting in the formation of an allylic carbocation and pyrophosphate (Figure 3.4). This ionization is then followed by the addition of a second molecule of FPP, and a subsequent deprotonation/cyclization to give the common intermediate presqualene diphosphate (PSPP). This PSPP intermediate is converted to dehydrosqualene via a redox neutral process by DSQS or to squalene in a reductive process by HSQS and an NADPH cofactor.<sup>76,131</sup>

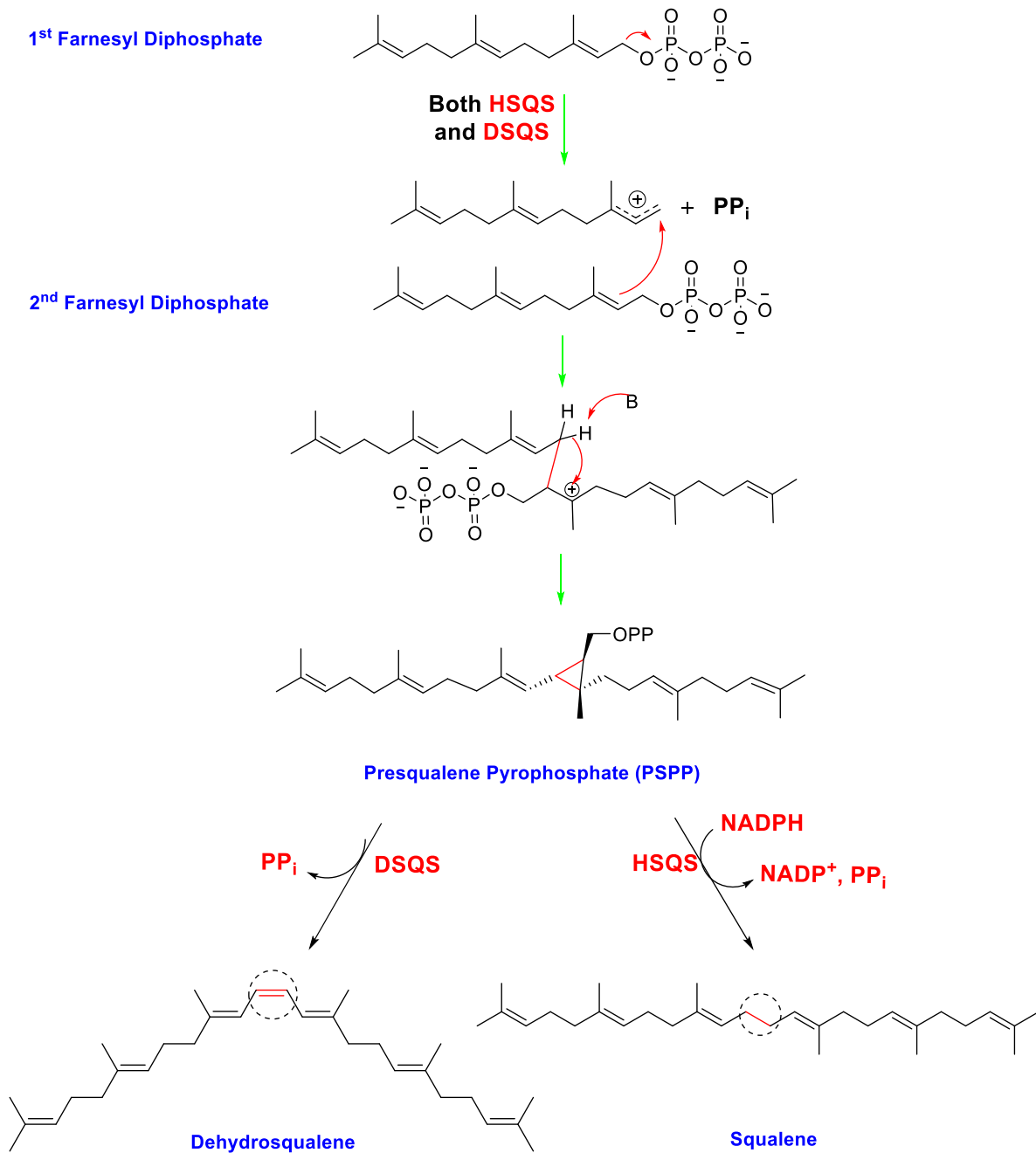


**Figure 3.4: The reactions catalyzed by HSQS and DSQS to produce squalene and dehydrosqualene, respectively. (P denotes a phosphate group).**

In the case of squalene synthase, the formation of presqualene diphosphate (PSPP) was proven to be rate determining, with the initial ionization of FPP as a very reasonable candidate for the rate determining step. This finding in turn makes the resultant allylic carbocation/pyrophosphate ion pair a reasonable target for inhibitor design (Figure 3.5).<sup>70,133,134</sup>

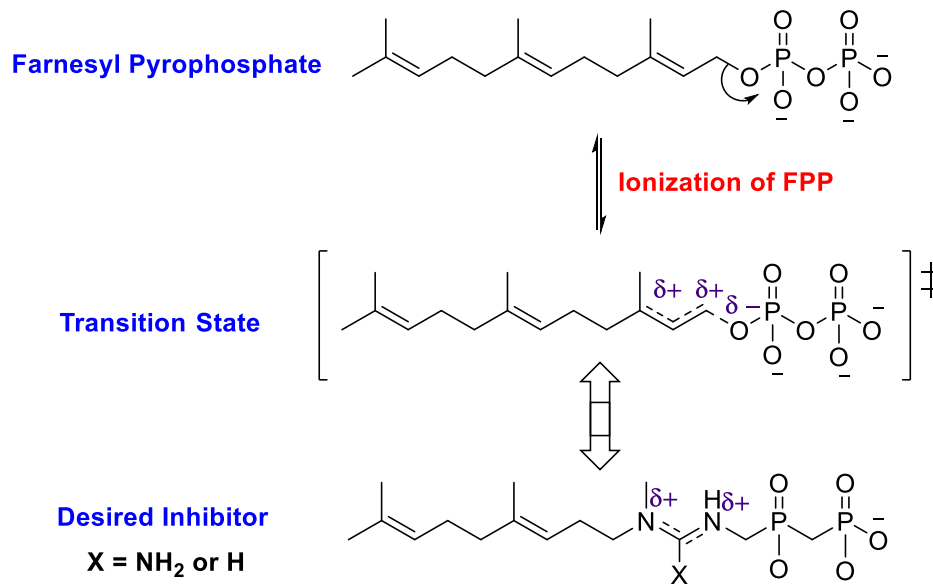


**Figure 3.5: Structure of the desired inhibitor mimicking the transition state of FPP dissociation.**

Since the goal was to inhibit enzymes that form either an allylic carbocation intermediate or a dissociative transition state bearing considerable carbocationic character at the allylic position, I decided to synthesize and evaluate inhibitors bearing a guanidinium or amidinium moiety appended to a pyrophosphate analogue and flanked by a hydrocarbon tail. These inhibitors should closely mimic the transition state/intermediate formed with farnesyl

diphosphate utilizing enzymes (HSQS and DSQS) (Figure 3.5). These functional groups not only provide the required positive charge, they also possess resonance structures that delocalize the positive charge over two/three  $sp^2$  hybridized nitrogen atoms, and enforce a planar geometry that more closely resembles the planarity of an allylic carbocation.

In this work, the inhibition strategy was tested on human squalene synthase (HSQS) and bacterial dehydroqualene synthase (DSQS) from *S. aureus* using three potential inhibitors. The guanidinium-based inhibitor **26** and the amidinium-based inhibitor **36** are mimics of the dissociative transition state. The urea-containing compound (inhibitor **34**) is an isosteric analogue of inhibitor **26** and it serves as a negative control to test for the importance of the positive charge in inhibition (Figure 3.6).

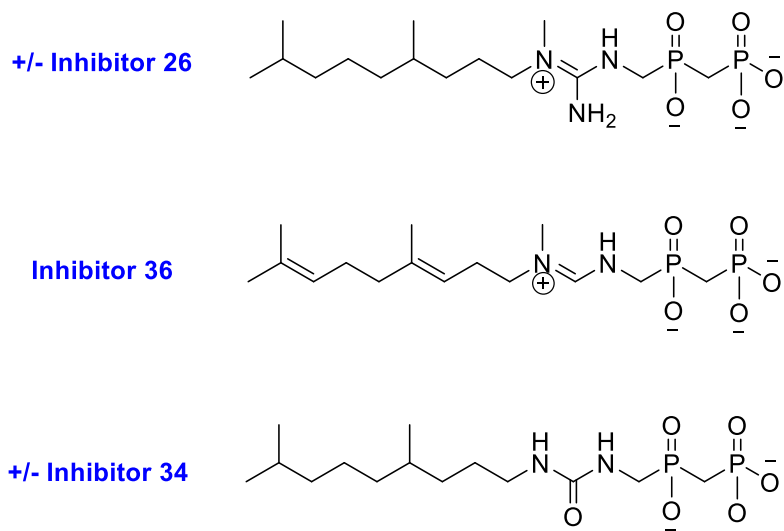


**Figure 3.6: Structure of inhibitors 26, 36 and 34.**

### 3.3 Synthesis of Inhibitors

#### 3.3.1 Synthesis of Inhibitor 26

The phosphinyl phosphonate amine intermediate **12** was prepared as described previously from diethyl phosphite, formaldehyde, and diethylmethylphosphonate in seven steps using literature methods. Compound **12** was treated with N,N' diBoc-thiourea, trifluoroacetic anhydride, and sodium hydride to give thiourea **23** (Figure 3.7).<sup>135</sup>

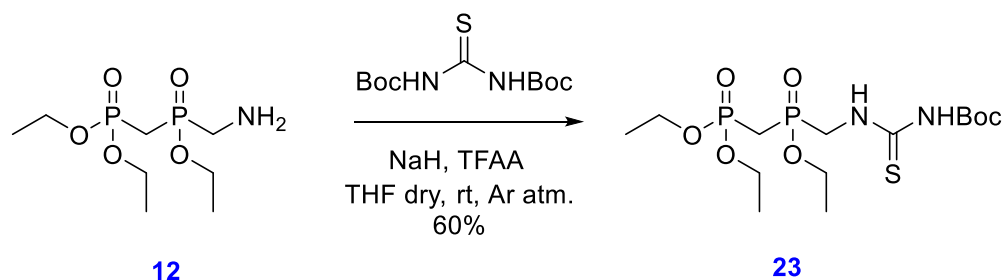


**Figure 3.7: Synthesis of the thiourea compound 23 via coupling of amine 12 and N,N' diBoc-thiourea.**

Thiourea **23** was initially coupled to compound **24** to prepare the unsaturated analogue of inhibitor **26** (Figure 3.8).<sup>136</sup> This coupling was achieved using the water soluble coupling reagent, 1-ethyl-3-(3-dimethyl-amino propyl) carbodiimide (EDC) and DIPEA, and provided compound **25**, which was purified by silica gel chromatography.<sup>136</sup> Treatment of compound **25** with trifluoroacetic acid (TFA) successfully removed the Boc protecting group. The resulting compound was then treated with TMSBr to remove the ethyl groups.<sup>136</sup>

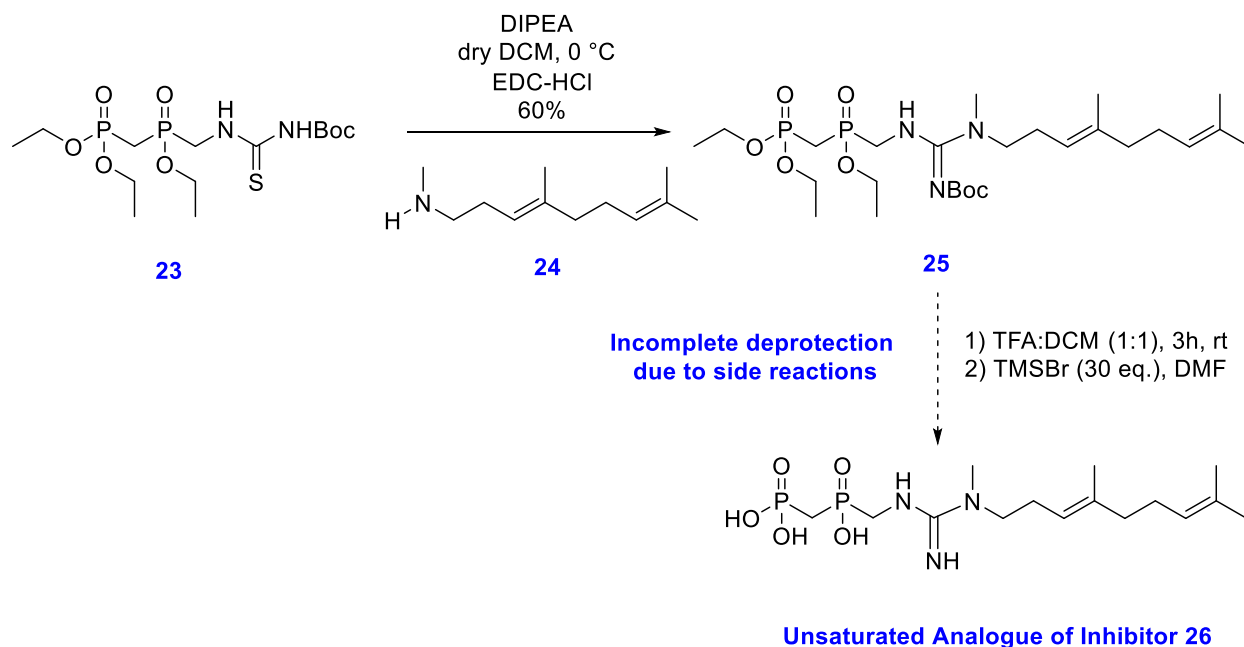


**Figure 3.8: Guanidinylation reaction and failed final inhibitor deprotection.**

However, all attempts to remove the ethyl groups with TMSBr (10 – 30 equivalents) were unsuccessful. At lower TMSBr concentrations, it was found that the reaction never went to completion and there was always incomplete deprotection, in which one or two ethyl groups are not removed even upon extended reaction times (Figure 3.9).

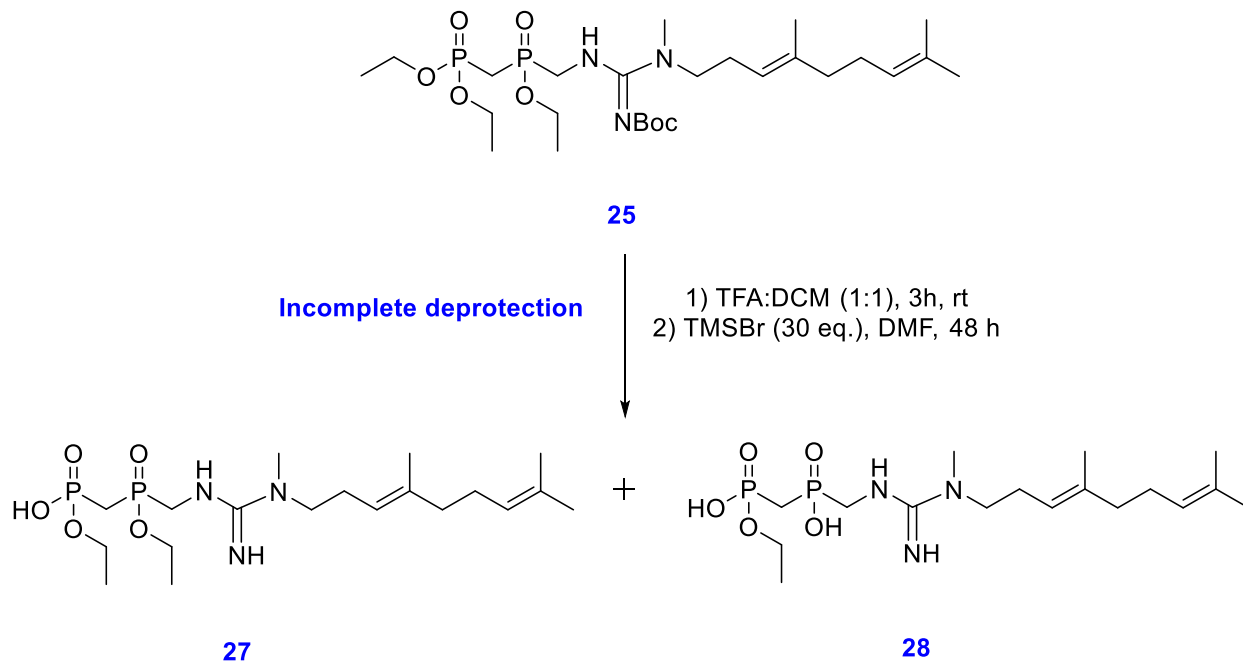
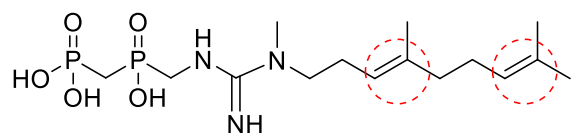


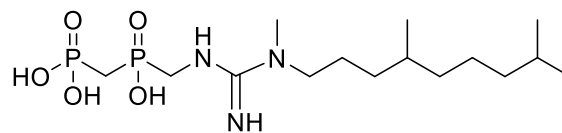
**Figure 3.9: Scheme showing side reactions encountered when using 30 equivalents of TMSBr in the deprotection of compound 25.**

When the amount of TMSBr used was increased to above 30 equivalents in an attempt to force the removal of the remaining ethyl groups, unwanted products were formed whose mass was consistent with the hydration of the alkene double bonds to give alcohols (Figure 3.10). Despite attempts to vigorously dry the solvent or to add a collidine base to help keep the medium neutral, side reactions of the alkene functionalities always occurred. It is possible that the water was introduced during the work-up, or that it was added via reactive brominated intermediates.





Unsaturated Analogue of Inhibitor 26



Inhibitor 26

**Figure 3.11: Structures of the unsaturated and saturated inhibitor 26.**

I synthesized the saturated version of the amine with the hydrophobic tail, compound **31**, by treating the unsaturated amine, compound **24**, with Pd/C under H<sub>2</sub> atmosphere (Figure 3.12).

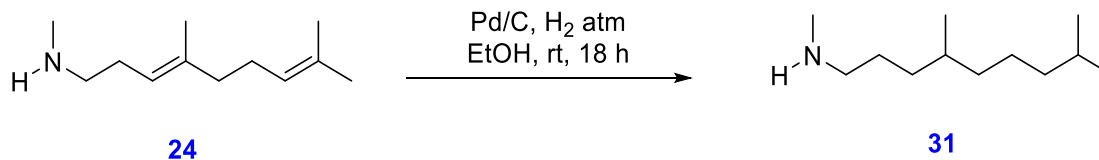


**Figure 3.12: Hydrogenation of unsaturated amine 24 to form the saturated racemic amine 31.**

Thiourea **23** was then coupled to the saturated racemic amine, compound **31** using EDC as a coupling reagent to give compound **32**.<sup>136</sup> The final deprotection of compound **32** became straightforward after removing the double bonds, since harsh acidic conditions could be used to deprotect it. Compound **32** was fully deprotected by refluxing in 4 N HCl for 48 hours to give inhibitor **26** (Figure 3.13).

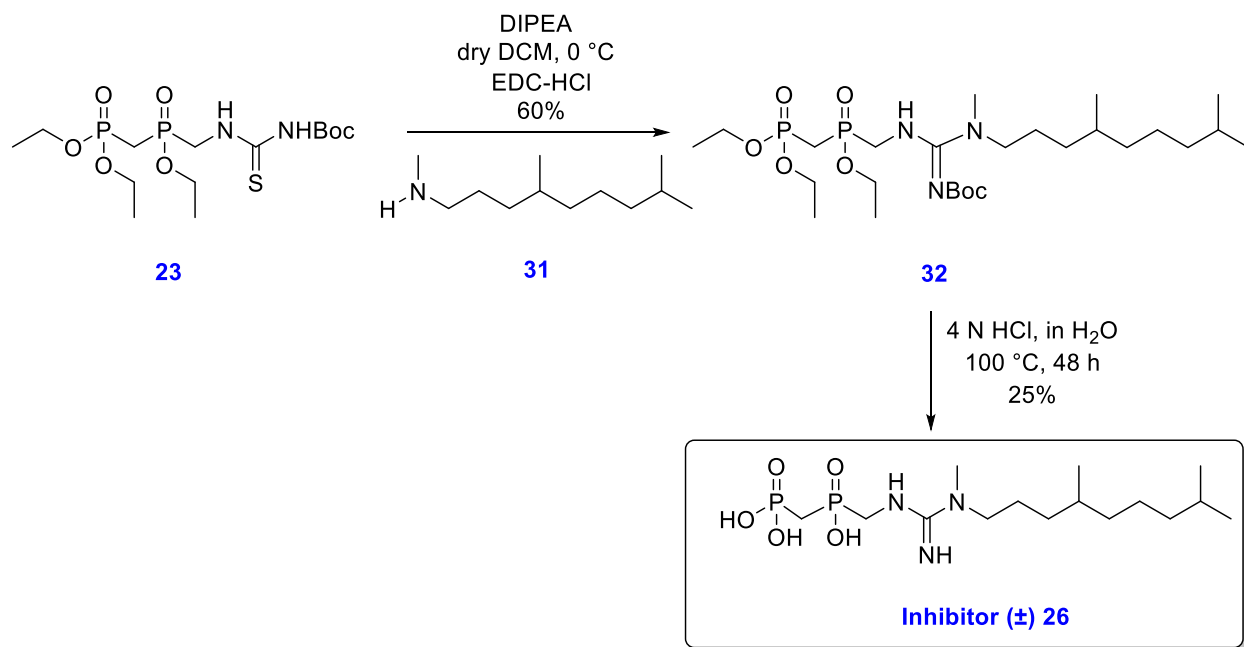


**Figure 3.13: Successful synthetic route for inhibitor (±) 26.**

Inhibitor **26** was then purified using anion-exchange chromatography. The crude reaction mixture was loaded onto a column of diethyl-aminoethanol (DEAE) cellulose (DE 52) anion exchange resin, which was eluted with various concentrations (0.01 – 0.1 M) of freshly prepared triethylammonium bicarbonate buffer (TEAB). All collected fractions were lyophilized and analyzed by <sup>1</sup>H and <sup>31</sup>P NMR spectroscopy to determine which fractions contained the final compound. The final compound was fully characterized by <sup>1</sup>H and <sup>31</sup>P NMR spectroscopy and mass spectrometry. The yield of the last step of synthesis was also determined by <sup>1</sup>H NMR spectroscopy with the addition of an internal standard of 1 mM 1,4-dioxane and integration of the appropriate signals. The yield was then estimated from <sup>1</sup>H NMR spectroscopy and the integration of the appropriate signals and was found to be approximately 25%.

### 3.3.2 Synthesis of Inhibitor 34

Three different approaches towards the synthesis of inhibitor **34** are described here. The first two approaches, pathway A and B, were not successful due to difficulties encountered during the synthesis. The third approach, pathway C, was successful and provided us the desired inhibitor in milligram quantities.

#### 3.3.2.1 Attempts Towards the Synthesis of Inhibitor 34: Pathway A

Pathway A is a short pathway using methodology described by C. Zhang *et al*, and is comprised of only two steps.<sup>138</sup> The first step involves reacting alcohol **9** with PhICl<sub>2</sub> (which is prepared *in situ* by suspending iodobenzene in hydrochloric acid containing 5% sodium hypochlorite) and sodium azide to make an *in situ* carbamoyl azide intermediate, which then reacts with amine **31** to produce the protected version of inhibitor **34**, compound **33**. The second step would involve treating compound **33** with TMSBr to remove the ethyl protecting groups and yield inhibitor **34** (Figure 3.14).<sup>118</sup>

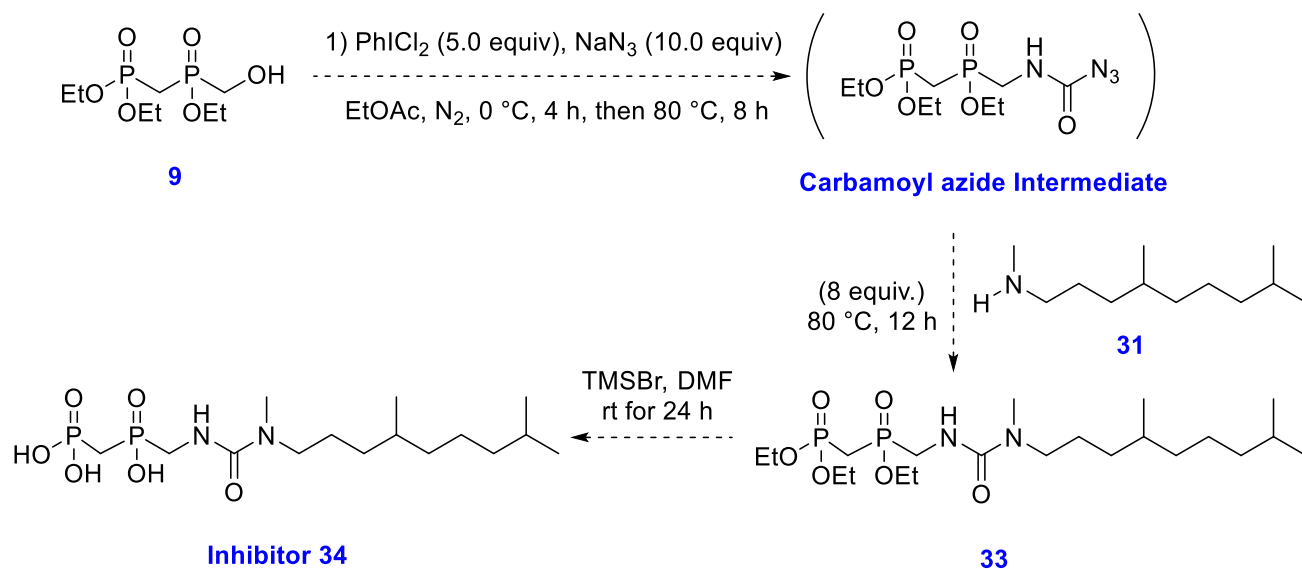


**Figure 3.14: Pathway A, an unsuccessful route towards inhibitor 34.**

Surprisingly, the first step never produced the desired product (compound **33**) and instead yielded many undesired products as analysed by mass spectrometry. NMR spectroscopy did not provide any insights since the spectra were messy and hard to interpret due to the many unknown peaks. The failure of this pathway led us to design pathway B (Figure 3.15).

### 3.3.2.2 Attempts Towards the Synthesis of Inhibitor 34: Pathway B

Another short pathway that also involve two steps, starts with the intermediate amine **12**<sup>118</sup>, that is treated with triphosgene in the presence of DIPEA in DCM, to form an isocyanate intermediate which then is coupled with amine **31** to give compound **33**.<sup>139</sup> The second step would involve treatment of compound **33** with TMSBr to remove the ethyl protecting groups (Figure 3.15).<sup>118</sup>

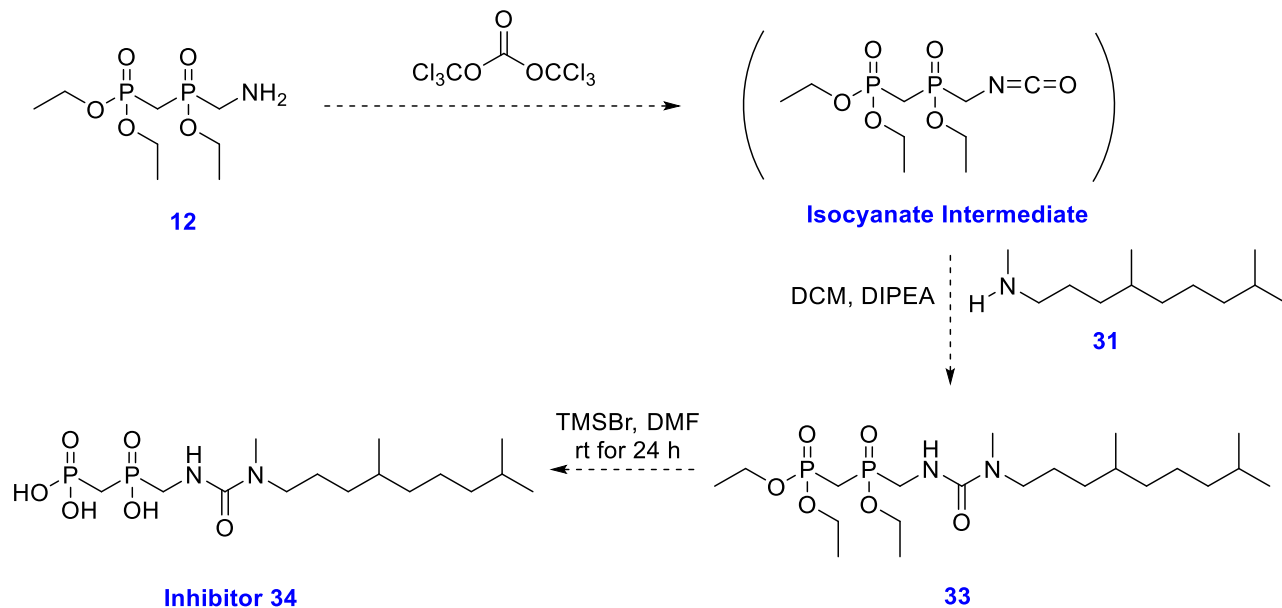


**Figure 3.15: Pathway B, unsuccessful route towards inhibitor 34.**

This approach also failed, since the product of the first step was never formed. Due to safety issues with possible phosgene release and/or hydrochloric acid gas, we did not try to optimize it. In addition, the third approach, pathway C (Figure 3.17), was running parallel to this approach and was successful.

### 3.3.2.3 Attempts Towards the Synthesis of Inhibitor 34: Pathway C

Pathway C was a successful approach to synthesize inhibitor **34** in a reasonable yield. This approach utilizes the amine **12**<sup>118</sup>, which was first protected with a Boc group in the presence of triethylamine base to give compound **35** (Figure 3.16).<sup>140</sup>

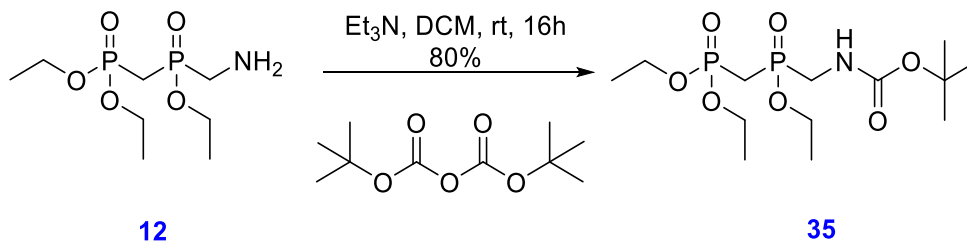


**Figure 3.16: Protection of the amine functional group by reacting it with diBoc.**

Compound **35** was then treated with triflic anhydride and 2-chloropyridine to produce an intermediate isocyanate that was immediately treated with racemic **31** to give racemic urea **33** (Figure 3.17).<sup>140</sup> Deprotection of urea **33** with TMSBr gave racemic inhibitor **34** which was purified by size exclusion chromatography.<sup>118</sup>

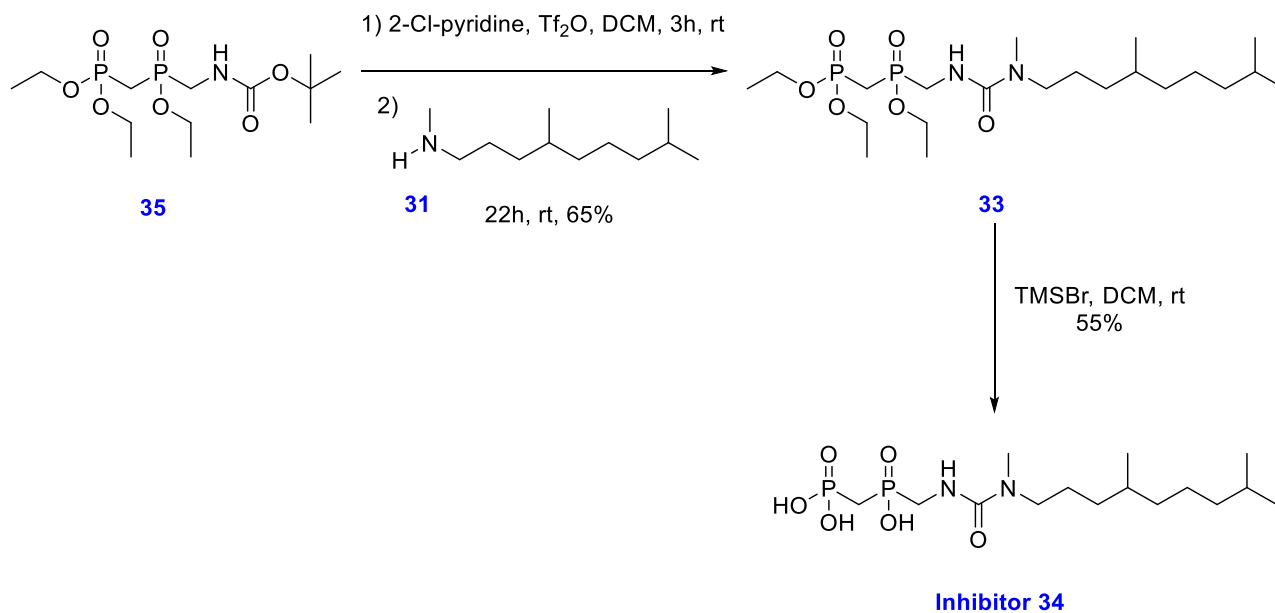


**Figure 3.17: Pathway C, the synthesis of inhibitor 34.**

### 3.3.3 Synthesis of Inhibitor 36

Inhibitor **36** was synthesized by another PhD student in the Tanner lab. It was synthesized from the literature known amine **12**<sup>118</sup> in three steps (Figure 3.18):

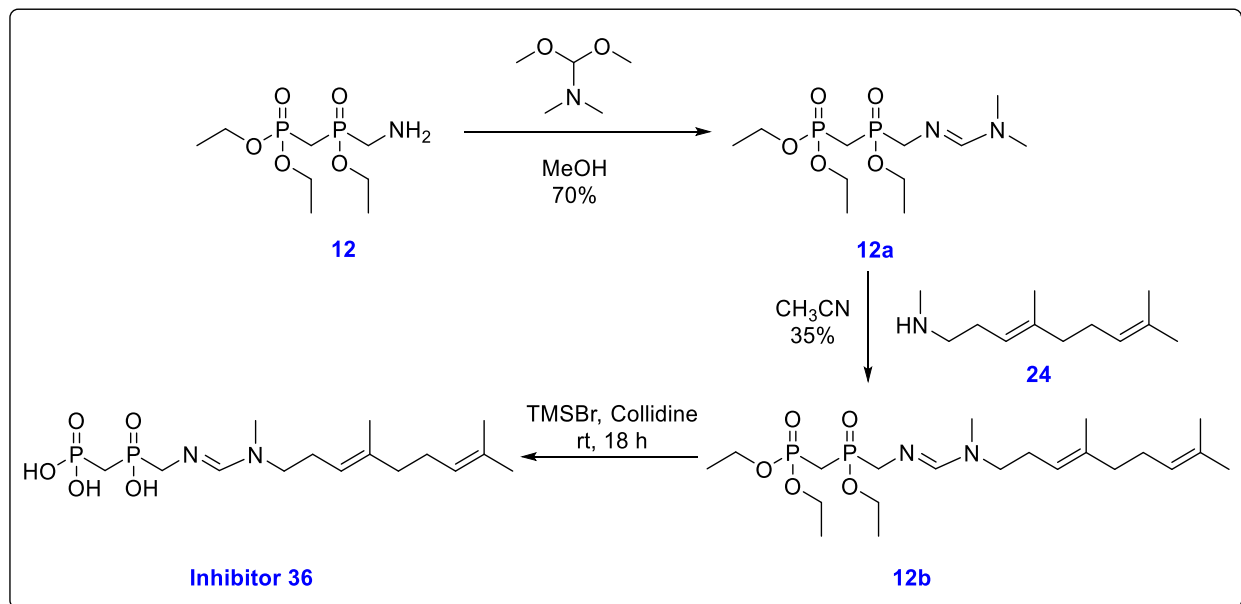


**Figure 3.18: Synthesis of inhibitor 36.** (this compound was synthesized by Taiya Adak)

### 3.4 Characterization of Inhibitors

All inhibitors were structurally characterized using <sup>1</sup>H and <sup>31</sup>P NMR spectroscopy and mass spectrometry. The yield of the final deprotection step as well as the concentration of stock solutions used in kinetics was determined by <sup>1</sup>H NMR spectroscopy. An internal standard of dioxane was added to the NMR samples and integration of the appropriate signals was used to quantify the inhibitor concentration.

Following the characterization of the inhibitors, we proceeded to the next steps: the overproduction and purification of HSQS and DSQS; and then the subsequent testing of inhibitors. The following sections will describe our inhibition studies with those inhibitors.

### **3.5 Overproduction and Purification of HSQS and DSQS**

The gene encoding for full length dehydrosqualene synthase from *Staphylococcus aureus* (DSQS) was synthesized and cloned into a pET28a(+) expression vector by Genscript. This includes a sequence encoding for an N-terminal hexa-histidine tag that allows for protein purification by immobilized metal affinity chromatography, a kanamycin resistance gene that facilitates the selection of transformed bacteria, and a T7 promoter/lac operon system for IPTG induction and protein expression.

It should be noted that HSQS has always been a problem to express and purify, due to solubility issues.<sup>141</sup> A study involving the truncation of the protein at both termini, ultimately showed that a doubly truncated protein (residues 31 – 370) was fully active and crystallizable.<sup>141</sup> Therefore, a codon optimized gene for doubly truncated human squalene synthase (residues 31–370) was synthesized and cloned into a pET28b expression vector, yielding pET28b-hSQS(31–370), and was provided to us by Dr. Jon Freeman.

### 3.6 Measurement of Enzyme Kinetics

#### 3.6.1 Continuous Coupled Assay

Inhibition kinetics were measured by a modification of a previously described continuous coupled assay for phosphate release (Figure 3.19).<sup>122</sup> This assay involves pyrophosphatase, which is a coupling enzyme added to hydrolyze the pyrophosphate byproduct into two molecules of phosphate (Pi). This phosphate (Pi) then reacts with 2-amino-6-mercapto-7-methylpurine ribonucleoside (MESG) as catalyzed by another coupling enzyme, purine nucleoside phosphorylase (PNPase), to generate ribose-1-phosphate and 2-amino-6-mercapto-7-methylpurine. The resulting purine product is monitored by an increase in absorbance at 360 nm.

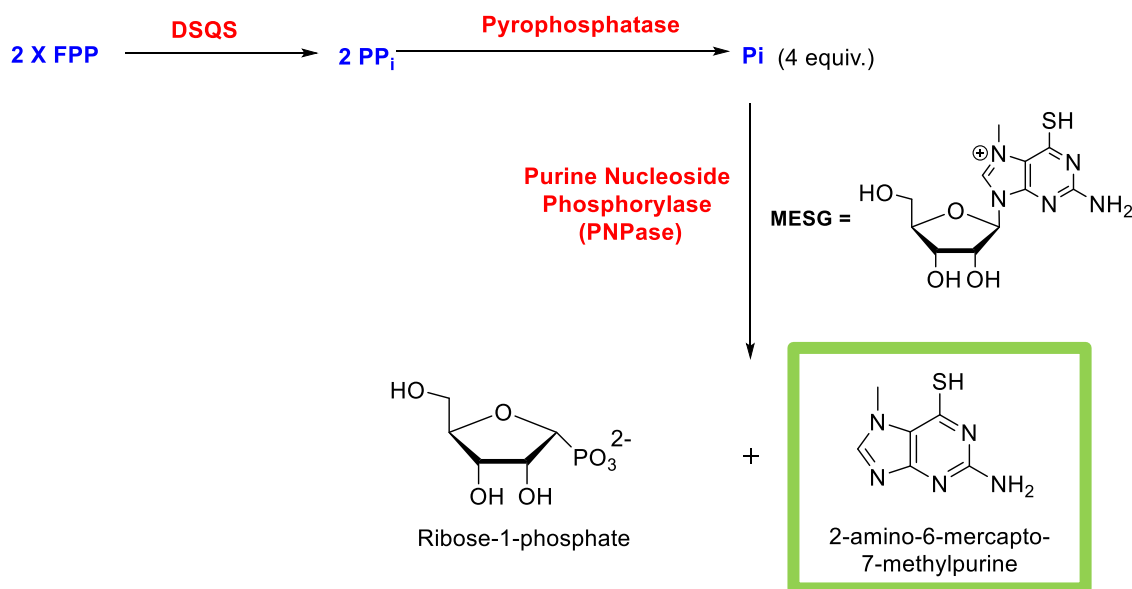


**Figure 3.19: Continuous coupled assay for phosphate release in the reaction catalyzed by DSQS. The inset shows the chromophore.**

Human squalene synthase (HSQS) utilizes NADPH during catalysis (Figure 3.20) with a  $K_m$  value of 430  $\mu\text{M}$ , which has a high absorbance that overlaps with that of the kinetic assay's chromophore; thereby interfering with the spectrophotometric assay.<sup>64,131</sup> Therefore, the use of the spectrophotometric assay in that case is prohibited in monitoring the kinetics of the full SQS reaction. It is noteworthy that the presqualene diphosphate (PSPP) intermediate can still be formed in the absence of NADPH and the first pyrophosphate moiety (PPi) is released as a byproduct (Figure 3.20).<sup>64</sup> Therefore, the rate of the first half reaction can be monitored by the release of the pyrophosphate byproduct using the spectrophotometric assay for phosphate release.

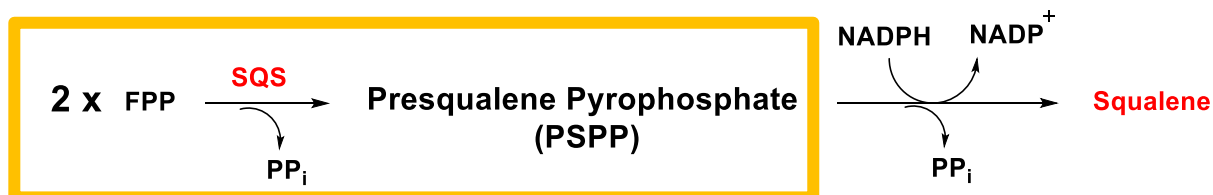


**Figure 3.20: The reaction catalyzed by SQS. The inset outlines the first half of the enzymatic reaction.**

Secondly, it has been found that inhibitors can still bind to the free HSQS enzyme (or perhaps a 1:1 FPP – enzyme complex) in the absence of NADPH, and they will compete with the FPP substrates.<sup>131</sup> Thus, the inhibition of the half reaction can be used to reflect the affinity of the inhibitors to the HSQS active site, and we were able to measure IC<sub>50</sub> values for this process. Due to the limitations of our assay, determinations of  $K_I$  values were not performed with the SQS enzyme.

In contrast, dehydrosqualene synthase (DSQS) does not utilize NADPH during catalysis (Figure 3.21), and there is no interference in the absorption spectrum.<sup>75</sup> Consequently, a full kinetic analyses to obtain a  $K_I$  value was performed with DSQS, using the spectrophotometric assay shown previously.

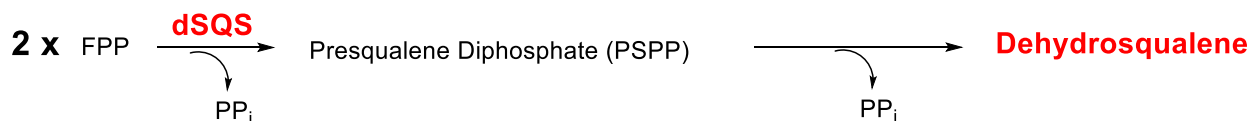


**Figure 3.21: The reaction catalyzed by DSQS.**

Prior to the measurement of inhibition constants, a Michaelis-Menten analysis was used to obtain the values of  $k_{cat}$  and  $K_m$  for the DSQS reaction. Initial velocities were measured at different concentrations of farnesyl diphosphate (FPP) incubated with  $MgCl_2$  (5 mM) and dehydrosqualene synthase in a HEPES buffer (pH 7.5) containing 5% ethanol. The kinetic parameters were then determined by fitting the initial velocities to the Michaelis-Menten equation and a hyperbolic kinetic profile was obtained with the following results  $k_{cat} = 0.39 \pm 0.01 \text{ s}^{-1}$ ,  $K_m = 25 \pm 5 \text{ }\mu\text{M}$ , and  $k_{cat}/K_m = 16 \times 10^3 \text{ M}^{-1}\text{s}^{-1}$  (Figure 3.22).

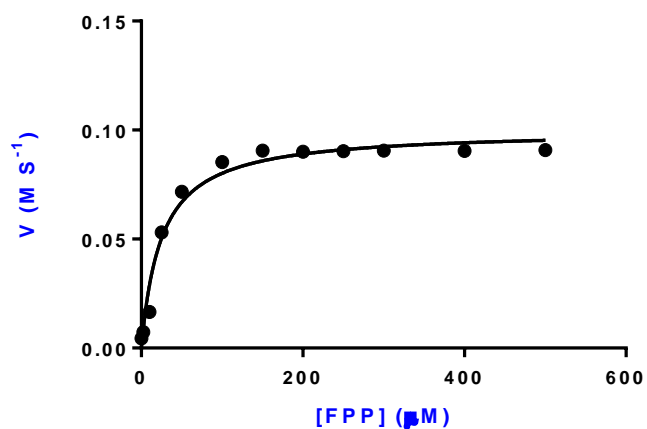


**Figure 3.22: A plot of initial velocity vs [FPP] for the reaction catalyzed by DSQS.** Kinetic parameters were obtained by fitting the data to the Michaelis Menten equation and were found to be as follows:  $k_{\text{cat}} = 0.39 \pm 0.01 \text{ s}^{-1}$ ,  $K_{\text{m}} = 25 \pm 5 \text{ } \mu\text{M}$ , and  $k_{\text{cat}}/K_{\text{m}} = 16 \times 10^3 \text{ M}^{-1}\text{s}^{-1}$

### 3.6.2 Inhibition Results and Discussion

In this study, a guanidinium/amidinium moiety was appended to a phosphinyl phosphonate group (a non-hydrolyzable analogue of pyrophosphate) to give inhibitors **26** and **36**, respectively. These were designed to act as a close mimic of the putative intermediates and/or transition states formed in the reactions catalyzed by HSQS and DSQS enzymes (Figure 3.23). A urea-containing inhibitor **34** was also prepared as a negative control.

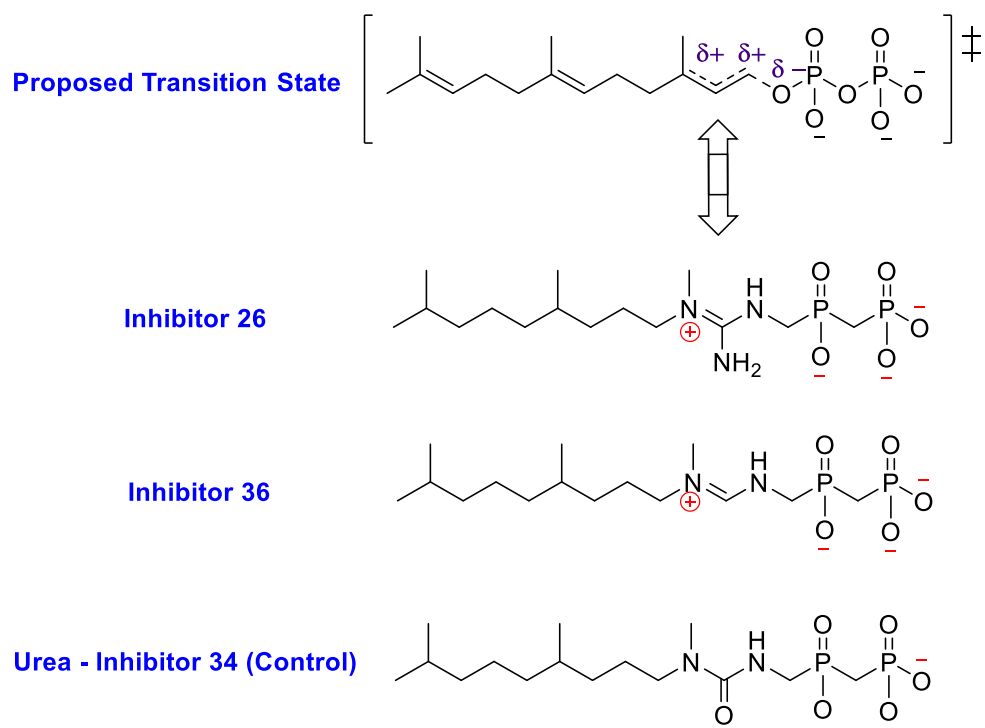


**Figure 3.23: A scheme showing how inhibitors 26 and 36 mimic the proposed transition state. The bottom structure shows the neutral urea-containing inhibitor 34 as a negative control.**

In the case of human squalene synthase (HSQS), only  $IC_{50}$  values on the inhibition of the first half reaction were determined ( $[FPP] = 50 \mu M$ ), due to the caveats mentioned in section 3.6.1. Linear initial rates indicated that product inhibition of this unnatural process (run in the absence of NADPH) was not problematic under these assay conditions. Inhibitors **26**, **36** and **34** were shown to bind with  $IC_{50}$  values of  $32 \pm 4 \mu M$ ,  $212 \pm 7 \mu M$  and  $1.5 \pm 1 \mu M$ , respectively (Figure 3.24).

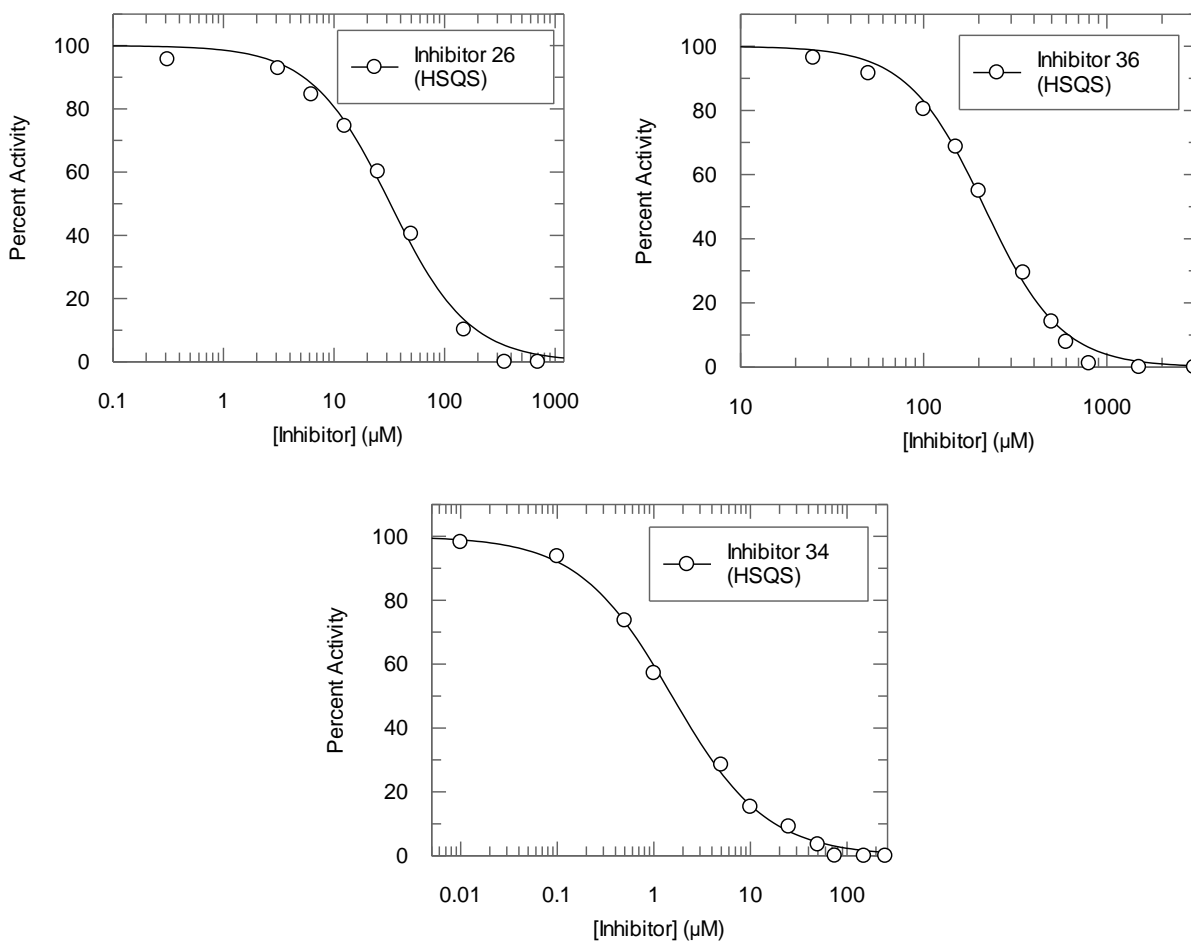


**Figure 3.24:  $IC_{50}$  determinations for the inhibition of the reaction catalyzed by HSQS ( $[FPP] = 50 \mu M$ ). Graphs show data for inhibitors 26, 36 and 34, respectively.**

Under identical concentrations of FPP, the  $IC_{50}$  values of inhibitors **26**, **36**, and **34** against dehydrosqualene synthase (DSQS) were found to be  $17 \pm 1 \mu\text{M}$ ,  $45 \pm 2 \mu\text{M}$ , and  $5.5 \pm 0.2 \mu\text{M}$ .

The  $IC_{50}$  curves for all three inhibitors are shown in Figure 3.25.

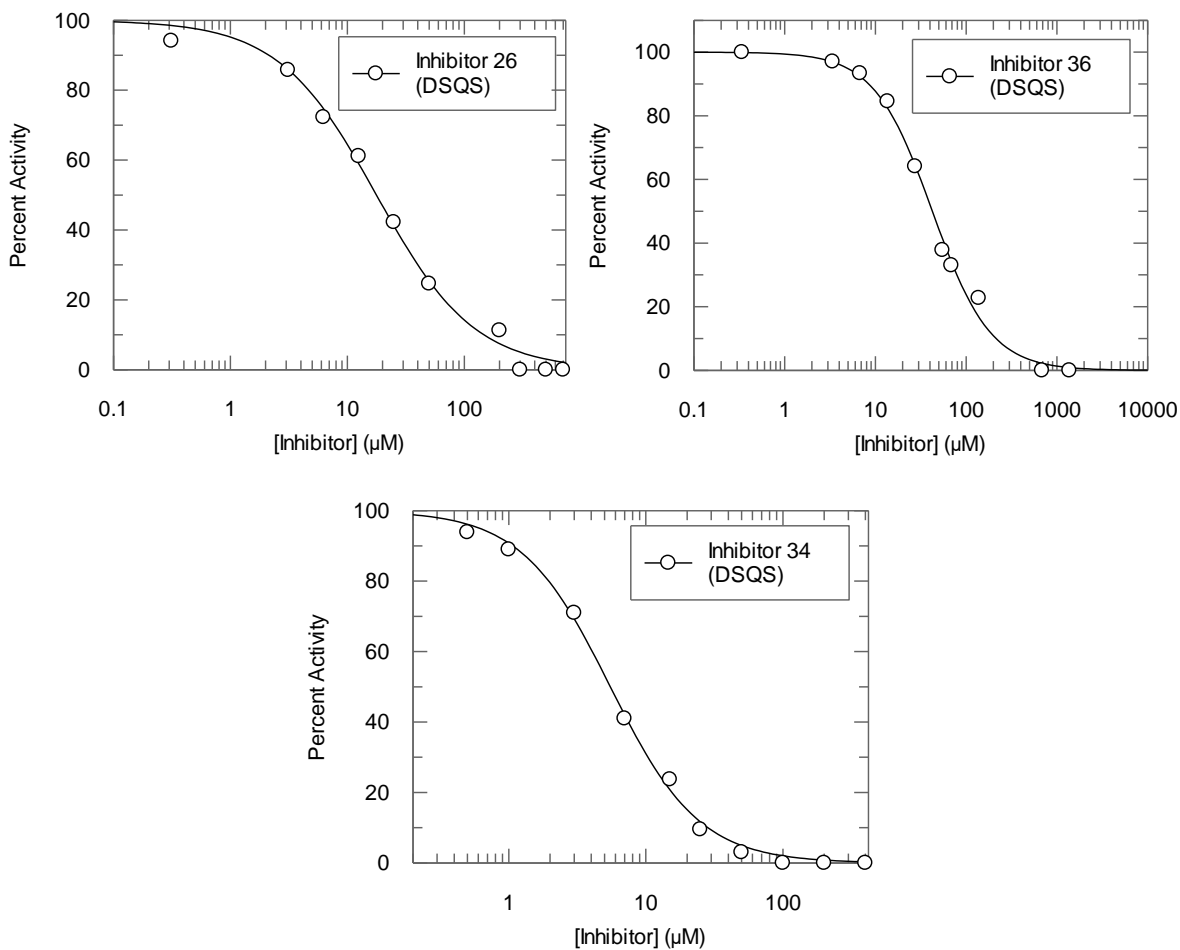


**Figure 3.25:  $IC_{50}$  determinations for the inhibition of the reaction catalyzed by DSQS ([FPP] =  $50 \mu\text{M}$ ). Graphs show data for inhibitors 26, 36 and 34, respectively.**

Surprisingly, the inhibition results with inhibitors **26** and **34** determined for both human squalene synthase (HSQS) and bacterial dehydrosqualene synthase (DSQS) enzymes indicate that the neutral urea-containing inhibitor **34** is the most potent of the three. These results indicate that the positive charge of the guanidinium moiety does not make a significant contribution to binding. Inhibitor **36**, the amidinium inhibitor, was the weakest of the three in both cases. The relatively good agreement between the trends in the measured  $IC_{50}$  values for both enzymes, suggests similar modes of binding to their inhibitors, and implies that the first half of the HSQS reaction, which lacks the NADPH cofactor, can be used as a reliable assay for evaluating the binding affinity of competitive inhibitors.

In the case of DSQS, where it was possible to monitor the kinetics of the complete reaction, we decided to obtain a  $K_I$  value and to probe whether the compounds act as competitive inhibitors. We varied the concentrations of both the inhibitors and the substrate. The linear initial velocities obtained for inhibitors **26**, **36**, and **34** were analyzed using the GraphPad Prism software, and the inhibition kinetic data were found to fit Michaelis-Menten models for competitive inhibition. The following values of  $K_I$  were calculated:  $1.9 \pm 0.2 \mu\text{M}$ ,  $4.2 \pm 0.7 \mu\text{M}$  and  $0.6 \pm 0.1 \mu\text{M}$ , respectively. The following Michaelis-Menten fit models were obtained for inhibitors **26**, **36**, and **34**, respectively, (Figure 3.26).

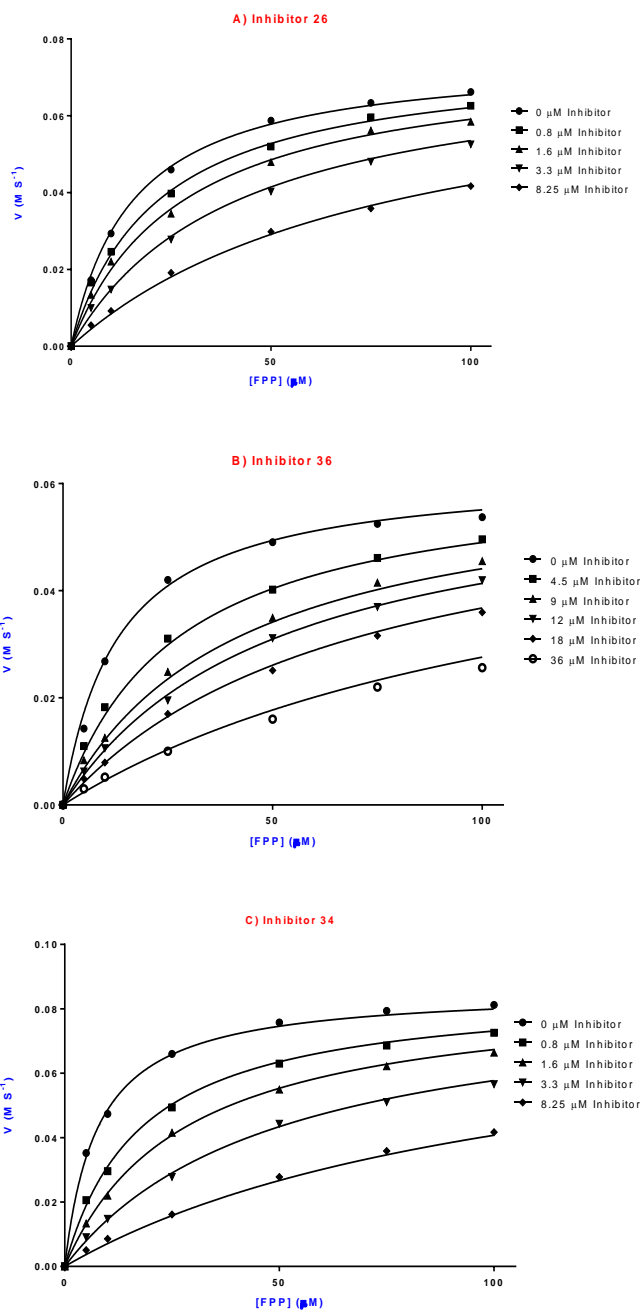


**Figure 3.26: Plot of rate versus FPP concentration for the inhibition of the DSQS reaction with fitting to the Michaelis-Menten equation for competitive inhibition. A) Data for inhibitor 26. B) Data for inhibitor 36. C) Data for inhibitor 34.**

Inhibitors **26**, **36** and **34** were confirmed to act as competitive inhibitors using Lineweaver-Burk plots (Figure 3.27).

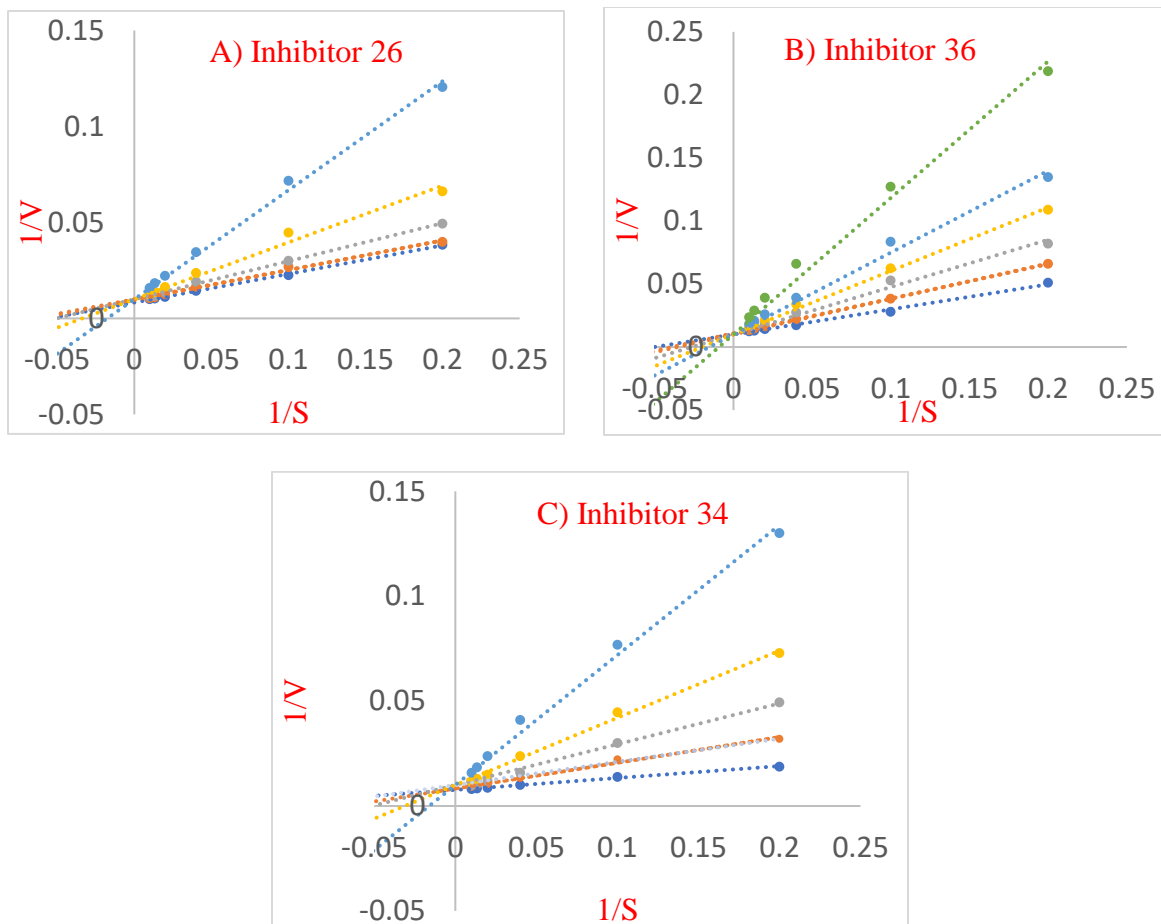


**Figure 3.27: Lineweaver-Burk plots for the inhibition of DSQS by inhibitors 26, 36, and 34.**

The color codes for the above Lineweaver-Burk plots are as follows: **A)** Inhibition by inhibitor **26** at the following concentrations: light blue = 8.25  $\mu\text{M}$ , yellow = 3.3  $\mu\text{M}$ , grey = 1.6  $\mu\text{M}$ , orange = 0.8  $\mu\text{M}$ , dark blue = 0  $\mu\text{M}$ . **B)** Inhibition by inhibitor **36** at the following concentrations: green = 36  $\mu\text{M}$ , light blue = 18  $\mu\text{M}$ , yellow = 12  $\mu\text{M}$ , grey = 9  $\mu\text{M}$ , orange = 4.5  $\mu\text{M}$ , dark blue = 0  $\mu\text{M}$ . **C)** Inhibition by inhibitor **34** at the following concentrations: light blue = 8.25  $\mu\text{M}$ , yellow = 3.3  $\mu\text{M}$ , grey = 1.6  $\mu\text{M}$ , orange = 0.8  $\mu\text{M}$ , dark blue = 0  $\mu\text{M}$ .

Since the  $K_I$  values are only an order of magnitude lower than the  $K_m$  values of the natural DSQS substrate FPP, inhibitors do not bind significantly more strongly than the substrate despite the former resembling the enzymatic reaction intermediates. Interestingly, the  $\text{NH}_2$  moiety of the guanidinium group in inhibitor **26**, and the absence of the unsaturation in the hydrocarbon chain, in inhibitor **36**, were not detrimental to binding as the  $K_I$  values are similar between the two inhibitors. The fact that the urea-containing inhibitor **34** was found to be slightly more potent than the guanidinium-containing inhibitor **26** indicates that the incorporation of the positive charge from the guanidinium moiety does not significantly increase the binding affinity. Since inhibitor **34** is effectively isosteric with inhibitor **26**, it would appear that the direct stabilization of the allylic carbocation intermediate is not a key factor in catalysis with these enzymes.

### 3.7 Conclusion and Summary

In this study three inhibitors were prepared: the first included a guanidinium group, the second included an amidinium group, and the last a was neutral urea-containing compound that was isosteric to the first inhibitor. These inhibitors were tested on human squalene synthase and bacterial dehydrosqualene synthase in order to test whether the inclusion of a positive charge, represented by the aforementioned guanidinium or amidinium groups, would significantly contribute to binding. These functional groups provide not only a positive charge but also possess resonance structures that delocalize the positive charge over two/three nitrogen atoms. This also introduces planarity to the inhibitors' structure. These structural and electronic factors were designed to mimic the putative allylic carbocation generated in the active site of the target enzymes. It would seem reasonable to suspect that these enzymes would have evolved to stabilize carbocationic intermediates and the transition states leading to them, therefore, it was believed that they would bind tightly to these inhibitors. Inhibitors **26** and **36** were found to inhibit dehydrosqualene synthase (DSQS) in the low micromolar range with  $K_I$  values fairly close to the  $K_m$  value for farnesyl diphosphate (FPP,  $K_m = 25 \mu\text{M}$ ) (Table 1). Unexpectedly, the inhibitor lacking a positive charge (urea-containing inhibitor **34**) did bind to DSQS slightly better than inhibitors **26** or **36**. In a similar fashion, inhibitors **26**, **36** and **34** were assayed, in the first half of the HSQS reaction, and similar trends of inhibition were observed.

	$K_I$ for DSQS ( $\mu\text{M}$ )	$\text{IC}_{50}$ for DSQS ( $\mu\text{M}$ ) <sup>a</sup>	$\text{IC}_{50}$ for SQS ( $\mu\text{M}$ ) <sup>a,b</sup>
Inhibitor <b>26</b>	$1.9 \pm 0.2$	$17 \pm 1$	$32 \pm 4$
Inhibitor <b>36</b>	$4.2 \pm 0.7$	$45 \pm 2$	$212 \pm 7$
Inhibitor <b>34</b>	$0.6 \pm 0.1$	$5.5 \pm 0.2$	$1.5 \pm 1$

**Table 1: Summary of kinetic constants measured with DSQS and SQS,<sup>a</sup> measured with [FPP] = 50  $\mu\text{M}$ . <sup>b</sup> measured for first half reaction in absence of NADPH**

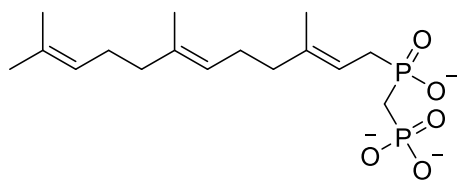
The hypothesis that the incorporation of guanidinium and amidinium groups should increase inhibitor potency is refuted by one of the following alternative hypotheses. One possibility is that there aren't any specific electrostatic interactions between the enzyme and the allylic carbocation during catalysis. For such a transformation to occur there are several carbocation rearrangements that must take place, and there are many distinct binding sites that need to be occupied by a carbocation during catalysis. Perhaps the enzyme does not need to evolve an active site that stabilizes all of them. Instead, the ionization of farnesyl diphosphate (FPP) may be initiated by the strong interactions of the  $\text{Mg}^{2+}$  cluster to the pyrophosphate leaving group as well as by the binding of the long hydrophobic tunnel to the FPP hydrophobic tail.<sup>63,75</sup> Optimizations of these binding interactions in the transition state for the initial ionization of farnesyl diphosphate (FPP), which leads to the formation of a stable tertiary/allylic carbocation and a stable leaving group, could suffice to promote ionization. Any electrostatic interactions required to stabilize the carbocation intermediate could be supplied by the adjacent pyrophosphate group in the ion pair, and the enzyme may not need to evolve them.

Another possibility is that the allylic carbocation may not be formed as a discrete intermediate, given the lack of direct evidence for the formation of such a species.<sup>134</sup> However, it seems somewhat unlikely that the cyclopropanation reaction, which leads to the formation of PSPP, occurs in a single concerted step and that it does not involve any carbocationic intermediates given the general acceptance of the formation of carbocation intermediates in most enzymatic reactions that utilize allylic diphosphates as substrates. It would be expected, even if this concerted reaction was operative, that the cyclopropanation transition state would bear considerable carbocationic character. Therefore, it would still be expected that inhibitors bearing a positive charge would bind more tightly than neutral inhibitors.

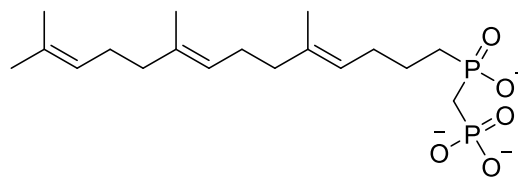
A final possibility that can account for these results, is that the guanidinium/amidinium cations may have not picked up the essential binding interactions for catalysis because of their mis-positioning in the active site. Since there are two FPP binding sites, and only one of them catalyzes the dissociation of FPP, it is possible that our inhibitor only occupies the "non-ionizing" FPP binding site. Therefore, the presence of a positive charge is not effective at increasing potency. However, earlier attempts to inhibit squalene synthase (SQS) with ammonium-containing FPP analogues seem to contradict this explanation. Biller *et al* reported, in one of the first studies on inhibitors of squalene synthase (SQS), that inhibitor **37**, a stable FPP analogue wherein both allylic and anhydride oxygen atoms were replaced with CH<sub>2</sub>, inhibited the reaction with an IC<sub>50</sub> of 31.5 μM (Figure 3.28).<sup>133</sup>

Moreover, in an attempt to approximate the transition state separation between the fragments, Biller *et al* synthesized inhibitors **38**, **39**, and **40** (Figure 3.28). In these compounds the farnesyl hydrocarbon tails and the same phosphinyl phosphonate moiety described in this work were connected through a variety of two atom linkers. With an IC<sub>50</sub> value of 67 μM, inhibitor **38** (with a two carbon linker) was a slightly weaker inhibitor of squalene synthase than inhibitor **37**.<sup>133</sup>

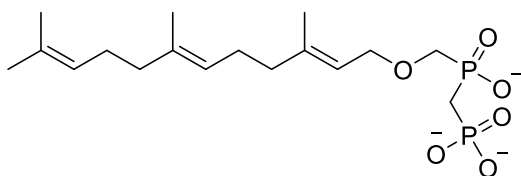
Biller *et al* replaced one methylene group with an oxygen atom to give inhibitor **39**, in order to position an H-bond acceptor within the active site acid. Interestingly, a profound increase in potency was observed for inhibitor **39**, as it was found to be 1300-fold more potent than its methylene analogue, inhibitor **38**. Inhibitor **39** inhibited squalene synthase with an IC<sub>50</sub> of 0.05 μM. On the other hand, when one methylene group was replaced with an ammonium functionality to give inhibitor **40**, the potency was reduced by 32-fold to give an IC<sub>50</sub> of 16 μM. A comparison of the results obtained with inhibitor **39** and inhibitor **40** clearly demonstrate that the inclusion of a positive charge does not improve binding in this system.<sup>133</sup>



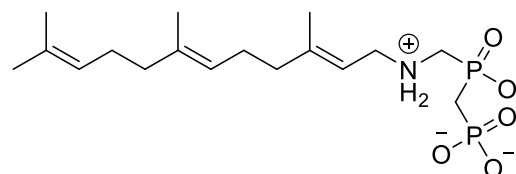
**Inhibitor 37**  
**IC<sub>50</sub> = 31.5 μM**



**Inhibitor 38**  
**IC<sub>50</sub> = 67 μM**



**Inhibitor 39**  
**IC<sub>50</sub> = 0.05 μM**



**Inhibitor 40**  
**IC<sub>50</sub> = 16 μM**

**Figure 3.28: Structures of inhibitors 37 – 40, with their IC<sub>50</sub> values.**

The ammonium-containing inhibitor **40** possesses a positive charge similar to inhibitors **26** and **36** described in this study and its IC<sub>50</sub> value is similar in magnitude (Figure 3.29). This work reveals the seemingly minimal advantage of the inclusion of a positive charge in the inhibitor design.

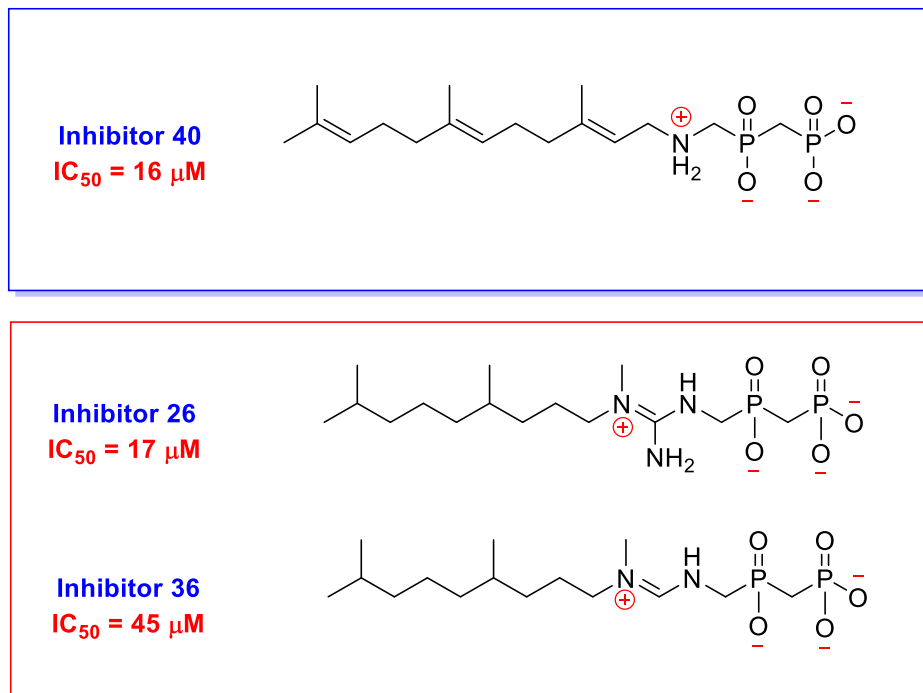


**Figure 3.29: The top box shows the structure and  $IC_{50}$  value of inhibitor 40. The bottom box shows the structures and  $IC_{50}$  values for both inhibitors 26 and 36 from our current study.**

Another example that suggests that SQS may not be directly stabilizing the allylic carbocation during catalysis involves lipophilic 1,1-bisphosphonates which are known to be potent inhibitors of many enzymes that utilize allylic pyrophosphate substrates.<sup>142</sup> For instance, inhibitor **41** (Figure 3.30), which is a bisphosphonate attached to a hydrocarbon tail, inhibits squalene synthase with an  $IC_{50}$  of 4.2  $\mu M$ . When replacing one methylene group with an ammonium functionality to give inhibitor **42** (Figure 3.30), inhibitor potency is attenuated: inhibitor **42** displayed an  $IC_{50}$  of 20  $\mu M$ . Studies described in this chapter, together with the aforementioned literature reports presented above, indicates that introducing a positive charge

into FPP analogues does not provide any additional binding to the SQS and DSQS enzyme, which indirectly supports our hypothesis mentioned above.

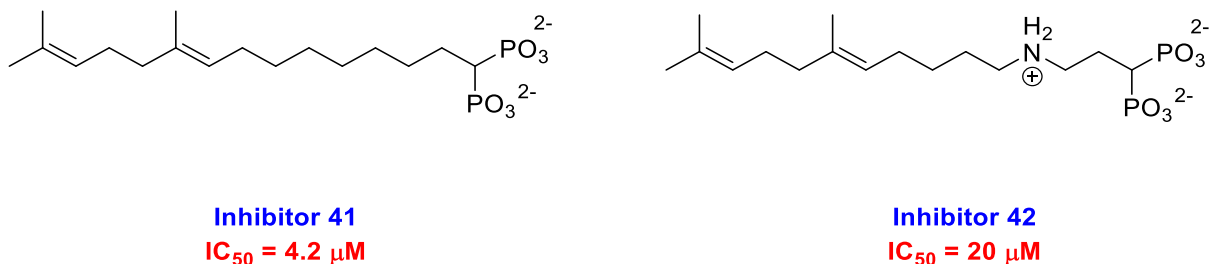


**Figure 3.30: Structures of inhibitors 41 and 42, with their  $IC_{50}$  values.**

In contrast, targeting the second half of the squalene synthase reaction using cationic inhibitors has had somewhat more success.<sup>143</sup> This half reaction involves the ionization of presqualene diphosphate (PSPP) and the release of a pyrophosphate moiety as a byproduct. Poulter and coworkers used a cationic inhibition strategy to design inhibitor **43** (Figure 3.31), which was found to be a potent inhibitor of squalene synthase.<sup>143</sup> Inhibitor **43** is designed to mimic the transition state/intermediate formed during the dissociation of the presqualene diphosphate intermediate (PSPP). It includes a positively charged ammonium group in an analogous position to that of the cyclopropylmethyl cation intermediate that would be expected to form, and was found to inhibit squalene synthase with an  $IC_{50}$  value of 5  $\mu M$ . Interestingly, inhibitor **43** binds to the SQS enzyme much better than the natural substrate PSPP by almost one order of magnitude, as its  $IC_{50}$  value compares favorably to the  $K_m$  value of 77  $\mu M$  for the conversion of PSPP into squalene. However, it should be noted that neutral isosteric analogues of inhibitor **43** were unavailable for comparison in this study.<sup>134,143</sup>

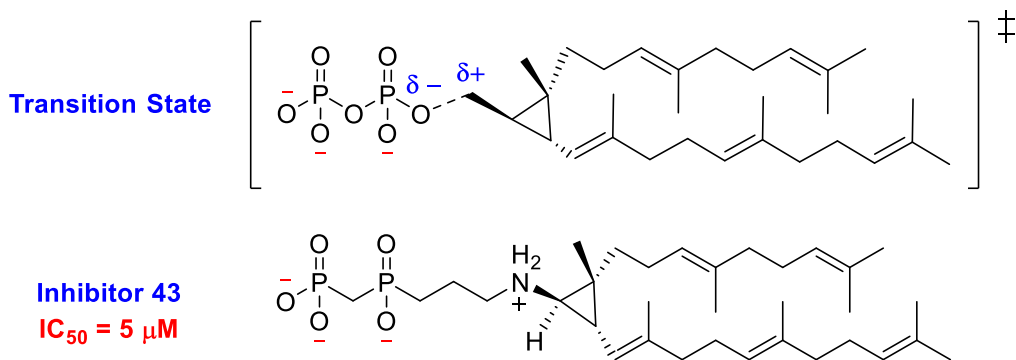
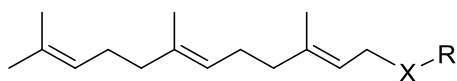


**Figure 3.31: The transition state for PSPP dissociation and structure of inhibitor 43, with its  $IC_{50}$  value.**

In another report <sup>144</sup>, the results supported the importance of incorporating a positive charge in squalene synthase inhibitors and suggested that the positive charge contributes significantly to the inhibitor's affinity for the enzyme active site. Interestingly, it showed that inhibitors such as **44** and **45** bound more tightly than their corresponding ether analogues, inhibitors **46** and **47**, by almost three orders of magnitude (Figure 3.32). <sup>144</sup> Their interpretation of this data was that the incorporation of the ammonium functionality in inhibitors, **44** and **45**, helps them to mimic the carbocation intermediate involved in the conversion of presqualene diphosphate (PSPP) to squalene in the second half of the SQS reaction. Moreover, several medicinal chemistry studies have previously reported very potent inhibitors with a positively charged ammonium functionality incorporated into their structures. <sup>145</sup>



**Inhibitor 44:** X = NH<sub>2</sub><sup>+</sup>, R = farnesyl, IC<sub>50</sub> = 48 μM

**Inhibitor 45:** X = NH<sub>2</sub><sup>+</sup>, R = (3-pyridyl)methyl, IC<sub>50</sub> = 0.05 μM

**Inhibitor 46:** X = O, R = farnesyl, IC<sub>50</sub> = 828 μM

**Inhibitor 47:** X = O, R = (3-pyridyl)methyl, IC<sub>50</sub> = 5 μM

**Figure 3.32: Structures of inhibitors 44 – 47, with their IC<sub>50</sub> values.**

Ammonium-containing inhibitors have been found to be very potent inhibitors for many families of enzymes, as the protonated amine effectively mimics carbocation intermediates and/or transition states.<sup>85,87,146</sup> For instance, several potent glycosidase inhibitors carry basic nitrogen in their structures.<sup>90,91,93</sup> These amino group-containing inhibitors serve to mimic the developing charge of an oxocarbenium ion-like transition state, and were shown to serve as potent inhibitors with *K<sub>I</sub>* values ranging from nanomolar to picomolar. The enzymes' affinity for a transition state/intermediate with a carbocationic character explains why the enzyme binds so tightly to these inhibitors.<sup>93</sup>

When we compare enzymes that promote the dissociation of allylic diphosphates to glycosidases, we find that the latter has a very poor leaving group (typically an alcohol). In addition, the leaving group in glycosidases lacks the capacity to be stabilized by charged hydrogen bonds or metal ion during catalysis, unlike the pyrophosphate leaving group in SQS. Most importantly, the substitution of sugars with many electron-withdrawing oxygen atoms, makes the oxocarbenium ion less stable than a tertiary allylic carbocation and thus high in

energy, which in turn will force the enzyme to evolve an active site that is capable of stabilizing it (or the corresponding transition state) in order to promote its formation during catalysis.<sup>124–128</sup>

Another interesting example that highlights the application of ammonium-containing inhibitors is observed with enzymes that generate tertiary carbocations from the protonation or alkylation of alkenes. A classic example is the development of isopentenyl diphosphate isomerase (IDI) inhibitors. One of the very potent inhibitors of this enzyme is inhibitor **48**, which is an ammonium-containing inhibitor (Figure 3.33). The appropriately positioned positively charged nitrogen atom makes inhibitor **48** a good mimic of the carbocationic intermediate, with a  $K_{\text{dis}}$  value less than 120 pM ( $K_{\text{dis}}$  was calculated from  $K_{\text{dis}} = \frac{k_{\text{off}}}{k_{\text{on}}}$ ).<sup>85,87,88</sup>

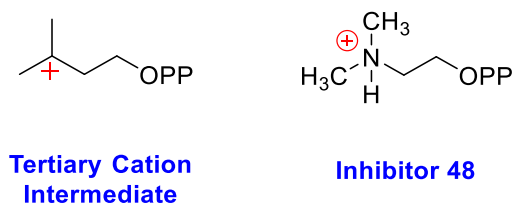


**Figure 3.33: Structure of the tertiary cation intermediate formed in the reaction of isopentenyl diphosphate isomerase and inhibitor 48.**

When comparing these enzymes to those involving the dissociation of allylic diphosphates, key differences emerge. Firstly, the lack of resonance stabilization in tertiary carbocations, makes them less stable than tertiary allylic carbocations. Secondly, catalysis can't be assisted by tight binding to a diphosphate moiety, given that there is no ionization in such

reactions.<sup>89</sup> Lastly, with no pyrophosphate to act as an ion pair in these enzymatic reactions, any stabilizing electrostatic interactions must come from the active site residues. Consequently, one would expect that this family of enzymes would evolve an active site that stabilizes these highly energetic carbocation intermediates by tight binding during catalysis.

All the aforementioned findings suggest that both dehydrosqualene synthase (DSQS) and squalene synthase (SQS) likely did not evolve an active site to stabilize the carbocationic intermediate formed from the heterolytic dissociation of the farnesyl diphosphate (FPP) substrate. Nevertheless, this conclusion can't be generalized to all families of enzymes that utilize allylic diphosphates in catalysis. Other allylic diphosphate-utilizing enzymes have been successfully inhibited with inhibitors bearing a protonated amine group. For instance, in the case of farnesyltransferase, an ammonium-containing inhibitor (Figure 3.34) has been reported with an IC<sub>50</sub> value of 14  $\mu$ M, its potency dropped more than 20 fold upon replacing the positively-charged amine group with a sulfur atom.<sup>147</sup>

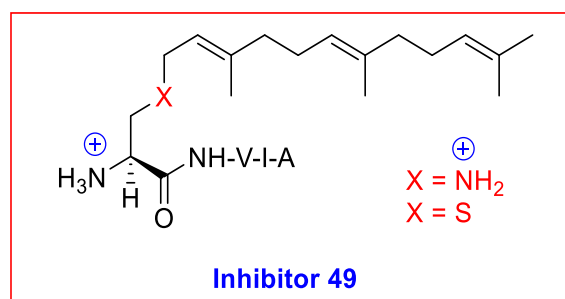


**Figure 3.34: Structure of inhibitor 49.**

In summary, this work suggests that, the development of inhibitors bearing a carbocationic character to mimic carbocation intermediate/transition state may be an effective approach to potent inhibitor design with some members of the above-mentioned enzyme families, but not necessarily with all of them.

### **3.8 Experimental Procedures**

#### **3.8.1 Materials and Methods**

All reagents were purchased from Sigma-Aldrich, Fluka, Toronto Research Chemicals Inc. (TRC), or Advanced ChemTech and used without further purification unless otherwise stated. D<sub>2</sub>O (99.9%) was purchased from Cambridge Laboratories. Dowex® 50WX8 (H<sup>+</sup> form) resin was purchased from Sigma-Aldrich. Triethylamine was distilled over CaH<sub>2</sub> under an atmosphere of Ar. Silica gel chromatography was performed using Silica Gel SiliaFlash F60 (230-400 mesh, Silicycle). Biogel P-2 size exclusion chromatography resin was purchased from Bio-Rad. <sup>1</sup>H NMR spectra were recorded on a Bruker AV400 spectrometer at a field strength of 400 MHz. Proton-decoupled <sup>31</sup>P NMR spectra were recorded on Bruker AV400 spectrometer at a field strength of 162 MHz. Mass spectra were obtained on a Waters Micromass LCT mass spectrometer using electrospray ionization (ESI-MS). Neutral compounds were detected as positive ions, and negatively charged compounds were detected as negative ions.

## 3.8.2 Synthesis of Inhibitors

### 3.8.2.1 Synthesis of Compound 31

Compound **24** (2 g, 11 mmol) was dissolved in EtOH (50 ml) and 10% Pd/C catalyst (200 mg) was added. The mixture was stirred under 1 atm of H<sub>2</sub> (g) for 18 h at rt. The catalyst was removed by filtration and the resulting filtrate was evaporated to dryness under reduced pressure giving compound **31** as a viscous oil (1.8 g, 99%) <sup>1</sup>H NMR (CDCl<sub>3</sub>, 400 MHz): δ ppm 2.56 (t, *J* = 6.2, 2H), 2.48 (s, 3H), 1.58 – 0.85 (m, 12H), 0.79 (d, *J* = 6.6 Hz, 9H). ESI-MS *m/z* 186.4 [M+H]<sup>+</sup>.

### 3.8.2.2 Synthesis of Inhibitor 26

#### 3.8.2.2.1 Synthesis of Compound 23

N, N-Di-Boc-thiourea (410 mg, 1.53 mmol) and NaH (80 mg, 2.1 mmol) were stirred in dry THF (20 ml) under argon for 25 min at 0 °C. Trifluoroacetic anhydride (300 μl, 1.75 mmol) was then added and the mixture was left stirring for 1 h at 0° C, followed by the addition of compound **12** (400 mg, 1.75 mmol). The reaction mixture was stirred at rt for 20 h, quenched with H<sub>2</sub>O, and the product was extracted with CH<sub>2</sub>Cl<sub>2</sub> (3 X 50 ml). The organic layers were dried over MgSO<sub>4</sub> and then concentrated under reduced pressure to yield a yellow oil. The crude product was purified using column chromatography (15%–100% EtOAc in petroleum ether) to afford compound **23** (400 mg, 60%). <sup>1</sup>H NMR (CDCl<sub>3</sub>, 400 MHz): δ ppm 10.09 (s, 1H), 8.09 (s,

1H), 4.47 (m, 2H), 4.34 – 4.05 (m, 6H), 2.54 (t,  $J = 17.3$  Hz, 2H), 1.47 (s, 9H), 1.24 (t,  $J = 7.1$  Hz, 6H), 1.19 (t,  $J = 5.1$  Hz, 3H).  $^{31}\text{P}$ - $\{^1\text{H}\}$  NMR ( $\text{CDCl}_3$ , 162 MHz):  $\delta$  ppm 19.72 (s), 40.05 (s). ESI-MS  $m/z$  433.1  $[\text{M}+\text{H}]^+$ .

### 3.8.2.2.2 Synthesis of Compound 32

Compound **23** (180 mg, 0.41 mmol), DIPEA (80  $\mu\text{l}$ , 0.41 mmol), EDC-HCl (170 mg, 0.83 mmol), and compound **31** (120 mg, 0.62 mmol) were dissolved in dry  $\text{CH}_2\text{Cl}_2$  (15 mL) at  $0^\circ\text{C}$  and stirred under argon for 25 h at rt. The reaction mixture was then quenched with  $\text{H}_2\text{O}$  and then extracted with  $\text{CH}_2\text{Cl}_2$  (3 X 50 ml). The organic layers were dried over  $\text{MgSO}_4$  and concentrated under reduced pressure to yield an oil. The crude product was purified using column chromatography (1-15% MeOH in EtOAc containing 5%  $\text{Et}_3\text{N}$ ) to afford compound **32** (140 mg, 60%).  $^1\text{H}$  NMR ( $\text{CDCl}_3$ , 400 MHz):  $\delta$  ppm 4.24 – 4.05 (m, 6H), 3.72 (m, 2H), 3.25 (m, 2H), 2.95 (s, 3H), 2.62 – 2.43 (m, 2H), 2.07 – 1.95 (m, 2H), 1.68 – 1.48 (m, 10H), 1.45 (s, 9H), 1.32 (m, 9H), 1.25 (m, 6H), 1.13 (t,  $J = 5.7$  Hz, 3H).  $^{31}\text{P}$ - $\{^1\text{H}\}$  NMR ( $\text{CDCl}_3$ , 162 MHz):  $\delta$  ppm 20.05 (s), 44.50 (s). HRMS (ESI)  $m/z$   $[\text{M} + \text{H}]^+$  calcd for  $\text{C}_{21}\text{H}_{47}\text{N}_3\text{O}_5\text{P}_2$  586.5711, found 586.5701.

### 3.8.2.2.3 Synthesis of Inhibitor 26

Compound **32** (100 mg, 0.17 mmol) was treated with 4 N HCl in H<sub>2</sub>O and stirred at 100° C for 48 h. The solution was then neutralized with NaOH (0.1 M) and concentrated under reduced pressure to yield a yellow oil. The compound was then dissolved in H<sub>2</sub>O (10 ml) and acidified with Dowex resin (H<sup>+</sup> form) to pH 1. The crude was then dissolved in H<sub>2</sub>O (10 ml), loaded onto a 50 mL column of size exclusion resin (Bio-Gel® P-2), and eluted with water. All fractions were lyophilized to dryness and analyzed using <sup>1</sup>H and <sup>31</sup>P NMR spectroscopy. Fractions containing inhibitor were redissolved in water, combined and lyophilized to give inhibitor **26** as a white solid (18 mg, 25%). <sup>1</sup>H NMR (MeOD, 400 MHz): δ ppm 3.55 (d, *J* = 8.6 Hz, 2H), 3.31 – 3.28 (m, 2H) 3.03 (s, 3H), 2.25 – 2.04 (m, 2H), 1.72 – 1.02 (m, 12H), 0.86 (d, *J* = 5.5 Hz, 9H). <sup>31</sup>P-<sup>1</sup>H NMR (MeOD, 162 MHz): δ ppm 18.66 (s), 33.04 (s). ESI-MS *m/z* 400.1 [M+H]<sup>+</sup>.

### 3.8.2.3 Synthesis of Inhibitor 34

#### 3.8.2.3.1 Synthesis of Compound 35

Compound **12** (300 mg, 1.09 mmol) was dissolved in dry CH<sub>2</sub>Cl<sub>2</sub> (15 mL), then Et<sub>3</sub>N (275 μl, 1.63 mmol) was added and the mixture was stirred under argon at rt for 30 min. Boc<sub>2</sub>O (300 mg, 1.32 mmol) was then added and the reaction was stirred at rt for 16 h. The reaction mixture was concentrated under reduced pressure and the crude product was purified using silica gel chromatography (25%–75% EtOAc in petroleum ether) to yield pure compound **35** (325 mg,

81%).  $^1\text{H}$  NMR ( $\text{CDCl}_3$ , 400 MHz):  $\delta$  ppm 4.30 – 4.06 (m, 6H), 3.55 – 3.65 (m, 2H), 2.60 – 2.36 (m, 2H), 1.49 (s, 9H), 1.45 – 1.25 (m, 6H), 1.24 – 1.19 (t,  $J = 7.6$  Hz 3H).  $^{31}\text{P}$ - $\{^1\text{H}\}$  NMR ( $\text{CDCl}_3$ , 162 MHz):  $\delta$  ppm 20.58 (s), 41.84 (s). ESI-MS  $m/z$  374.3  $[\text{M}+\text{H}]^+$ .

### 3.8.2.3.2 Synthesis of Compound 33

Compound **35** (80 mg, 0.21 mmol) was placed in a round-bottom flask followed by dry  $\text{CH}_2\text{Cl}_2$  (10 mL). 2-Chloropyridine (60  $\mu\text{l}$ , 0.63 mmol) was added, followed by trifluoromethanesulfonic anhydride (60  $\mu\text{l}$ , 0.31 mmol), and the reaction mixture was stirred for 50 min at rt. Then  $\text{Et}_3\text{N}$  (1.8 mL, 1.26 mmol) followed by the compound  $\pm\mathbf{31}$  (116 mg, 0.62 mmol) was added, and the reaction mixture was stirred at rt for 20 h. The crude product was purified using silica gel chromatography (10%–50% EtOAc in petroleum ether) to afford compound **33** (66 mg, 65%).  $^1\text{H}$  NMR ( $\text{CDCl}_3$ , 400 MHz):  $\delta$  ppm 4.28 – 4.06 (m, 6H), 3.6 – 3.72 (m, 2H), 2.95 (m, 2H), 2.76 (s, 3H), 1.85 – 1.75 (m, 2H), 1.56 – 1.03 (m, 21H), 0.88 – 0.94 (m, 9H).  $^{31}\text{P}$ - $\{^1\text{H}\}$  NMR ( $\text{CDCl}_3$ , 162 MHz):  $\delta$  ppm 22.50 (s), 45 (s). ESI-MS  $m/z$  483.9  $[\text{M}-\text{H}]^-$ .

### 3.8.2.3.3 Synthesis of Inhibitor 34

Compound **33** (100 mg, 0.21 mmol) was treated with TMSBr (1 mL) in  $\text{CH}_2\text{Cl}_2$  (10 mL) and stirred at rt for 18 h. The solution was then neutralized with NaOH (0.1 M) and was subsequently concentrated under reduced pressure to yield a yellow oil. The compound was then dissolved in  $\text{H}_2\text{O}$  (10 mL) and acidified with Dowex resin ( $\text{H}^+$  form) to pH 1. The crude was then dissolved in  $\text{H}_2\text{O}$  (10 mL), loaded onto a 50 mL column of size exclusion resin (Bio-Gel®P-2)

and eluted with water. All fractions were lyophilized to dryness and analyzed using  $^1\text{H}$  and  $^{31}\text{P}$  NMR spectroscopy. Fractions containing inhibitor were redissolved in water, combined and lyophilized to give inhibitor **34** as a white solid (48 mg, 56%).  $^1\text{H}$  NMR ( $\text{D}_2\text{O}$ , 400 MHz):  $\delta$  ppm 3.68 – 3.24 (m, 4H), 2.96 (s, 3H), 2.15 – 2.09 (m, 2H), 1.73 – 0.95 (m, 12H), 0.92 (s, 9H).  $^{31}\text{P}$ - $\{^1\text{H}\}$  NMR ( $\text{D}_2\text{O}$ , 162 MHz):  $\delta$  ppm 14.79 (s), 36.93 (s). ESI-MS  $m/z$  399.2  $[\text{M}-\text{H}]^-$ .

### 3.8.3 General Enzyme Methods

Centrifugal filters (4 mL 10 000 MWCO) were purchased from Millipore. Isopropyl- $\beta$ -D-1-thiogalactopyranoside (IPTG) was purchased from Invitrogen. Chelating Sepharose® Fast resin was purchased from Pharmacia Biotech. Protein concentrations were determined by the method of Bradford on a Cary 3E UV-Vis spectrophotometer using bovine serum albumin as standard. These measurements were performed at room temperature. Protein purity was assessed using SDS-PAGE. The enzyme kinetic assays were carried out on a Cary 300 UV-Vis spectrometer with a Cary temperature controller attached. All kinetic parameters were determined from the fit of initial velocities to the Michaelis-Menten equation:  $v_0 = \frac{V_{max} \cdot [\text{S}]}{K_M + [\text{S}]}$ .

Inhibition kinetics were determined using:  $v_0 = \frac{V_{max} \cdot [\text{S}]}{K_M (1 + \frac{[\text{I}]}{K_I}) + [\text{S}]}$ .  $\text{IC}_{50}$  values were calculated using

this equation:  $y = \frac{100\%}{1 + \left(\frac{x}{\text{IC}_{50}}\right)^s}$ , where "s" is the slope factor, x is the inhibitor concentration and y is

the percent activity.

### 3.8.3.1 Overproduction and Purification of HSQS and DSQS

The gene encoding for dehydrosqualene synthase from *S. aureus* MS4 was synthesized and cloned into a pET28a(+) vector at the BamH1 and Sall restriction sites, by Genscript. A stop codon was added after the DSQS gene to prevent expression of pET28a's optional C-terminal His tag. Expression of the resulting plasmid, pETa-DSQS results in a protein expressed with an N-terminal His tag and T7 tag. The codon optimized gene for doubly truncated human squalene synthase (residues 31-370) was synthesized by GenScript and cloned into a pET28b expression vector (Novagen) via the *NdeI/XhoI* restriction sites, yielding pET28b-hSQS(31-370) (provided to us by Dr Jon Freeman). A stop codon was added after the SQS gene to prevent expression of pET28b's optional C-terminal His tag. The resulting construct encoded HSQS (31-370) with an N-terminal His tag followed by a thrombin protease recognition site. Both plasmids were used to transform chemically competent *Escherichia coli* expression strain Rosetta(DE3) pLysS (Novagen) following the Inoue method. Overproduction of DSQS and SQS was achieved following a modification of a previously described procedure.<sup>148</sup> Transformed cells were grown at 37 °C in 1 L of Terrific Broth (TB) medium containing 30 µg/mL kanamycin until an OD<sub>600</sub> of 0.6 was reached. Cells were induced for overproduction by the addition of 120 mg (1 mM) of isopropyl-β-D-1-thiogalactopyranoside (IPTG). After growing at 24 °C for an additional 24 hours, cells were harvested and lysed with a French press in Tris-HCl buffer (50 mM, pH 8.0) containing dithiothreitol (2 mM), NaCl (500 mM), MgCl<sub>2</sub> (2 mM), CHAPS (4 mM), imidazole (20 mM), aprotinin (1 µg mL<sup>-1</sup>), and pepstatin A (1 µg mL<sup>-1</sup>).

The lysate was cleared by centrifugation (34 155g, 45 min) and filtration through a 0.22 mm filter. A column containing chelating Sepharose fast flow resin (GE Healthcare, 10 mL) was charged with 100 mM NiSO<sub>4</sub> and washed with Tris-HCl buffer (50 mM, pH 8.0) containing NaCl (500 mM) and imidazole (5 mM). The clarified lysate was loaded onto the column and eluted with same buffer but containing imidazole at 5, 20, 100, and 500 mM. Fractions containing the desired enzyme eluted after the addition of 500 mM imidazole as analyzed by Bradford assay. <sup>129</sup> Glycerol (10%) was added to the resulting eluent before flash freezing with liquid N<sub>2</sub>. Typically, 20-30 mg of enzyme was purified from 1 L of culture. Enzymes were found to be more than 90% pure as analyzed by SDS-PAGE.

### **3.8.3.2 Measurements of Inhibition Kinetics**

Kinetic parameters of dehydrosqualene synthase (DSQS) were measured by a modification of a previously described continuous coupled assay for phosphate release. The concentrations of stock solutions of FPP were determined by <sup>1</sup>H NMR spectroscopy with the addition of an internal standard of 1 mM 1,4-dioxane and integration of the appropriate signals. A cuvette containing 50 mM HEPES buffer (pH 7.50, final volume 1000 μL, containing 5% EtOH), MgCl<sub>2</sub> (5 mM), farnesyl diphosphate (50 μM, added from a stock solution prepared in 40% EtOH), 2-amino-6-mercapto-7-methylpurine ribonucleoside (MESG) (20 μM), purine nucleoside phosphorylase (PNPase) (1 unit), and inorganic pyrophosphatase (PPase) (0.5 unit) was thermally equilibrated for 5 min at 37 °C. The enzymatic reaction was initiated by the addition of dehydrosqualene synthase (MW = 37000 g/mol, 0.04 nmol/ml) and the rate was calculated from the observed increase of absorption at 360 nm ( $\epsilon = 11000 \text{ M}^{-1} \cdot \text{cm}^{-1}$ ) after

accounting for the 4:1 ratio of phosphate to dehydrosqualene. Kinetic parameters were determined from the fit of initial velocities to the Michaelis-Menten equation. SQS kinetics were determined in the same fashion but (MW = 37000 g/mol, 0.05 nmol/ml) of enzyme was added and the 2:1 ratio of phosphate to squalene was accounted for. Inhibition kinetics were described as above, but with the incubation of inhibitors **26**, **36** and **34** at various concentrations. The kinetic parameters  $k_{cat}$  and  $K_m$ , the inhibition constants  $IC_{50}$  and  $K_I$ , and their associated errors, were determined by fitting the initial velocity data to the Michaelis-Menten equation using non-linear regression. Every experiment was repeated 3 times and the resulting kinetic constants never differed by more than 20%. Data obtained on different days with different batches of enzyme could result in kinetic constants that differed from those reported above by up to 25%.

## Chapter 4: The Inhibition of Type 1 Isopentenyl Diphosphate Isomerase by Guanidinium-Based Inhibitors

### Guanidinium-Based Inhibitors

#### 4.1 Introduction

In the previous two chapters, we described the use of guanidinium-based inhibitors against enzymes that catalyze the ionization of allylic diphosphates. We found limited success with this approach and rationalized that the enzymes may not bind the carbocation tightly. In this chapter, we turn our attention to an enzyme that generates a less stable carbocation and not an ion pair. Such an enzyme would likely have evolved to bind tightly to the carbocation.

Organisms utilizing the mevalonate pathway (MVA) critically rely on isopentenyl diphosphate isomerase (IDI), since the loss of its activity is lethal to them.<sup>80,81,87</sup> It is noteworthy that IDI catalyzes the interconversion of isopentenyl diphosphate (IPP) and dimethylallyl diphosphate (DMAPP) (Figure 4.1), the fundamental precursors for the biosynthesis of more than 70 000 isoprenoid natural products.<sup>149,150</sup>

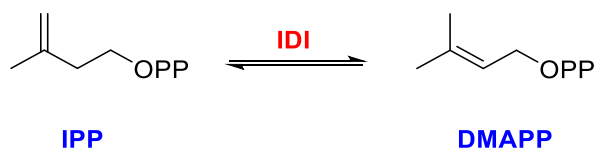


**Figure 4.1: The reaction catalyzed by IDI.**

## 4.2 Design of Inhibitors

Several studies reported that the isomerization reaction catalyzed by IDI involves a tertiary carbocation.<sup>79,82,85,87–89,150</sup> The Poulter and Abeles groups concluded that the isomerization reaction proceeds by a stepwise protonation – deprotonation reaction mechanism that involves a tertiary carbocationic intermediate (see Figures 1.41 and 1.44 in Chapter One). This was further confirmed when they studied the inhibitory effect of inhibitor **48** (nitrogen isopentenyl diphosphate analogue) (Figure 4.2).<sup>85,87,88</sup>

The ammonium-containing inhibitor **48** provides a close mimic to the carbocationic intermediate, as it places a positively charged nitrogen atom in an analogous position to that of the carbocation (Figure 4.2). The fact that this inhibitor shows potent activity against IDI ( $K_{\text{dis}} = 120 \text{ pM}$ ), supports the existence of a tertiary carbocation intermediate.<sup>88</sup>

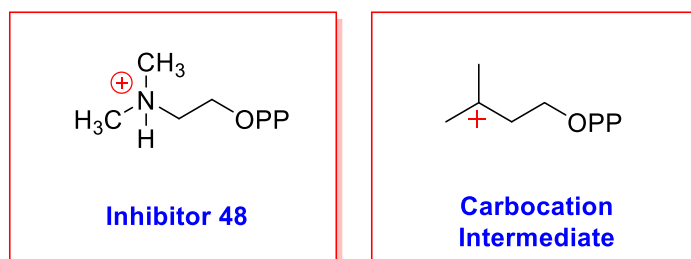


**Figure 4.2: The structures of inhibitor 48 and the carbocation intermediate formed in the IDI reaction.**

Based on the aforementioned results, a positively charged DMAPP analogue should be a potent inhibitor of IDI, and we suspected that inhibitors **2**, **3** and **4** (described in chapter two) may be useful with other enzymes that generate carbocationic intermediates, such as IDI (Figure 4.3). One potential advantage that these inhibitors may have, is that the positive charge resides on  $sp^2$ -hybridized atoms, that may more closely mimic the geometry of the carbocation. Therefore, we decided to test the inhibitory activity of the three inhibitors against isopentenyl diphosphate isomerase (IDI). Inhibitor **2** contains a positively charged guanidinium functionality. Inhibitor **3** has an ammonium group and retains the positive charge, but it is mispositioned in the active site. Inhibitor **4** (the negative control) is sterically similar to inhibitor **2** but lacks any charges. The compounds were synthesized and characterized as mentioned in chapter two (section 2.3).

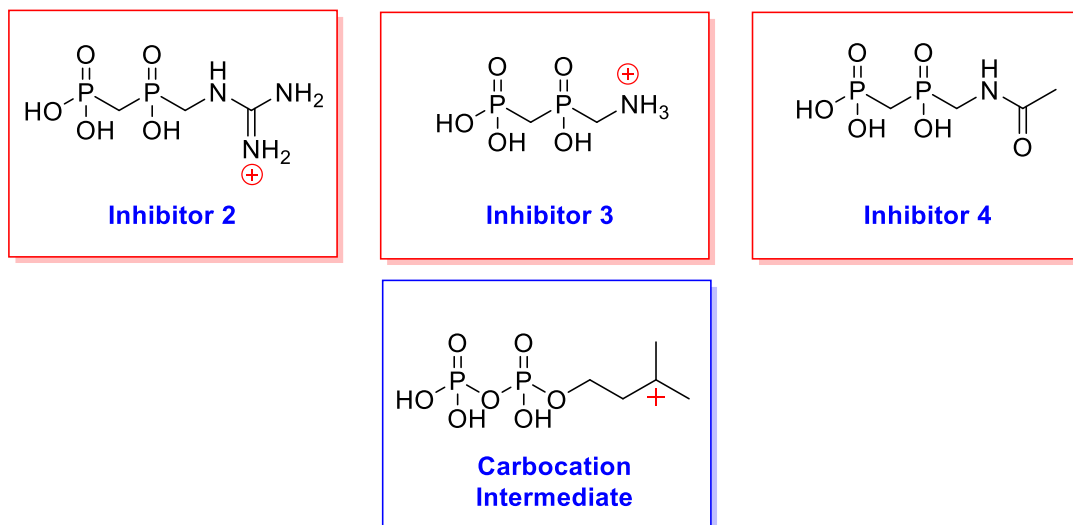


**Figure 4.3:** The three red boxes show the structures of inhibitors **2**, **3** and **4**, respectively.

The blue box shows the structure of the carbocation intermediate formed in the IPP-catalyzed reaction.

### 4.3 Enzyme Kinetics

The isomerization reaction catalyzed by isopentenyl diphosphate isomerase (IDI) does not involve the ionization of DMAPP and therefore, the release of PPi cannot be directly used to monitor the enzymatic reaction spectrophotometrically.<sup>79,88</sup> Consequently, we designed a new enzymatic assay that utilizes 4-dimethylallyl tryptophan synthase (4-DMATS, see section 1.4.3) as a coupling enzyme (Figure 4.4). The DMAPP produced by IDI is rapidly consumed by the 4-DMATS-catalyzed prenylation of tryptophan, and a pyrophosphate group is released as a byproduct. The previously described continuous coupled assay for phosphate release was then employed.<sup>122</sup> Since the 4-DMATS reaction releases pyrophosphate (PPi) as a byproduct, pyrophosphatase was added to catalyze its hydrolysis into two equivalents of phosphate. This phosphate (Pi) then acts as a substrate for the coupling enzyme purine nucleoside phosphorylase (PNP), which acts on 2-amino-6-mercapto-7-methylpurine ribonucleoside (MESG) to generate ribose-1-phosphate and 2-amino-6-mercapto-7-methylpurine as products. MESG shows a maximum UV absorbance at 330 nm at a neutral pH, while 2-amino-merapto-7-methylpurine shows a maximum UV absorbance at 360 nm. Therefore, the kinetics of the isopentenyl diphosphate isomerase catalytic reaction can be followed by an increase in absorption at 360 nm. It should be noted that, 4-DMATS has been extensively studied in the Tanner lab and therefore, a plasmid suitable for high level overproduction of the enzyme is readily available.<sup>55,130</sup>

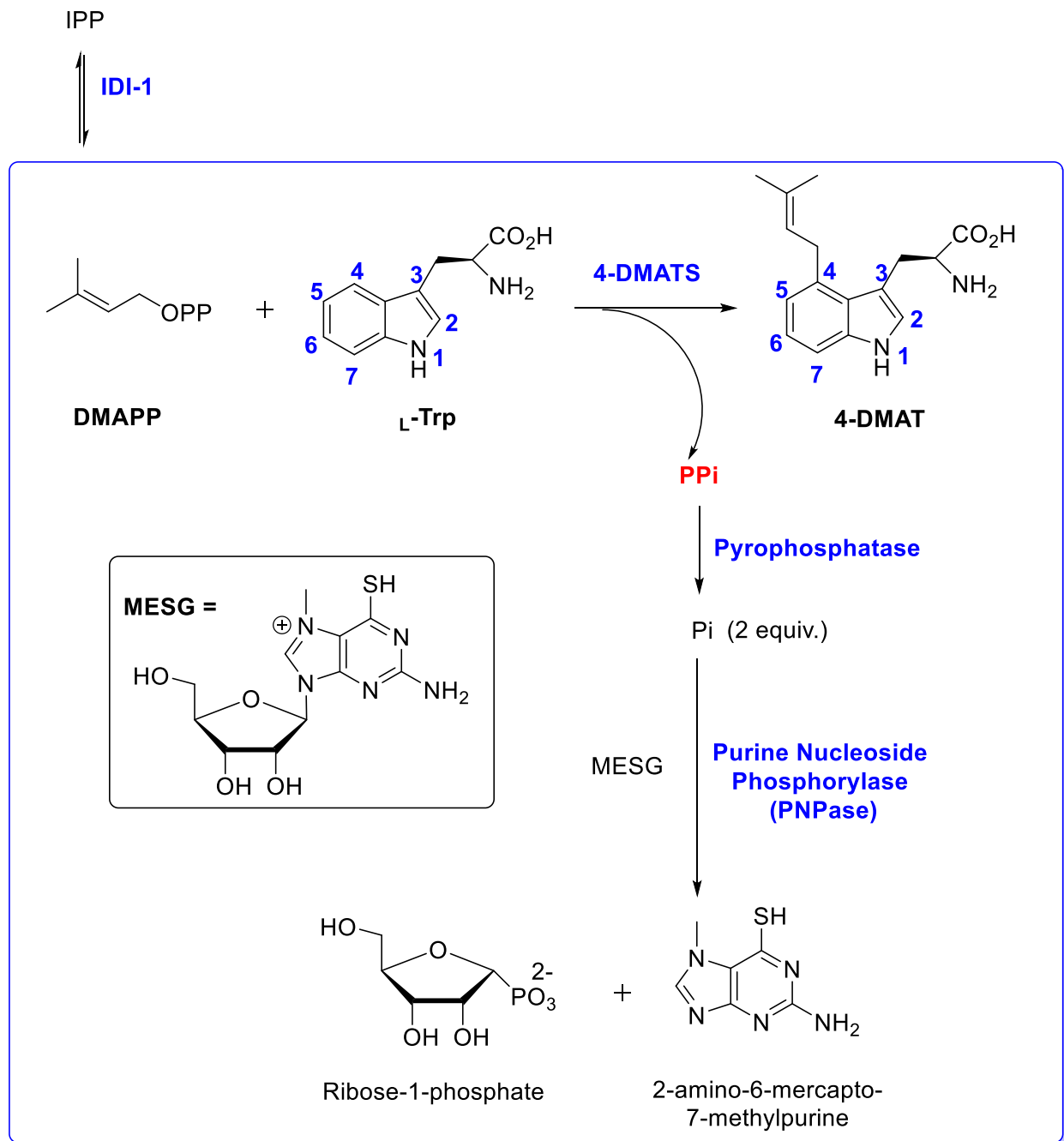


**Figure 4.4: The continuous coupled assay for the reaction catalyzed by isopentenyl diphosphate isomerase (IDI). The blue inset shows the continuous coupled assay for the reaction catalyzed by 4-DMATS.**

### 4.3.1 Overproduction and Purification of IDI and 4-DMATS

The gene encoding for isopentenyl diphosphate isomerase from *Escherichia coli* (IDI-1), was synthesized and cloned into a pET-28a(+) expression vector at the *NdeI*-*BamHI* restriction sites by Genscript. This includes a sequence encoding for an N-terminal hexa-histidine tag that allows for protein purification by immobilized metal affinity chromatography, a kanamycin resistance gene that facilitates the selection of transformed bacteria, and a T7 promoter/lac operon system for IPTG induction and protein expression. The overproduction of IDI was performed differently from other enzymes, as I had to add IPTG after cooling down the medium to 12 °C and then I left it growing at 18 °C for an additional 26 hours. Approximately 40 mg of enzyme was obtained from 1 liter of cell culture and it was found to be more than 90% pure as analyzed by SDS-PAGE (Figure A.1). The enzyme could be stored at – 80 °C without a significant loss of activity for at least 4 months. 4-Dimethylallyl diphosphate synthase (4-DMATS) was overproduced and purified as described previously.<sup>55,130</sup>

### 4.3.2 Measurements of Kinetic Parameters for the 4-DMATS reaction

Kinetic constants ( $k_{\text{cat}}$  and  $K_m$ ) of the reaction catalyzed by 4-DMATS were obtained using a previously described continuous coupled assay for phosphate release (Figure 4.4).<sup>122</sup> The enzymatic reaction was initiated by the addition of 4-DMATS (0.4 nmol/ml) and the rate was calculated from the observed increase of absorption at 360 nm ( $\epsilon = 11000 \text{ M}^{-1}\text{cm}^{-1}$ ). The initial velocities were measured at a series of different concentrations of dimethylallyl diphosphate (DMAPP) (1  $\mu\text{M}$  - 40.0  $\mu\text{M}$ ), while keeping the concentration of L-tryptophan constant (30  $\mu\text{M}$ ).

By fitting the data to the Michaelis-Menten equation, a hyperbolic kinetic profile was observed (Figure 4.5) with the following kinetic parameters values as follows:  $k_{cat} = 0.51 \pm 0.05 \text{ s}^{-1}$  and  $K_m = 10.5 \pm 0.5 \text{ }\mu\text{M}$ . These values agree with the literature and indicates full activity of the coupling enzyme.<sup>55</sup>

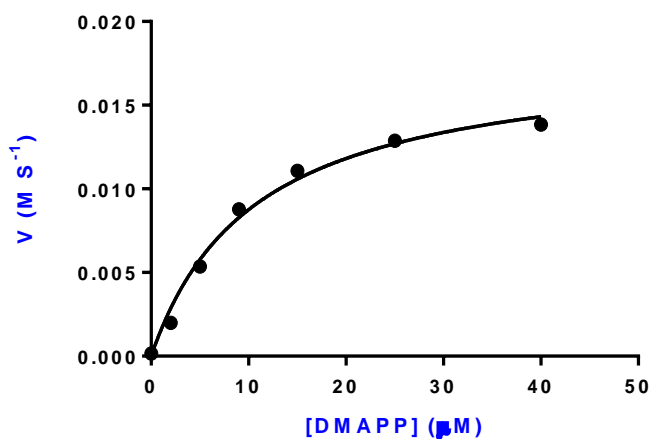


**Figure 4.5: A plot of initial velocity vs. DMAPP concentration for the reaction catalyzed by 4-DMATS. The kinetic parameters were determined by fitting the data to the Michaelis-Menten equation and are as follows:  $k_{cat} = 0.51 \pm 0.05 \text{ s}^{-1}$  and  $K_m = 10.5 \pm 0.5 \text{ }\mu\text{M}$ .**

### 4.3.3 Measurement of Kinetics Parameters for the IDI reaction and Inhibition Kinetics

The kinetic parameters ( $k_{cat}$  and  $K_m$ ) for the isomerization reaction catalyzed by IDI were determined with the continuous coupled assay that utilized 4-DMATS as a coupling enzyme (Figure 4.4). In this case the enzymatic reaction was initiated by the addition of IDI (0.06 nmol/ml) and the initial velocities were measured at a series of different concentrations of isopentenyl diphosphate (IPP) (1  $\mu\text{M}$  - 50.0  $\mu\text{M}$ ). A hyperbolic kinetic profile was obtained upon

fitting the data to the Michaelis-Menten equation and give the following kinetic parameters values:  $k_{\text{cat}} = 0.88 \pm 0.08 \text{ s}^{-1}$  and  $K_{\text{m}} = 8.5 \pm 0.5 \text{ }\mu\text{M}$  (Figure 4.6).

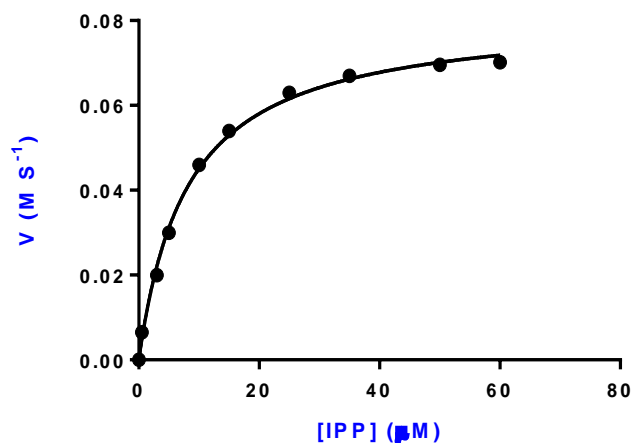


**Figure 4.6: A plot of initial velocity vs. IPP concentration for the reaction catalyzed by IDI-1. The kinetic parameters were determined by fitting the data to the Michaelis-Menten equation and are as follows:  $k_{\text{cat}} = 0.88 \pm 0.08 \text{ s}^{-1}$  and  $K_{\text{m}} = 8.5 \pm 0.5 \text{ }\mu\text{M}$ .**

The inhibition of the isopentenyl diphosphate isomerase (IDI) reaction by inhibitors **2**, **3** and **4** was studied using the aforementioned continuous coupled assay for DMAPP formation. Inhibition kinetics were performed as described above, but with the inclusion of inhibitors **2** – **4** at different concentrations. We first tested the inhibitory effect of these inhibitors against the coupling enzyme, 4-DMATS, to ensure that they would not interfere with the coupled assay. The three inhibitors showed undetectable inhibition of 4-DMATS when tested at low micromolar concentrations and partial inhibition when tested with millimolar range. Thus, the DMAPP assay could be used with inhibitors that are in the micromolar range or lower.

The  $IC_{50}$  values for inhibitors **2** – **4** were determined by measuring the initial velocities of the IDI catalyzed reaction at a series of different inhibitor concentrations (varying from 0  $\mu\text{M}$  – 1000  $\mu\text{M}$ ) while keeping the concentration of isopentenyl diphosphate (IPP) (10  $\mu\text{M}$ ) constant. The  $IC_{50}$  values for inhibitors **2**, **3** and **4** were found to be  $300 \pm 10$  nM,  $15 \pm 3$   $\mu\text{M}$  and  $190 \pm 7$   $\mu\text{M}$ , respectively (Figure 4.7). The results indicate that the positively charged guanidinium-based inhibitor **2**, benefits from electrostatic interactions in the active site more than the natural substrate ( $K_m = 8.5 \pm 0.5$   $\mu\text{M}$ ). It is almost three orders of magnitude more potent than the neutral inhibitor, **4**, presumably because it is a good mimic of the carbocationic intermediate. The  $IC_{50}$  of inhibitor **3** was similar to the  $K_m$  of DMAPP, indicating that proper positioning of the positive charge is important for tight binding.

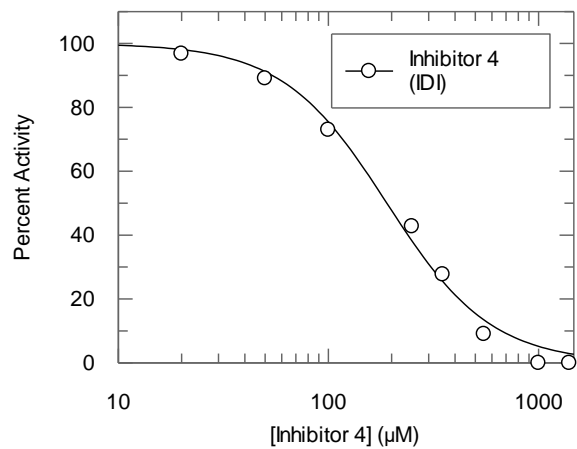
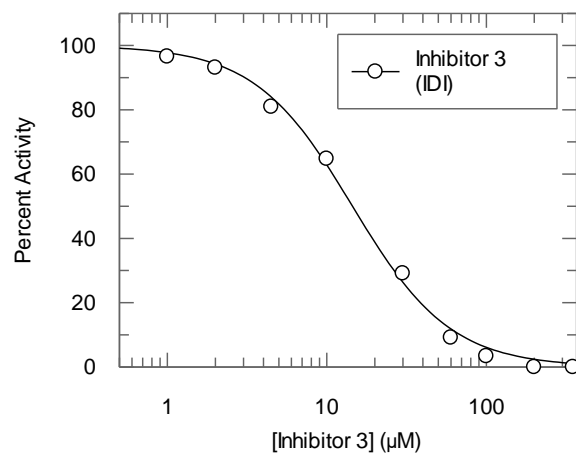
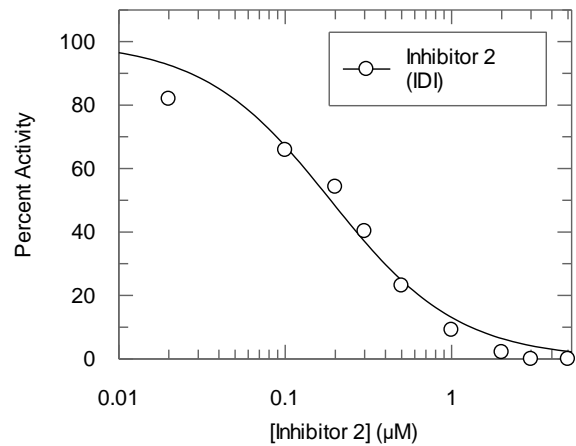


**Figure 4.7: IC<sub>50</sub> curves for inhibitors 2 – 4, respectively, against IDI-1.**

To obtain  $K_I$  values and the mode of inhibition for inhibitors **2**, **3**, and **4**, we measured initial velocities while varying the concentrations of both the inhibitor and the substrate. The linear initial velocities obtained for inhibitors **2**, **3**, and **4** were analyzed using the GraphPad Prism software, and the inhibition kinetic data were found to fit the Michaelis-Menten fit models for competitive inhibition (Figure 4.8). The following values of  $K_I$  were calculated:  $120 \pm 3$  nM,  $4.2 \pm 0.2$   $\mu$ M and  $51.7 \pm 0.9$   $\mu$ M, respectively. The corresponding Lineweaver-Burke plots are shown in Figure 4.9. As suggested by the  $IC_{50}$  values, inhibitor **2** was much more potent than the neutral control, inhibitor **4**. Since the enzyme concentration (57 nM) is approaching the value of  $K_I$  (120 nM), the assumption that [I] is greater than the [E] may not hold for all data points. The Morrison equation ( $K_I^{app} = K_I(1 + \frac{[S]}{K_M})$ ) has been used to treat data where this assumption does not hold. Application of this equation to our data did not change the value of  $K_I$  by more than 10%, suggesting the error introduced by making this assumption is minimal. <sup>151</sup>

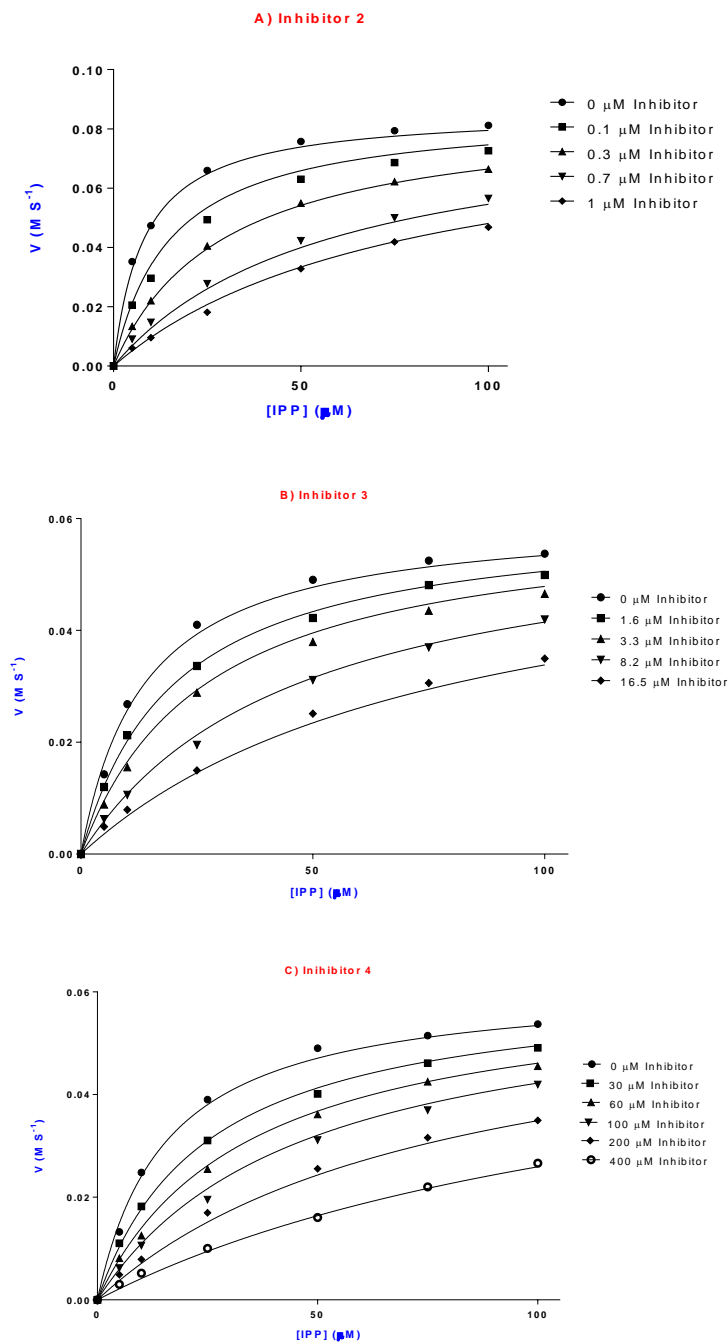


**Figure 4.8: Plot of rate versus IPP concentration for the inhibition of the IDI reaction with fitting to the Michaelis-Menten equation for competitive inhibition. A) Data for inhibitor 2. B) Data for inhibitor 3. C) Data for inhibitor 4.**

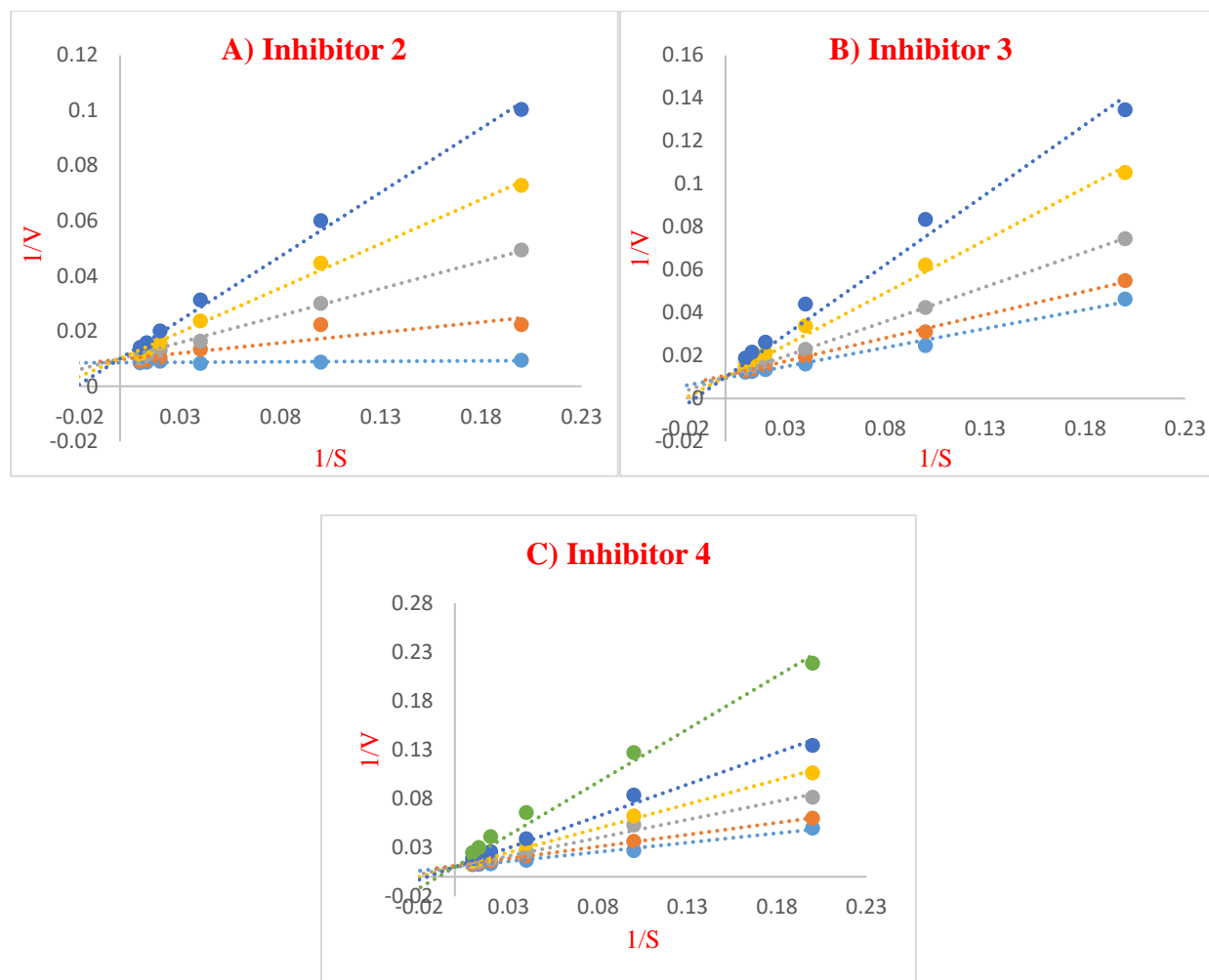


**Figure: Figure 4.9: Lineweaver-Burk plots for the inhibition of IDI by inhibitors 2, 3, and 4.** The color codes for the above Lineweaver-Burk plots are as follows: A) Inhibition by inhibitor 2 at the following concentrations: dark blue = 1  $\mu$ M, yellow = 0.7  $\mu$ M, grey = 0.3  $\mu$ M, orange = 0.1  $\mu$ M, light blue = 0  $\mu$ M. B) Inhibition by inhibitor 3 at the following concentrations: dark blue = 16.5  $\mu$ M, yellow = 8.2  $\mu$ M, grey = 3.3  $\mu$ M, orange = 1.6  $\mu$ M, light blue = 0  $\mu$ M. C) Inhibition by inhibitor 4 at the following concentrations: green = 400  $\mu$ M, dark blue = 200  $\mu$ M, yellow = 100  $\mu$ M, grey = 60  $\mu$ M, orange = 30  $\mu$ M, light blue = 0  $\mu$ M.

#### 4.4 Summary of Chapter Four and Overall Thesis Conclusion

In this study, we used inhibitors (**2**, **3** and **4**) (Figure 4.10) to target the tertiary carbocation-generating enzyme, isopentenyl diphosphate isomerase (IDI). These inhibitors were initially designed to target the allylic carbocation generating enzyme (farnesyl diphosphate synthase), but they showed weak inhibition. Many scenarios were envisioned to explain this observation, one of which is that the enzyme did not bind significantly to the allylic carbocation.

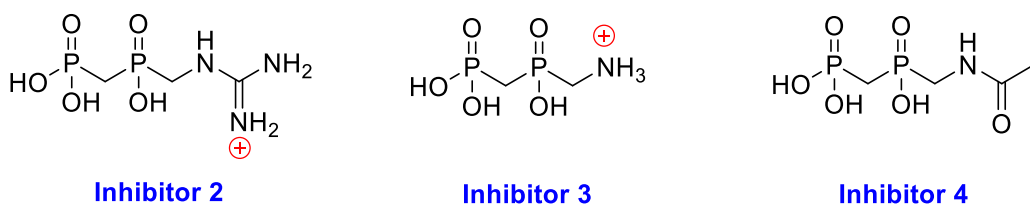


**Figure 4.10: Structures of inhibitors 2, 3 and 4.**

This study was initiated to probe the effectiveness of the inclusion of a guanidinium functionality into inhibitors of isopentenyl diphosphate isomerase (IDI). The guanidinium functionality in inhibitor **2** possesses a planar and delocalized positive charge in a position analogous to that of the tertiary carbocation generated by the enzyme in the active site. The ammonium-containing inhibitor **3**, possesses a positive charge but is mispositioned in the active site, and inhibitor **4** is a negative control to test for the necessity of the positive charge for tight binding. It was expected that the tertiary carbocation generating enzyme, IDI, would bind tightly

to inhibitor **2**, since it is known that this enzyme has evolved to stabilize a carbocation intermediate.

Inhibitors **2**, **3** and **4** were found to be competitive inhibitors of isopentenyl diphosphate isomerase with the following  $K_I$  values:  $120 \pm 3$  nM,  $4.2 \pm 0.2$   $\mu$ M and  $51.7 \pm 0.9$   $\mu$ M, respectively. It is noteworthy that inhibitor **2**, bearing a planar delocalized cation, inhibits IDI with nanomolar affinity which is almost eighty fold lower than the value of  $K_m$  for IPP. Inhibitor **3** inhibits the enzyme with a low micromolar affinity that is similar to the  $K_m$  value of IPP. We reasoned that the guanidinium functionality in inhibitor **2** allows the positive charge to be positioned in the active site in an analogous position to that of the intermediate carbocation, so that the inhibitor benefits from the favorable electrostatic interactions provided by the active site of the enzyme.

The ammonium-containing inhibitor **3** possesses a positive charge, but in a different location to that of the terminal nitrogen(s) of the guanidinium group. It inhibits the enzyme with a  $K_I$  value similar to the  $K_m$  value of the natural substrate. Inhibitor **4** was also a weak inhibitor of IDI, since it lacks the positive charge which seems to be a key factor for tight binding in the active site of the enzyme. The inclusion of the positive charge positioned at the right location in the inhibitor of isopentenyl diphosphate isomerase (IDI) had a dramatic effect on binding interactions in the active site.

In a similar fashion, inhibitor **48** (Figure 4.2) binds to IDI extremely tightly with a  $K_{\text{dis}}$  value of 120 pM.<sup>85,87,88</sup> While inhibitor **2** is less potent than NIPP, it has the advantage of being hydrolytically stable. The aforementioned results indicate that the isomerase has evolved an active site that stabilizes the high energy tertiary carbocation, presumably via favorable electrostatic interactions with negatively-charged residues in the active site. This is required in the absence of electrostatic stabilization through ion pair formation, that occurs with enzymes that dissociate allylic diphosphates.<sup>68</sup> The use of ammonium-containing inhibitors has been a very successful strategy in order to design selective and potent inhibitors for many families of enzymes, since the amine groups bind in their conjugate acid forms thus effectively mimicking the developing positive charge on carbocationic intermediates and/or transition states.<sup>85,87,88</sup>

The glycosidase family of enzymes is an interesting example that highlights this strategy.<sup>91-93,99,152</sup> They had to evolve an active site to stabilize the high energy oxocarbenium ion through electrostatic interactions with negatively-charged residues (in this case it is believed to be carboxylate basic residues) in the active site. In the active site of glycosidases as opposed to glycosyl transferases, the generated oxocarbenium ion lacks the capacity to be stabilized by negatively charged ion pairs (such as pyrophosphate), which in turn forces the enzyme to evolve in order to stabilize it. It is noteworthy that several of the most potent glycosidase inhibitors carry a basic nitrogen in their framework, that is required for potency. This shines the light on the importance of a positive charge in inhibitors of these enzymes.<sup>91-93,99,152</sup>

The use of ammonium-containing inhibitors has been successful for enzymes that generate tertiary carbocations from either protonation (such as in this study) or alkylation of alkenes (such as in the case of geranylgeranyl diphosphate synthase (GGPPS), see section 1.6.3 in chapter one).<sup>101</sup> The GGPPS enzyme forms a high energy tertiary carbocation by the addition of an alkene to an allylic carbocation. Steiger *et al.* designed inhibitor **49** (Figure 4.11) which is a mechanism-based inhibitor designed to mimic the developing positive charge on the putative high energy tertiary carbocation intermediate formed during catalysis.<sup>101</sup>

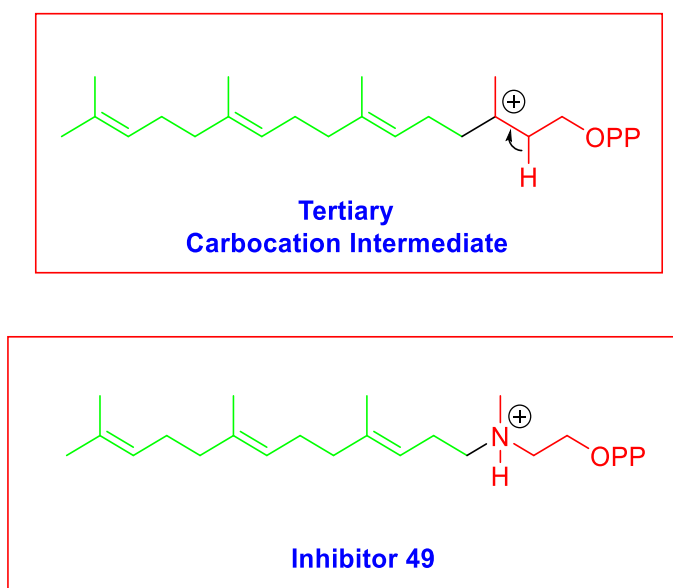


**Figure 4.11: Structures of inhibitor 49 and the tertiary carbocation intermediate formed in the reaction catalyzed by GGPPS.**

When comparing reactions that involve the generation of tertiary carbocations via protonation to those involving the dissociation of allylic diphosphates, key differences emerge. Firstly, tertiary carbocations are only stabilized by hyperconjugation, while allylic carbocations are also stabilized by resonance. Therefore, the latter are more stable and their need for stabilization from the enzyme may be less. Secondly, tertiary carbocation-generating enzymes lack the capacity to use tight binding to a diphosphate moiety to initiate catalysis, given that there is no pyrophosphate ionization in such reactions.<sup>79,82,85,87</sup> Perhaps most importantly, there is no pyrophosphate byproduct in the active site, which acts as an ion pair and stabilizes the carbocation via electrostatic interactions.

An emerging theme that came from work in this thesis was that the incorporation of the guanidinium group as a carbocation mimic was successful with enzymes that generate a tertiary cation by protonation, but not successful in enzymes that catalyze the dissociation of an allylic diphosphate to make an allylic cation-ion pair.

In the case of IDI, the inclusion of the positive charge at the right location in inhibitor **2** had a dramatic effect on binding affinity and produced a nanomolar inhibitor, while the neutral inhibitor **4** had a very low affinity towards the enzyme. Contrarily, all three inhibitors were weak inhibitors of HFPPS. We concluded that, in the case of HFPPS, the enzyme did not need to evolve an active site to directly stabilize the carbocation, since there is a pyrophosphate group in the active site that stabilizes the carbocation via electrostatic interactions, and the carbocation is resonance stabilized. Therefore, the inclusion of a positive charge in the inhibitor design was not successful.

Similar findings were obtained in our studies with the bacterial enzyme DSQS. We designed analogues of the guanidinium-based inhibitors flanked with a long hydrocarbon tail, as well as a structurally similar amidinium-based inhibitor. To test for the effectiveness of incorporating a positive charge in these inhibitors, we designed a negative control inhibitor, urea-containing inhibitor. The inhibitors of DSQS were more potent than with HFPPS, likely because the enzyme recognizes the lipophilic tails, however, the inclusion of a positive charge into the inhibitor design did not increase potency.

This latter discussion on HFPPS and DSQS is somewhat contrary to literature reports that suggests cationic inhibitors are the most potent inhibitors of HFPPS.<sup>123</sup> Upon further inspection however, it is evident that the location of the positive charge in these inhibitors is not too important for binding affinity. In addition, the absence of the positive charge does not cause a dramatic difference in binding as previously discussed (section 2.6). Therefore, the majority of binding energy likely comes from recognition of the bisphosphonate backbone that is used in almost all of the potent inhibitors, as they are known to be potent metal chelators.<sup>148,153–155</sup> While the work in this thesis suggests that some enzymes that catalyze the dissociation of allylic diphosphates do not need to evolve to stabilize the resulting carbocation, the conclusion does not need to be universal. In the case of farnesyltransferase, an ammonium-containing inhibitor has been reported with an  $IC_{50}$  value of 14  $\mu M$ , it's  $IC_{50}$  increased to 200  $\mu M$  upon replacing the positively-charged amine group with a sulfur atom.<sup>147</sup>

In summary, the work conducted in this thesis on: human farnesyl diphosphate synthase (HFPPS), human squalene synthase (HSQS), bacterial dehydrosqualene synthase (DSQS) and isopentenyl diphosphate isomerase (IDI-1) suggests that, the development of inhibitors bearing a carbocationic character to mimic the developing positive charge on a carbocationic intermediate/transition state is likely to be most successful in enzymes that form a higher energy carbocation that is not ion-paired.

#### 4.5 Overall Thesis Future Directions

Future directions of research that arise from this work would likely involve attempts to increase the potency of the IDI inhibitor. Inhibitor **2** did act as a competitive inhibitor of isopentenyl diphosphate isomerase (IDI) with a  $K_I$  in the nanomolar range. To increase the inhibitor potency even further, we could increase the distance between the guanidinium functionality and the pyrophosphate analogue backbone by adding another methylene group to give inhibitor **50** (Figure 4.12). The new inhibitor **50** positions the positive charge at a more analogous location to that of the carbocation intermediate. In this compound the partial positive charge on all three nitrogen atoms may now contribute to binding.

In our original design of inhibitor **2** the replacement of the P-O-P bridging oxygen with a methylene was used to prevent decomposition problems arising from the P-O-P hydrolyzable bond (see section 2.2). It appeared that the positively charged guanidinium group helped to promote the hydrolysis. However, if the guanidinium functionality was removed one carbon further away from the P-O-P bond to give inhibitor **51** (Figure 4.12), it could lead to an inhibitor

that is stable to hydrolysis. It is anticipated that the pyrophosphate mimic in inhibitor **51** will more closely resemble DMAPP than the phosphonyl phosphinate of inhibitors **2 – 4**.

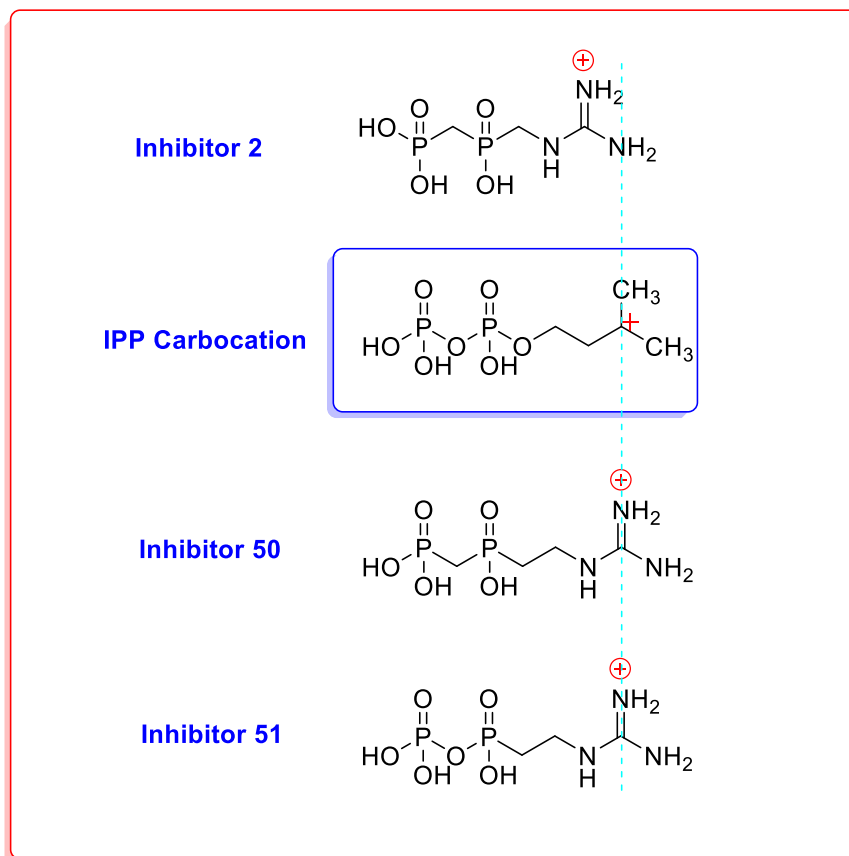


**Figure 4.12: Structures of the IPP carbocationic intermediate, inhibitor 2 and the proposed inhibitors 50 and 51.**

## 4.6 Experimental Procedures

### 4.6.1 Synthesis of Inhibitors

Inhibitors **2**, **3** and **4** were synthesized and quantified as described in chapter two of this thesis (section 2.8.2)

### 4.6.2 General Enzyme Methods

Centrifugal filters (4 mL 10 000 MWCO) were purchased from Millipore. Acryl-cuvettes used in enzyme kinetic assays were from Sarstedt. Chelating Sepharose® Fast resin was purchased from Pharmacia Biotech. Protein concentrations were determined by the method of Bradford on a Cary 3E UV-Vis spectrophotometer using bovine serum albumin as standard.<sup>129</sup> All measurements were performed at room temperature. Protein purity was assessed using SDS-PAGE, stained with Coomassie blue according to Laemmli. 185 Molecular weight standards for SDS-PAGE were BSA (66 kDa) and carbonic anhydrase (29 kDa), both purchased from Sigma. The enzyme kinetic assays were carried out on a Cary 300 UV-Vis spectrometer with a Cary temperature controller attached. Protein concentrations were determined by the Bradford assay using a commercial kit (Bio-Rad). 4-DMATS was overproduced and purified as described previously.<sup>55</sup> All kinetic parameters were determined from the fit of initial velocities to the

Michaelis-Menten equation:  $v_0 = \frac{V_{max} \cdot [S]}{K_M + [S]}$ . Inhibition kinetics were determined using:  $v_0 =$

$\frac{V_{max} \cdot [S]}{K_M (1 + \frac{[I]}{K_I}) + [S]}$  and the Morrison equation:  $K_I^{app} = K_I (1 + \frac{[S]}{K_M})$ .<sup>151</sup> IC<sub>50</sub> values were calculated

using this equation:  $y = \frac{100\%}{1 + \left(\frac{x}{IC_{50}}\right)^s}$ , where "s" is the slope factor. x is the inhibitor concentration

and y is the percent activity.

#### 4.6.2.1 Overproduction and Purification of Isopentenyl Diphosphate Isomerase (IDI)

The gene encoding for isopentenyl diphosphate isomerase (IDI-1) from *Escherichia coli* was synthesized and cloned into a pET-28a(+) expression vectors (Novagen/EMD Millipore) at the NdeI-BamHI restriction sites, respectively, by GenScript®. This plasmid, IDI-1/pET-28a(+) was used to transform chemically competent *Escherichia coli* expression strain Rosetta(DE3) pLysS (Novagen) following the Inoue method.<sup>130</sup> Overproduction of IDI-1 enzyme was achieved following a modified procedure.<sup>84</sup> Transformed cells were grown at 37 °C in 1 L of Terrific Broth (TB) medium containing 30 µg/mL kanamycin until an OD<sub>600</sub> of 0.5 was reached. Cells were induced for overproduction by the addition of 120 mg (1 mM) of isopropyl-1-thio-β-D-galactopyranoside (IPTG) after cooled down to 12 °C. After growing at 18 °C for an additional 26 hours, cells were harvested and lysed with a French press in Tris-HCl buffer (50 mM, pH 7.5) containing dithiothreitol (DTT, 2 mM), aprotinin (1 µg mL<sup>-1</sup>), and pepstatin A (1 µg mL<sup>-1</sup>). The lysate was cleared by centrifugation (34 155g, 45 min) and filtered through a 0.22 mm filter. A column containing chelating Sepharose fast flow resin (GE Healthcare, 10 mL) was charged with 100 mM NiSO<sub>4</sub> and washed with Tris-HCl buffer (50 mM, pH 7.5) containing NaCl (500 mM) and imidazole (5 mM). The clarified lysate of each enzyme was loaded onto the column and eluted with same buffer but containing imidazole at 5 – 500 mM. Fractions containing the desired enzyme eluted after the addition of 500 mM imidazole as analyzed by the Bradford assay.<sup>129</sup> Glycerol (10%) was added to the resulting eluent before flash freezing with liquid N<sub>2</sub>. Typically, 40 mg of each enzyme was purified from 1 L of culture. Enzymes were found to be more than 90% pure as analyzed by SDS-PAGE (Figure A.1)

#### 4.6.2.2 Measurement of Kinetic constants for 4-DMATs and Inhibition Testing

The kinetic parameters ( $K_m$  and  $k_{cat}$ ) of 4-dimethylallyl tryptophan synthase (4-DMATs) were measured using a previously described continuous coupled assay for phosphate release.<sup>122</sup> The concentrations of stock solutions of dimethylallyl diphosphate (DMAPP) and tryptophan were determined by <sup>1</sup>H NMR spectroscopy with the addition of an internal standard of 1 mM 1,4-dioxane and integration of the appropriate signals. A cuvette containing 50 mM Tris-HCl buffer (pH 7.50, final volume 1000  $\mu$ L), MgCl<sub>2</sub> (5 mM), varying concentrations of dimethylallyl diphosphate (DMAPP) (1  $\mu$ M – 40  $\mu$ M), a constant concentration of tryptophan (30  $\mu$ M), 2-amino-6-mercapto-7-methylpurine ribonucleoside (MESG) (20  $\mu$ M), purine nucleoside phosphorylase (PNPase) (1 unit), and inorganic pyrophosphatase (PPase) (0.5 unit) was thermally equilibrated for 5 min at 37 °C. The enzymatic reaction was initiated by the addition of 4-DMATs (MW = 52000 g/mol, 0.45 nmol/ml), and the rate was calculated from the observed increase of absorption at 360 nm ( $\epsilon = 11000 \text{ M}^{-1}\text{cm}^{-1}$ ). Kinetic parameters were determined from the fit of initial velocities to the Michaelis-Menten equation. Inhibition kinetics were performed as described above, but with the incubation of inhibitors **2**, **3** and **4** at various concentrations. The kinetic parameters  $k_{cat}$  and  $K_m$ , and their associated errors, were determined by fitting the initial velocity data to the Michaelis-Menten equation using non-linear regression. Every experiment was repeated 3 times and the resulting kinetic constants never differed by more than 20%. Data obtained on different days with different batches of enzyme could result in kinetic constants that differed from those reported above by up to 25%.

### 4.6.2.3 Measurements of IDI-1 Enzyme and Inhibition Kinetics

In order to measure the kinetic parameters of isopentenyl diphosphate isomerase (IDI-1), another coupling enzyme, 4-DMATS, was added to our previously described continuous assay. The concentrations of stock solutions of isopentenyl diphosphate (IPP) were determined by  $^1\text{H}$  NMR spectroscopy with the addition of an internal standard of 1 mM 1,4-dioxane and integration of the appropriate signals. A cuvette containing 50 mM Tris-HCl buffer (pH 7.50, final volume 1000  $\mu\text{L}$ ),  $\text{MgCl}_2$  (5 mM), isopentenyl diphosphate (IPP) (10  $\mu\text{M}$ ), tryptophan (30  $\mu\text{M}$ ), 2-amino-6-mercapto-7-methylpurine ribonucleoside (MESG) (20  $\mu\text{M}$ ), purine nucleoside phosphorylase (PNPase) (1 unit), and inorganic pyrophosphatase (PPase) (0.5 unit) was thermally equilibrated for 5 min at 37  $^\circ\text{C}$ . In a similar fashion to 4-DMATS, enzymatic reaction was initiated by the addition of (MW = 21000 g/mol, 0.06 nmol/ml) of the enzyme, and the rate was calculated from the observed increase of absorption at 360 nm ( $\epsilon = 11000 \text{ M}^{-1}\cdot\text{cm}^{-1}$ ). Kinetic parameters were determined from the fit of initial velocities to the Michaelis-Menten equation. Inhibition kinetics were described as above, but with the incubation of inhibitors **2**, **3** and **4** at various concentrations. The kinetic parameters  $k_{\text{cat}}$  and  $K_{\text{m}}$ , the inhibition constants  $\text{IC}_{50}$  and  $K_{\text{I}}$ , and their associated errors, were determined by fitting the initial velocity data to the Michaelis-Menten equation using non-linear regression. Every experiment was repeated 3 times and the resulting kinetic constants never differed by more than 20%. Data obtained on different days with different batches of enzyme could result in kinetic constants that differed from those reported above by up to 25%.

## Bibliography

- (1) Christianson, D. W. *Structural Biology and Chemistry of the Terpenoid Cyclases*; 2006; Vol. 106. <https://doi.org/10.1021/cr050286w>.
- (2) Dale Poulter, C. Biosynthesis of Non-Head-to-Tail Terpenes. Formation of L'-1 and 1'-3 Linkages. *Acc. Chem. Res.* **1990**, *23* (3), 70–77. <https://doi.org/10.1021/ar00171a003>.
- (3) Greenhagen, B.; Chappell, J. Molecular Scaffolds for Chemical Wizardry: Learning Nature's Rules for Terpene Cyclases. *Proc. Natl. Acad. Sci.* **2002**, *98* (24), 13479–13481. <https://doi.org/10.1073/pnas.261562898>.
- (4) Poulter, C. D.; Rilling, H. C. The Prenyl Transfer Reaction. Enzymatic and Mechanistic Studies of the 1'-4 Coupling Reaction in the Terpene Biosynthetic Pathway. *Acc. Chem. Res.* **1978**, *11* (8), 307–313. <https://doi.org/10.1021/ar50128a004>.
- (5) Henrick, C. A. The Synthesis of Insect Sex Pheromones. *Tetrahedron* **1977**. [https://doi.org/10.1016/0040-4020\(77\)80372-4](https://doi.org/10.1016/0040-4020(77)80372-4).
- (6) Averhoff, W. W.; Richardson, R. H. Multiple Pheromone System Controlling Mating in *Drosophila Melanogaster*. *Proc. Natl. Acad. Sci. U. S. A.* **1976**. <https://doi.org/10.1073/pnas.73.2.591>.
- (7) Ginzel, M. D.; Hanks, L. M. Contact Pheromones as Mate Recognition Cues of Four Species of Longhorned Beetles (Coleoptera: Cerambycidae). *J. Insect Behav.* **2003**. <https://doi.org/10.1023/A:1023911701159>.
- (8) Farag, M. A.; Al-Mahdy, D. A.; Meyer, A.; Westphal, H.; Wessjohann, L. A. Metabolomics Reveals Biotic and Abiotic Elicitor Effects on the Soft Coral Sarcophyton Ehrenbergi Terpenoid Content. *Sci. Rep.* **2017**, *7* (1), 1–11.

<https://doi.org/10.1038/s41598-017-00527-8>.

- (9) Deguerry, F.; Pastore, L.; Wu, S.; Clark, A.; Chappell, J.; Schalk, M. The Diverse Sesquiterpene Profile of Patchouli, *Pogostemon Cablin*, Is Correlated with a Limited Number of Sesquiterpene Synthases. *Arch. Biochem. Biophys.* **2006**, *454* (2), 123–136. <https://doi.org/10.1016/j.abb.2006.08.006>.
- (10) De Clercq, E. Current Lead Natural Products for the Chemotherapy of Human Immunodeficiency Virus (HIV) Infection. *Med. Res. Rev.* **2000**, *20* (5), 323–349. [https://doi.org/10.1002/1098-1128\(200009\)20:5<323::AID-MED1>3.0.CO;2-A](https://doi.org/10.1002/1098-1128(200009)20:5<323::AID-MED1>3.0.CO;2-A).
- (11) Monocytic Promoting Apoptosis Induction of Apoptosis in Liver Tumors by The. **1995**, 1995.
- (12) Robert, A.; Dechy-Cabaret, O.; Cazelles, J.; Meunier, B. From Mechanistic Studies on Artemisinin Derivatives to New Modular Antimalarial Drugs. *Acc. Chem. Res.* **2002**, *35* (3), 167–174. <https://doi.org/10.1021/ar990164o>.
- (13) McMorris, T. C.; Lira, R.; Gantzel, P. K.; Kelner, M. J.; Dawe, R. Sesquiterpenes from the Basidiomycete *Omphalotus Illudens*. *J. Nat. Prod.* **2000**, *63* (11), 1557–1559. <https://doi.org/10.1021/np9904760>.
- (14) De Schutter, J. W.; Shaw, J.; Lin, Y. S.; Tsantrizos, Y. S. Design of Potent Bisphosphonate Inhibitors of the Human Farnesyl Pyrophosphate Synthase via Targeted Interactions with the Active Site “capping” Phenyls. *Bioorganic Med. Chem.* **2012**, *20* (18), 5583–5591. <https://doi.org/10.1016/j.bmc.2012.07.019>.
- (15) Cerqueira, N. M. F. S. A.; Oliveira, E. F.; Gesto, D. S.; Santos-Martins, D.; Moreira, C.; Moorthy, H. N.; Ramos, M. J.; Fernandes, P. A. Cholesterol Biosynthesis: A Mechanistic Overview. *Biochemistry* **2016**, *55* (39), 5483–5506.

- <https://doi.org/10.1021/acs.biochem.6b00342>.
- (16) Tarshis, L. C.; Proteau, P. J.; Kellogg, B. A.; Sacchettini, J. C.; Poulter, C. D. Regulation of Product Chain Length by Isoprenyl Diphosphate Synthases. *Proc. Natl. Acad. Sci.* **1996**, *93* (26), 15018–15023. <https://doi.org/10.1073/pnas.93.26.15018>.
- (17) Dickschat, J. S. Bacterial Terpene Cyclases. *Natural Product Reports*. 2016. <https://doi.org/10.1039/c5np00102a>.
- (18) Starks, C. M.; Back, K.; Chappell, J.; Noel, J. P. Structural Basis for Cyclic Terpene Biosynthesis by Tobacco 5-Epi- Aristolochene Synthase. *Science* (80-. ). **1997**. <https://doi.org/10.1126/science.277.5333.1815>.
- (19) Steele, C. L.; Crock, J.; Bohlmann, J.; Croteau, R. Sesquiterpene Synthases from Grand Fir ( *Abies Grandis* ) . *J. Biol. Chem.* **2002**, *273* (4), 2078–2089. <https://doi.org/10.1074/jbc.273.4.2078>.
- (20) Buhaescu, I.; Izzedine, H. Mevalonate Pathway: A Review of Clinical and Therapeutical Implications. *Clin. Biochem.* **2007**, *40* (9–10), 575–584. <https://doi.org/10.1016/j.clinbiochem.2007.03.016>.
- (21) Yeganeh, B.; Wiechec, E.; Ande, S. R.; Sharma, P.; Moghadam, A. R.; Post, M.; Freed, D. H.; Hashemi, M.; Shojaei, S.; Zeki, A. A.; et al. Targeting the Mevalonate Cascade as a New Therapeutic Approach in Heart Disease, Cancer and Pulmonary Disease. *Pharmacol. Ther.* **2014**, *143* (1), 87–110. <https://doi.org/10.1016/j.pharmthera.2014.02.007>.
- (22) Rääkkönen, J.; Mönkkönen, H.; Auriola, S.; Mönkkönen, J. Mevalonate Pathway Intermediates Downregulate Zoledronic Acid-Induced Isopentenyl Pyrophosphate and ATP Analog Formation in Human Breast Cancer Cells. *Biochem. Pharmacol.* **2010**, *79* (5), 777–783. <https://doi.org/10.1016/j.bcp.2009.10.003>.

- (23) Gao, J.; Chu, X.; Qiu, Y.; Wu, L.; Qiao, Y.; Wu, J.; Li, D. Discovery of Potent Inhibitor for Farnesyl Pyrophosphate Synthase in the Mevalonate Pathway. *Chem. Commun.* **2010**, 46 (29), 5340–5342. <https://doi.org/10.1039/c0cc00992j>.
- (24) Rääkkönen, J.; Taskinen, M.; Dunford, J. E.; Mönkkönen, H.; Auriola, S.; Mönkkönen, J. Correlation between Time-Dependent Inhibition of Human Farnesyl Pyrophosphate Synthase and Blockade of Mevalonate Pathway by Nitrogen-Containing Bisphosphonates in Cultured Cells. *Biochem. Biophys. Res. Commun.* **2011**, 407 (4), 663–667. <https://doi.org/10.1016/j.bbrc.2011.03.070>.
- (25) Cornforth, J. W.; Cornforth, R. H.; Popják, G.; Yengoyan, L. On the Biosynthesis of Cholesterol. *J. Biol. Chem.* **1966**, 241, 3970–3987. [https://doi.org/10.1016/S0003-9861\(53\)80011-1](https://doi.org/10.1016/S0003-9861(53)80011-1).
- (26) Liang, P. H.; Ko, T. P.; Wang, A. H. J. Structure, Mechanism and Function of Prenyltransferases. *Eur. J. Biochem.* **2002**, 269 (14), 3339–3354. <https://doi.org/10.1046/j.1432-1033.2002.03014.x>.
- (27) Ayong, L.; DaSilva, T.; Mauser, J.; Allen, C. M.; Chakrabarti, D. Evidence for Prenylation-Dependent Targeting of a Ykt6 SNARE in Plasmodium Falciparum. *Mol. Biochem. Parasitol.* **2011**, 175 (2), 162–168. <https://doi.org/10.1016/j.molbiopara.2010.11.007>.
- (28) Harris, C. M.; Poulter, C. D. Recent Studies of the Mechanism of Protein Prenylation. *Nat. Prod. Rep.* **2000**, 17 (2), 137–144. <https://doi.org/10.1039/a904110i>.
- (29) E., O. Targeting Isoprenoid Biosynthesis for Drug Discovery: Bench to Bedside. *Acc. Chem. Res.* **2010**, 43 (9), 1216–1226. <https://doi.org/10.1021/ar100026v> LK - <http://sfx.library.uu.nl/utrecht?sid=EMBASE&iissn=00014842&id=doi:10.1021%2Far100>

- 026v&atitle=Targeting+isoprenoid+biosynthesis+for+drug+discovery%3A+Bench+to+be  
dside&stitle=Acc.+Chem.+Res.&title=Accounts+of+Chemical+Research&volume=43&is  
sue=9&spage=1216&epage=1226&aulast=Oldfield&aufirst=Eric&aunit=E.&aufull=Oldf  
ield+E.&coden=ACHRE&isbn=&pages=1216-1226&date=2010&aunit1=E&aunitm=.
- (30) Ochocki, J. D.; Distefano, M. D. Prenyltransferase Inhibitors: Treating Human Ailments from Cancer to Parasitic Infections. *Medchemcomm* **2013**, *4* (3), 476–492.  
<https://doi.org/10.1039/c2md20299a>.
- (31) Chung, Y. T.; Matkowskyj, K. A.; Li, H.; Bai, H.; Zhang, W.; Tsao, M. S.; Liao, J.; Yang, G. Y. Overexpression and Oncogenic Function of Aldo-Keto Reductase Family 1B10 (AKR1B10) in Pancreatic Carcinoma. *Mod. Pathol.* **2012**, *25* (5), 758–766.  
<https://doi.org/10.1038/modpathol.2011.191>.
- (32) Cohen, L. H.; Pieterman, E.; Van Leeuwen, R. E. W.; Du, J.; Negre-Aminou, P.; Valentijn, A. R. P. M.; Overhand, M.; Van Der Marel, G. A.; Van Boom, J. H. Inhibition of Human Smooth Muscle Cell Proliferation in Culture by Farnesyl Pyrophosphate Analogues, Inhibitors of in Vitro Protein:Farnesyl Transferase. *Biochem. Pharmacol.* **1999**, *57* (4), 365–373. [https://doi.org/10.1016/S0006-2952\(98\)00322-0](https://doi.org/10.1016/S0006-2952(98)00322-0).
- (33) Membranes, C. Modification Reactions Ras-Related Gtpases And. **1994**, 181–205.
- (34) Dolence, J. M.; Dale Poulter, C. A Mechanism for Posttranslational Modifications of Proteins by Yeast Protein Farnesyltransferase (Ras/Prenyl Transfer/Farnesyl Diphosphate). *Biochemistry* **1995**, *92* (May), 5008–5011.
- (35) Osman, A.; G. Niles, E.; T. Loverde, P. Characterization of the Ras Homologue of Schistosoma Mansoni. *Mol. Biochem. Parasitol.* **1999**, *100* (1), 27–41.  
[https://doi.org/10.1016/S0166-6851\(99\)00029-8](https://doi.org/10.1016/S0166-6851(99)00029-8).

- (36) Wang, K. C.; Ohnuma, S. ichi. Isoprenyl Diphosphate Synthases. *Biochimica et Biophysica Acta - Molecular and Cell Biology of Lipids*. 2000.  
[https://doi.org/10.1016/S1388-1981\(00\)00136-0](https://doi.org/10.1016/S1388-1981(00)00136-0).
- (37) Tarshis, L. C.; Proteau, P. J.; Kellogg, B. A.; Sacchettini, J. C.; Poulter, C. D. Regulation of Product Chain Length by Isoprenyl Diphosphate Synthases. *Proc. Natl. Acad. Sci. U. S. A.* **1996**. <https://doi.org/10.1073/pnas.93.26.15018>.
- (38) Chen, A.; Dale Poulter, C.; Kroon, P. A. Isoprenyl Diphosphate Synthases: Protein Sequence Comparisons, a Phylogenetic Tree, and Predictions of Secondary Structure. *Protein Sci.* **1994**. <https://doi.org/10.1002/pro.5560030408>.
- (39) Holloway, P.; Popják, G. The Purification of 3,3-Dimethylallyl- and Geranyl-Transferase and of Isopentenyl Pyrophosphate Isomerase from Pig Liver. *Biochem. J.* **1967**, *104* (1), 57–70. <https://doi.org/10.1042/bj1040057>.
- (40) Choi, S. R.; Breugst, M.; Houk, K. N.; Poulter, C. D.  $\Delta$ -Deuterium Isotope Effects As Probes for Transition-State Structures of Isoprenoid Substrates. *J. Org. Chem.* **2014**, *79* (8), 3572–3580. <https://doi.org/10.1021/jo500394u>.
- (41) Popják, G.; Cornforth, J. Substrate Stereochemistry in Squalene Biosynthesis. *Biochem. J.* **1966**, *101* (3), 553–568. <https://doi.org/10.1042/bj1010553>.
- (42) J. KEVIN DORSEY, JUDITH A. DORSEY, A.; PORTER, J. W. The Purification and Properties of Pig Liver Geranyl Pyrophosphate Synthetase. *J. Biol. Chem.* **1966**, *241* (22), 5353–5360.
- (43) Poulter, C. D.; Wiggins, P. L.; Le, A. T. Farnesylpyrophosphate Synthetase. A Stepwise Mechanism for the V-4 Condensation Reaction. *J. Am. Chem. Soc.* **1981**, *103* (13), 3926–3927. <https://doi.org/10.1021/ja00403a054>.

- (44) Tarshis, L. C.; Sacchettini, J. C.; Yan, M.; Poulter, C. D. Crystal Structure of Recombinant Farnesyl Diphosphate Synthase at 2.6-Å Resolution. *Biochemistry* **1994**, *33* (36), 10871–10877. <https://doi.org/10.1021/bi00202a004>.
- (45) Song, L.; Poulter, A. C. D. Yeast Farnesyl-Diphosphate Synthase: Site-Directed Mutagenesis of Residues in Highly Conserved Prenyltransferase Domains I and II (Sitedirected Mutants/Kinetic Cntn/Immunoaffluty Chromatography). *Biochemistry* **1994**, *91* (April), 3044–3048.
- (46) Tong, H.; Holstein, S. A.; Hohl, R. J. Simultaneous Determination of Farnesyl and Geranylgeranyl Pyrophosphate Levels in Cultured Cells. *Anal. Biochem.* **2005**, *336* (1), 51–59. <https://doi.org/10.1016/j.ab.2004.09.024>.
- (47) Hooff, G. P.; Wood, W. G.; Kim, J. H.; Igbavboa, U.; Ong, W. Y.; Muller, W. E.; Eckert, G. P. Brain Isoprenoids Farnesyl Pyrophosphate and Geranylgeranyl Pyrophosphate Are Increased in Aged Mice. *Mol. Neurobiol.* **2012**, *46* (1), 179–185. <https://doi.org/10.1007/s12035-012-8285-6>.
- (48) Huang, C. C.; Hightower, K. E.; Fierke, C. A. Mechanistic Studies of Rat Protein Farnesyltransferase Indicate an Associative Transition State. *Biochemistry* **2000**, *39* (10), 2593–2602. <https://doi.org/10.1021/bi992356x>.
- (49) Poulter, C. D.; Rilling, H. C. Prenyltransferase: The Mechanism of the Reaction. *Biochemistry* **1976**, *15* (5), 1079–1083. <https://doi.org/10.1021/bi00650a019>.
- (50) Laskovics, F. M.; Poulter, C. D. Prenyltransferase: Determination of the Binding Mechanism and Individual Kinetic Constants for Farnesylpyrophosphate Synthetase by Rapid Quench and Isotope Partitioning Experiments. *Biochemistry* **1981**, *20* (7), 1893–1901. <https://doi.org/10.1021/bi00510a027>.

- (51) Tahir, S. K.; Gu, W. Z.; Zhang, H. C.; Leal, J.; Lee, J. Y.; Kovar, P.; Saeed, B.; Cherian, S. P.; Devine, E.; Cohen, J.; et al. Inhibition of Farnesyltransferase with A-176120, a Novel and Potent Farnesyl Pyrophosphate Analogue. *Eur. J. Cancer* **2000**, *36* (9), 1161–1170. [https://doi.org/10.1016/S0959-8049\(00\)00067-8](https://doi.org/10.1016/S0959-8049(00)00067-8).
- (52) Cohen, L. H.; Valentijn, A. R. P. M.; Roodenburg, L.; Van Leeuwen, R. E. W.; Huisman, R. H.; Lutz, R. J.; Van Der Marel, G. A.; Van Boom, J. H. Different Analogues of Farnesyl Pyrophosphate Inhibit Squalene Synthase and Protein: Farnesyltransferase to Different Extents. *Biochem. Pharmacol.* **1995**, *49* (6), 839–845. [https://doi.org/10.1016/0006-2952\(94\)00454-T](https://doi.org/10.1016/0006-2952(94)00454-T).
- (53) Weller, V. A.; Distefano, M. D. Measurement of the  $\alpha$ -Secondary Kinetic Isotope Effect for a Prenyltransferase by MALDI Mass Spectrometry [2]. *J. Am. Chem. Soc.* **1998**, *120* (31), 7975–7976. <https://doi.org/10.1021/ja980353m>.
- (54) Park, J.; Matralis, A. N.; Berghuis, A. M.; Tsantrizos, Y. S. Human Isoprenoid Synthase Enzymes as Therapeutic Targets. *Front. Chem.* **2014**, *2* (July), 1–21. <https://doi.org/10.3389/fchem.2014.00050>.
- (55) Luk, L. Y. P.; Tanner, M. E. Mechanism of Dimethylallyltryptophan Synthase: Evidence for a Dimethylallyl Cation Intermediate in an Aromatic Prenyltransferase Reaction. *J. Am. Chem. Soc.* **2009**, *131* (39), 13932–13933. <https://doi.org/10.1021/ja906485u>.
- (56) Gebler, J. C.; Woodside, A. B.; Poulter, C. D. Dimethylallyltryptophan Synthase. an Enzyme-Catalyzed Electrophilic Aromatic Substitution. *J. Am. Chem. Soc.* **1992**, *114* (19), 7354–7360. <https://doi.org/10.1021/ja00045a004>.
- (57) Henneman, L.; Van Cruchten, A. G.; Kulik, W.; Waterham, H. R. Inhibition of the Isoprenoid Biosynthesis Pathway; Detection of Intermediates by UPLC-MS/MS. *Biochim.*

- Biophys. Acta - Mol. Cell Biol. Lipids* **2011**, 1811 (4), 227–233.  
<https://doi.org/10.1016/j.bbalip.2011.01.002>.
- (58) Liscum, L. Cholesterol Biosynthesis. In *Biochemistry of Lipids, Lipoproteins and Membranes*; 2008. <https://doi.org/10.1016/B978-044453219-0.50016-7>.
- (59) Rohmer, M.; Knani, M.; Simonin, P.; Sutter, B.; Sahm, H. Isoprenoid Biosynthesis in Bacteria: A Novel Pathway for the Early Steps Leading to Isopentenyl Diphosphate. *Biochem. J.* **1993**. <https://doi.org/10.1042/bj2950517>.
- (60) Chappell, J. Biochemistry and Molecular Biology of the Isoprenoid Biosynthetic Pathway in Plants. *Annual Review of Plant Physiology and Plant Molecular Biology*. 1995.  
<https://doi.org/10.1146/annurev.pp.46.060195.002513>.
- (61) Withers, S. T.; Keasling, J. D. Biosynthesis and Engineering of Isoprenoid Small Molecules. *Applied Microbiology and Biotechnology*. 2007.  
<https://doi.org/10.1007/s00253-006-0593-1>.
- (62) Mizioro, H. M. Enzymes of the Mevalonate Pathway of Isoprenoid Biosynthesis. *Archives of Biochemistry and Biophysics*. 2011. <https://doi.org/10.1016/j.abb.2010.09.028>.
- (63) Pandit, J.; Danley, D. E.; Schulte, G. K.; Mazzalupo, S.; Pauly, T. A.; Hayward, C. M.; Hamanaka, E. S.; Thompson, J. F.; Harwood, H. J. Crystal Structure of Human Squalene Synthase. A Key Enzyme in Cholesterol Biosynthesis. *J. Biol. Chem.* **2000**, 275 (39), 30610–30617. <https://doi.org/10.1074/jbc.M004132200>.
- (64) Jarstfer, M. B.; Zhang, D. L.; Poulter, C. D. Recombinant Squalene Synthase. Synthesis of Non-Head-to-Tail Isoprenoids in the Absence of NADPH. *J. Am. Chem. Soc.* **2002**, 124 (30), 8834–8845. <https://doi.org/10.1021/ja020410i>.
- (65) Altman, L. J.; Ash, L.; Kowerski, R. C.; Epstein, W. W.; Larsen, B. R.; Rilling, H. C.;

- Muscio, F.; Gregonis, D. E. Prephytoene Pyrophosphate. A New Intermediate in the Biosynthesis of Carotenoids. *J. Am. Chem. Soc.* **1972**, *94* (9), 3257–3259.  
<https://doi.org/10.1021/ja00764a073>.
- (66) Washburn, N. Letters No. 18,. **1977**, No. 18, 1555–1558.
- (67) Cornforth, A. J. W.; Cornforth, R. H.; Donninger, C.; Popjak, G.; Ryback, G.; Schroepfer, G. J. Studies on the Biosynthesis of Cholesterol . XVII . The Asymmetric Synthesis of a Symmetrical Molecule Source : Proceedings of the Royal Society of London . Series B , Biological Sciences , Vol . 163 , No . 993 , A Discussion on Detailed Stereochemistry Of. **1966**, *163*.
- (68) Blagg, B. S. J.; Jarstfer, M. B.; Rogers, D. H.; Poulter, C. D. Recombinant Squalene Synthase. A Mechanism for the Rearrangement of Presqualene Diphosphate to Squalene. *J. Am. Chem. Soc.* **2002**, *124* (30), 8846–8853. <https://doi.org/10.1021/ja020411a>.
- (69) Rilling, H. C.; Poulter, C. D.; Epstein, W. W.; Larsen, B. Studies on the Mechanism of Squalene Biosynthesis. Presqualene Pyrophosphate, Stereochemistry and a Mechanism for Its Conversion to Squalene. *J. Am. Chem. Soc.* **1971**, *93* (7), 1783–1785.  
<https://doi.org/10.1021/ja00736a038>.
- (70) Jarstfer, M. B.; Blagg, B. S. J.; Rogers, D. H.; Poulter, C. D. Biosynthesis of Squalene. Evidence for a Tertiary Cyclopropylcarbanyl Cationic Intermediate in the Rearrangement of Presqualene Diphosphate to Squalene. *J. Am. Chem. Soc.* **2002**, *118* (51), 13089–13090. <https://doi.org/10.1021/ja963308s>.
- (71) Christianson, D. W. Structural and Chemical Biology of Terpenoid Cyclases. *Chemical Reviews*. 2017. <https://doi.org/10.1021/acs.chemrev.7b00287>.
- (72) Zhang, H.; Varlamova, O.; Vargas, F. M.; Falany, C. N.; Leyh, T. S.; Gu, P.; Ishii, Y.;

- Spencer, T. a; Shechter, I. Function-Structure Studies and Identification of Three Enzyme Squalene Synthase \*. *J. od Biol. Chem.* **1998**, *273* (20), 9424–9429.  
<https://doi.org/10.1074/jbc.273.20.12515>.
- (73) Dr., E. O. P. D. D. and F.-Y. L. Terpene Biosynthesis: Modularity Rules Eric. *Bone* **2008**, *23* (1), 1–7. <https://doi.org/10.1038/jid.2014.371>.
- (74) Wendt, K. U.; Schulz, G. E.; Corey, E. J.; Liu, D. R. ChemInform Abstract: Enzyme Mechanisms for Polycyclic Triterpene Formation. *ChemInform* **2010**, *31* (46), no-no.  
<https://doi.org/10.1002/chin.200046288>.
- (75) Lin, F.-Y.; Liu, C.-I.; Liu, Y.-L.; Zhang, Y.; Wang, K.; Jeng, W.-Y.; Ko, T.-P.; Cao, R.; Wang, A. H.-J.; Oldfield, E. Mechanism of Action and Inhibition of Dehydrosqualene Synthase. *Proc. Natl. Acad. Sci.* **2010**, *107* (50), 21337–21342.  
<https://doi.org/10.1073/pnas.1010907107>.
- (76) Pelz, A.; Wieland, K. P.; Putzbach, K.; Hentschel, P.; Albert, K.; Götz, F. Structure and Biosynthesis of Staphyloxanthin from *Staphylococcus Aureus*. *J. Biol. Chem.* **2005**, *280* (37), 32493–32498. <https://doi.org/10.1074/jbc.M505070200>.
- (77) Chia-I Liu, George Y. Liu, Yongcheng Song, Fenglin Yin, Mary E. Hensler, Wen-Yih Jeng, Victor Nizet, Andrew H. Wang, E. O. References and Notes 1. **2008**, No. March, 1391–1395.
- (78) Moise, A. R.; Al-Babili, S.; Wurtzel, E. T. Mechanistic Aspects of Carotenoid Biosynthesis. *Chem. Rev.* **2014**, *114* (1), 164–193. <https://doi.org/10.1021/cr400106y>.
- (79) Berthelot, K.; Estevez, Y.; Deffieux, A.; Peruch, F. Isopentenyl Diphosphate Isomerase: A Checkpoint to Isoprenoid Biosynthesis. *Biochimie* **2012**, *94* (8), 1621–1634.  
<https://doi.org/10.1016/j.biochi.2012.03.021>.

- (80) Durbecq, V.; Clantin, B.; Bompard-Gilles, C.; Stalon, V.; Droogmans, L.; Sainz, G.; Oudjama, Y.; Tricot, C.; Villeret, V.; Caillet, J. Crystal Structure of Isopentenyl Diphosphate:Dimethylallyl Diphosphate Isomerase. *EMBO J.* **2001**, *20* (7), 1530–1537. <https://doi.org/10.1093/emboj/20.7.1530>.
- (81) Lee, S.; Poulter, C. D. Escherichia Coli Type I Isopentenyl Diphosphate Isomerase: Structural and Catalytic Roles for Divalent Metals. *J. Am. Chem. Soc.* **2006**, *128* (35), 11545–11550. <https://doi.org/10.1021/ja063073c>.
- (82) Street, I. P.; Coffman, H. R.; Baker, J. A.; Poulter, C. D. Identification of Cys139 and Glu207 As Catalytically Important Groups in the Active Site of Isopentenyl Diphosphate: Dimethylallyl Diphosphate Isomerase. *Biochemistry* **1994**, *33* (14), 4212–4217. <https://doi.org/10.1021/bi00180a014>.
- (83) Street, I. P.; Christensen, D. J.; Poulter, C. D. Hydrogen Exchange during the Enzyme-Catalyzed Isomerization of Isopentenyl Diphosphate and Dimethylallyl Diphosphate. *J. Am. Chem. Soc.* **1990**, *112* (23), 8577–8578. <https://doi.org/10.1021/ja00179a049>.
- (84) Chen, H.; Li, M.; Liu, C.; Zhang, H.; Xian, M.; Liu, H. Enhancement of the Catalytic Activity of Isopentenyl Diphosphate Isomerase (IDI) from *Saccharomyces Cerevisiae* through Random and Site-Directed Mutagenesis. *Microb. Cell Fact.* **2018**, *17* (1), 1–14. <https://doi.org/10.1186/s12934-018-0913-z>.
- (85) Reardon, J. E.; Abeles, R. H. Time-Dependent Inhibition of Isopentenyl Pyrophosphate Isomerase by 2-(Dimethylamino)Ethyl Pyrophosphate. *J. Am. Chem. Soc.* **1985**, *107* (13), 4078–4079. <https://doi.org/10.1021/ja00299a054>.
- (86) Wouters, J.; Oudjama, Y.; Stalon, V.; Droogmans, L.; Poulter, C. D. Crystal Structure of the C67A Mutant of Isopentenyl Diphosphate Isomerase Complexed with a Mechanism-

- Based Irreversible Inhibitor. *Proteins Struct. Funct. Genet.* **2004**, *54* (2), 216–221.  
<https://doi.org/10.1002/prot.10573>.
- (87) Muehlbacher, M.; Poulter, C. D. Isopentenyl Diphosphate:Dimethylallyl Diphosphate Isomerase. Irreversible Inhibition of the Enzyme by Active-Site-Directed Covalent Attachment. *J. Am. Chem. Soc.* **1985**, *107* (26), 8307–8308.  
<https://doi.org/10.1021/ja00312a107>.
- (88) Muehlbacher, M.; Poulter, C. D. Isopentenyl-Diphosphate Isomerase: Inactivation of the Enzyme with Active-Site-Directed Irreversible Inhibitors and Transition-State Analogues. *Biochemistry* **1988**, *27* (19), 7315–7328. <https://doi.org/10.1021/bi00419a021>.
- (89) Neti, S. S.; Pan, J. J.; Poulter, C. D. Mechanistic Studies of the Protonation-Deprotonation Reactions for Type 1 and Type 2 Isopentenyl Diphosphate:Dimethylallyl Diphosphate Isomerase. *J. Am. Chem. Soc.* **2018**, *140* (40), 12900–12908.  
<https://doi.org/10.1021/jacs.8b07274>.
- (90) Winchester, B.; Fleet, G. W. J. Amino-Sugar Glycosidase Inhibitors: Versatile Tools for Glycobiologists. *Glycobiology* **1992**, *2* (3), 199–210.  
<https://doi.org/10.1093/glycob/2.3.199>.
- (91) Asano, N. Glycosidase Inhibitors: Update and Perspectives on Practical Use. *Glycobiology* **2003**, *13* (10), 93–104. <https://doi.org/10.1093/glycob/cwg090>.
- (92) Carlo, R. V.; Garcia, A.; Hammond, D.; Blade, L. M. Amino-Sugar Glycosidase Inhibitors: Versatile Tools for Glycobiologists. **1999**. [https://doi.org/10.1002/\(sici\)1521-3773\(19990315\)38:6<750::aid-anie750>3.0.co;2-6](https://doi.org/10.1002/(sici)1521-3773(19990315)38:6<750::aid-anie750>3.0.co;2-6).
- (93) Gloster, T. M.; Davies, G. J. Glycosidase Inhibition: Assessing Mimicry of the Transition State. *Org. Biomol. Chem.* **2010**, *8* (2), 305–320. <https://doi.org/10.1039/b915870g>.

- (94) Davies, G. J.; Tolley, S. P.; Henrissat, B.; Hjort, C.; Schiilein, M. Structures of Oligosaccharide-Bound Forms of the Endoglucanase V from *Humicola Insolens* at 1.9 Å Resolution. *Biochemistry* **1995**, *34* (49), 16210–16220.  
<https://doi.org/10.1021/bi00049a037>.
- (95) The Structure of Nojirimycin, a Piperidinose Sugar Antibiotic. *J. Antibiot. (Tokyo)*. **1966**, *19* (6), 288–292.
- (96) Gao, K.; Zheng, C.; Wang, T.; Zhao, H.; Wang, J.; Wang, Z.; Zhai, X.; Jia, Z.; Chen, J.; Zhou, Y.; et al. In Depth Study: A Re-Evaluation of Styrene and Noise Exposures in the Fiberglass-Reinforced Plastic Boat Manufacturing Industry. *Molecules* **2016**, *21* (11).  
<https://doi.org/10.3390/molecules21111600>.
- (97) Stevens, K. L.; Molyneux, R. J. In Depth Study: A Re-Evaluation of Styrene and Noise Exposures in the Fiberglass-Reinforced Plastic Boat Manufacturing Industry. *J. Chem. Ecol.* **1988**, *14* (6), 1467–1473. <https://doi.org/10.1007/BF01012418>.
- (98) Chavan, S. R.; Gavale, K. S.; Khan, A.; Joshi, R.; Kumbhar, N.; Chakravarty, D.; Dhavale, D. D. Iminosugars Spiro-Linked with Morpholine-Fused 1,2,3-Triazole: Synthesis, Conformational Analysis, Glycosidase Inhibitory Activity, Antifungal Assay, and Docking Studies. *ACS Omega* **2017**, *2* (10), 7203–7218.  
<https://doi.org/10.1021/acsomega.7b01299>.
- (99) Pino-Gonzalez, M. S.; Romero-Carrasco, A.; Calvo-Losada, S.; Oña-Bernal, N.; Quirante, J. J.; Sarabia, F. Synthesis of Tetrazole Fused Azepanes and Quantum Chemical Topology Study on the Mechanism of the Intramolecular Cycloaddition Reaction. *RSC Adv.* **2017**, *7* (79), 50367–50371. <https://doi.org/10.1039/c7ra10899k>.
- (100) Schröder, S. P.; Wu, L.; Artola, M.; Hansen, T.; Offen, W. A.; Ferraz, M. J.; Li, K. Y.;

- Aerts, J. M. F. G.; Van Der Marel, G. A.; Codée, J. D. C.; et al. Gluco-1 H -Imidazole: A New Class of Azole-Type  $\beta$ -Glucosidase Inhibitor. *J. Am. Chem. Soc.* **2018**, *140* (15), 5045–5048. <https://doi.org/10.1021/jacs.8b02399>.
- (101) Steiger, A.; Pyun, H. J.; Coates, R. M. Synthesis and Characterization of Aza Analogue Inhibitors of Squalene and Geranylgeranyl Diphosphate Synthases. *J. Org. Chem.* **1992**, *57* (12), 3444–3449. <https://doi.org/10.1021/jo00038a038>.
- (102) Zhang, Y.; Cao, R.; Yin, F.; Hudock, M. P.; Guo, R.; Mukherjee, S.; Gao, Y.; Robinson, H.; Song, Y.; No, J. H.; et al. Lipophilic Bisphosphonates as Dual Farnesyl / Geranylgeranyl Diphosphate Synthase Inhibitors : An X-Ray and NMR Investigation By Department of Chemistry , University of Illinois at Urbana-Champaign , 600 South Mathews Department of Orthopedic Surgery , Gr. **2009**, No. 7, 1–2.
- (103) Artz, J. D.; Dunford, J. E.; Arrowood, M. J.; Dong, A.; Chruszcz, M.; Kavanagh, K. L.; Minor, W.; Russell, R. G. G.; Ebetino, F. H.; Oppermann, U.; et al. Targeting a Uniquely Nonspecific Prenyl Synthase with Bisphosphonates to Combat Cryptosporidiosis. *Chem. Biol.* **2008**, *15* (12), 1296–1306. <https://doi.org/10.1016/j.chembiol.2008.10.017>.
- (104) Russell, R. G. G. Bisphosphonates: The First 40 Years. *Bone* **2011**, *49* (1), 2–19. <https://doi.org/10.1016/j.bone.2011.04.022>.
- (105) Holstein, S. A.; Cermak, D. M.; Wiemer, D. F.; Lewis, K.; Hohl, R. J. Phosphonate and Bisphosphonate Analogues of Farnesyl Pyrophosphate as Potential Inhibitors of Farnesyl Protein Transferase. *Bioorganic Med. Chem.* **1998**, *6* (6), 687–694. [https://doi.org/10.1016/S0968-0896\(98\)00034-0](https://doi.org/10.1016/S0968-0896(98)00034-0).
- (106) De Schutter, J. W.; Zaretsky, S.; Welbourn, S.; Pause, A.; Tsantrizos, Y. S. Novel Bisphosphonate Inhibitors of the Human Farnesyl Pyrophosphate Synthase. *Bioorganic*

- Med. Chem. Lett.* **2010**, *20* (19), 5781–5786. <https://doi.org/10.1016/j.bmcl.2010.07.133>.
- (107) Wiemer, A. J.; Tong, H.; Swanson, K. M.; Hohl, R. J. Digeranyl Bisphosphonate Inhibits Geranylgeranyl Pyrophosphate Synthase. *Biochem. Biophys. Res. Commun.* **2007**, *353* (4), 921–925. <https://doi.org/10.1016/j.bbrc.2006.12.094>.
- (108) Strates, B. S.; Firschein, H. E.; Urist, M. R. Alkaline Phosphatase and Failure of Calcification under the Influence of a Diphosphonate. *BBA - Gen. Subj.* **1971**, *244* (1), 121–124. [https://doi.org/10.1016/0304-4165\(71\)90127-9](https://doi.org/10.1016/0304-4165(71)90127-9).
- (109) Widler, L.; Jaeggi, K. A.; Glatt, M.; Müller, K.; Bachmann, R.; Bisping, M.; Born, A. R.; Cortesi, R.; Guiglia, G.; Jeker, H.; et al. Highly Potent Geminal Bisphosphonates. From Pamidronate Disodium (Aredia) to Zoledronic Acid (Zometa). *J. Med. Chem.* **2002**, *45* (17), 3721–3738. <https://doi.org/10.1021/jm020819i>.
- (110) Lacbay, C. M.; Mancuso, J.; Lin, Y. S.; Bennett, N.; Götte, M.; Tsantrizos, Y. S. Modular Assembly of Purine-like Bisphosphonates as Inhibitors of Hiv-1 Reverse Transcriptase. *J. Med. Chem.* **2014**, *57* (17), 7435–7449. <https://doi.org/10.1021/jm501010f>.
- (111) Ebetino, F. H.; Hogan, A. M. L.; Sun, S.; Tsoumpra, M. K.; Duan, X.; Triffitt, J. T.; Kwaasi, A. A.; Dunford, J. E.; Barnett, B. L.; Oppermann, U.; et al. The Relationship between the Chemistry and Biological Activity of the Bisphosphonates. *Bone* **2011**, *49* (1), 20–33. <https://doi.org/10.1016/j.bone.2011.03.774>.
- (112) Szajnman, S. H.; Montalvetti, A.; Wang, Y.; Docampo, R.; Rodriguez, J. B. Bisphosphonates Derived from Fatty Acids Are Potent Inhibitors of Trypanosoma Cruzi Farnesyl Pyrophosphate Synthase. *Bioorganic Med. Chem. Lett.* **2003**, *13* (19), 3231–3235. [https://doi.org/10.1016/S0960-894X\(03\)00663-2](https://doi.org/10.1016/S0960-894X(03)00663-2).
- (113) Martin, M. B.; Arnold, W.; Heath, H. T.; Urbina, J. A.; Oldfield, E. Nitrogen-Containing

- Bisphosphonates as Carbocation Transition State Analogs for Isoprenoid Biosynthesis. *Biochem. Biophys. Res. Commun.* **1999**. <https://doi.org/10.1006/bbrc.1999.1404>.
- (114) Lin, Y. S.; Park, J.; De Schutter, J. W.; Huang, X. F.; Berghuis, A. M.; Sebag, M.; Tsantrizos, Y. S. Design and Synthesis of Active Site Inhibitors of the Human Farnesyl Pyrophosphate Synthase: Apoptosis and Inhibition of ERK Phosphorylation in Multiple Myeloma Cells. *J. Med. Chem.* **2012**, *55* (7), 3201–3215. <https://doi.org/10.1021/jm201657x>.
- (115) Coukell, A. J.; Markham, A. Pamidronate. A Review of Its Use in the Management of Osteolytic Bone Metastases, Tumour-Induced Hypercalcaemia and Paget's Disease of Bone. *Drugs and Aging* **1998**, *12* (2), 149–168. <https://doi.org/10.2165/00002512-199812020-00007>.
- (116) Kavanagh, K. L.; Guo, K.; Dunford, J. E.; Wu, X.; Knapp, S.; Ebetino, F. H.; Rogers, M. J.; Russell, R. G. G.; Oppermann, U. The Molecular Mechanism of Nitrogen-Containing Bisphosphonates as Antiosteoporosis Drugs. *Proc. Natl. Acad. Sci.* **2006**, *103* (20), 7829–7834. <https://doi.org/10.1073/pnas.0601643103>.
- (117) Studies, P. Indole Prenyltransferases : Mechanistic Studies and Inhibitor Design. **2015**.
- (118) Flohr, A.; Aemissegger, A.; Hilvert, D.  $\alpha$ -Functionalized Phosphonylphosphinates: Synthesis and Evaluation as Transcarbamoylase Inhibitors. *J. Med. Chem.* **1999**, *42* (14), 2633–2640. <https://doi.org/10.1021/jm991008q>.
- (119) Bernatowicz, M. S.; Youling, W.; Matsueda, G. R. 1H-Pyrazole-1-Carboxamide Hydrochloride: An Attractive Reagent for Guanylation of Amines and Its Application to Peptide Synthesis. *J. Org. Chem.* **1992**, *57* (8), 2497–2502. <https://doi.org/10.1021/jo00034a059>.

- (120) Gers, T.; Kunce, D.; Markowski, P.; Izdebski, J. Reagents for Efficient Conversion of Amines to Protected Guanidines. *Synthesis (Stuttg)*. **2003**, *2004* (01), 37–42.  
<https://doi.org/10.1055/s-2003-44374>.
- (121) Zhang, Y.; Zhu, W.; Liu, Y. L.; Wang, H.; Wang, K.; Li, K.; No, J. H.; Ayong, L.; Gulati, A.; Pang, R.; et al. Chemo-Immunotherapeutic Antimalarials Targeting Isoprenoid Biosynthesis. *ACS Med. Chem. Lett.* **2013**. <https://doi.org/10.1021/ml4000436>.
- (122) Webb, M. R. A Continuous Spectrophotometric Assay for Inorganic Phosphate and for Measuring Phosphate Release Kinetics in Biological Systems. *Proc. Natl. Acad. Sci.* **2006**, *89* (11), 4884–4887. <https://doi.org/10.1073/pnas.89.11.4884>.
- (123) Kotsikorou, E.; Oldfield, E. A Quantitative Structure-Activity Relationship and Pharmacophore Modeling Investigation of Aryl-X and Heterocyclic Bisphosphonates as Bone Resorption Agents. *J. Med. Chem.* **2003**, *46* (14), 2932–2944.  
<https://doi.org/10.1021/jm030054u>.
- (124) Olah, G. A.; Clifford, P. R.; Halpern, Y.; Johanson, R. G. Stable Carbocations. CXIX. Carbon-13 Nuclear Magnetic Resonance Spectroscopy Study of the Structure of Allyl Cations. *J. Am. Chem. Soc.* **1971**, *93* (17), 4219–4222.  
<https://doi.org/10.1021/ja00746a022>.
- (125) Martin, A.; Arda, A.; Désiré, J.; Martin-Mingot, A.; Probst, N.; Sinaÿ, P.; Jiménez-Barbero, J.; Thibaudeau, S.; Blériot, Y. Catching Elusive Glycosyl Cations in a Condensed Phase with HF/SbF<sub>5</sub> Superacid. *Nat. Chem.* **2016**, *8* (2), 186–191.  
<https://doi.org/10.1038/nchem.2399>.
- (126) Amyes, T. L.; Jencks, W. P. Lifetimes of Oxocarbenium Ions in Aqueous Solution from Common Ion Inhibition of the Solvolysis of  $\alpha$ -Azido Ethers by Added Azide Ion. *J. Am.*

- Chem. Soc.* **1989**, *111* (20), 7888–7900. <https://doi.org/10.1021/ja00202a033>.
- (127) Richard, J. P.; Amyes, T. L.; Toteva, M. M. Formation and Stability of Carbocations and Carbanions in Water and Intrinsic Barriers to Their Reactions. *Acc. Chem. Res.* **2001**, *34* (12), 981–988. <https://doi.org/10.1021/ar0000556>.
- (128) Rablen, P. R.; Perry-Freer, N. A. How the Arrangement of Alkyl Substituents Affects the Stability of Delocalized Carbocations. *J. Org. Chem.* **2018**, *83* (7), 4024–4033. <https://doi.org/10.1021/acs.joc.8b00415>.
- (129) BRADFORD, M. M. A Rapid and Sensitive Method for the Quantitation Microgram Quantities of Protein Utilizing the Principle of Protein-Dye Binding. **2000**, *254*, 481. [https://doi.org/10.1016/0003-2697\(76\)90527-3](https://doi.org/10.1016/0003-2697(76)90527-3).
- (130) Inoue, H.; Nojima, H.; Okayma, H. High Efficiency Transformation of *Escherichia Coli* with Plasmids. *Gene* **1990**, *96*, 23–28.
- (131) Abdelmagid, W. M.; Aduk, T.; Freeman, J. O.; Tanner, M. E. Studies with Guanidinium- and Amidinium-Based Inhibitors Suggest Minimal Stabilization of Allylic Carbocation Intermediates by Dehydrosqualene and Squalene Synthases. *Biochemistry* **2018**, *57* (38), 5591–5601. <https://doi.org/10.1021/acs.biochem.8b00731>.
- (132) Stein, E. A.; Bays, H.; O'Brien, D.; Pedicano, J.; Piper, E.; Spezzi, A. Lapaquistat Acetate: Development of a Squalene Synthase Inhibitor for the Treatment of Hypercholesterolemia. *Circulation* **2011**, *123* (18), 1974–1985. <https://doi.org/10.1161/CIRCULATIONAHA.110.975284>.
- (133) Biller, S. A.; Sofia, M. J.; DeLange, B.; Forster, C.; Gordon, E. M.; Harrity, T.; Rich, L. C.; Ciosek, C. P. The First Potent Inhibitor of Squalene Synthase: A Profound Contribution of an Ether Oxygen to Inhibitor-Enzyme Interaction. *J. Am. Chem. Soc.*

- 1991**, *113* (22), 8522–8524. <https://doi.org/10.1021/ja00022a050>.
- (134) Radisky, E. S.; Poulter, C. D. Squalene Synthase: Steady-State, Pre-Steady-State, and Isotope-Trapping Studies. *Biochemistry* **2000**, *39* (7), 1748–1760. <https://doi.org/10.1021/bi9915014>.
- (135) Yin, B. L.; Liu, Z. G.; Zhang, J. C.; Li, Z. R. N, N-Di-Boc-Substituted Thiourea as a Novel and Mild Thioacylating Agent Applicable for the Synthesis of Thiocarbonyl Compounds. *Synthesis (Stuttg)*. **2010**, No. 6, 991–999. <https://doi.org/10.1055/s-0029-1219273>.
- (136) Linton, B. R.; Carr, A. J.; Orner, B. P.; Hamilton, A. D. A Versatile One-Pot Synthesis of 1,3-Substituted Guanidines from Carbamoyl Isothiocyanates. *J. Org. Chem.* **2000**, *65* (5), 1566–1568. <https://doi.org/10.1021/jo991458q>.
- (137) Beytia, E., Qureshi, A. A., and Porter, J. W. Squalene Synthetase 3. Mechanism of Reaction. **1867**, *248* (5).
- (138) Zhang, C.; Wang, W.-K.; He, T. Dramatic Solvent Effect in the One-Pot Synthesis of Substituted Ureas Directly from Primary Alcohols Using the Combined Reagent of Iodobenzene Dichloride and Sodium Azide in Ethyl Acetate. *Synthesis (Stuttg)*. **2012**, *44* (19), 3006–3014. <https://doi.org/10.1055/s-0032-1316745>.
- (139) Cotarca, L.; Geller, T.; Répási, J. Bis(Trichloromethyl)Carbonate (BTC, Triphosgene): A Safer Alternative to Phosgene? *Org. Process Res. Dev.* **2017**, *21* (9), 1439–1446. <https://doi.org/10.1021/acs.oprd.7b00220>.
- (140) Spyropoulos, C.; Kokotos, C. G. One-Pot Synthesis of Ureas from Boc-Protected Amines. *J. Org. Chem.* **2014**, *79* (10), 4477–4483. <https://doi.org/10.1021/jo500492x>.
- (141) Thompson, J. F.; Danley, D. E.; Mazzalupo, S.; Milos, P. M.; Lira, M. E.; Harwood, H. J.

- Truncation of Human Squalene Synthase Yields Active, Crystallizable Protein. *Arch. Biochem. Biophys.* **1998**, *350* (2), 283–290. <https://doi.org/10.1006/abbi.1997.0502>.
- (142) Ciosek, C. P.; Magnin, D. R.; Harrity, T. W.; Logan, J. V. H.; Dickson, J. K.; Gordon, E. M.; Hamilton, K. A.; Jolibois, K. G.; Kunselman, L. K.; Lawrence, R. M.; et al. Lipophilic 1,1-Bisphosphonates Are Potent Squalene Synthase Inhibitors and Orally Active Cholesterol Lowering Agents in Vivo. *J. Biol. Chem.* **1993**, *268* (33), 24832–24837.
- (143) Poulter, C. D.; Capson, T. L.; Thompson, M. D.; Bard, R. S. Squalene Synthetase. Inhibition by Ammonium Analogues of Carbocationic Intermediates in the Conversion of Presqualene Diphosphate to Squalene. *J. Am. Chem. Soc.* **1989**, *111* (10), 3734–3739. <https://doi.org/10.1021/ja00192a036>.
- (144) Prashad, M.; Kathawala, F. G.; Scallen, T. N-(Arylalkyl)Farnesylamines: New Potent Squalene Synthetase Inhibitors. *J. Med. Chem.* **1993**, *36* (10), 1501–1504. <https://doi.org/10.1021/jm00062a026>.
- (145) Sealey-Cardona, M.; Cammerer, S.; Jones, S.; Ruiz-Pérez, L. M.; Brun, R.; Gilbert, I. H.; Urbina, J. A.; González-Pacanowska, D. Kinetic Characterization of Squalene Synthase from *Trypanosoma Cruzi*: Selective Inhibition by Quinuclidine Derivatives. *Antimicrob. Agents Chemother.* **2007**, *51* (6), 2123–2129. <https://doi.org/10.1128/AAC.01454-06>.
- (146) Narula, A. S.; Rahier, A.; Benveniste, P.; Schuber, F. 24-Methyl-25-Azacycloartanol, an Analogue of a Carbonium Ion High-Energy Intermediate, Is a Potent Inhibitor of (S) - Adenosyl-L-Methionine: Sterol C-24-Methyltransferase in Higher Plant Cells. *J. Am. Chem. Soc.* **1981**, *103* (9), 2408–2409. <https://doi.org/10.1021/ja00399a045>.
- (147) Cassidy, P. B.; Poulter, C. D. Transition State Analogs for Protein Farnesyltransferase. *J. Am. Chem. Soc.* **1996**, *118* (36), 8761–8762. <https://doi.org/10.1021/ja961214c>.

- (148) Song, Y.; Lin, F. Y.; Yin, F.; Hensler, M.; Poveda, C. A. R.; Mukkamala, D.; Cao, R.; Wang, H.; Morita, C. T.; Pacanowska, D. G.; et al. Phosphonosulfonates Are Potent, Selective Inhibitors of Dehydrosqualene Synthase and Staphyloxanthin Biosynthesis in *Staphylococcus Aureus*. *J. Med. Chem.* **2009**, *52* (4), 976–988. <https://doi.org/10.1021/jm801023u>.
- (149) Wouters, J.; Oudjama, Y.; Barkley, S. J.; Tricot, C.; Stalon, V.; Droogmans, L.; Poulter, C. D. Catalytic Mechanism of *Escherichia Coli* Isopentenyl Diphosphate Isomerase Involves Cys-67, Glu-116, and Tyr-104 as Suggested by Crystal Structures of Complexes with Transition State Analogues and Irreversible Inhibitors. *J. Biol. Chem.* **2003**, *278* (14), 11903–11908. <https://doi.org/10.1074/jbc.M212823200>.
- (150) Street, I. P.; Poulter, C. D. Isopentenyl diphosphate:Dimethylallyl diphosphate Isomerase: Construction of a High-Level Heterologous Expression System for the Gene from *Saccharomyces Cerevisiae* and Identification of an Active-Site Nucleophile. *Biochemistry* **1990**, *29* (32), 7531–7538. <https://doi.org/10.1021/bi00484a023>.
- (151) Ellenbroek, B.; Abizaid, A.; Amir, S.; de Zwaan, M.; Parylak, S.; Cottone, P.; Zorrilla, E. P.; Price, L. H.; Harrison, B. J.; Pantelis, C.; et al. *Equilibrium Dissociation Constant*; 2010. [https://doi.org/10.1007/978-3-540-68706-1\\_796](https://doi.org/10.1007/978-3-540-68706-1_796).
- (152) Ermert, P.; Vasella, A.; Weber, M.; Rupitz, K.; Withers, S. G. Configurationally Selective Transition State Analogue Inhibitors of Glycosidases. A Study with Nojiritetrazoles, a New Class of Glycosidase Inhibitors. *Carbohydr. Res.* **1993**. [https://doi.org/10.1016/0008-6215\(93\)84160-8](https://doi.org/10.1016/0008-6215(93)84160-8).
- (153) Zhang, Y.; Cao, R.; Yin, F.; Hudock, M. P.; Guo, R. T.; Krysiak, K.; Mukherjee, S.; Gao, Y. G.; Robinson, H.; Song, Y.; et al. Lipophilic Bisphosphonates as Dual

Farnesyl/Geranylgeranyl Diphosphate Synthase Inhibitors: An X-Ray and Nmr Investigation. *J. Am. Chem. Soc.* **2009**, *131* (14), 5153–5162.

<https://doi.org/10.1021/ja808285e>.

- (154) Sanders, J. M.; Gómez, A. O.; Mao, J.; Meints, G. A.; Van Brussel, E. M.; Burzynska, A.; Kafarski, P.; González-Pacanowska, D.; Oldfield, E. 3-D QSAR Investigations of the Inhibition of Leishmania Major Farnesyl Pyrophosphate Synthase by Bisphosphonates. *J. Med. Chem.* **2003**, *46* (24), 5171–5183. <https://doi.org/10.1021/jm0302344>.
- (155) Chia-I Liu, George Y. Liu, Yongcheng Song, Fenglin Yin, Mary E. Hensler, Wen-Yih Jeng, Victor Nizet, Andrew H. Wang, E. O. A Cholesterol Biosynthesis Inhibitor Blocks Staphylococcus Aureus Virulence. **2008**, No. March, 1391–1395.

## **Appendix**

### **NMR Spectra of Selected Compounds and SDS-PAGE**

**SDS-PAGE of IDI, DSQS, HFPPS and HSQS Enzymes (left to right)**

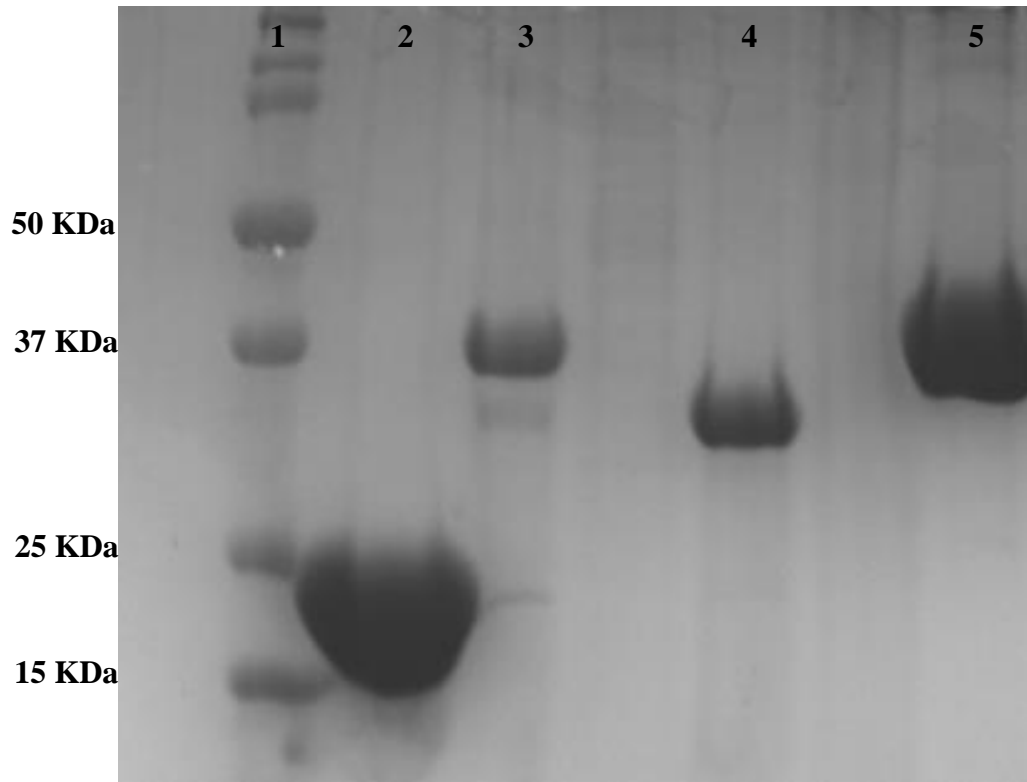


**Figure A.1:** SDS-PAGE showing IDI, DSQS, HFPPS and HSQS Enzymes (from left to right, respectively). Lane 1: molecular weight standards; Lane 2: pure IDI; Lane 3: pure DSQS; Lane 4: pure HFPPS; Lane 5: pure HSQS.

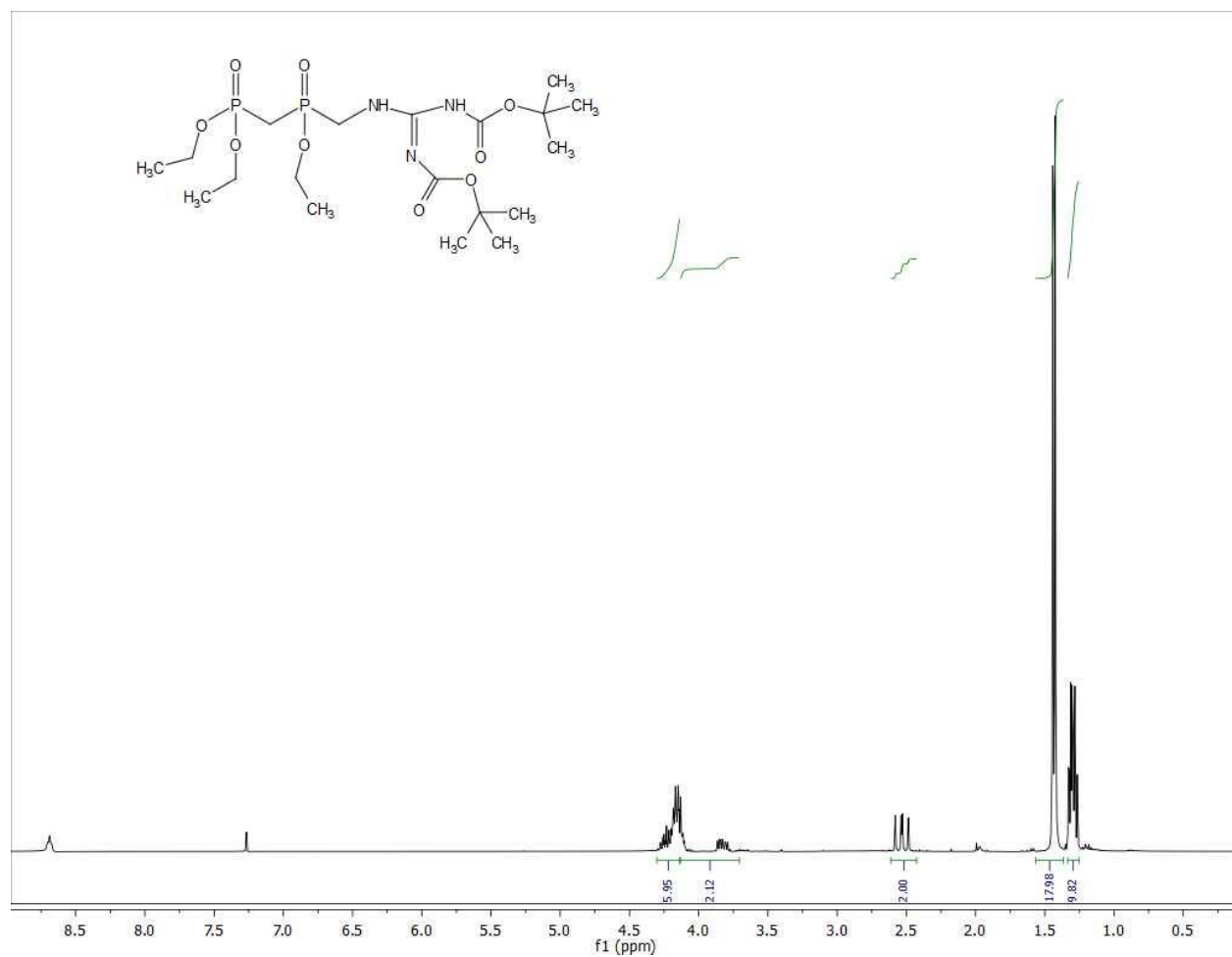


**Figure A.2:** <sup>1</sup>H NMR spectrum of compound 14 (CDCl<sub>3</sub>, 400 MHz)

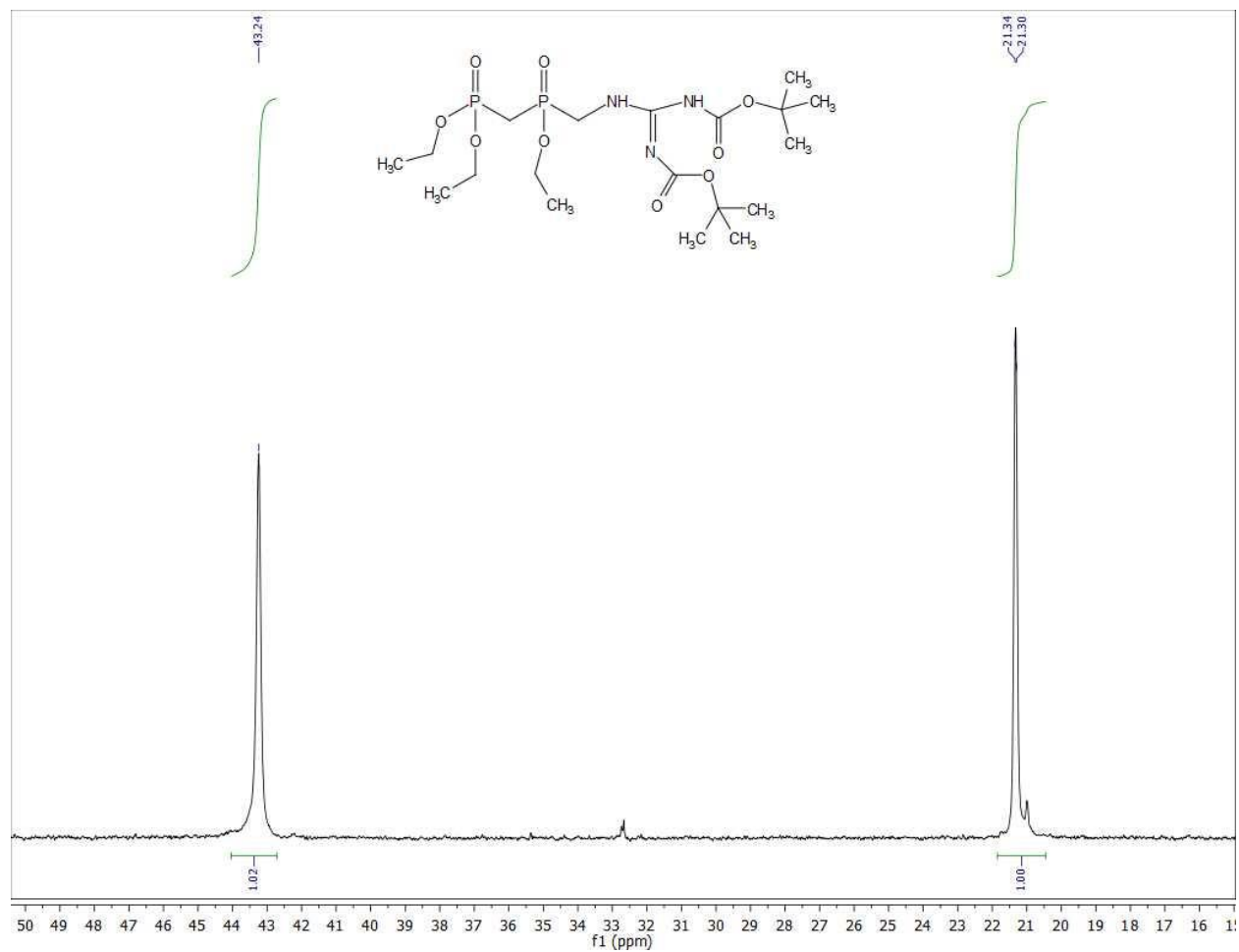


**Figure A.3:**  $^{31}\text{P}$ - $\{^1\text{H}\}$  NMR spectrum of compound **14** ( $\text{CDCl}_3$ , 162 MHz)

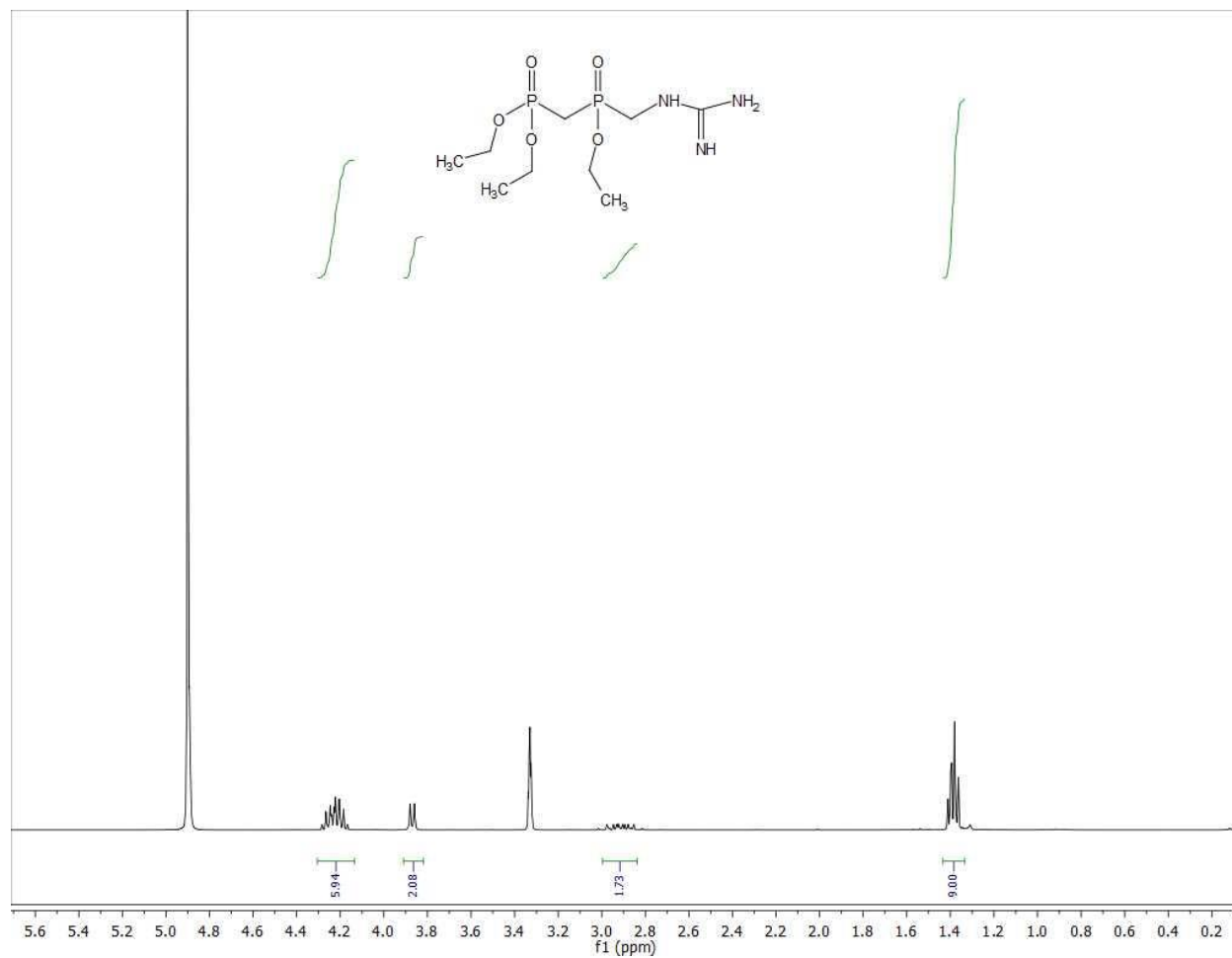


**Figure A.4:** <sup>1</sup>H NMR spectrum of compound **13** (MeOD, 400 MHz)

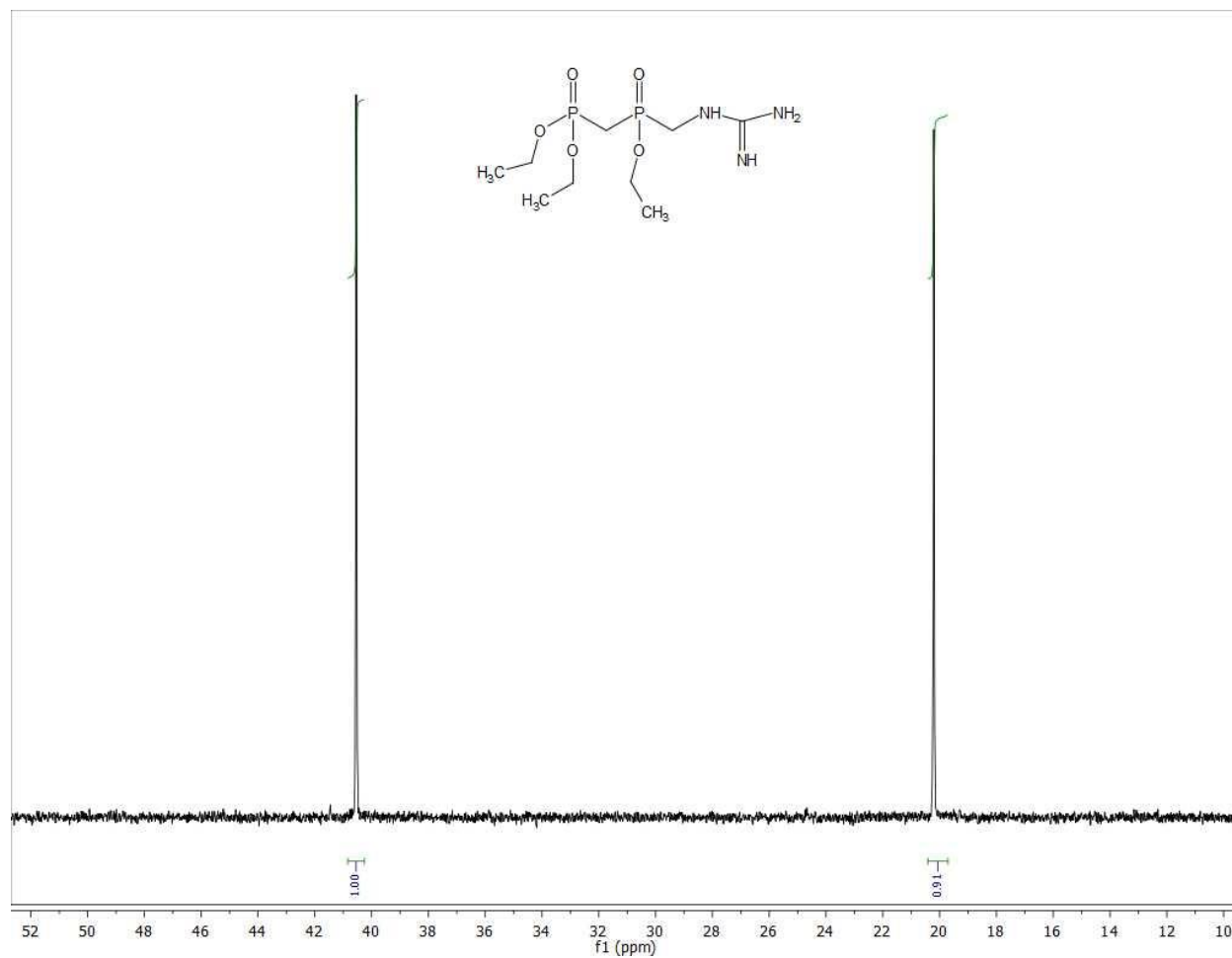


**Figure A.5:**  $^{31}\text{P}$ - $\{^1\text{H}\}$  NMR spectrum of compound 13 (MeOD, 162 MHz)

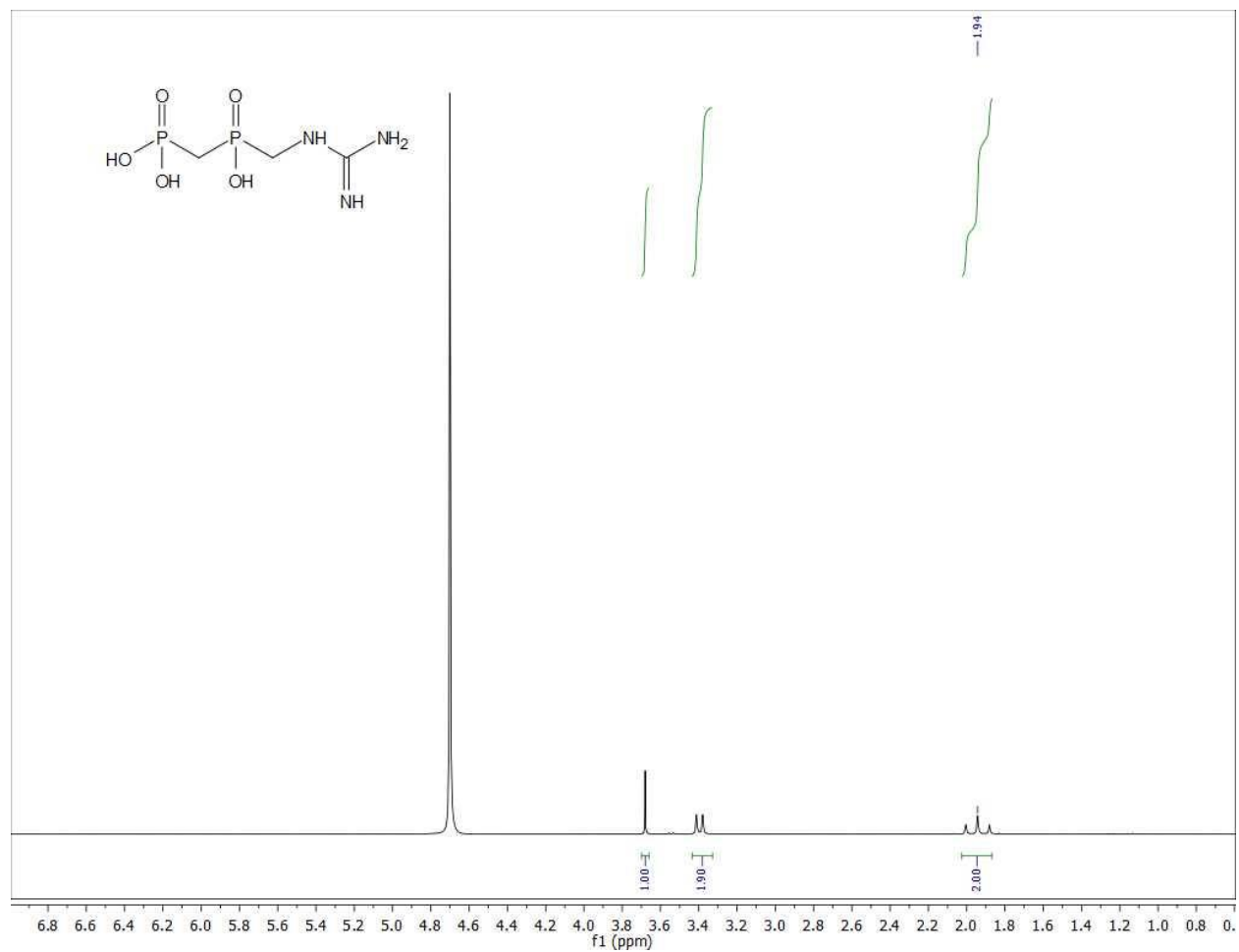


**Figure A.6:**  $^1\text{H}$  NMR spectrum of inhibitor 2 ( $\text{D}_2\text{O}$ , 400 MHz)

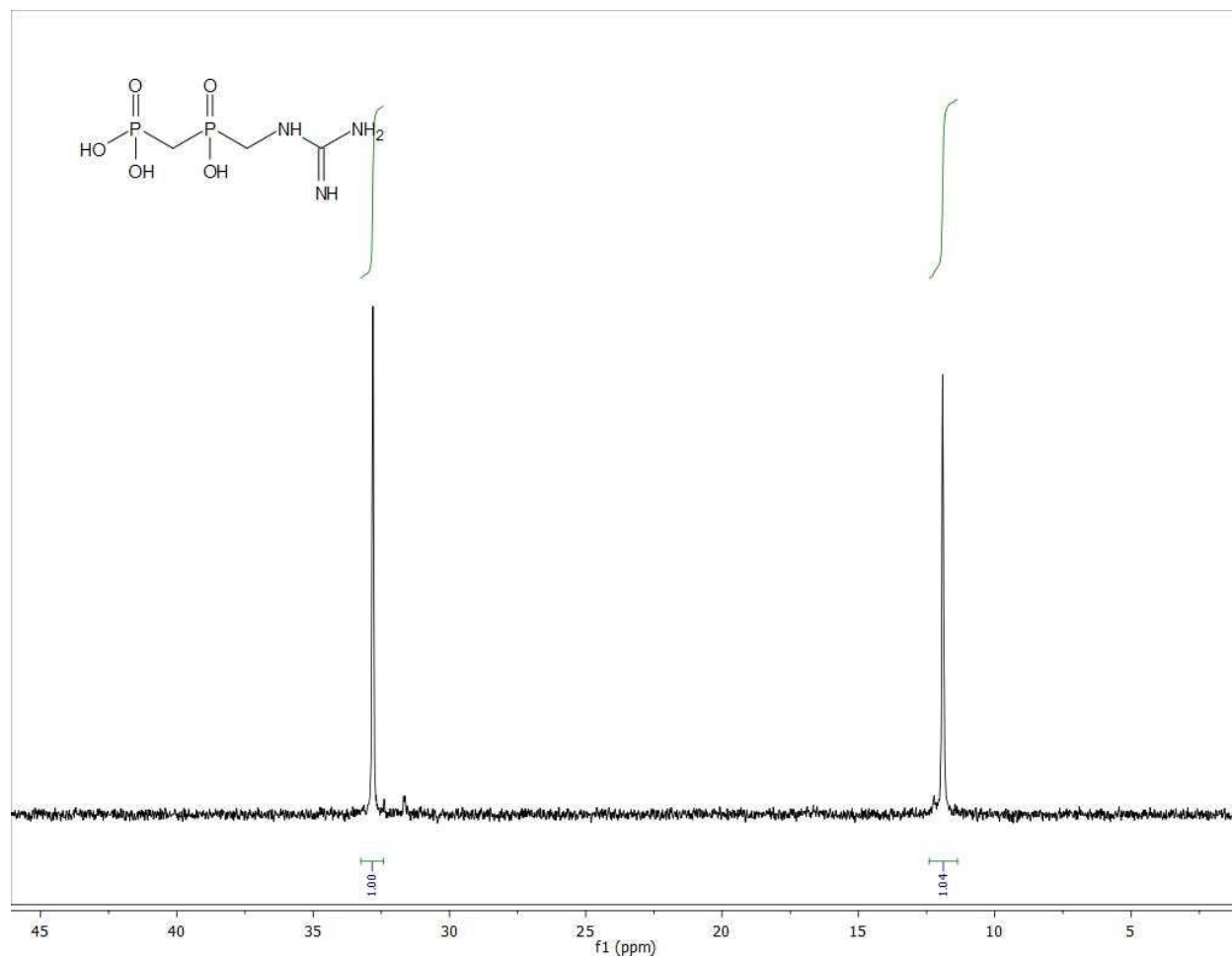


**Figure A.7:**  $^{31}\text{P}\{-^1\text{H}\}$  NMR spectrum of inhibitor 2 ( $\text{D}_2\text{O}$ , 162 MHz)

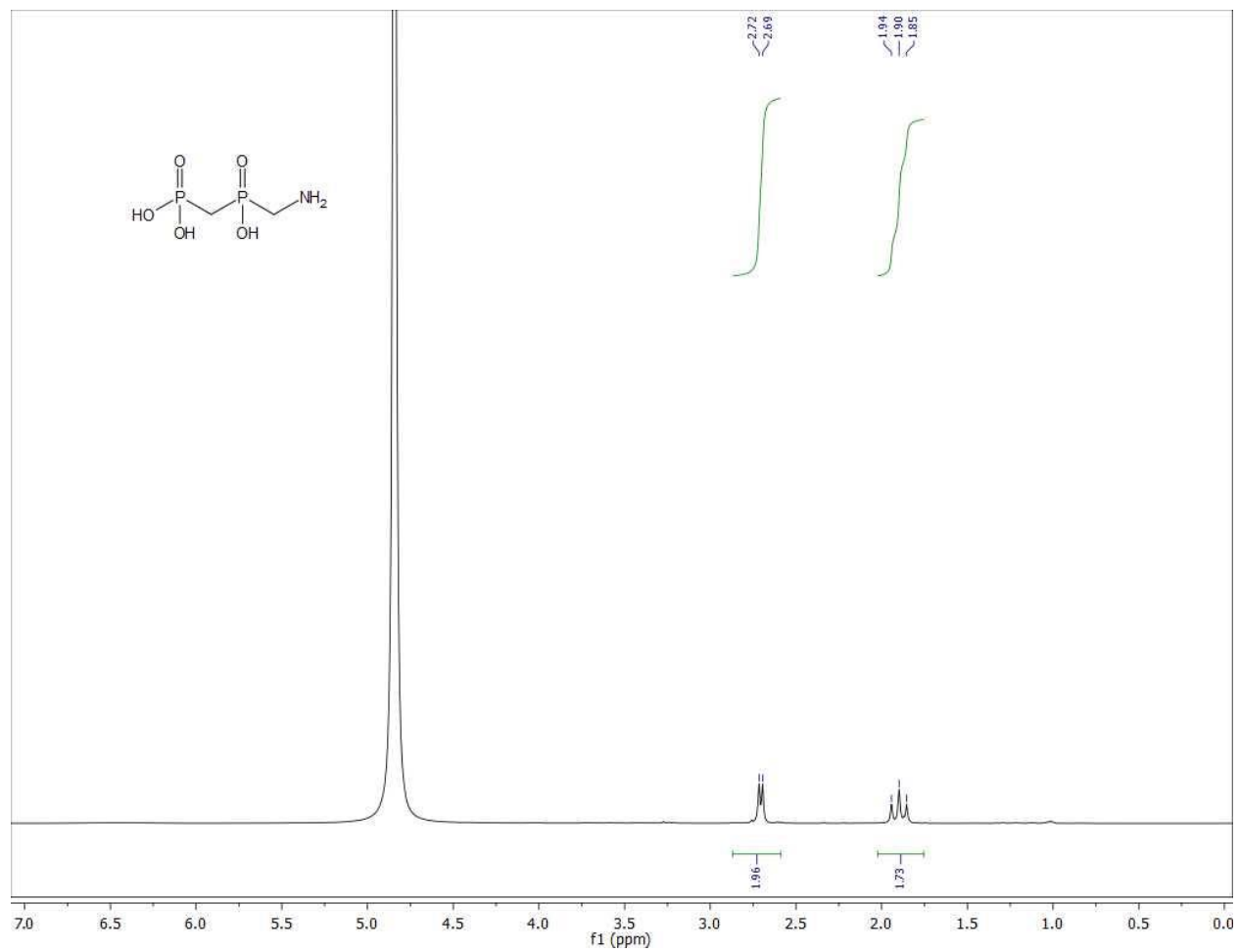


**Figure A.8:**  $^1\text{H}$  NMR spectrum of inhibitor 3 ( $\text{D}_2\text{O}$ , 400 MHz)

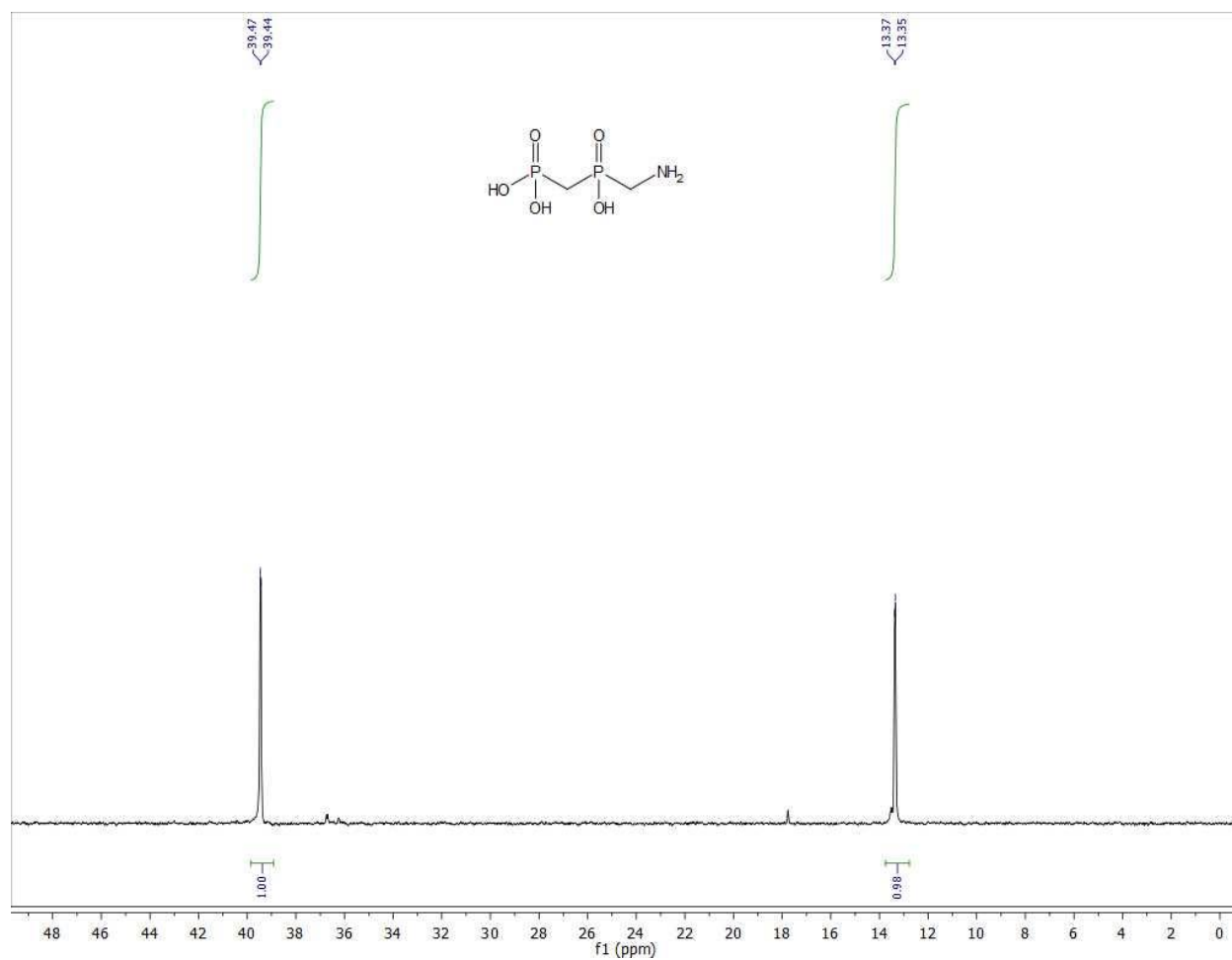


**Figure A.9:**  $^{31}\text{P}\{-^1\text{H}\}$  NMR spectrum of inhibitor **3** ( $\text{D}_2\text{O}$ , 162 MHz)

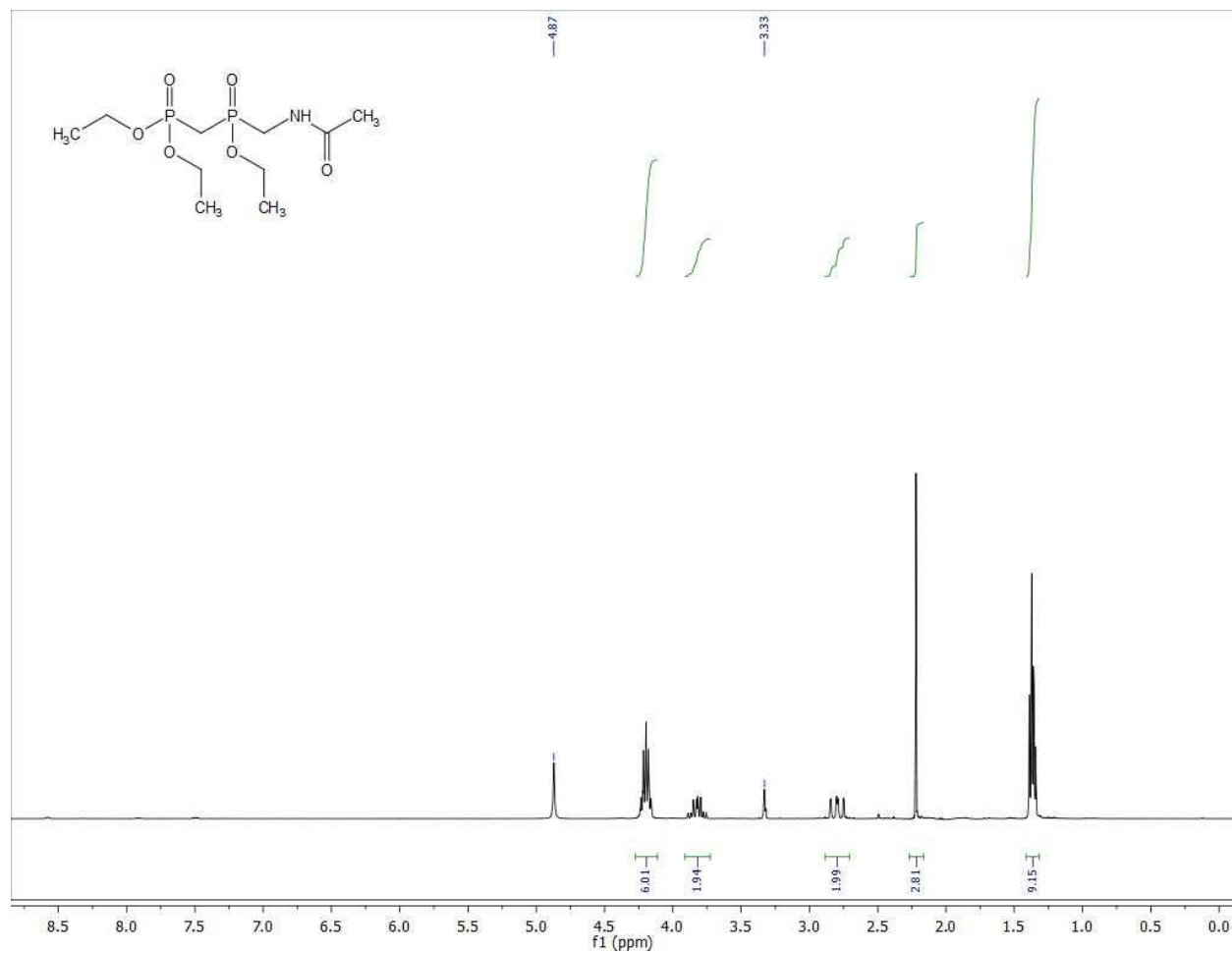


**Figure A.10:** <sup>1</sup>H NMR spectrum of compound **15** (MeOD, 400 MHz)

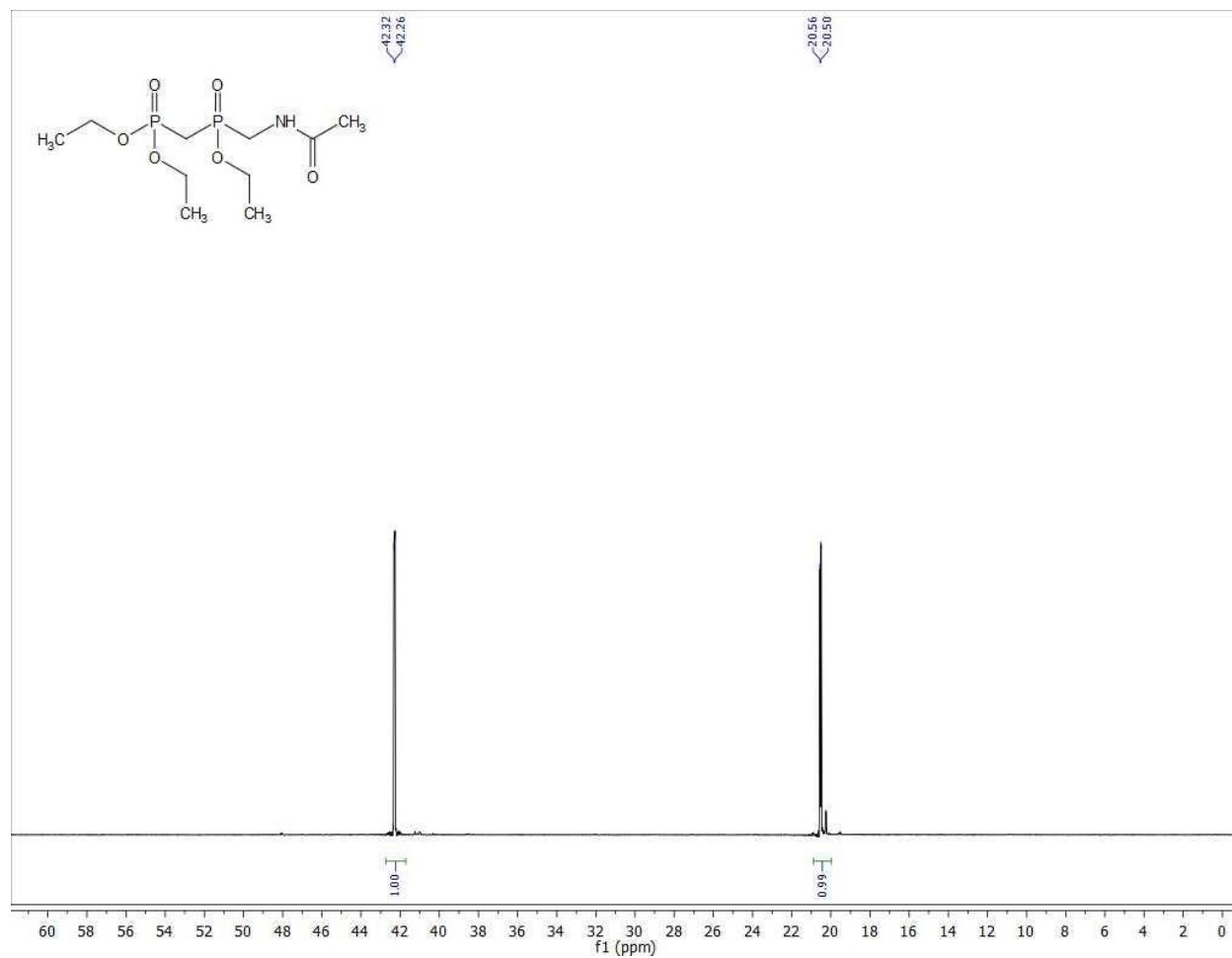


**Figure A.11:**  $^{31}\text{P}\{-^1\text{H}\}$  NMR spectrum of compound **15** (MeOD, 162 MHz)

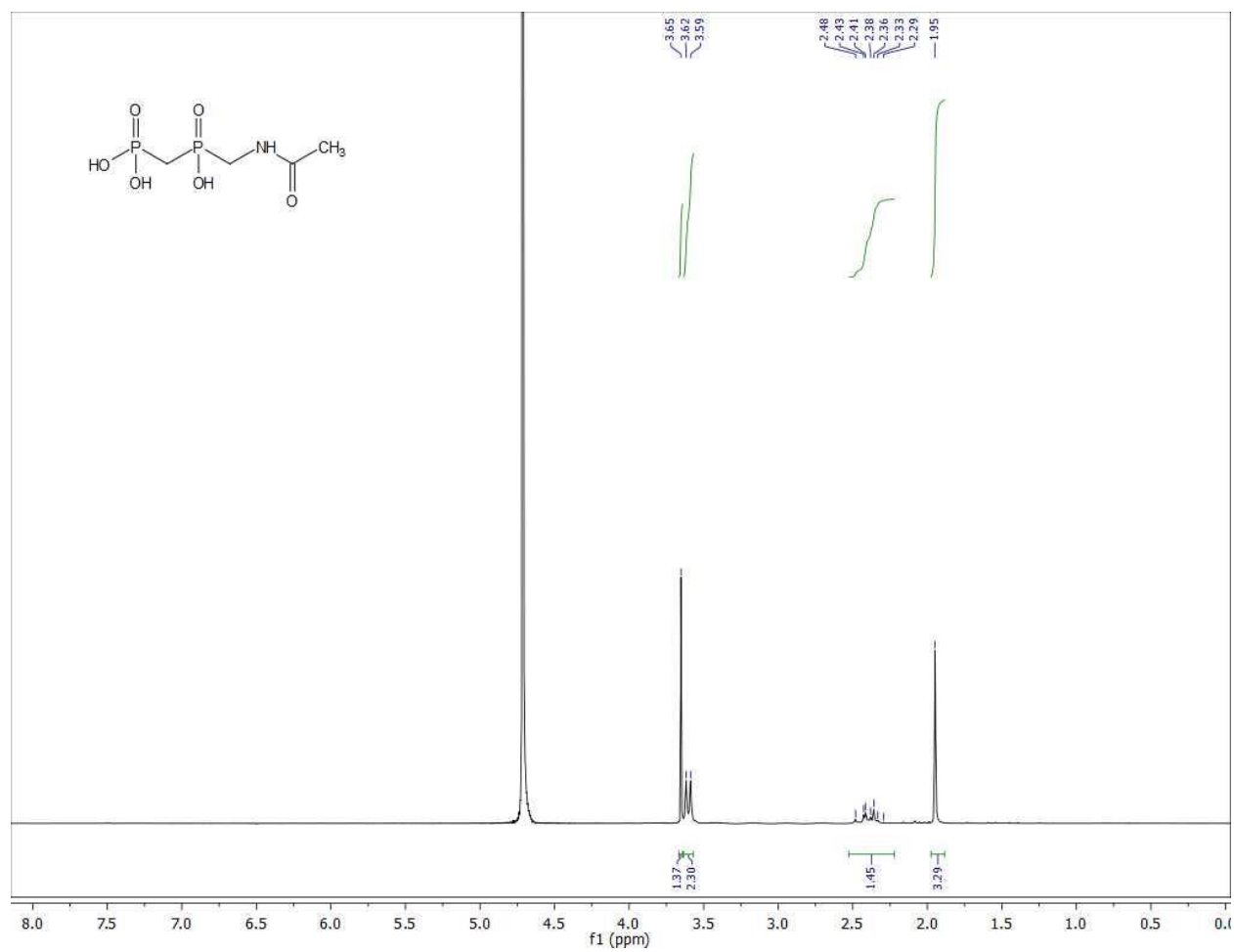


**Figure A.12:**  $^1\text{H}$  NMR spectrum of inhibitor 4 ( $\text{D}_2\text{O}$ , 400 MHz)

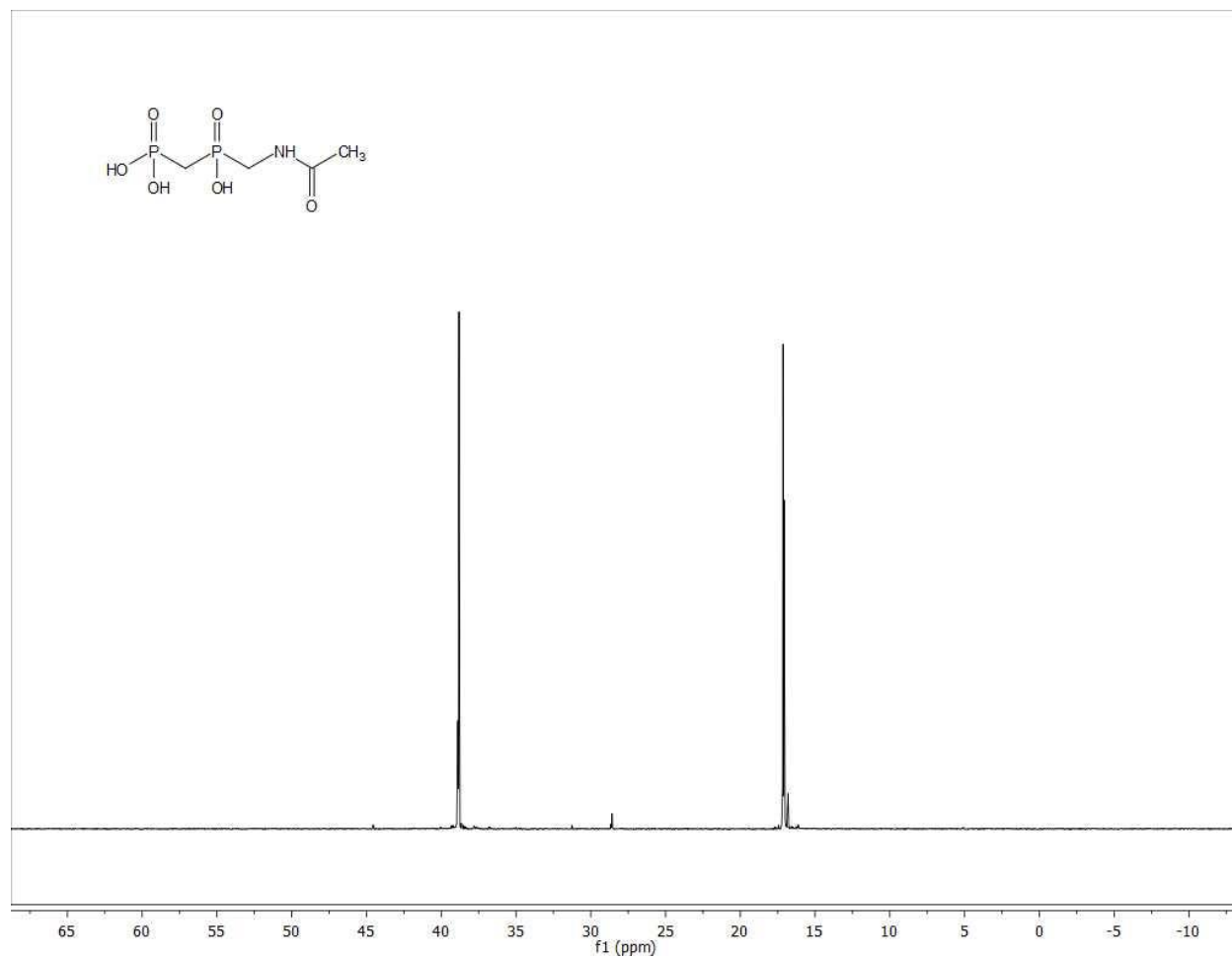


**Figure A.13:**  $^{31}\text{P}$ - $\{^1\text{H}\}$  NMR spectrum of inhibitor 4 ( $\text{D}_2\text{O}$ , 162 MHz)

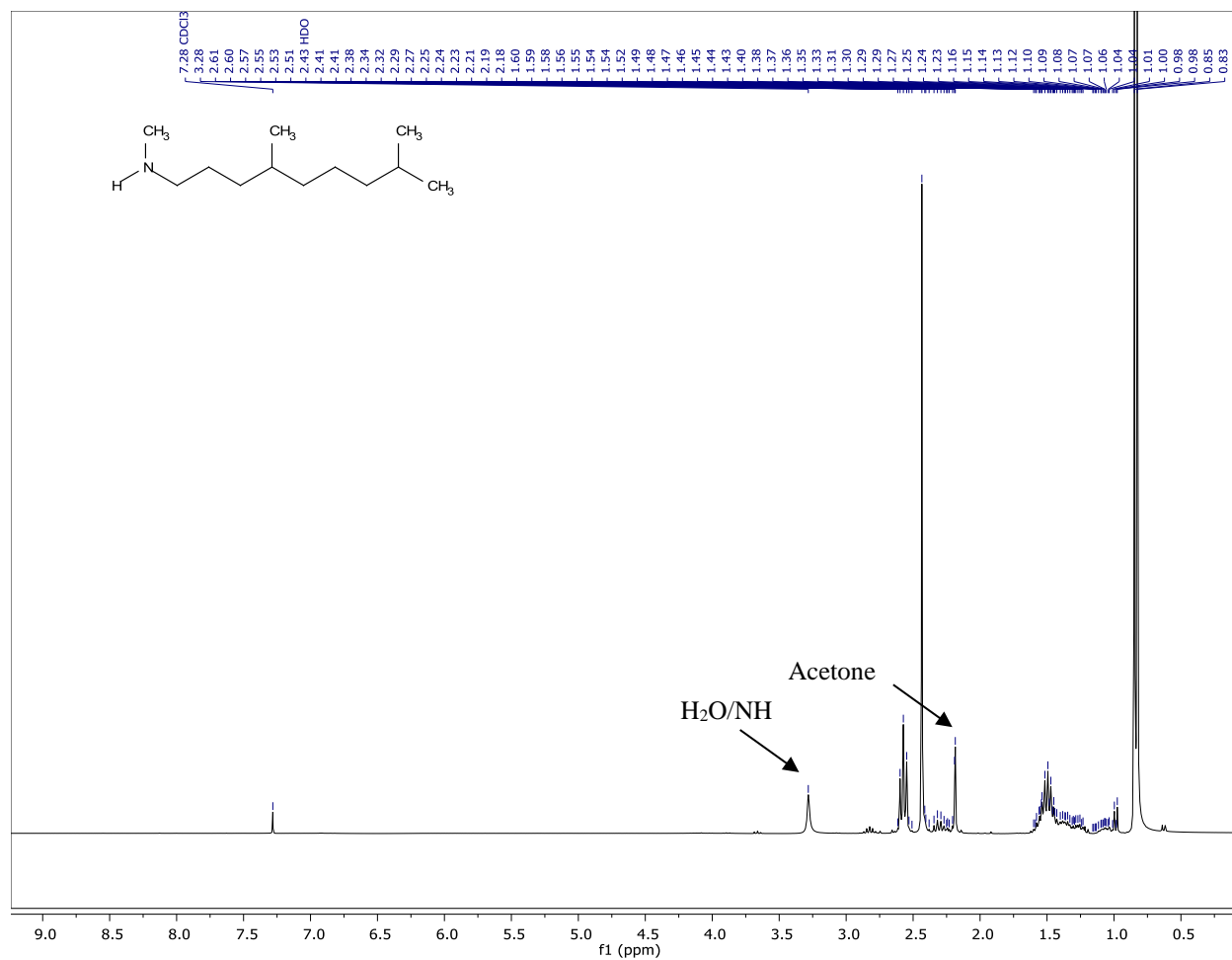


**Figure A.14:** <sup>1</sup>H NMR spectrum of compound **31** (CDCl<sub>3</sub>, 400 MHz)

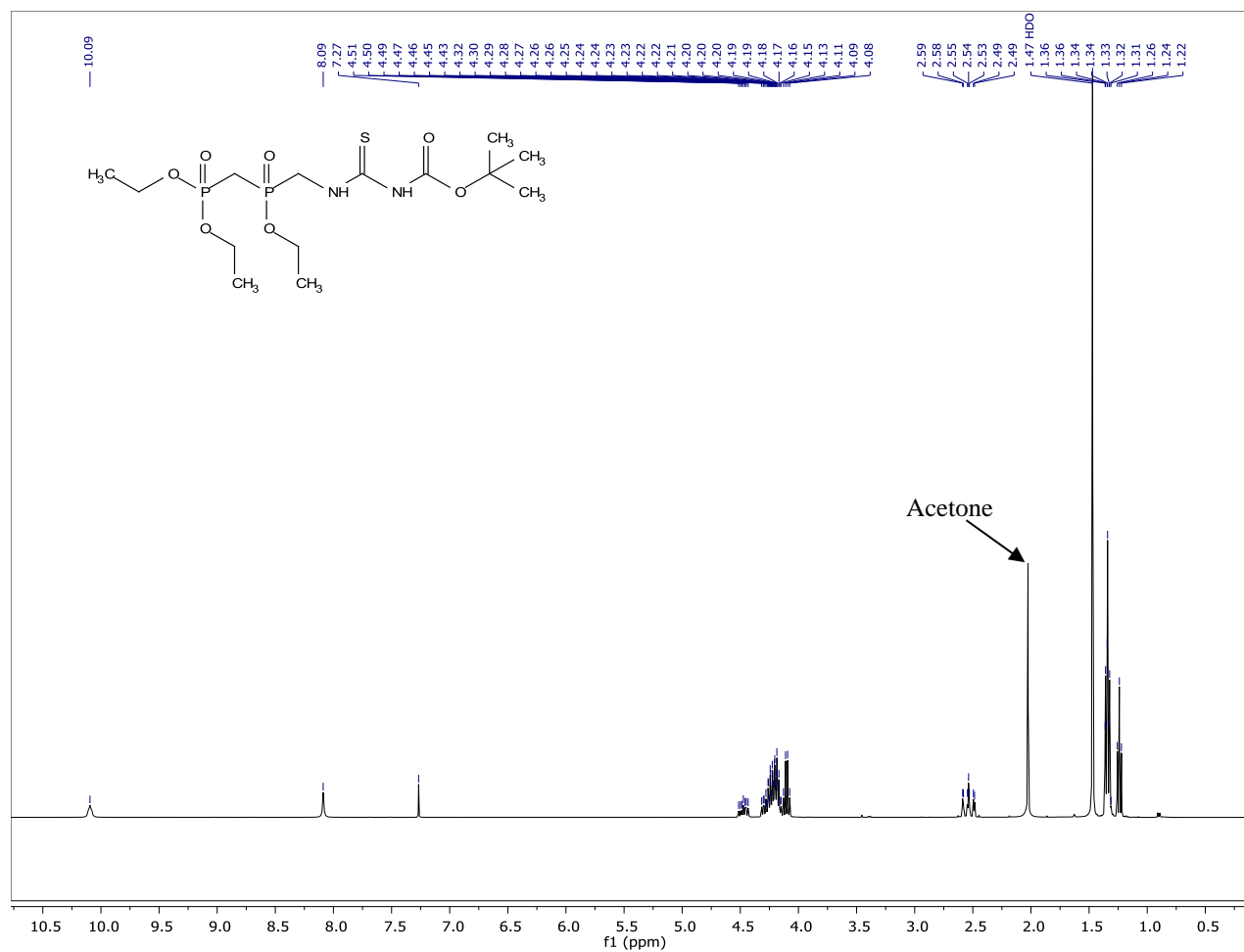


**Figure A.15:** <sup>1</sup>H NMR spectrum of compound **23** (CDCl<sub>3</sub>, 400 MHz)

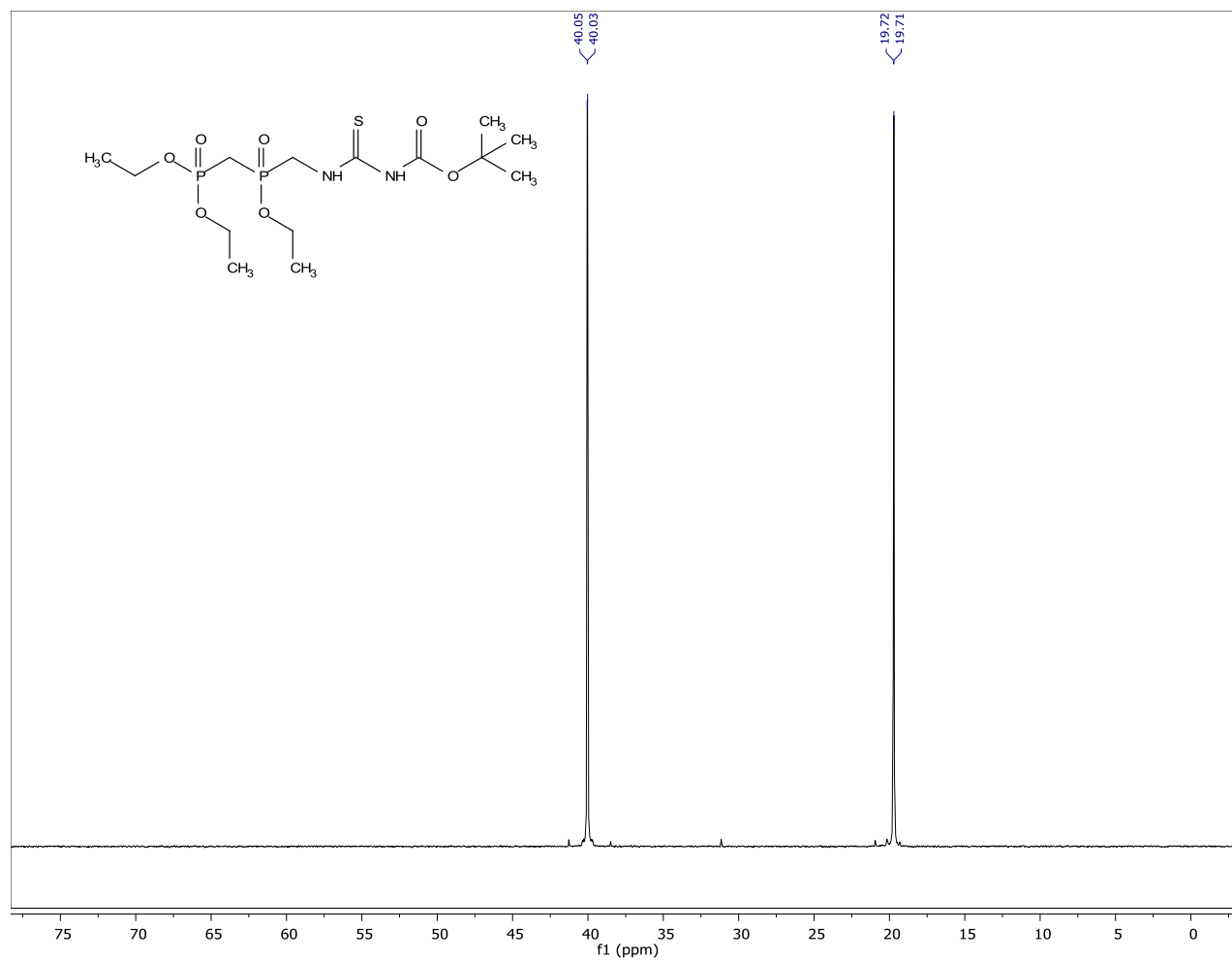


**Figure A.16:**  $^{31}\text{P}\{-^1\text{H}\}$  NMR spectrum of compound **23** ( $\text{CDCl}_3$ , 162 MHz)

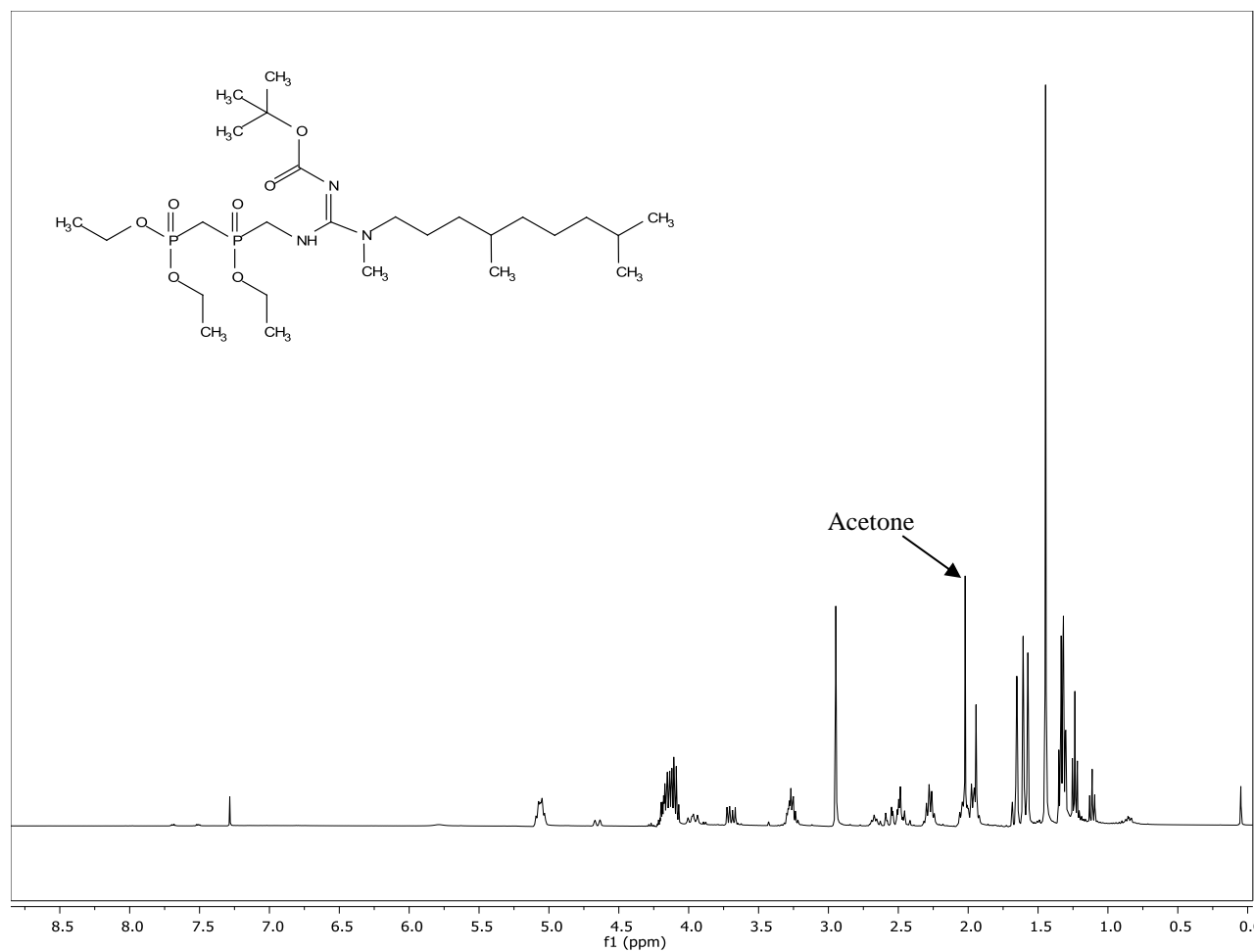


**Figure A.17:** <sup>1</sup>H NMR spectrum of compound **32** (CDCl<sub>3</sub>, 400 MHz)

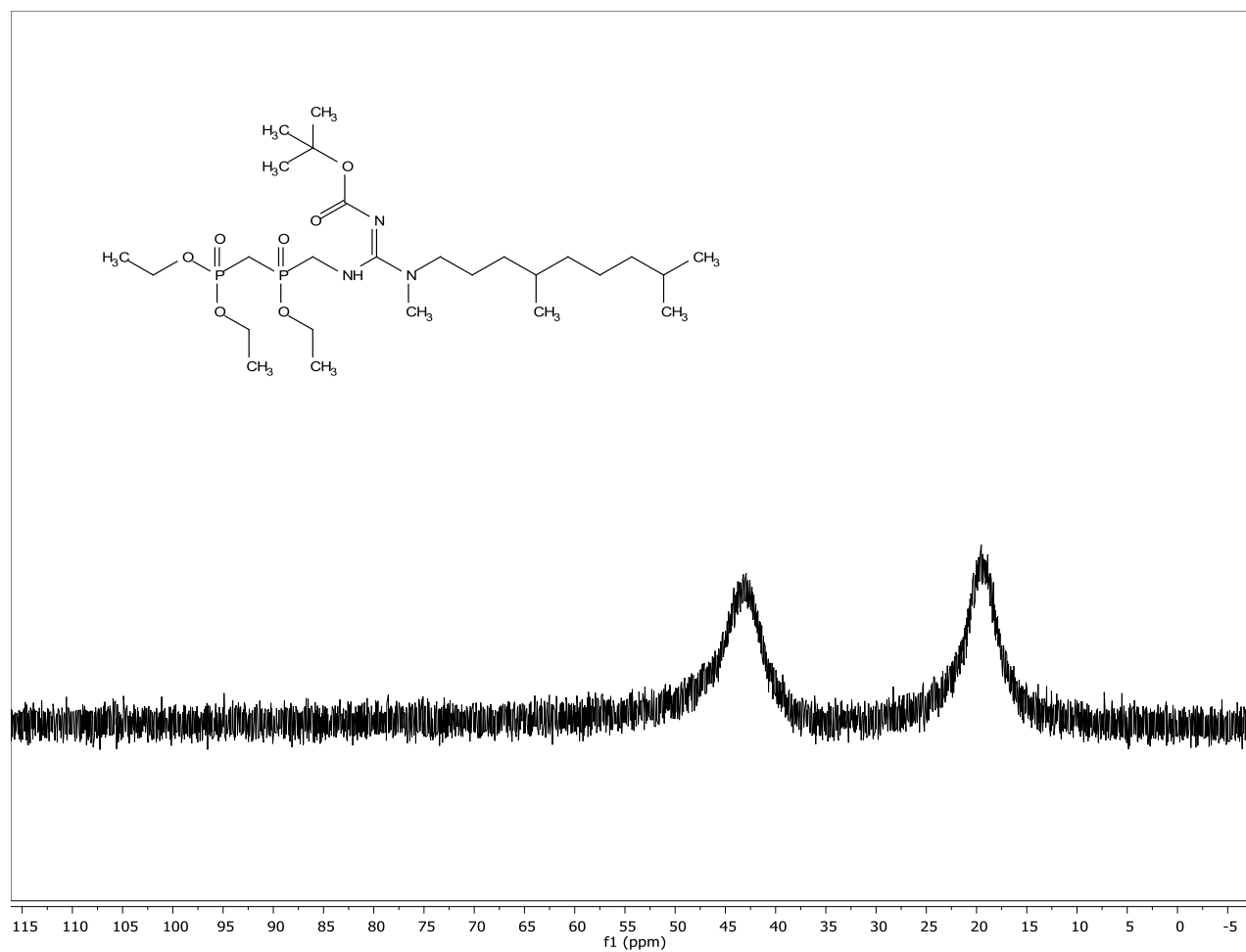


**Figure A.18:**  $^{31}\text{P}\{-^1\text{H}\}$  NMR spectrum of compound **32** ( $\text{CDCl}_3$ , 162 MHz)

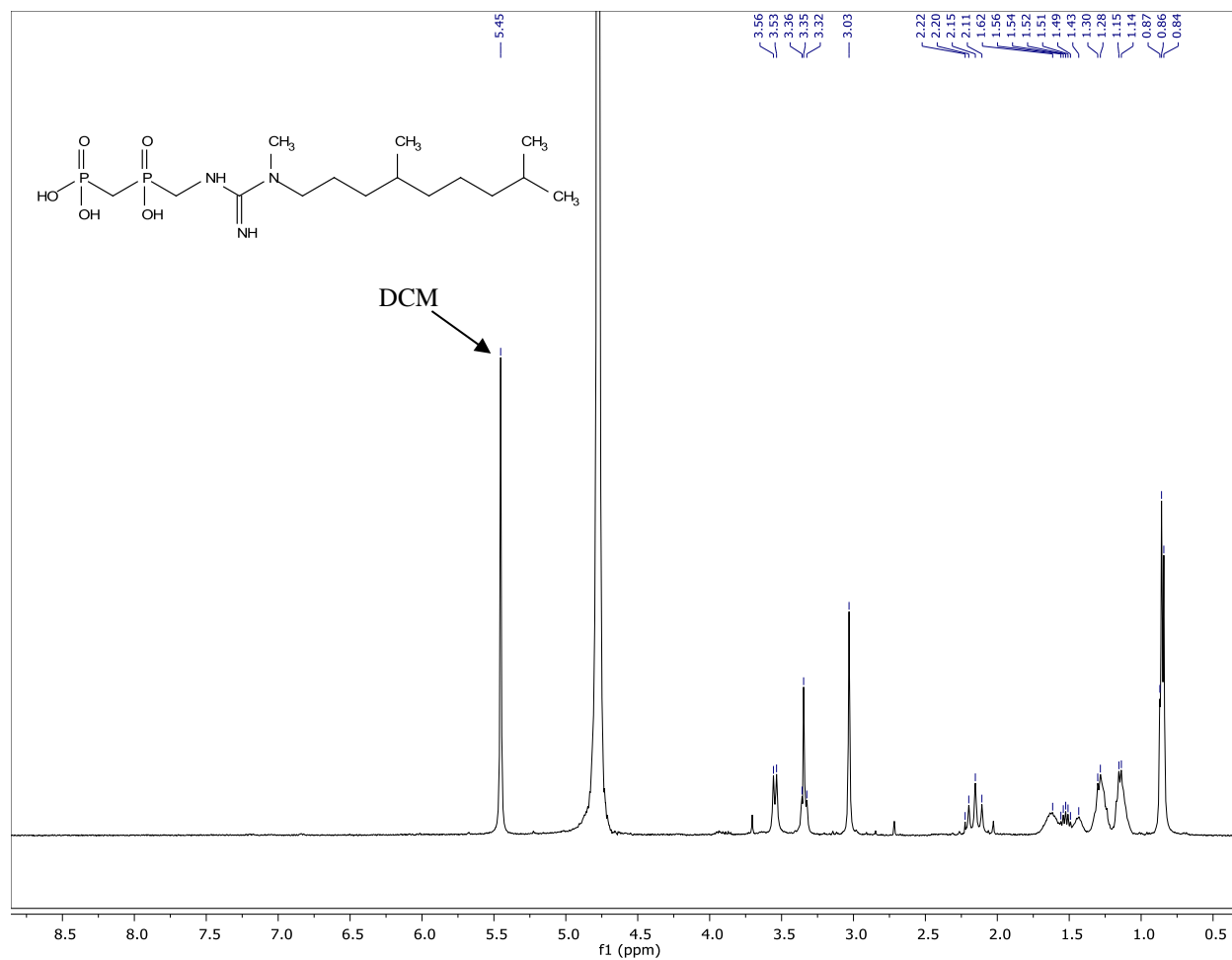


**Figure A.19:** <sup>1</sup>H NMR spectrum of inhibitor **26** (MeOD, 400 MHz)

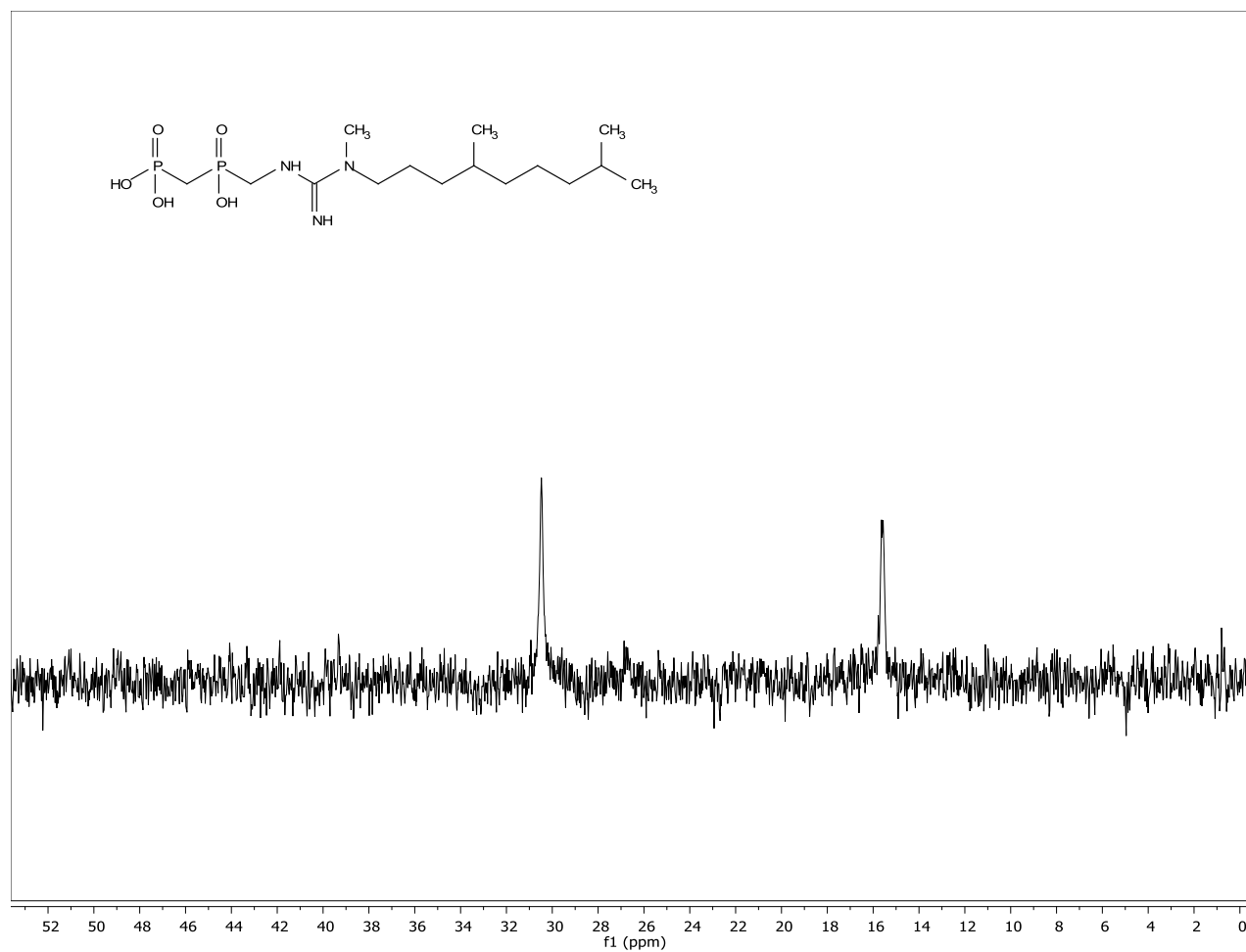


**Figure A.20:**  $^{31}\text{P}\{-^1\text{H}\}$  NMR spectrum of inhibitor **26** ( $\text{CDCl}_3$ , 162 MHz)

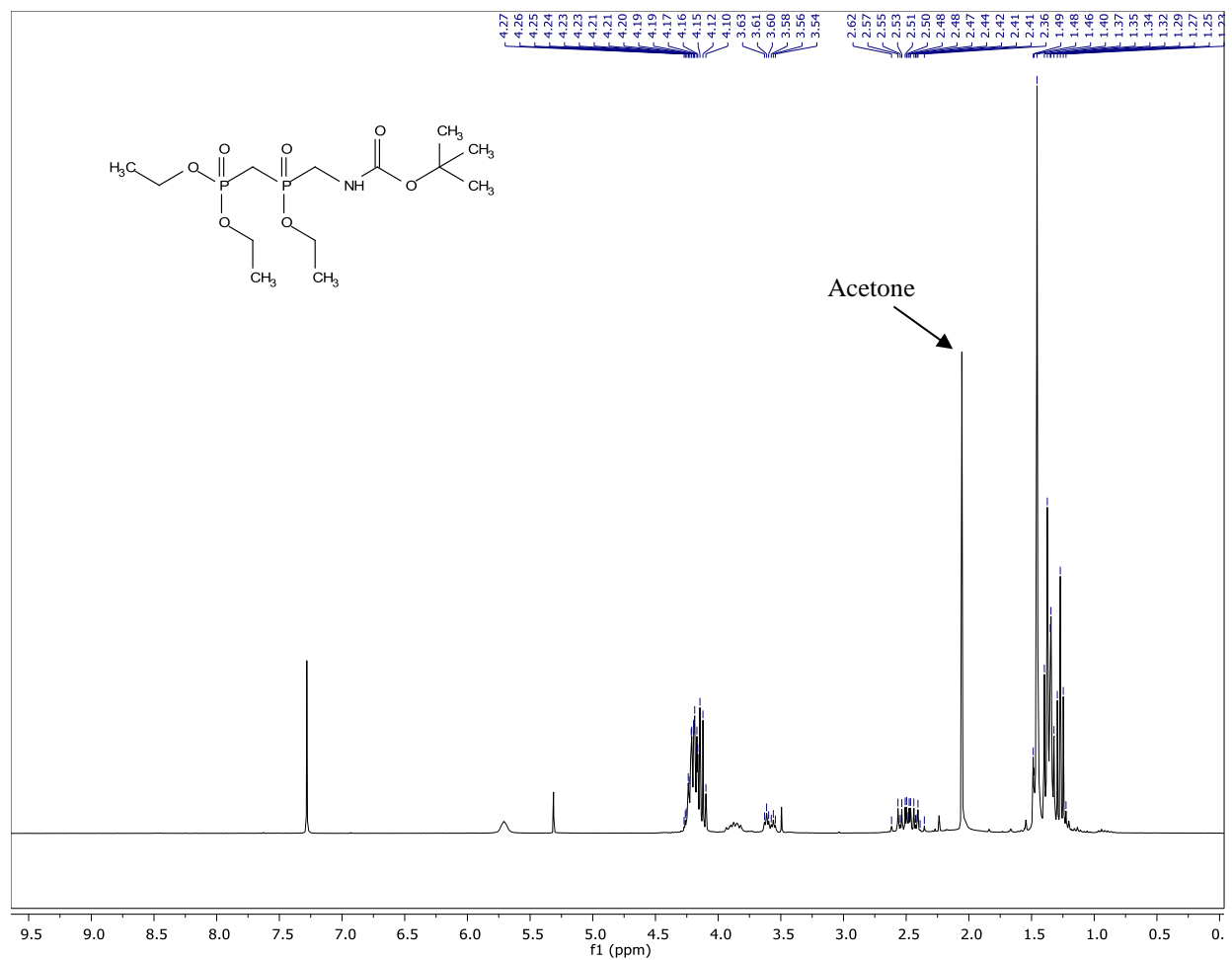


**Figure A.21:**  $^1\text{H}$  NMR spectrum of compound **35** ( $\text{CDCl}_3$ , 400 MHz)

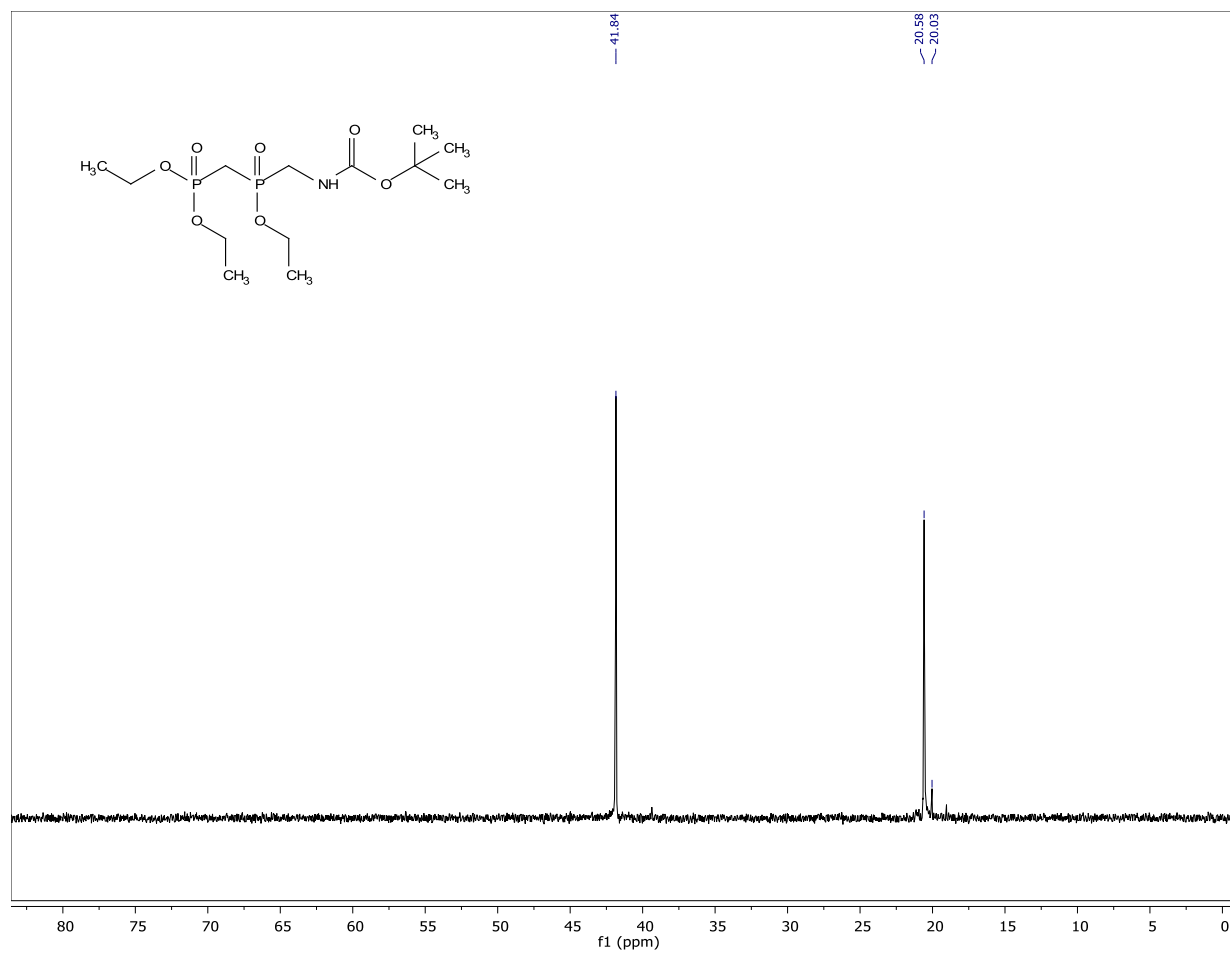


**Figure A.22:**  $^{31}\text{P}\{-^1\text{H}\}$  NMR spectrum of compound **35** ( $\text{CDCl}_3$ , 162 MHz)

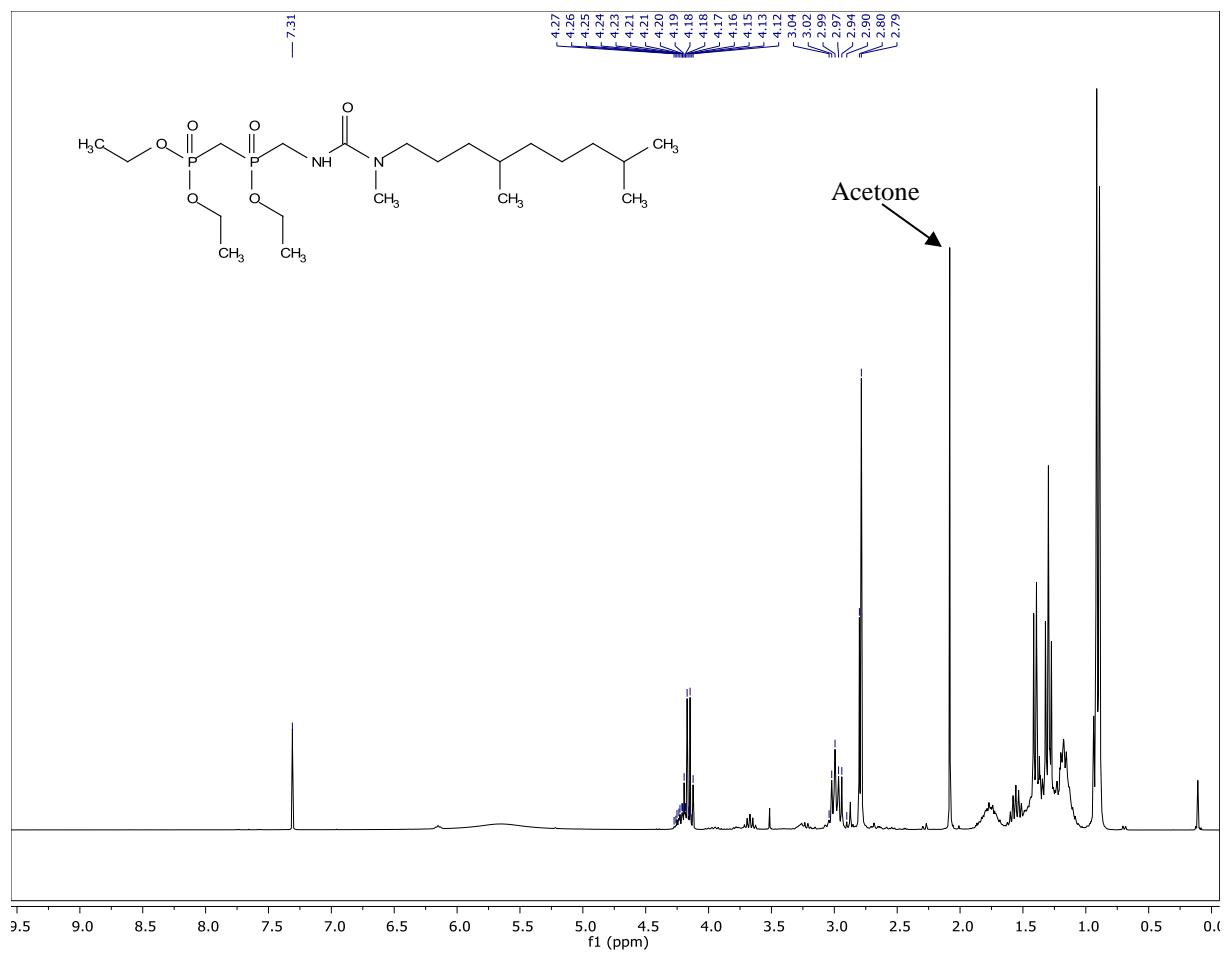


**Figure A.23:**  $^1\text{H}$  NMR spectrum of compound **33** ( $\text{CDCl}_3$ , 400 MHz)

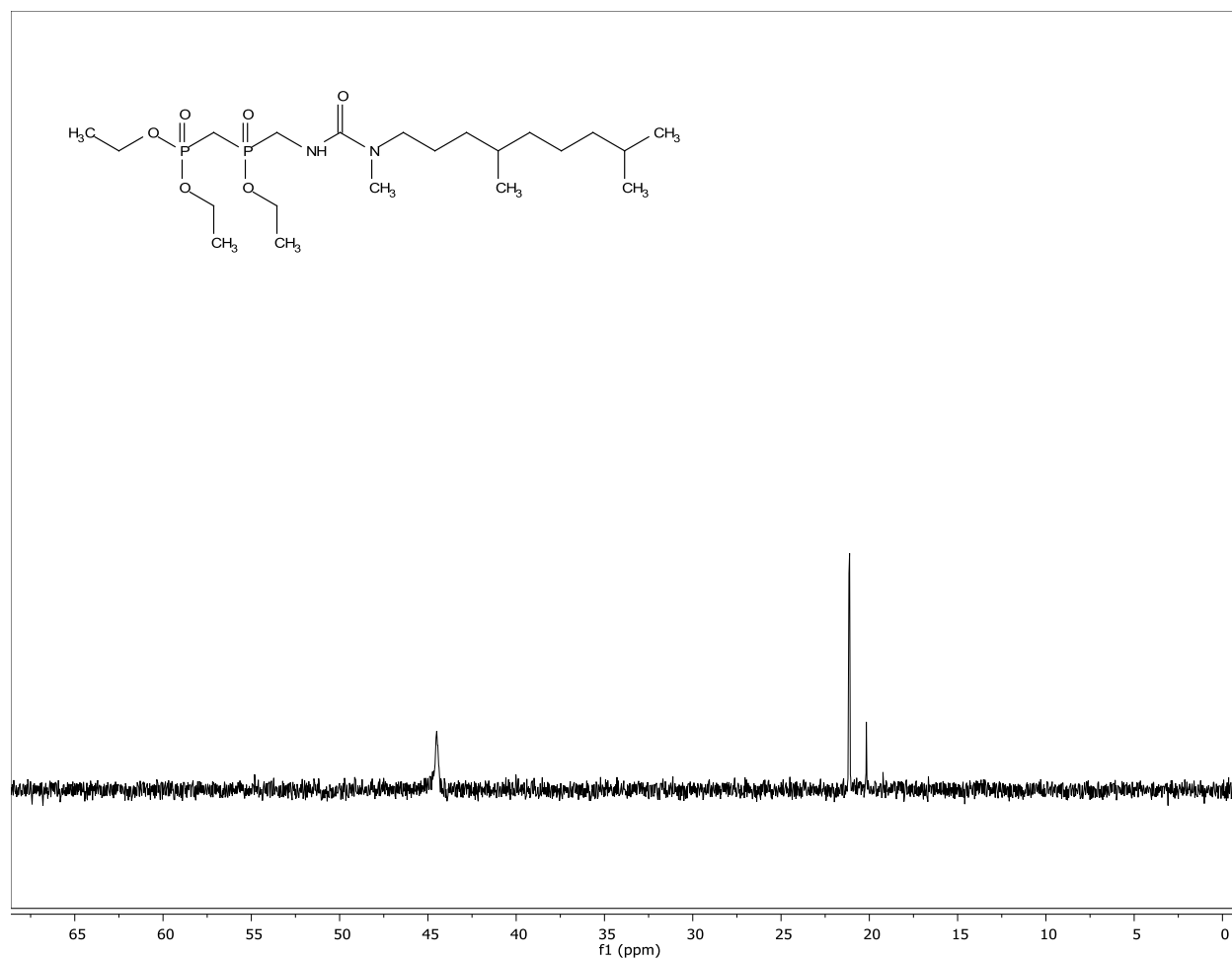


**Figure A.24:**  $^{31}\text{P}\{-^1\text{H}\}$  NMR spectrum of compound **33** ( $\text{CDCl}_3$ , 162 MHz)

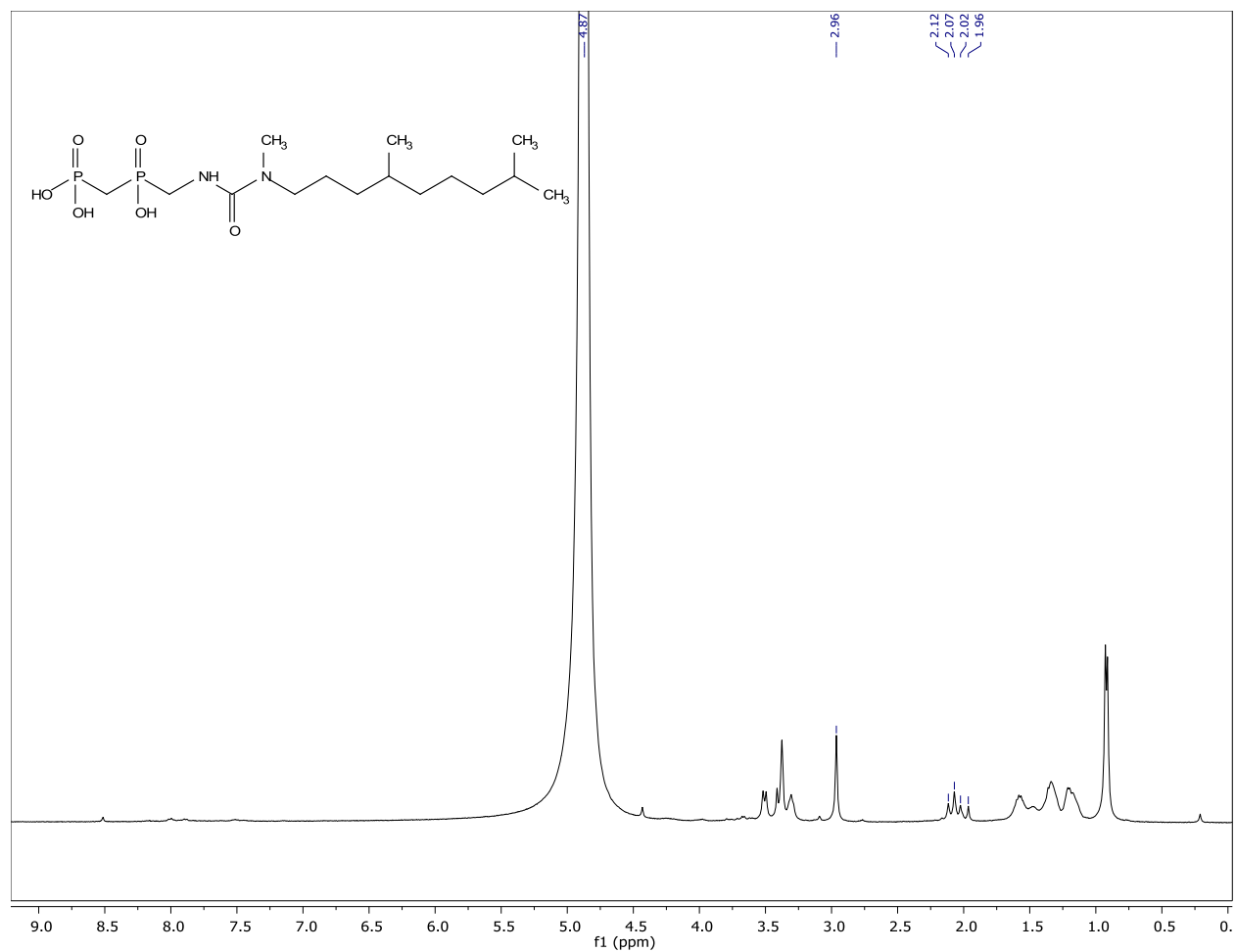


**Figure A.25:** <sup>1</sup>H NMR spectrum of inhibitor **34** (D<sub>2</sub>O, 400 MHz)

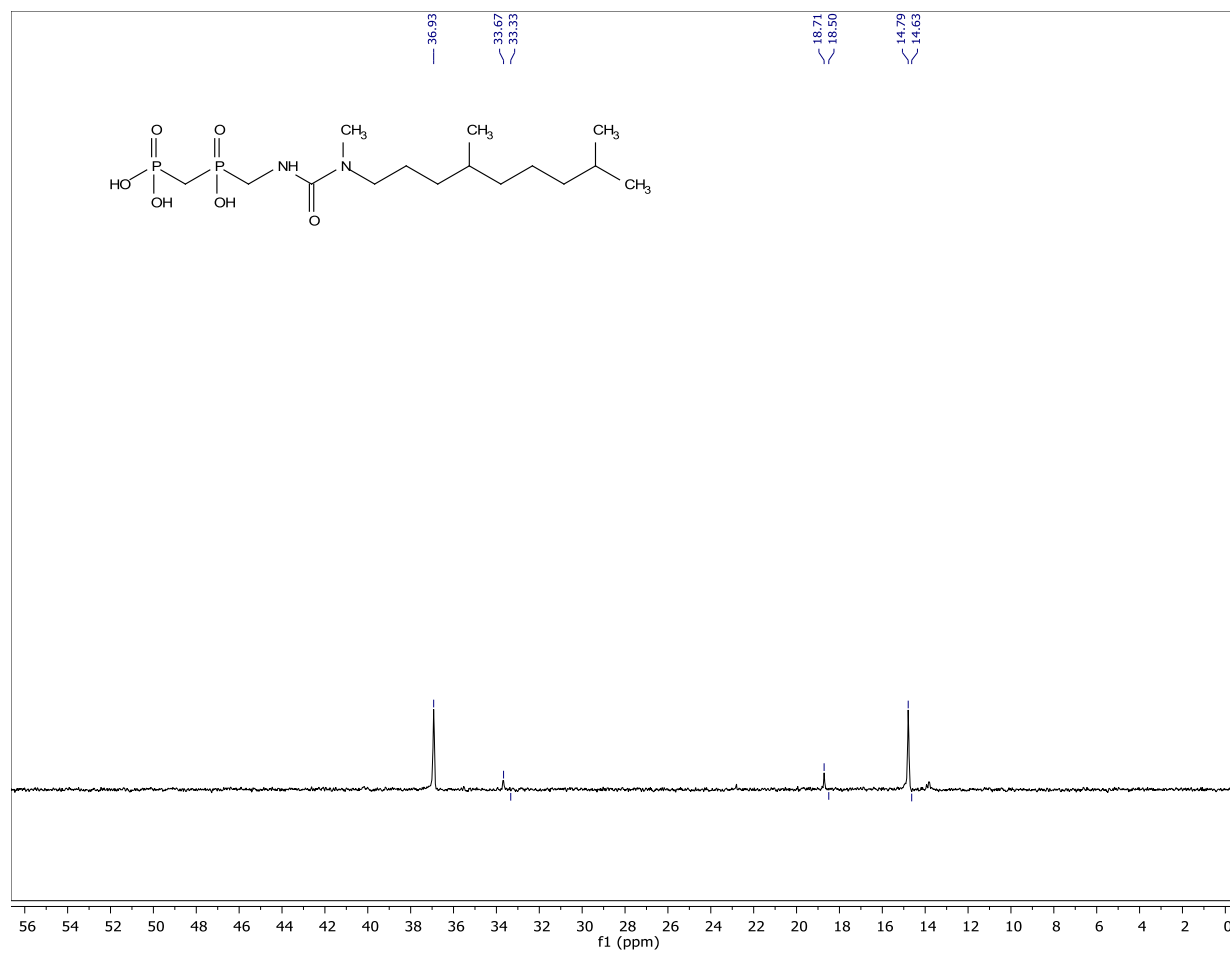


**Figure A.26:**  $^{31}\text{P}\{-^1\text{H}\}$  NMR spectrum of inhibitor **34** ( $\text{D}_2\text{O}$ , 162 MHz)